A Numerical Modelling Study of Tropical Cyclone Sidr (2007): Sensitivity Experiments Using the Weather Research and Forecasting (WRF) Model

---

A thesis submitted in fulfilment of the
requirements for the Degree
of Master of Science in Geography
in the University of Canterbury
by Tristan J. Shepherd
University of Canterbury
2008

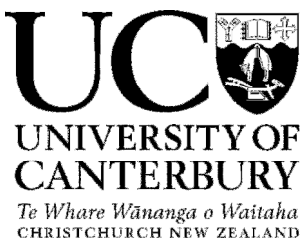

Table of Contents

List of Figures

List of Tables

List of abbreviations used in the text

AMSR-E	The Advanced Microwave Scanning Radiometer for Earth Observing System
Aqua EOS	Earth Observing System (Aqua mission)
BMJ	Betts-Miller-Janjic
CAPE	Convective Available Potential Energy
CISK	Conditional Instability of the Second Kind
CP	Convective Parameterisation
CRED	Center for Research on the Epidemiology of Disasters
dd/mm/yy	Date/Month/Year (format for dates in this thesis)
E	East
EL	Equilibrium Line
EnKF	Ensemble Kalman Filter
F-16	Flight 16
GD	Grell-Devenyi
GFDL	Geophysical Fluid Dynamics Laboratory
GFS	Global Forecast System
IBM-P575	International Business Machines Corporation- Power Model 575 computer
JTWC	Joint Typhoon Warning Centre
KF	Kain-Fritsch
KF_48	Kain-Fritsch 48 hour simulation
KF_72	Kain-Fritsch 72 hour simulation
KF_108	Kain-Fritsch 108 hour simulation
Lat	Latitude
Long	Longitude
LCL	Lifting Condensation Level
LFC	Level of Free Convection
LST	Local Standard Time (Bangladesh local time)
MM5	Pennsylvania State University-National Center for Atmospheric Research Mesoscale Model
MODIS	Moderate Resolution Imaging Spectrometer
MYJ	Mellor-Yamada-Janjic

N	North
Navy/NRL	United States Naval Research Laboratory
NCAR	National Center for Atmospheric Research
NCEP	National Centers for Environmental Prediction
No Cu	No Cumulus
PBL	Planetary Boundary Layer
PCP	Precipitation and Cloud Parameterisation
PCT	Polarization Corrected Temperature
PV	Potential Vorticity
PVU	Potential Vorticity Units
RH	Relative Humidity
RIP4	Read-Interpolate-Plot Version 4
S	South
SSMI	Special Sensor Microwave Imager
SST	Sea Surface Temperature simulation
TMI	TRMM Microwave Imager
TRMM	Tropical Rainfall Measuring Mission
W	West
WPS	WRF Pre-Processing
WRF-ARW	Advanced Weather Research and Forecasting
WSM6	WRF Single Moment 6 Class
YSU	Yonsei University
3DVAR	Three-Dimensional Variational Assimilation

List of symbols used in the text

°C	Temperature in degrees Celsius
°	Direction in degrees
dBz	Decibel
GHz	Gigahertz
g kg^{-1}	Grams per kilogram
hPa	Pressure
hr	Hour
J kg^{-1}	Joules per kilogram
K	Kelvin
kg	Kilogram
km	Kilometre
m	Metre
m s^{-1}	Metres per second
m^2 s^{-1}	Metres squared per second
mm	Millimetre
mm/hr	Millimetres per hour
x, y, z	Cartesian coordinates along the three axes
z	Height
Δ	Change increment
%	Percent

Acknowledgments

Firstly, my sincere thanks to Jesus Christ, my Lord.

This research was supported by the financial assistance of Lady Diana Isaac, and the Isaac Wildlife Trust. I am thankful that they are supporting of young students who want to advance the scientific understanding of interactions between people and the environment. The Sir Neil Isaac Scholarship in Geography and Environmental Sciences is a fine tribute to the late Sir Neil Isaac, and may it continue for many years to come.

This work is the culmination of 20 years in the New Zealand education system, and before I embark on a PhD overseas it is a good time to reflect. I have, in that time, been fortunate to have received inspiration from a number of passionate teachers. My memories of the creative atmosphere in every classroom at Elmwood Normal are still so fresh in my mind, as are the days I spent becoming a young man at St Andrews College. In particular, my time at St Andrews developed me into an intelligent, well read, well spoken, and critical thinking student. I will always remember the opportunity Barry Maister granted me, when he selected me to attend St Andrews. I would not be where I am today if he had not. I also would like to thank Dr Jeni Curtis for developing my English skills (although perfection is still a long way off!); Keith Toner for his passionate Maths classes; and Reverend Hamish Galloway for his spiritual guidance. These are people with incredible character and skill, and were inspiring teachers. I hope that I will make as good a teacher in the coming years.

The tertiary education sector has brought many challenges and joys, and I am better for it. The Geography department at Canterbury University is full of dedicated staff that work hard in their teaching roles. I would like to express my thanks to all departmental staff that have had a role in my seven years here. In particular, I would like to thank Dr Burn Hockey who was a great friend and lecturer during my studies. For this master's research, I am greatly indebted to my supervisors Dr Peyman Zawar-Reza and Professor Andy Sturman, who have provided me with some excellent atmospheric knowledge and skills. I have appreciated the time that Peyman has invested in me so that I can operate numerical models; and Andy has a wealth of atmospheric knowledge, and it has been a pleasure to have been taught by him. In addition to my supervisors, I would like to thank: Paul Bealing for converting this document to a PDF; and Marney Brosnan for producing an excellent map of Bangladesh. I would also like to thank Basit Kahn for the time he spent with me manipulating code for experiments. These people are a reflection of the quality of staff and students we have in this department. Finally, I must thank Colin McMurtie and Tony Dale who run and maintain the university's supercomputer- you guys are brilliant. I look forward to seeing the high performance computing facility thrive at this university.

To my family and friends in all places: your support and interest has been a shining light during a very challenging and stressful 12 months of work. Thanks especially to Kelvin Walst and Lynton Brocklehurst for your encouragement and support. Thanks mum for the 'meals on wheels', and dad for your brains. I guess I should thank 'Billy' for putting up with my annoying brotherly ways. To my best friend Nick Letham: you are a great man, thank you for your advice, support, and continual friendship.

God bless and see you all soon!
T J SHEPHERD November, 2008.

Abstract

The tropical cyclone is a majestic, yet violent atmospheric weather system occurring over tropical waters. Their majesty evolves from the significant range of spatial scales they operate over: from the mesoscale, to the larger synoptic-scale. Their associated violent winds and seas, however, are often the cause of damage and destruction for settlements in their path.

Between 10/11/07 and 16/11/07, tropical cyclone Sidr formed and intensified into a category 5 hurricane over the southeast tropical waters of the northern Indian Ocean. Sidr tracked west, then north, during the course of its life, and eventually made landfall on 15/11/07, as a category 4 cyclone near the settlement of Barguna, Bangladesh. The storm affected approximately 2.7 million people in Bangladesh, and of that number 4234 were killed.

In this study, the dynamics of tropical cyclone Sidr are simulated using version 2.2.1 of Advanced Weather Research and Forecasting — a non-hydrostatic, two-way interactive, triply-nested-grid mesoscale model. Three experiments were developed examining model sensitivity to ocean-atmosphere interaction; initialisation time; and choice of convective parameterisation scheme. All experiments were verified against analysed synoptic data. The ocean-atmosphere experiment involved one simulation of a cold sea surface temperature, fixed at 10 °C; and simulated using a 15 km grid resolution. The initialisation experiment involved three simulations of different model start time: 108-, 72-, and 48-hours before landfall respectively. These were simulated using a 15 km grid resolution. The convective experiment consisted of four simulations, with three of these using a different implicit convective scheme. The three schemes used were, the Kain-Fritsch, Betts-Miller-Janjic, and Grell-Devenyi ensemble. The fourth case simulated convection explicitly. A nested domain of 5km grid spacing was used in the convective experiment, for high resolution modelling. In all experiments, the Eta-Ferrier microphysics scheme, and the Mellor-Yamada-Janjic planetary boundary layer scheme were used.

As verified against available observations, the model showed considerable sensitivity in each of the experiments. The model was found to be well suited for combining ocean-atmosphere interactions: a cool sea surface caused cyclone Sidr to dissipate within 24 hours. The initialisation simulations indicated moderate model sensitivity to initialisation time: variations were found for both cyclone track and intensity. Of the three simulations, an initialisation time 108 hours prior to landfall, was found to most accurately represent cyclone Sidr's track and intensity. Finally, the convective simulations showed that considerable differences were found in cyclone track, intensity, and structure, when using different convective schemes. The Kain-Fritsch scheme produced the most accurate cyclone track and structure, but the rainfall rate was spurious on the sub-grid-scale. The Betts-Miller-Janjic scheme resolved realistic rainfall on both domains, but cyclone intensity was poor. Of particular significance, was that explicit convection produced a similar result to the Grell-Devenyi ensemble for both model domain resolutions.

Overall, the results suggest that the modelled cyclone is highly sensitive to changes in initial conditions. In particular, in the context of other studies, it appears that the combination of convective scheme, microphysics scheme, and boundary layer scheme, are most significant for accurate track and intensity prediction.

Chapter 1

Introduction

1.1 Context

The tropical cyclone (also known as a hurricane or typhoon) is one of nature's most majestic yet fierce and unrelenting natural hazards. Tropical cyclones are certainly of great beauty when they occur over the vast tropical oceans of Earth, but when these storms come into the vicinity of people in coastal settlements, they can become quite devastating. Such destructive potential was witnessed from North American Hurricane's Katrina (2005) and Andrew (1992), while many lives were lost as a result of northern Indian Ocean's Cyclone Bhola (1970) and the *Bangladesh cyclone* of 1991.

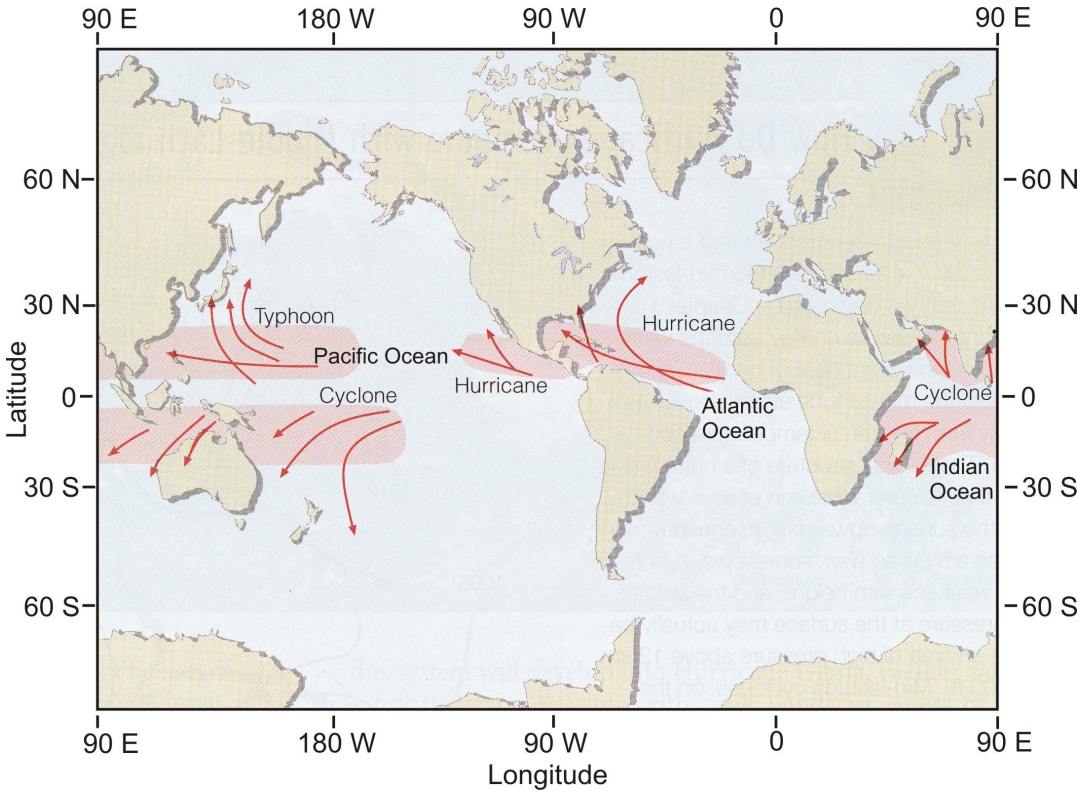

Figure 1.1: The three principal genesis regions of tropical cyclones as described by Emanuel (2005) (adapted from Ahrens 2007).

According to Emanuel (2005), tropical cyclones develop in three principle belts (Figure 1.1). The first belt extends from the western tropical Atlantic, through the Gulf of Mexico to the eastern North Pacific Ocean. The second stretches west of the central North Pacific across the South China Sea, the Bay of Bengal, and ending in the Arabian Sea. The third and final belt extends from the central South Pacific across the South Indian Ocean to the

coast of Africa. The reasons for cyclones forming in these specific regions are outlined in Chapter 2.

A hurricane's intensity is measured in a number of ways. The most universal measure is the Saffir-Simpson hurricane damage potential scale (Saffir and Simpson 1974), which classifies a tropical cyclone from category 1 (minimal damage), to category 5 (catastrophic). This intensity measure is based on a hurricane's wind speed, central pressure, and associated storm surge (Table 1.1). Wind speeds are a sustained 1 minute average at 10 m height. On average, 84 tropical disturbances develop each year and of that only 45 on average make category 1 hurricane status (Emanuel 2005).

Table 1.1: Saffir – Simpson hurricane intensity scale (Saffir and Simpson 1974).

Category	Central pressure (hPa)	Maximum wind speed (m s^{-1})	Storm surge (m)	Damage
Tropical depression	–	<17	–	–
Tropical Storm	–	17–32	–	–
1	≥980	33–42	1–1.5	Minimal
2	965–979	43–49	2–2.5	Moderate
3	945–964	50–58	3–3.5	Extensive
4	920–944	59–69	4–5.5	Extreme
5	<920	>69	>5.5	Catastrophic

Between 10/11/07 and 16/11/07, tropical cyclone Sidr, a category 5 hurricane, reportedly claimed the lives of 4,234 people in Bangladesh (Center for Research on the Epidemiology of Disasters (CRED), International Disaster Database 2008). An event of this magnitude occurring in a region of the world that is poorly developed and relatively ill-equipped to respond to such weather events often means its effects are amplified. Indeed, the death toll was almost double that of Hurricane Katrina — a category 5 cyclone occurring in the north-central Gulf Coast in 2005, and one of the five deadliest hurricanes in United States history — and the aftermath of Sidr much worse than Katrina's damage to New Orleans in 2005. It should be noted, however, that cyclone warnings, response times and rescue efforts have improved since the 1991 *Bangladesh Cyclone* which claimed 138,000 lives.

Disasters like Sidr provide impetus for research and education to better understand hurricanes in order to reduce society's vulnerability to hurricane-related impacts.

According to Pielke and Pielke (1997), lessons learnt from successes and failures in reducing vulnerability to hurricanes have the potential to contribute to efforts to reduce societal vulnerability to extreme weather events more generally. Research has an important role in contributing to this reduction of risk.

The majority of scholarly research regarding tropical cyclones has been to understand their structure, development and dynamics, and then transfer this knowledge into accurate numerical weather forecasting models so that lives might be saved. Most of the earliest theoretical studies such as Syono (1953), Yanai (1961), Lily (1960), Malkus and Riehl (1960), Estoque (1962), Charney and Eliassen (1964), Rosenthal (1964) Ooyama (1964), and Gray and Shea (1973), made use of available observational data to construct a framework of the general structure and physical processes within a hurricane. It was well established by the mid-1960s that hurricanes form from a perturbation in an easterly wave, and are driven by latent heat release from cumulus convection (Kuo 1964). It was not until the 1980s when the first theory that recognised the ocean has a dominant role in the intensity of hurricanes was derived. Indeed, the study of Emanuel (1986) that recognised the hurricane operates as a Carnot heat engine, revolutionised the conceptual understanding of hurricane genesis and intensification. Furthermore, the advent of the numerical model was an incredible step forward in the representation of cyclones, especially their inner core structures, unlocking a wealth of potential studies, forecasting developments and applications for understanding cyclones.

Numerical studies of tropical cyclones date back to as early as the mid-1950s, when a core group of research scientists developed two-dimensional axisymmetric hurricane models to help understand these convective systems. An excellent review of early numerical models and research is provided by Anthes (1982). In particular, the work of Rosenthal (1964), Kuo (1965), and Ooyama (1964, 1969, 1971) paved the way for developments in this field. These early numerical studies examined the role of latent heat release and the effect of convective parameterisation, which are arguably the most important processes in the tropical cyclone environment. Because these axisymmetric models ignored flow variations on the horizontal plane, they were rather crude. There were, however, some advanced studies conducted with the axisymmetric model such as Kurihara (1975), Yamasaki (1977), Rosenthal (1978), Anthes and Chang (1978) and, Chang and Anthes (1979). These were restricted, however, because of what Rosenthal (1979) described as ineffective closure mechanisms in the model, and inability to simulate asymmetrical flow. This was

because these models could not realistically simulate latent heat release, because closure in model parameterisation schemes was yet to be developed. Indeed, while Rosenthal (1979) found the growth of a tropical cyclone is significantly affected when the convective parameterisation (CP) and form of the cloud are altered, further use of these numerical methods seemed of little benefit until closure for CP in a model could be obtained.

Fortunately, two significant developments occurred during the 1980s and 1990s that allowed for more realistic simulation of convective heating and cumulus parameterisation. The first was the improvement of the three-dimensional asymmetric model. In fact, three-dimensional asymmetric models had been in use for some time, with significant studies by Anthes et al. (1971*a*, 1971*b*), Anthes (1972), and Kurihara and Tuleya (1974), but these were rather crude. Advances in computing power during the 1980s and 1990s, however, meant higher grid resolutions for three-dimensional models were now obtainable. This allowed for simulation of inner core structures and spiral rain bands (Willoughby et al. 1982). The second significant development was the advent of more robust CP schemes providing the necessary closure for more accurate simulations of convective cloud structures. In particular, the schemes of Fritsch and Chappell (1980*a*, 1980*b*), Betts and Miller (1986), Grell et al. (1991, 1993), and Kain and Fritsch (1993) were an improvement in the implicit representation of cumulus convection and precipitation processes on coarse model domains.

In recent years, a number of very high resolution three-dimensional asymmetric numerical models have been developed. These have improved the treatment of model governing equations, and have been used for hurricane research. Such models include the National Atmospheric and Oceanic Administration's Geophysical Fluid Dynamics Laboratory (GFDL) hurricane model, Pennsylvania State University-National Center for Atmospheric Research mesoscale model (MM5), and the Weather Research and Forecasting (WRF) model. MM5 was replaced by WRF after its conception in 2002, and was initially not regarded suitable for hurricane research. A proof-of-concept study, however, found it to be a suitable forecast and research tool for hurricanes (Davis et al. 2006). Since that time a limited number of cases have been conducted with WRF, and more are required to realise the potential of this model for simulating high resolution, detailed, dynamical structures of hurricanes. More specifically, WRF initialisation studies by Nolan et al. (2002), Rosier (2005), Guo et al. (2006), Snyder and Chen (2006), Davis and Holland (2007), Pattanayak and Mohanty (2008); and CP studies by Rosier (2005), Gentry and Lackmann (2006), Li

and Pu (2006), and Bassill and Morgan (2008), serve as an excellent foundation for this research. It is apparent, however, that very few WRF convective studies exist in the scholarly literature. This is significant because there is evidence for sensitivity of tropical cyclone prediction to choice of CP scheme (Puri and Miller 1990; Davis and Bosart 2002). Thus it is important to examine the effect of CP schemes with fundamentally different formulations. This forms one of the reasons for this study, as outlined in the rationale.

This research adds to the body of scientific knowledge on numerical research of tropical cyclones using WRF to conduct a series of simulations of tropical cyclone Sidr. A number of experiments are conducted that examine the ocean-atmosphere interaction, model initialisation time, and CP scheme on cyclone dynamics and life cycle. The motivations of this work are outlined in the rationale, and the research objectives indicate what this study aims to achieve.

1.2 Rationale

There are a number of important considerations that make this study important. Firstly, Bangladesh and surrounding regions are often overlooked for cyclone research studies. The reason for this is generally due to the lack of observational equipment located in this region. For example, only one cyclone detection radar exists in the Indian Ocean region, and it is based in Calcutta, so coverage is generally poor. Furthermore, there are no known reconnaissance aircraft in this region, virtually ruling out any direct measurement of events. Indeed, cyclone studies of this region rely heavily on the use of remotely sensed imagery, which can be limiting due to sensor error, and timing of image acquisition. In addition, the majority of scholarly research on hurricanes is conducted in North America, and most studies tend to focus on Atlantic hurricanes. The work presented here is an attempt to rectify the imbalance that exists between the plethora of North American cyclone studies, and the minimal Indian Ocean cyclone studies. It is hoped that this study will raise awareness of the need to include this region in more complex and detailed hurricane modelling investigations. Secondly, there have been a limited number of hurricane case studies undertaken with WRF to date, and even fewer studies that examine the role of CP schemes for hurricane events. Thirdly, it is important (for both humanitarian and practical reasons) to conduct tropical cyclone research to assist communities affected by these events. A greater amount of knowledge and understanding available to draw upon when planning and responding to these events is critical. This is particularly relevant in

Bangladesh, an area that relies on only one meteorological centre for warnings, and the good will of researchers to investigate events in this region so that appropriate forecasts can be derived. Finally, there are several meteorological centres around the globe that predict tropical cyclones and forecast their paths. This research could assist those organisations to further understand tropical cyclone dynamics and their effects.

1.3 Thesis objectives

The aim of this research is to use WRF to conduct a series of sensitivity experiments investigating the dynamics, environmental interactions, and life cycle of tropical cyclone Sidr. This aim is divided into four research objectives:

- Examine the synoptic and mesoscale atmospheric processes that led to the development of tropical cyclone Sidr.

- Examine the influence of sea surface temperature on tropical cyclone intensity, energy exchanges, life cycle, and structure, and test the suitability of WRF for coupling ocean-atmosphere processes.

- Examine the role of model initial conditions on the intensity and track of cyclone Sidr.

- Examine the sensitivity of the simulated hurricane to various CP schemes.

The following research questions aim to answer these objectives:

1. What were the observed atmospheric developments that lead to the genesis of Sidr, and its continued intensification? What significant hurricane structural characteristics existed?

2. What effect does a cool sea surface temperature have on hurricane intensification and energy exchange?

3. How important is model initialisation time for prediction of cyclone track and intensity?

4. What differences in cyclone track, intensity, and structure exist between the CP experiments?

5. Which CP experiment resolved the most realistic precipitation rates?

6. What do the precipitation rates indicate about the operation of each CP scheme, and what implications does this have for the operation of the precipitation and cloud parameterisation (PCP) scheme?

1.4 Thesis structure

Chapter 2 presents relevant background information on the processes involved in tropical cyclone formation. The chapter also outlines mesoscale meteorological modelling, and some of the processes involved relevant to this study. Chapter 3 discusses the methodological approach used and presents the model experimental design and WRF technical description. In Chapter 4, details cyclone Sidr's development and life cycle, using a range of observational data are presented. Chapter 5 describes an experiment examining the role of ocean-atmosphere interaction, which also forms a basic diagnostic test of the model. Chapter 6 presents results from initialisation experiments, where the model start time was varied to determine the most accurate cyclone forecast. Chapter 7 presents the results of the CP experiments. Chapter 8 revisits the objectives of this thesis, and discusses the major findings in relation to other work. The thesis is concluded in Chapter 9.

Chapter 2
Tropical cyclones and numerical modelling

2.1. Introduction

This chapter presents relevant background information for the understanding of this thesis. The processes of tropical cyclone formation are discussed before some of the more advanced physical processes are explained. A background of mesoscale meteorological modelling is provided, with an explanation of WRF, and some relevant studies are also introduced. Finally, an explanation of the role of CP, a major component of this thesis, concludes this chapter.

2.2 The Tropical Cyclone

There are a number of key texts and research papers that have contributed to the advancement of theoretical understanding of tropical cyclones over the last half-century (Miller 1958; Kuo 1964; Gray and Shea 1973; Anthes 1982; Gray 1982; Willoughby et al. 1982; Chan 1984; Marks 1985; Emanuel 1986; Pielke 1990; Cione et al. 2000; Emanuel 2004; Chan et al. 2002; Black PG, et al. 2007). This advancement of knowledge would not have been possible without the introduction of more sophisticated observational equipment, including satellite remote sensing, dropsondes, reconnaissance aircraft, and cyclone detection radar. This has allowed for more accurate interpretation of the physical and dynamical interactions in the hurricane environment. For example, recent research using reconnaissance aircraft has allowed for direct eye wall observation. In addition, dropsondes have provided more accurate measurements of the thermodynamic structure inside the eye, eye wall and spiral rain bands of hurricanes (Black ML, et al. 2006).

Numerical weather prediction models have also played a major role in developing and testing a variety of hurricane theories, and improving hurricane. Over the past 20 years the research emphasis appears to have diverted away from theoretical cyclone studies, to more of an applied approach using models. In particular, research appears devoted to the representation of convection in models, and hurricane track forecasting. There are some well accepted, fundamental principles behind tropical cyclone development that date back 30 years, but these are sometimes questioned, which requires a continuation of theoretical

research. This section describes tropical cyclone development and life cycle using such theories, and examines some of the more complicated processes that this thesis investigates.

2.2.1 Environmental controls

2.2.1.1 Controls on formation

According to Pielke (1990), observations have shown that certain conditions in the physical environment are required for the formation of a hurricane. These are:

1. Sea surface temperatures greater than 26 °C, to a depth of at least 60 m.
2. A region of low-level horizontal wind convergence (generally a pre-existing region of low surface pressure).
3. Little or no vertical wind shear (wind speed and direction changes with height) between the lower- and upper-troposphere.
4. A moist low- to mid-level troposphere to encourage and support convection.
5. A location poleward of 5° latitude.

There is considerable debate surrounding which of these criteria are the most important or need to occur first. Generally, if all the above conditions are satisfied, however, then genesis occurs. One particular theory on the genesis process was outlined in Pielke (1990), where a decision tree that the American National Hurricane Centre uses to determine genesis (Figure 2.1) was given as an example. It is clear from Figure 2.1 that the state of atmospheric circulation (specifically a zone of low level convergence) in the tropics must first be favourable before any of the other environmental factors are considered.

2.2.1.2 Controls on intensity

An excellent review of past studies on the environmental controls of tropical cyclone intensity is presented in Emanuel et al. (2004). Such studies have focussed on certain properties of the atmospheric environment like vertical wind shear and the horizontal wind, and dynamical features like disturbances in the upper-level environment. Emanuel et al. (2004) claimed that atmospheric environmental factors were being studied too heavily by hurricane scientists, and that an ocean-atmosphere approach was needed. This is because it

has been shown that hurricanes alter the surface temperature of the ocean (Price 1981). In addition, Gallacher et al. (1989) showed that a decrease in ocean temperature of 2.5 K near the eye of a hurricane would shut down energy production in the hurricane environment. Other studies by Khain and Ginis (1991), Bender et al. (1993), and Schade and Emanuel (1999) confirm that a cool sea surface has a strong negative feedback on tropical cyclone intensity.

Emanuel et al. (2004) devised a new ocean-atmosphere model that provided a means of testing a number of atmospheric environmental factors with feedback from the sea surface. This allowed for new observations of the controls of tropical cyclone intensity. A number of factors were found to influence hurricane intensity, including potential intensity, storm track, wind shear, upper-ocean thermal structure, bathymetry, and land surface characteristics. Results also concluded that forecasts are rendered increasingly uncertain in the presence of wind shear. In addition, and perhaps the most important finding of this decade, was that accurate forecasts of tropical cyclone intensity require good knowledge of the upper-ocean thermal structure. For example, the cyclones studied by Emanuel et al. (2004) showed that climatological upper-ocean thermal conditions were inadequate for accurate intensity prediction. Thus, the importance of including ocean measurements and processes alongside atmospheric processes is critical to accurate forecasting and intensity prediction of hurricanes.

Having identified the environmental controls of hurricane development and intensity, it is appropriate to explain the importance and role of these for hurricane formation.

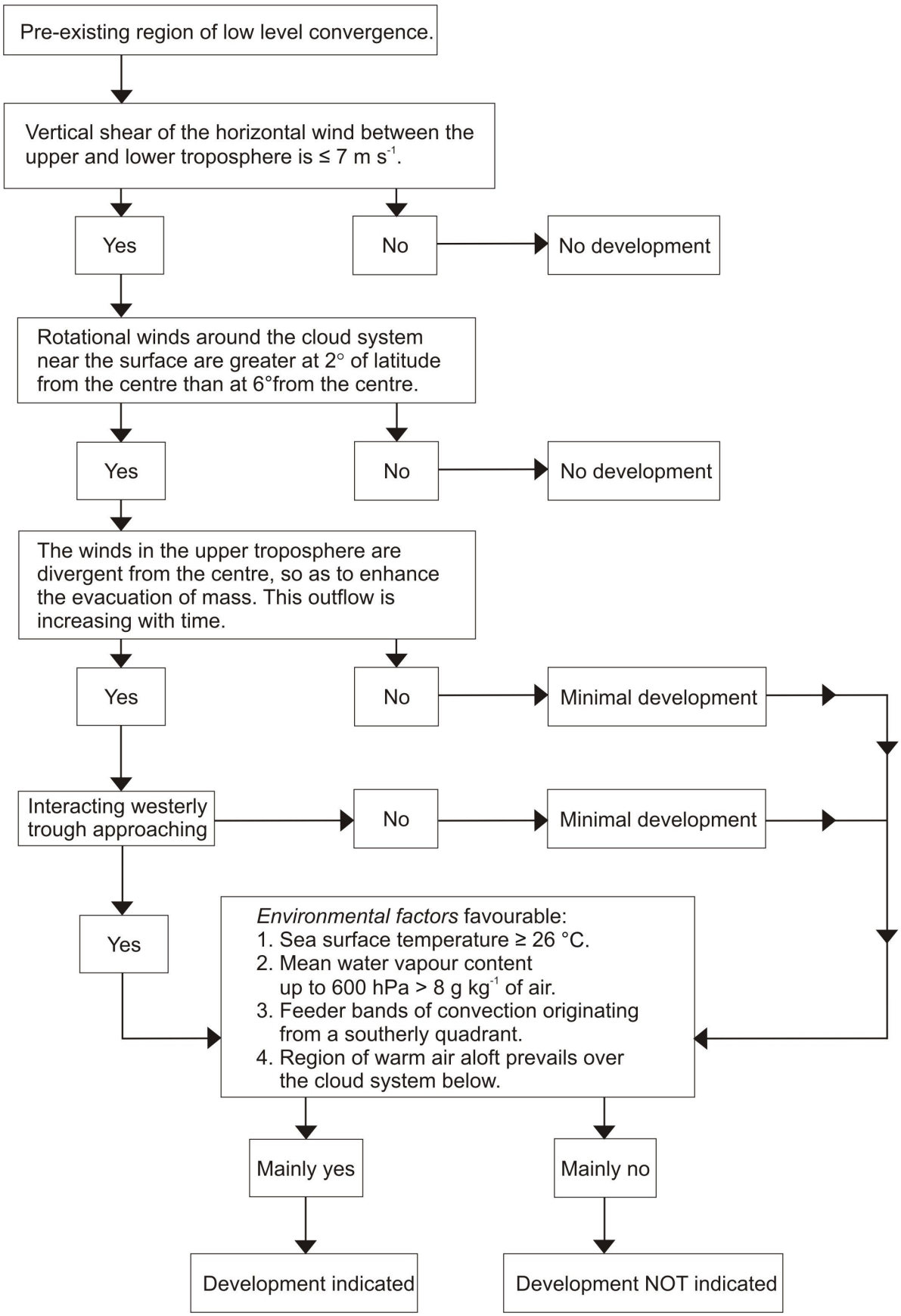

Figure 2.1: An example of a decision tree used by the American National Hurricane Centre to determine whether a tropical cyclone will develop (adapted from Pielke 1990).

2.2.2 Structure and life cycle

According to Anthes (1982), a tropical cyclone undergoes three stages during its life cycle — genesis, maturity, and decay.

2.2.2.1 Genesis

During genesis, the cyclone environment is represented by a relatively disorganised array of clouds and squalls. This is associated with a wave perturbation in the easterly trade wind flow at, or close to the surface (Figure 2.2a). A perturbation like this enhances low-level convergence such that air will flow toward a centre of convergence. In doing so, if sea surface temperatures are sufficiently warm enough then the boundary layer air will entrain moisture as it flows across the sea surface. It has been shown that latent heat supply is a fundamental component to cyclone development (Kurihara and Tuleya 1981). This boundary layer flow has the effect of enriching the lower-troposphere with heat and moisture, and as the air rises from forced uplift at the convergence centre, it begins to condense forming turbulent cumulus clouds. If the middle- troposphere is sufficiently moist, then cumulus clouds will not evaporate. If there is minimal vertical wind shear present, then the cumulus will continue to grow reaching the upper- troposphere. This convective process forms very deep cumulonimbus clouds (Figure 2.2b), which are efficient transporters of heat and moisture. Downdraughts that form in these clouds are also effective at removing any dry air that might be present in the middle-troposphere. This process assists with the increase in saturation of the atmosphere. Cumulonimbus can only be sustained with adequate divergence assisted by a westerly trough at upper-levels. The divergence acts to ventilate the system. The air eventually subsides at roughly 400 km from the cyclone, where it returns to the surface. The subsequent coupling of the lower- and upper-troposphere and the cycle that is produced from this process — the Carnot cycle (Figure 2.6) means the hurricane can be described as a thermal heat engine (Pielke 1990). In this sense, a hurricane converts thermal energy associated with heat and moisture from the ocean, into mechanical energy (Stull 1999). The air-sea interaction and Carnot cycle will be discussed in a later section.

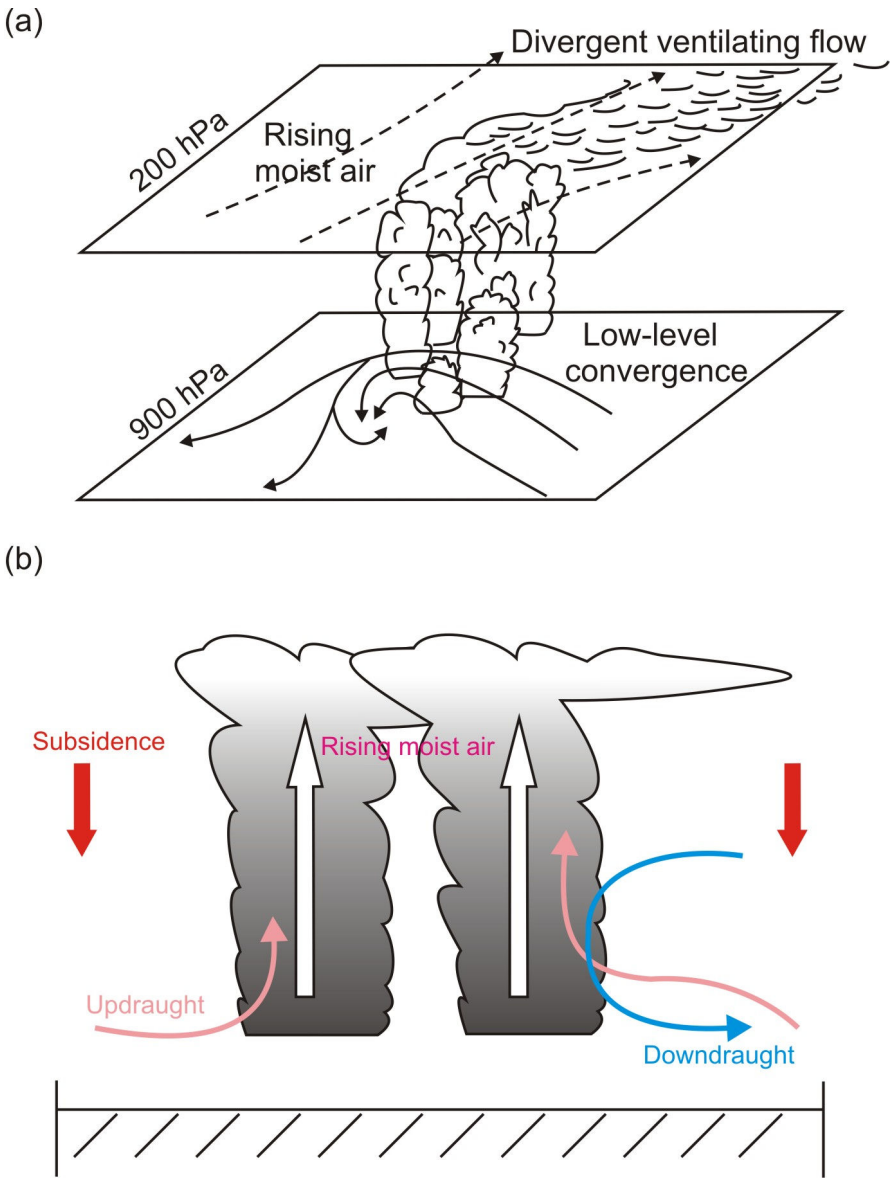

Figure 2.2: Hypothesised atmospheric conditions during tropical cyclone genesis. In Figure 2.2a, the perturbation of an easterly wave at 900 hPa continues to form a developing convergence zone. Rising moist air is supported by an upper-level southwesterly flow providing ventilation (Anthes 1982). A structural representation of the developing hurricane is shown in Figure 2.2b. Updraughts allow moist air to rise and cool, while dry air is removed from the mid-level by downdraughts. At this stage, solitary tropical convective clouds start to converge (Emanuel 2005).

For a tropical cyclone to subsequently develop from a disorganised mass of convective clouds to an organised structure operating as a Carnot heat engine, means that some other processes must occur. Indeed, according to Pielke (1990), there are a number of factors assisting further development. Firstly, the amount of mass removed at the upper-levels must be greater than the amount of mass converging at the surface. This serves to lower the surface pressure resulting in additional low-level convergence. This supports deep cumulus convective development and transports additional moisture from the surface to upper-levels. Secondly, as the low-level convergence intensifies, the Coriolis force becomes less important and is replaced by the centrifugal force. The observed response is the

countervailing tendency of an air parcel to be spun out of the inward spiral because the air is achieving a larger rotation rate as it spirals in towards the centre. Over time it becomes increasingly difficult for the air to reach the convergence centre as the centrifugal force increases, which assists formation of the hurricane eye. Thirdly, spiralling in of moist air parcels leads to the formation of cumulonimbus spiral bands. These bands occur in localised regions of the curved inflow. They are also known as feeder bands because they enhance the low-level flow in their vicinity, resulting in a more favourable environment of moisture and temperature for deep convection. Finally, when minimal hurricane force winds of 33 m s^{-1} are achieved (see Table 1.1 in Chapter 1), air parcels will no longer reach the centre of low pressure. Instead air blows tangentially to lines of constant pressure. This region is known as the eye wall and is the part of the hurricane that contains the most intense wind speeds and precipitation rates. The development of an eye wall is one of the major distinguishing factors between a tropical storm and a hurricane (Pielke 1990). Indeed, these processes help the tropical cyclone to intensify towards maturity.

An example of a decision tree similar to Figure 2.1 can also be used to estimate whether an existing tropical cyclone will intensify. This is shown in Figure 2.3. The presence of a feeder band is a large factor in the decision process.

For intensification to continue, the principal environmental factors and processes needed for genesis must remain satisfied until at least a category 1 hurricane on the Saffir-Simpson scale is reached. Once this is achieved a hurricane will continue its intensification towards maturity, and persist until environmental conditions change so that it decays. Indeed, according to Pielke (1997), the requirements for the continuance of a hurricane are less restrictive than those for its development. This explains why hurricanes often track into areas well beyond their source region. The effect that removing these requirements have on the hurricane will be explored in the decay section.

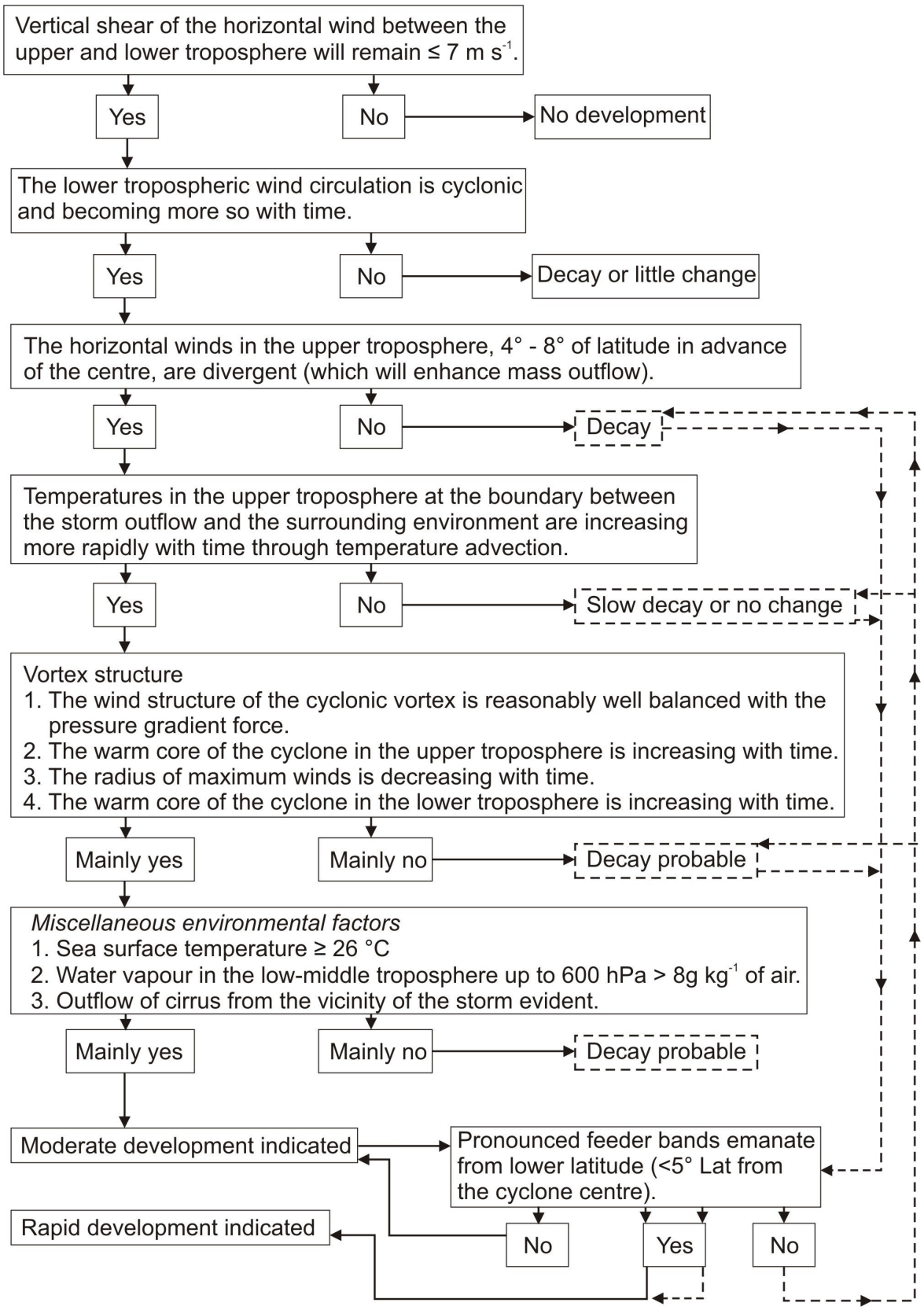

Figure 2.3: An example of a decision tree used to determine if a tropical cyclone will undergo further intensification. The presence of a spiralling feeder band, or spiral rain band becomes a large factor in the intensification decision process. Dashed lines indicate the check of this condition for each of the associated dashed boxes (Pielke 1990).

2.2.2.2 Maturity

At maturity, the tropical cyclone exhibits strong rotational circulation with a large axisymmetric component and clouds which are well organised about a centre of low pressure (Figure 2.4). This is the stage during the life cycle where the central pressure of the eye is deepest. The maximum wind speed is also at peak intensity. A well developed eye will be present which has little or no cloud caused by subsiding, dry air. An eye wall of most intense wind speed and heavy convective thunderstorms will radiate out from the eye. A number of significant spiral rain bands are generally present, separated by areas of light precipitation. Sometimes these features might be concealed by a dense layer of cirrus aloft. This is caused by air diverging at the limits of the upper-atmosphere. The features of a mature hurricane are illustrated in Figure 2.4.

The processes that bring a hurricane to maturity were described in the genesis section. The most important process to reiterate is the increased intensity of convergence and rotation at the centre. The eye wall intensifies because of this increased convergence as air can no longer reach the centre of the storm and is forced to concentrate around a ring about the centre. The mature stage is usually defined as the time of maximum potential intensity determined from the ocean-atmosphere interaction, and the rate of heating in the storm system (Emanuel 1988).

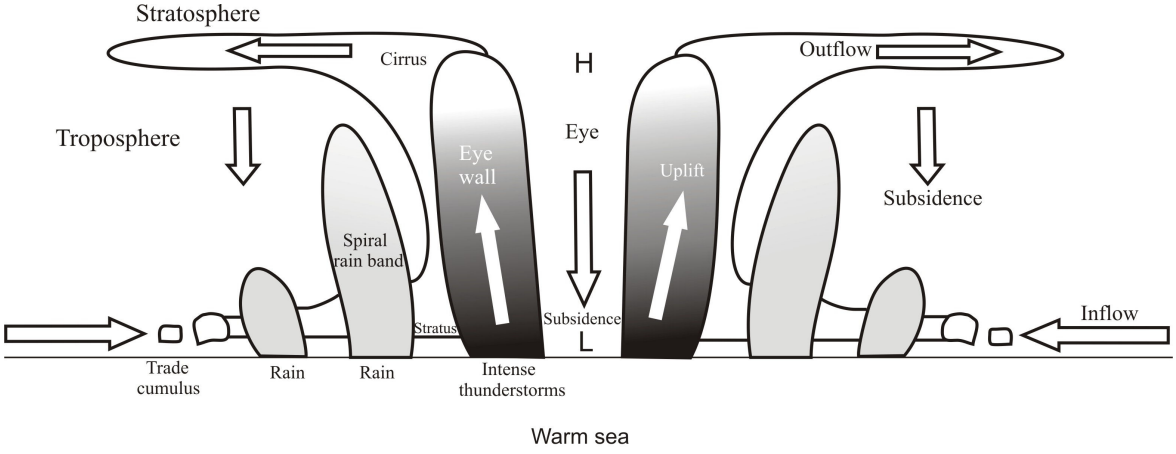

Figure 2.4: Idealised structure of a mature hurricane. Environmental air flows are indicated by the arrows. Precipitation is heaviest in the eye wall and spiral rain bands — these are regions of deep convection. The eye is a region of calm, subsiding air that forms a unique feature of the mature hurricane. The pressure at the surface is as expected relatively low when compared to pressures away from the storm. As a result of dynamic interactions between the surface and rising air, upper-level air spirals out anticyclonically, cooling in the process and forms distinct caps of cirrus aloft (Stull 1999).

2.2.2.2.1 A mature hurricane model

A number of atmospheric parameters of a mature hurricane that were conceptualised in Stull (1999) are shown here in a composite diagram: Figure 2.5. It is worthwhile to discuss some of the features of a mature hurricane, as shown by Stull (1999). Firstly, at maturity, the pressure difference between the eye and surrounding environment will be at its greatest (Figure 2.5b). This is often used as a measure of hurricane strength, such that the greater the pressure difference, the more intense a hurricane will be. Secondly, the tangential velocity will peak. The profile of tangential velocity of a mature hurricane will show an increase from the outer environment to the eye wall and then decrease rapidly towards the eye (Figure 2.5c). A study of 4 hurricanes presented in Stull (1999) showed that the critical radius of maximum velocity was in the range of 20–30 km, which is roughly the definition of the outer eye wall for these hurricanes. The commonality suggests that this is an expected value of most mature hurricanes, but the small sample size means uncertainty for individual events remains. Finally, vertical velocity will be at a maximum. At radii less than that of the maximum tangential winds, the air converging towards the centre rapidly piles up, and rises out of the boundary layer as thunderstorm convection within the eye wall (Figure 2.5d).

2.2.2.3 Decay

A tropical cyclone will start to decay when it encounters unfavourable environmental conditions. These conditions are — an environment that does not contain moist tropical air provided from a warm sea surface; dry land; a region of intense vertical wind shear; and an unfavourable large-scale flow aloft. These are essentially elements of the environmental controls required for genesis listed previously. A series of physical processes occur that act to dissipate the hurricane, and these are common to all environmental conditions, whether over land or water.

As the source and release of latent heat is diminished by the effect of land or cool water, the upper-level divergence weakens, mean temperature in the core decreases, and central pressure increases. As a consequence of the weakening pressure gradient, the eye wall expands outward, and because angular momentum becomes increasingly conserved, the cyclonic tangential winds diminish rapidly. With the warm moisture source either removed or inhibited and evaporation dominating, any remaining convection acts to dry out the

boundary layer. This process of drying and cooling continues until the pressure gradient aloft is totally diminished, and if cyclonic flow aloft results, subsequent filling of the eye.

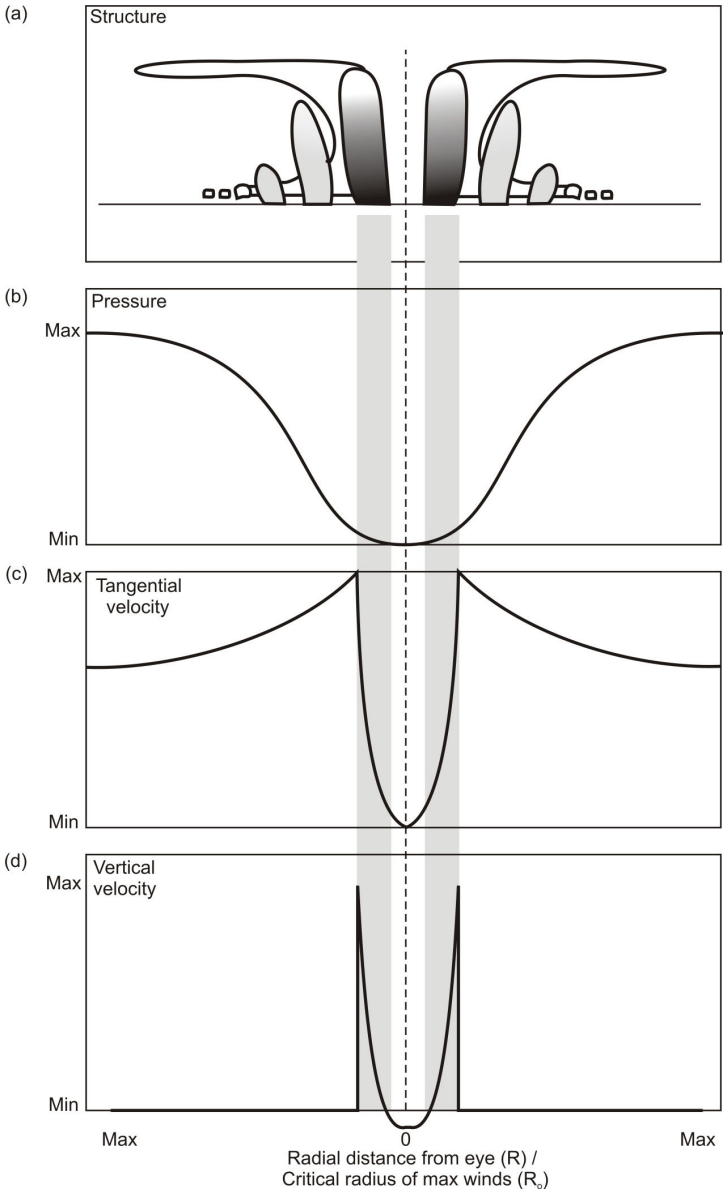

Figure 2.5: Composite hurricane structure based on an idealised model. The profiles are derived by dividing the radial distance from the eye by the critical radius of maximum winds, found in the eye wall. The eye wall is represented by the shaded area in the middle of the profile. Maximum and minimum on the y axis refer to the highest and lowest possible values that are calculated for each quantity explained in the text. Pressure is lowest in the eye (2.5b); tangential winds are at a maximum at the outer eye wall (2.5c), which is the same for vertical velocity (2.5d). Vertical velocity is negative in the eye due to subsidence (Stull 1999).

2.2.3 Physical processes

According to Ooyama (1982), the tropical cyclone is a complex system of interacting physical processes and multi-scale interactions. Ooyama (1982) recognised that there was still much information required on these processes despite a number of established theories, such as Oyama (1964), Charney and Eliassen (1964), and Gray and Shea (1973),

that helped to explain hurricane genesis. As a result, considerable research using models has been undertaken to find answers. It is now well recognised that there are three major physical processes governing hurricanes, namely — energy exchange at the air-sea interface; environmental interactions with surrounding large-scale features in the atmosphere; and internal dynamics such as cloud microphysics (Black, PG et al. 2007). There is still conjecture surrounding the roles of each of these physical processes including which one dominates. This is indicated by the numerous theories to explain genesis and intensification.

The three major physical processes are explained to illustrate some of the more complicated and intimate interactions that occur in the hurricane environment, which have an impact on genesis, intensity, and cyclone track.

2.2.3.1 Cumulus convective processes

An essential modelling component of this research investigates the effect of cumulus convective processes when using CP schemes. It is important, therefore, to outline some of the key theoretical understandings of the role of cumulus convection.

It has been shown that much of the latent heat released in hurricanes results from buoyant cumulus convection, due to a decrease in potential temperature with height up to 600 hPa (Gray and Shea 1973). Above this level, ascent of saturated air may result in stable, layered clouds (such as cirrus) and non-convective latent heat release (Anthes 1982). Research has also shown that cumulus-scale motions and large scale tropical disturbances enhance each other, so that a process of cooperation is initiated, and a hurricane develops through the cumulative effect of cumulus clouds (Charney and Eliassen 1964; Ooyama 1964). This forms the basis of the Conditional Instability of the Second Kind (CISK) theory. CISK states that as heating increases, so does horizontal convergence (resulting from convection), which increases the rate of low-level vorticity. This forms a positive feedback system that enhances development of further convective cloud and eventual hurricane growth if sustained.

Some problems have been identified with CISK during the early stages of cyclone development. According to Gray (1982), the theory had reasonable applicability for later stages of intensification, despite the following issues. Firstly, only a small portion of a

disturbance's inflow is driven by boundary layer convergence. The majority of a cyclone's inflow occurs above the boundary layer. Secondly, temperature increases due to condensation are overestimated. This is because an assumption that a balance between the initial wind and pressure field exists, which produces a wind increase due to condensational heating. Thirdly, the energy gain of the tropical cyclone can only come from a vertical mass balancing circulation from surface energy fluxes, not horizontal energy convergence. The fourth issue was that CISK does not deal with weather system non-intensification, which is a problem because some significant non-intensifying storms have considerable rainfall and moisture convergence. Finally, the theory does not account for the need of the disturbance to draw large amounts of vapour from the ocean, to enhance the energy flux required for intensification.

In response to these limitations, some improvements to the CISK theory were then made by Gray (1982), where it was found that the relative frequency and intensity of rain band formation was crucial to the development of hurricanes. As stated, the organisation of convective rain bands is vital to the localised enhancement of the low-level flow in their vicinity, resulting in a more favourable environment of moisture and temperature for deep convection. Accounting for rain band formation provided the necessary enhancement of the surface energy flux that was required to maintain CISK during the initial stages of cyclone development.

Because of the failure of CISK to account for supply of energy from the ocean, a new theory was put forward that incorporated the ocean into the genesis equation. Emanuel (1986) suggested there was an intimate link between the ocean and the atmosphere. The subsequent comparison of a hurricane to a Carnot heat cycle resulted in a new physical process of air-sea interaction developed by Emanuel (1986).

2.2.3.2 Air-sea interaction

As stated the hurricane can be regarded as a thermal heat engine, which operates under the theory of the Carnot cycle (Figure 2.6), (Emanuel 1986). This can be described in the context of a hurricane, as boundary layer air at A that initially flows in toward a convergence centre at B, acquiring moist entropy from the sea surface. This is followed by an ascent of this air through the troposphere with outflow to large radius at C where heat is released. The circuit is completed when the air eventually loses enough heat through

cooling at point D to subside and return to its ambient potential temperature at point A. In essence, the cycle is fuelled by latent heat supply from the boundary layer and maintained by its release aloft.

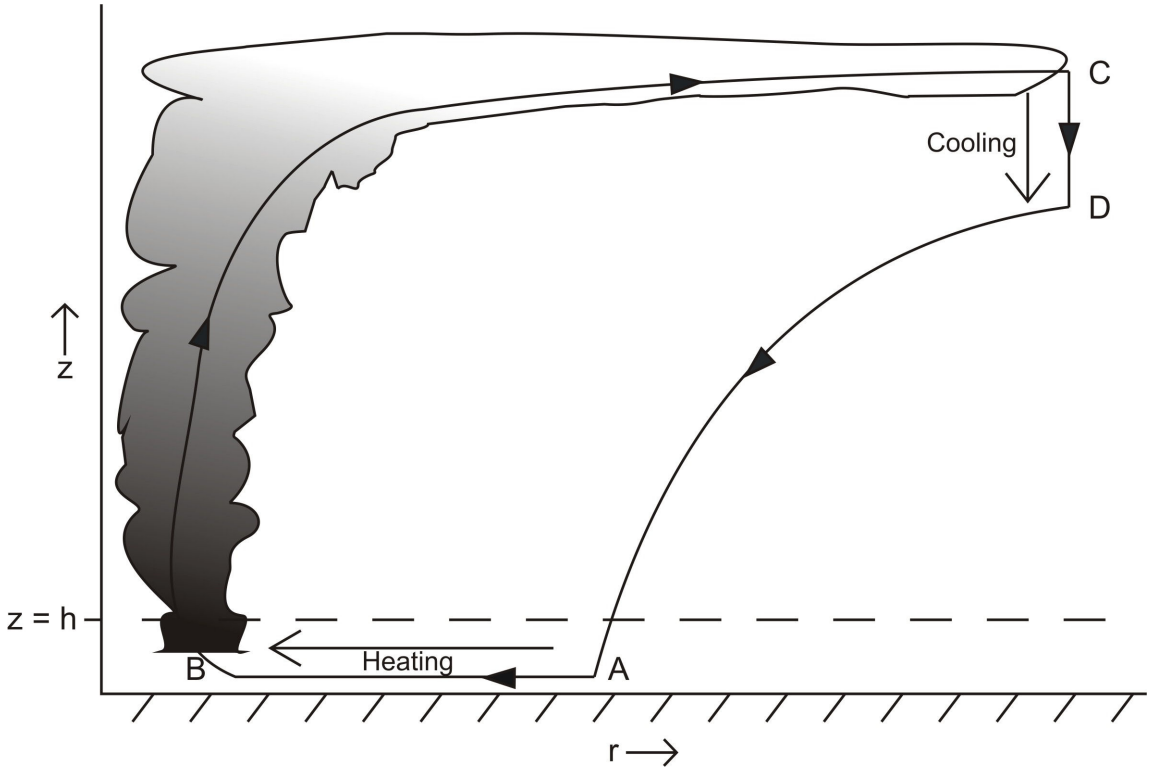

Figure 2.6: The energy cycle for a mature hurricane represented as a Carnot heat engine. Boundary layer air flows from A to B, undergoing heating as it entrains moisture, the air rises at B and flows outward to C. As it subsides from C to D it cools, and returns to its starting point at A. Note that r is equal to radius increasing from the centre, z is equal to height increasing with altitude, and z = h is the height of the boundary layer (Emanuel 1986).

According to Liu et al. (1997), studies have shown that sea surface temperature tends to control the supply of latent heat to a hurricane. This affects the general development and intensification of a hurricane. Indeed, Emanuel (1986, 1988) showed how the mechanical energy available from the thermodynamic Carnot cycle balanced the frictional dissipation. This balance was expressed as the work done against friction. Fundamental to this expression is thermodynamic efficiency and the total heat gain from the sea surface. The greater heat gained from the surface results in greater work done against friction in the boundary layer. If this friction can be overcome, then air is able to freely converge, rise, release latent heat as it cools, and eventually subside, which completes the Carnot cycle (Figure 2.6). If, however, friction cannot be overcome due to a loss in net heating or an imbalance in the cycle (such as lack of cooling aloft), represented by thermodynamic inefficiency, then a cyclone will not develop. Pertinent to this is sea surface temperature, because thermodynamic efficiency is mostly proportional to the temperature of the sea surface. Emanuel (1986) concluded that if sea surface temperature is less than 26 °C, then

the depth of the conditionally neutral or unstable layer is too shallow to form a tropical cyclone. This is primarily because the thermodynamic efficiency is too small.

2.2.3.3 Environmental interactions: steering flow

The hurricane can be described as a mesoscale feature with a synoptic scale supportive system (Ooyama 1982). As such, a number of complicated flows occurring across different scales can influence hurricane movement. Indeed, as stated by Emanuel (2005), the physics of hurricane motion has been a longstanding problem. Moreover, prediction of hurricane movement is arguably the most important component of hurricane research, as many lives have been lost from failure to accurately predict cyclone tracks over the last half century.

The highly complicated nature of the tropical hurricane environment means that a number of flows and processes must be accounted for. Firstly, according to Emanuel (2005), it has been shown that hurricanes move with the background flow in which they live (Figure 2.7a-d). Figure 2.7a-d shows idealised flow patterns in a tropical environment at a single altitude. A simple east to west background flow (Figure 2.7a) and a hurricane-like vortex (Figure 2.7b) can be added together to examine the influence of the vortex on the east to west flow. In the case of a strong vortex (Figure 2.7c) the impact of the vortex on the background wind flow is obvious, where the wind on the north side of the storm is stronger because its rotation is adding to the background easterlies. The impact of the vortex is more difficult to assess in the case of a weak vortex (Figure 2.7d), where it becomes a challenge for forecasters to accurately predict the hurricane centre. In these idealised cases, the hurricane would move west at the speed of the background flow, but because hurricanes are usually embedded in background flows that change direction and speed with altitude, an average of surfaces must be taken over the depth of the storm. Unfortunately, nature is more complicated than an idealised motion, because hurricanes change their background flow through the atmosphere. Thus, a hurricane vortex flow and background flow affect each other. This leads to the second point.

A hurricane also moves as a result of flow within a vortex. This is measured through absolute vorticity, which is the rate of spin about a vertical axis. Figure 2.8a illustrates the concept of air movement around a hurricane and the resultant spin that air in different regions acquires. Air moving in this manner creates two subsidiary vortices called *beta gyres* which act to steer a cyclone northwestward in the northern hemisphere. This steering

flow is known as *beta drift* and must be accounted for in a forecast. Finally, the last significant affect on hurricane movement is again related to the concept of vorticity. As stated previously, a divergent zone aloft is required for hurricane intensification, and because the airflow at upper-levels is in the opposite direction to the flow at the surface, the rising air starts to spin anticyclonically. The resultant upper-level anticyclone can be quite large when compared to the surface cyclone. In cases where the background airflow is minimal, then a particularly intense anticyclone can form aloft, and if some vertical wind shear is present, this anticyclone can be blown to one side of the surface cyclone. The flow around the surface cyclone can then push the surface cyclone off course (Figure 2.8b). This can be a particularly strong effect, and is often analysed by examining upper-level wind charts and identifying regions of anticyclonic potential vorticity (PV) anomalies.

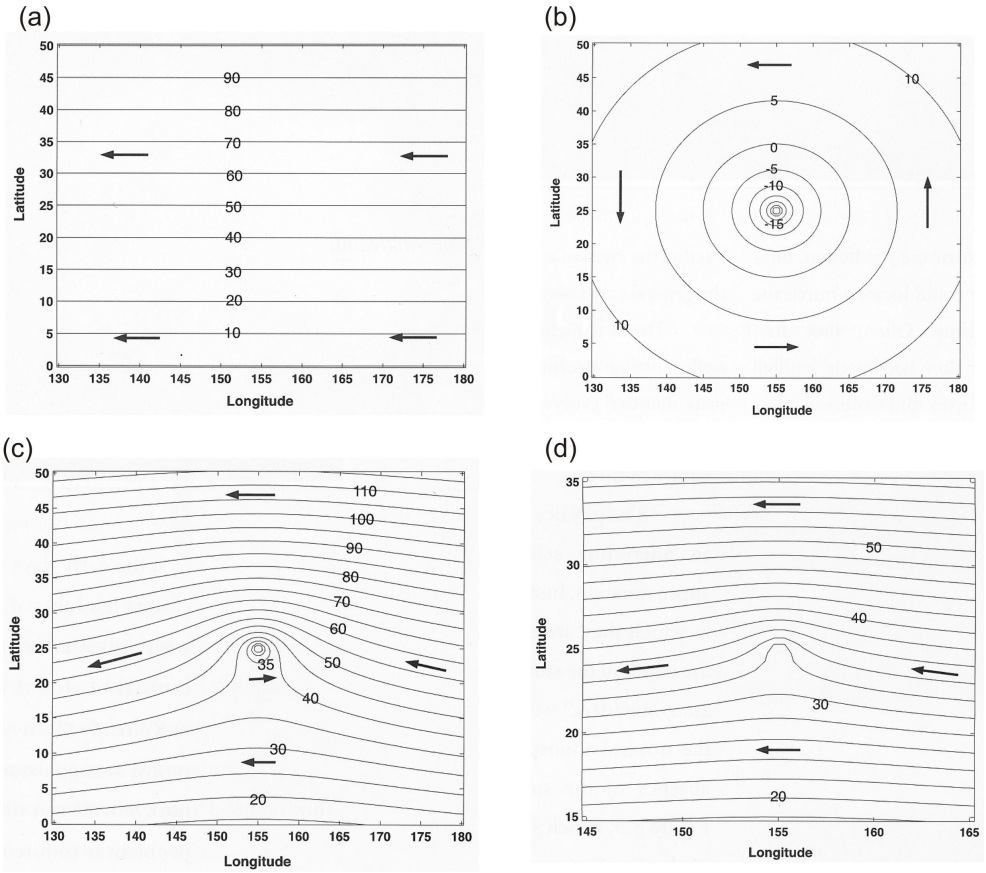

Figure 2.7: Some idealised tropical flow patterns for (a) a simple east to west flow, (b) a circular hurricane vortex, (c) when (a) and (b) are added together in the case of a strong vortex, and (d) when (a) and (b) are added together in the case of a weak vortex (Emanuel 2005).

A number of studies confirm that anticyclonic outflow at upper-levels, resulting from asymmetry in PV can steer tropical cyclones (Wu and Emanuel 1993, 1995*a*, 1995*b*; Wang and Holland 1996*a*, 1996*b*; Dengler and Reeder 1997; Henderson et al. 1999; Shapiro and Franklin 1999; Chan et al. 2002; Davis and Bosart 2002). The influence of PV forms an aspect of the initialisation and CP scheme analysis in this study.

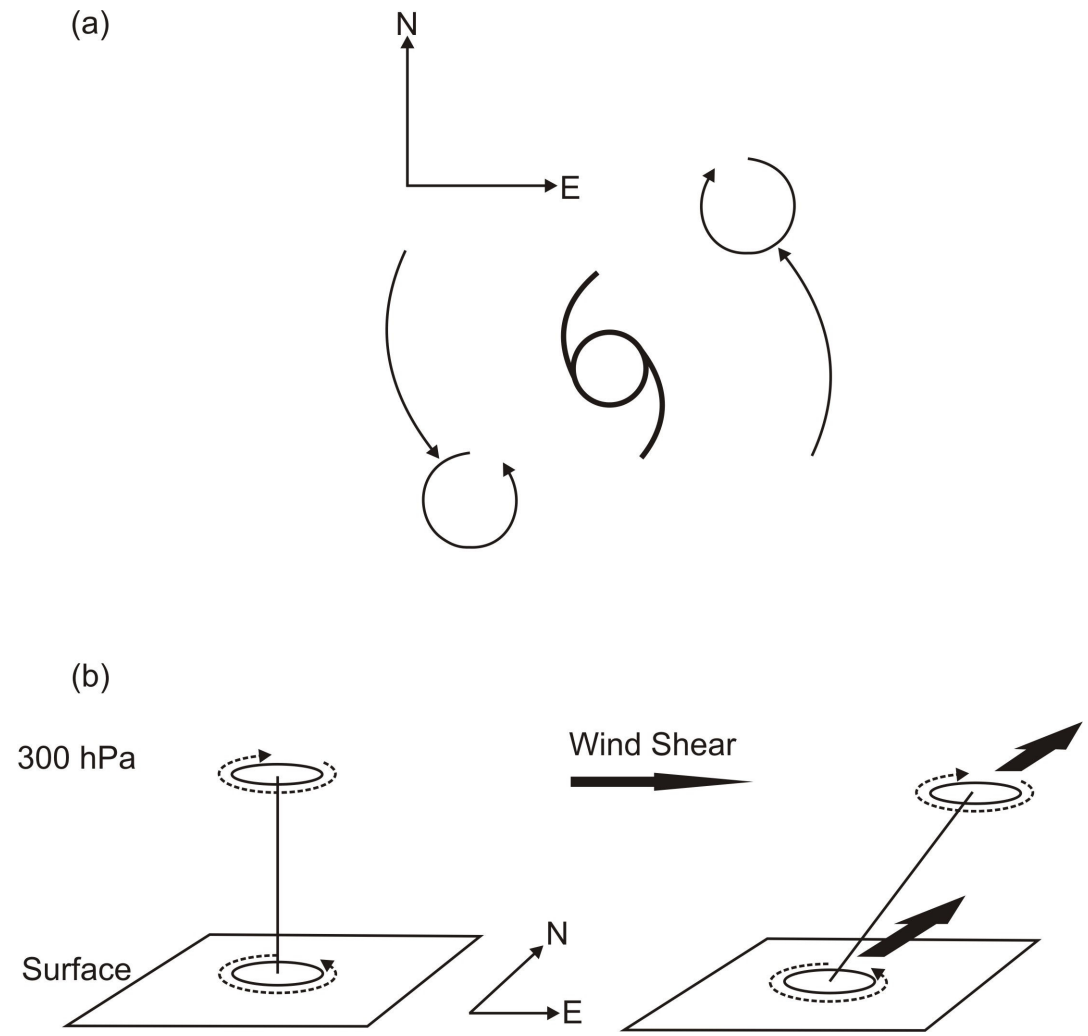

Figure 2.8: More complicated effects on hurricane movement. In (a) the concept of *beta gyres* is illustrated, where the subsidiary vortices that form from airflow on the west and east sides of the hurricane act to steer the hurricane northwestwards. In (b) an upper-level anticyclone that forms from vorticity through the hurricane column can be pushed to one side of the surface cyclone by vertical wind shear. The rotation of the anticyclone acts to steer the surface cyclone (Emanuel 2005).

2.3 Mesoscale meteorological modelling

Having described the theoretical processes of hurricanes, it is now important to outline numerical modelling. An explanation of the mesoscale model and its application to this research is covered. The concepts used in this study are also discussed.

2.3.1 The mesoscale

The mesoscale occurs between the micro- and synoptic-scales of motion and can be defined as having a horizontal distance between a few kilometres to about 700 km (Figure 2.9), (Sturman and Tapper 2006). The vertical scale is commonly observed to extend from tens of metres to the depth of the troposphere. The mesoscale model, therefore, operates

within this defined range, and encompasses phenomena from large cumulus clouds to tropical cyclones. In modelling terms, mesoscale is also defined as those atmospheric systems that have a horizontal extent large enough for the hydrostatic approximation to the vertical pressure to be valid, yet small enough for larger scale winds to not be appropriate as approximations for the actual wind (Pielke 2002).

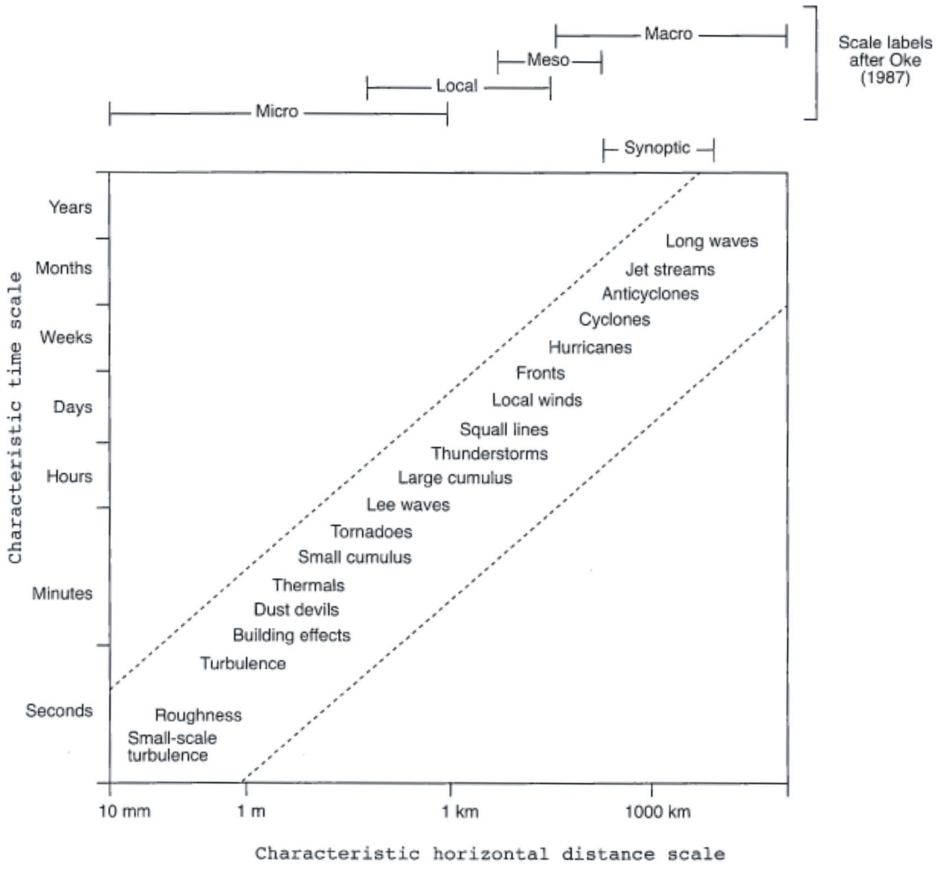

Figure 2.9: Atmospheric scales of motion and associated phenomena with respect to horizontal distance and time scales. The mesoscale can be defined as occurring between a few kilometres to about 700 km, with features lasting anywhere between a day and a week (Sturman and Tapper 2006).

2.3.2 General background of mesoscale modelling

To study simulations of atmospheric phenomena effectively, one must have a good understanding of both the physical and mathematical foundations of a numerical model. This must also be in partnership with knowledge of how a particular atmospheric system operates. Two approaches to simulating mesoscale phenomena exist, through physical models (building replicas of the ground or building surfaces, and testing them in wind tunnels), and mathematical models. This study uses a mathematical model approach, which employs algebra and calculus to solve equations that allow the simulation of atmospheric features. Some equations used in modelling analysis such as the governing equations,

cannot be fully solved and as such require a technique in the form of a numerical model, to find approximate solutions. According to Pielke (2002), there are three purposes of model use, to provide diagnostic evaluations (interpolation of data throughout a region), process studies (improvement of atmospheric understanding), and predictions (weather forecasts). This research uses a diagnostic approach.

The basic set of mathematical equations governing mesoscale numerical models are a set of conservation principles. According to Pielke (2002), these are conservation of mass, heat, motion, water, and gaseous materials. In order to complete a successful simulation, these equations must be solved simultaneously. In the most basic conceptual sense, a three-dimensional atmospheric model domain can be regarded as a cube with mass inputs and outputs (Figure 2.10). Fundamentally, mass into and out of the box must equal the change of mass inside the box, because the atmosphere has neither mass sinks nor sources. A model's governing equations are responsible for this rearrangement of mass and finding approximate solutions to the equations. In addition, within this cube are grid points, which are the points in the model where atmospheric variables are computed. A grid point contains the average value for a volume of surrounding air (Stull 1999). This volume is often referred to as a grid cell, and its size is dependent on the dimensions of the three Cartesian directions (x, y, z). These grid cells are spaced at regular intervals inside the model domain as shown in Figure 2.10. The size of a grid cell determines model resolution, and is a general indication of the quality of simulations. Generally, very high resolutions of the order of 1–5 km are desirable for the modelling of tropical cyclones. This is because of the need to resolve small cumulus clouds, which often occur on very small spatial scales (less than 1 km).

Figure 2.10 also illustrates one possible grid point configuration, and is also the configuration used in this research. In this case, one grid point is located in the centre of the grid cell. It is often desirable to have more grid points than just one at the centre. Indeed, grid points can be placed at the sides, top and bottom of a grid cell (Stull 1999). This is because it is quite advantageous to represent different atmospheric variables at different locations. For example, in the case of tropical cyclone research, it would make good sense to place points on the sides to capture vertical and horizontal flows into and out of the system. Unfortunately, due to the computational demand of such a configuration, it was not possible to achieve that in this study. In addition, the more grid points there are means the effects of model interpolation of data between points will be minimised. This

reduces the errors associated with interpolation, but due to computational demands it is still impossible to have a large number of grid points in a high resolution grid cell.

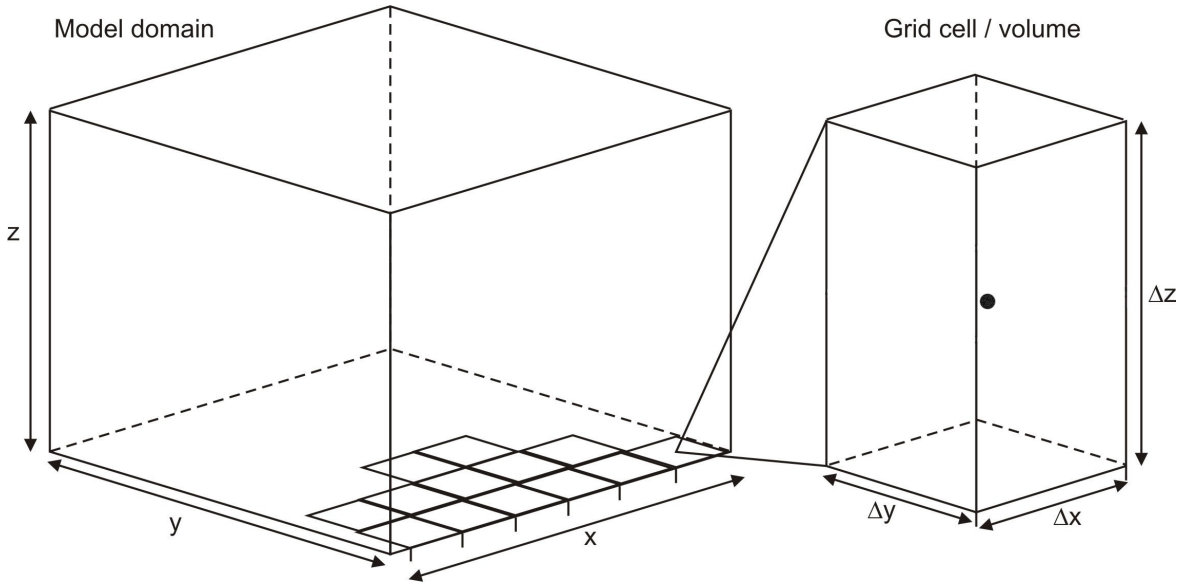

Figure 2.10: A conceptual example of a three-dimensional model domain, grid cell, and one grid point (black circle in the centre of the grid cell). The model domain is calculated from Cartesian directions x, y and z. The model resolution is always represented by the Cartesian directions Δx and Δy, which is the size of the grid cell two-dimensionally in the model domain.

During a numerical simulation of an atmospheric feature there are many complex interactions that occur. This makes models a very complicated tool for studying the atmosphere. Indeed, this task is complicated by the range of atmospheric processes that must be accounted for through parameterisation schemes. If such parameterisations contain inaccuracies, a chain reaction of negative events might be set off that impact upon the process being modelled. This is sometimes referred to as the Lorenz effect (Devaney 2003). A very simple example might be accounting for short wave radiation in the simulation of a cumulus cloud. A series of assumptions are made based on the theoretical understanding of radiative processes in the atmosphere, and are accounted for in the model by means of a short wave radiation parameterisation scheme. If, for instance, this scheme made an incorrect assumption about the feedback from the cumulus cloud to the short wave radiation flux, then this might offset the radiation budget. This error might compound and affect the development of further cumulus clouds in the environment modelled. When extrapolating this example to the likes of a tropical cyclone simulation, it becomes clear that errors in parameterisation can impact upon modelled processes such as heat and moisture distribution in cumulus clouds, which will ultimately affect the forecasting of hurricane intensity.

2.3.3 Weather Research and Forecasting: a mesoscale model

The Advanced Research WRF three-dimensional mesoscale modelling system was originally developed by the National Centers for Atmospheric Research (NCAR) in 2002, and a number of versions have since been released. The model is designed for a variety of applications, including both idealised and real data cases. This study uses the real data component of the model, drawing upon particular aspects of its intended design — those of parameterisation and forecast research. A more detailed explanation of the model's technical aspects is given in the methodology chapter.

2.4 Numerical simulation of tropical cyclones

Relevant numerical studies of tropical cyclones were identified in Chapter 1. This section describes WRF specific studies that are of relevance to this research.

2.4.1 Tropical cyclone studies using WRF

WRF is a relatively new model and its ability for accurate tropical cyclone forecasting and research is still somewhat unknown. Indeed, it was not specifically developed for tropical cyclone research, but to simulate continental, deep, moist convection using grid resolutions of less than 10 km (Davis et al. 2006). In recent studies, however, WRF has shown incredible potential to accurately simulate the dynamics and inner core structure of a tropical cyclone. This is due, in part, to a new moving nest system that allows for a grid resolution of 1 km or less (Davis and Holland 2007). Some WRF hurricane studies — Nolan et al. (2002), Rosier (2005), Guo et al. (2006), Snyder and Chen (2006), Davis et al. (2006), Davis and Holland (2007), and Pattanayak and Mohanty (2008) have tested the effect of model initial conditions on hurricane track and intensity. Only a handful of studies: Rosier (2005), Gentry and Lackmann (2006), Li and Pu (2006), and Bassill and Morgan (2008) have examined convective precipitation for hurricane events. This seems rather surprising given the importance of CP scheme selection on hurricane intensity and track simulation, but not unexpected because WRF has not been in service long.

2.4.2.1 Initialisation studies

Model initialisation remains one of the most important requirements for obtaining an accurate tropical cyclone track and intensity forecast. There are a multitude of initial conditions that can be adjusted to test forecast accuracy, such as simulation start time, physics schemes, type of meteorological dataset, and time step. Some advanced initialisation studies with WRF have included the use of an Ensemble Kalman Filter (EnKF) that allows for real-time updating of cyclone position during the forecast. Furthermore, the introduction of *vortex bogussing* or a *synthetic vortex* has allowed for more accurate representation of cyclone structure and location at the start of the simulation (Bender et al. 2004; Snyder and Chen 2006).

This research focuses on model start time, so only considers studies that use this as an initialisation control. It is apparent that there are few studies also using this technique. Indeed, of the literature surveyed, only two WRF studies were discovered, that of Davis et al. (2006) and Pattanayak and Mohanty (2008). This might be due to the fact that there are more advanced initialisation procedures currently being tested, such as Three-Dimensional Variational Assimilation (3DVAR). Nonetheless, it is still pertinent to examine what appears to be the most basic of initialisation methods. Indeed, sometimes it is best to limit the number of assumptions or the technicality of a simulation because of the highly complicated nature of modelling.

2.4.2.2 Convective parameterisation scheme studies

Most of the uncertainty surrounding tropical cyclone research lies with the representation of cumulus convection in the model, rather than the models themselves. As previously stated, convection is fundamental to the transportation of heat and moisture in a cyclone. WRF's governing equations are well equipped to conduct simulations of cyclones, but the schemes it uses need refining. This is an ongoing process that develops over time as scientists gain an improved understanding of the physics of cumulus convection. The testing of current CP schemes is therefore paramount to most cyclone sensitivity studies, but has not been studied in great detail with WRF. Indeed, as already stated, only a few CP studies using WRF are known, namely, Rosier (2005), Gentry and Lackmann (2006), Li and Pu (2006), and Bassill and Morgan (2008). These studies have shown that the choice of CP scheme affects the intensity of the cyclone, the structure, and precipitation rate.

Thus, it is important to outline what CP is, how it works, and the types of CP scheme used in WRF.

2.5 Cloud and convective parameterisation in models

A parameter is a numerical or other measurable factor forming one of a set that defines a system or sets the conditions of its operation. To *parameterise* therefore is to describe or represent in terms of a parameter or parameters. The atmospheric sciences discipline has many governing systems of equations that mathematically represent and parameterise the physical processes of the atmosphere. According to Jacobsen (1999), a parameterised equation is an equation in which one parameter is expressed in terms of at least two other parameters. For example, the equation of state is a parameterised equation which relates pressure (one parameter) to temperature and air density (two other parameters). Numerical models are a prime example of the implementation of such parameterised equations to resolve atmospheric processes.

An objective of this research is to examine the effects of different CP schemes for this event. Thus, it is of interest to explore how a numerical model parameterises cloud microphysical processes, and more specifically, the parameterisation schemes used by WRF.

Jacobsen (1999) stated that cloud motions in mesoscale models are sub-grid-scale phenomena and thus must be parameterised. This is due to the horizontal resolutions of this type of model, which require estimations of the effects of sub-grid-scale cumulus clouds on the model-scale environment. Individual cloud cells are often smaller than the grid spacing chosen or available for the simulation. Parameterisation is necessary to properly release latent heat on a realistic time scale in sub-grid-scale convective columns (Skamarock et al. 2005). Furthermore, deep convection overturns the atmosphere, affecting mesoscale dynamics such as vertical stability, heat and moisture redistribution, and cloud development which affects surface heating. All these processes are crucial to the development and intensification of a tropical cyclone, and parameterisation accounts for these large-scale atmospheric effects. If parameterisation is not used, then forecast errors are expected.

According to ‘How models produce precipitation and clouds’ (COMET program 2000), there are two fundamental parameterisations governing cloud and precipitation processes in a numerical model. The first is the PCP scheme, often referred to as the microphysics scheme in the model. PCP represents the model parameterisation of cloud and precipitation processes that remove excess moisture, and operates on the sub-grid scale. The second is the CP scheme, a method that accounts for convective effects through the redistribution of temperature and moisture in a grid column, reducing atmospheric instability. CP also operates on the sub-grid scale and prevents the PCP from creating un-realistic large scale convection. CP can be thought of as a control mechanism for PCP. The parameterisations are detailed in subsequent sections, and the CP schemes used in this study are also outlined.

2.5.1 Precipitation and cloud parameterisation schemes

As stated, PCP refers to model parameterisation of cloud and precipitation processes. Initially, some dynamical forcing of air is required to produce saturation, for instance large-scale convergence. Clouds and precipitation are developed in a PCP when latent heating of condensation results from rising motion. In the event of precipitation, evaporative cooling of the air in the layers below where the precipitation is formed results. The resultant cooling is part of a feedback process that may act to strengthen the initial circulation that produced the clouds and precipitation. This intensification will release further latent heat into the atmosphere, continuing the cycle.

There are two PCP techniques for generating clouds and precipitation, namely inferred clouds (no modelling of the cloud occurs) and predicted clouds (clouds are modelled). Firstly, inferred schemes are a traditional approach where a PCP operates by predicting Relative Humidity (RH) to infer the presence of clouds over vertical layers based on a RH saturation threshold. Most schemes set RH equal to 100% saturation as a critical threshold for cloud formation, but sometimes values between 75% and 85% have been used to account for scattered precipitation. The advantage of an inferred scheme is the speed at which they run, saving computational time, but the major disadvantage is that they are not physically realistic. For instance, precipitation is the direct result of RH, rather than being formed by a cloud. Furthermore, because of the coarse grid spacing of models, dynamical mesoscale features such as hurricanes will not be modelled at proper intensity, which throws off the moisture budget and precipitation forecast. Finally, recent technological

advances have led to more realistic operational PCP schemes that predict cloud water and internal cloud processes. This type of PCP is more accurate for hurricane research. Predicted cloud schemes can be either simple or complex. The simple cloud scheme forecasts precipitation from cloud water only, whereas the complex scheme predicts precipitation from internal cloud processes, including multiple cloud types.

WRF has a variety of PCP techniques available for selection. This study uses the latter of the two PCP techniques, in the form of a simple cloud scheme, namely the Eta-Ferrier PCP scheme. This scheme is actually a derivative of the fundamental simple cloud scheme described in 'How models produce precipitation and clouds' (COMET program 2000), making it slightly more advanced than a classic simple cloud scheme. The Eta scheme, as it is commonly referred to, is described in the following section.

2.5.1.1 The Eta-Ferrier PCP scheme

The Eta scheme (Ferrier et al. 2002) incorporates some of the most important complex microphysical processes, such as hydrometeor classes, which makes it a rather unique simple cloud scheme. Hydrometeors are divided into four precipitation classes, these are — suspended cloud liquid water droplets; rain; large ice (graupel, ice, snow); and small suspended cloud ice. The most important feature of this scheme is that hydrometeors can grow and shrink in size. Precipitation also falls to the ground at appropriate speeds and can be advected as part of the total condensate while falling. This allows for a range of atmospheric phenomena to be modelled. There are, however, some significant limitations arising from the treatment of hydrometeors, which imposes restrictions on the types of phenomena allowed for. For example, mixed forms of precipitation are allowed to fall together, rather than being separated into their respective classes. This makes it difficult to track the types of precipitation and their location in the cloud column. Furthermore, coarse grid-scale convective scheme interactions are extremely limited. For instance, the high RH threshold (98%) for 12 km grid cells that use the Eta PCP, means little grid-scale precipitation occurs in advance of convection. This means the CP will do more in convective situations, which can lead to negative consequences. For example, the Betts-Miller-Janjic (BMJ) CP scheme often leaves the sounding too dry for grid-scale condensation except at very cold temperatures where saturation with respect to ice occurs at a much lower RH with respect to water.

According to ‘Eta precipitation and clouds parameterisation’ (COMET program 2000), the Eta scheme uses the following steps to account for deep convective cloud processes. Firstly, upward motion in a moist lower-troposphere drives conditions towards saturation. Cloud water is produced for all moist air parcels that exceed the threshold RH. Cloud water represents the cloud structure. The greater the amount of cloud water, the larger the raindrops will be. Secondly, the cloud water content and cloud depth are increased if large-scale moisture supply continues. Cloud water is converted to rain at a specified rate determined by the auto-conversion threshold, and this is calculated from the grid resolution. Precipitation type is determined from rain drop size; heavy rain is assumed to have a large average drop size. As the rain falls it collects cloud water through a process of collision, such that in lower parts of the cloud most of the rain is produced from falling raindrops rather than auto-conversion. Thirdly, at this stage of cloud development, because a significant amount of moisture is going into making the cloud deeper and increasing the water content, precipitation rates tend to be less than the amount of water entering the environment. This provides an upper-bound on the precipitation rate such that precipitation rates produced by this PCP scheme may be considerably smaller if much of the water has to be used to bring the atmosphere to saturation and bring the cloud water content up to the auto-conversion threshold. In the fourth step, the glaciation process will trigger if cloud temperature reaches −10 °C, and a considerable amount of cloud ice and snow can form. As cloud ice falls it collides with rain, freezing on contact, and creates graupel. During the penultimate step the mixed-phase graupel zone descends through the cloud, but not as fast as water droplets. Plentiful moisture supply will maintain saturation with respect to water in this graupel zone of the cloud. Finally, all precipitation processes become active when the ice at the very top of the cloud falls below the specified melting level. As ice particles fall, they collect cloud water, which can increase the precipitation rate over the upper-bound. This anomaly is caused because water is falling that already entered the cloud column at a prior time in the cloud development. The cloud will eventually dissipate once it cannot maintain moisture saturation over the specified RH threshold.

2.5.2 PCP coupling to the convective parameterisation scheme

As stated, a model must also use a CP scheme to relieve instability *before* the PCP scheme tries to form grid-scale convection. If a model does not use a CP scheme or if it fails to relieve instability, then a PCP scheme will make grid-scale convection anywhere there is upward motion and sufficient moisture. This can lead to substantial errors in the amount of

forecast precipitation. It is, therefore, highly recommended that a PCP scheme is coupled with a CP scheme. An explanation of the fundamentals of the CP scheme is now provided.

2.5.3 Convective parameterisation schemes

According to Baldwin and Kain (2006), CP is a technique used to predict the collective effects of many convective clouds that may exist within a single grid element, as a function of larger-scale processes and/or conditions. When activated, a CP computes the changes in temperature and moisture that would occur at each vertical level if convection developed in the given grid point environment. These convective processes are resolved in numerical models using the vertical momentum equation to reproduce cloud structure.

CP schemes need to account for 6 different convective processes (Figure 2.11). These six processes are convective initiation, deep convection, shallow convection, vertical heating and cooling, vertical drying and moistening, and precipitation. It is important that a CP scheme attempts to account for these processes because, convection serves as a means to transport latent heat and moisture upward. If this is not done, then inaccuracies in the moisture budget arise. This has significant implications for tropical cyclones, which are driven by cumulus convective processes.

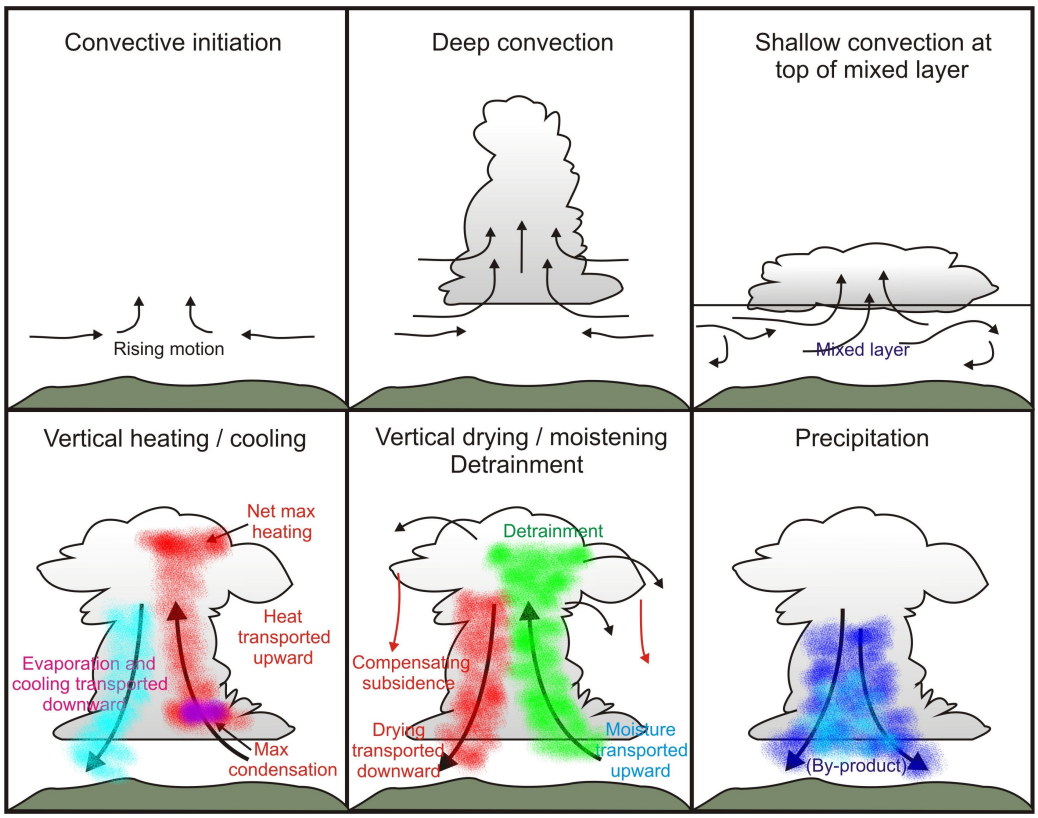

Figure 2.11: The 6 different convective processes CP schemes must account for (adapted from 'How models produce precipitation and clouds', COMET program 2000).

A CP scheme must also answer three key questions (‘Convective Parameterisation in Models’, Baldwin 1998). These are:

1. How do large scale processes control the initiation, location, and intensity of convection?

2. What are the properties of parameterised clouds (moist-convective processes)?

3. How does convection modify the environment (feedback)?

These questions form the basis for many different CP schemes, and all schemes have a different approach to answering them. Regarding the first question, the method a CP scheme uses to evaluate large-scale processes is often referred to as the dynamic control of the model. To calculate the intensity of large scale convection, a CP scheme will also incorporate a closure mechanism. The second question refers to the properties of the clouds, and how the scheme models the moist-convective processes. This is either using the convective adjustment or mass-flux technique. There is also a technique that represents cumulus clouds explicitly using no CP scheme, but very high resolutions are required for this method. The last question a CP scheme must consider is what to do with, and how to represent, the solutions to the first two questions in the large-scale model environment. This is known as feedback from the sub-grid-scale CP scheme to the PCP scheme. In a sense, the convective feedback modifies the large-scale environment.

The closure and feedback mechanisms alluded to above will be described in conjunction with each CP scheme, as these differ depending on the scheme used. Arguably, the most important component of the CP scheme is the method it uses to treat the moist-convective processes. As stated, this is either using the convective adjustment technique, the mass-flux technique, or by explicitly resolving the cloud with no CP scheme. The following sub-sections outline the fundamentals of each.

2.5.3.1 Convective adjustment

Convective adjustment is a process by which model simulated temperature and moisture profiles are adjusted towards reference temperature and moisture profiles. The reference profiles are specific to the environment that is being modelled. Reference profiles are

created from observational data of that particular environment. This technique does not model an individual cumulus cloud column unlike the mass-flux technique, only the sounding profiles for humidity and temperature are manipulated. Precipitation is calculated by the amount of condensate released when the modelled moisture and temperature profiles are adjusted back to the reference profiles. A conceptual illustration of how this process works is shown in Figure 2.12.

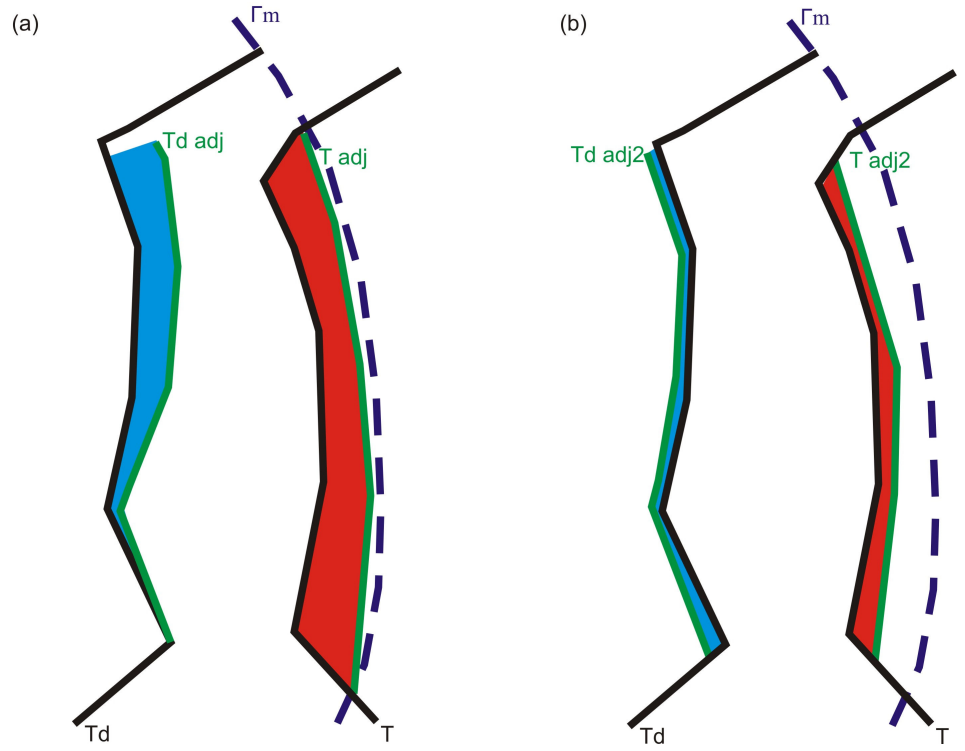

Figure 2.12: The concept of convective adjustment using temperature (T) and moisture (Td) reference profiles (black lines). During the initial stage (Figure 2.12a), *first guess* (model simulated) profiles are calculated (green lines), where the difference between the reference and model profiles is the amount of moisture gained (blue area) and warming undergone (red area). During the final stage (Figure 2.12b), the model profiles are shifted to conserve enthalpy. The precipitation released by adjustment is both the revised red and blue areas in Figure 2.12b.

2.5.3.2 Mass flux

The mass-flux technique explicitly simulates the individual cloud column based on a one-dimensional cloud model derived by Kain and Fritsch (1990). The mass-flux technique represents actual cloud processes in a model which are illustrated conceptually in Figure 2.13. Mass-flux refers to the magnitude of vertical motion inside the cloud, and is a measure of the inflow and outflow within the cloud spectrum. As Figure 2.13 shows, there are a number of inflows and outflows that contribute to the overall mass-flux. This includes lateral mixing at the sides of the cloud, and turbulent mixing at the cloud top.

Mass-flux also uses temperature and moisture profiles in a similar way to convective adjustment to determine if a parcel of air can undergo deep convection. If conditions for deep convection are satisfied, a cloud will be modelled. The advantage of this technique is that mass-flux parameterisation provides information on the nature and distribution of the precipitation types produced by the PCP scheme. This can be beneficial when using the Eta PCP scheme. Another advantage of explicitly simulating the cloud structure is that mass-flux accounts for downdraughts, which allows for more accurate mesoscale responses than in the convective adjustment method. This is due to the affect downdraughts have on cooling and drying parts of the lower-troposphere. If downdraughts are taken into account, then this allows for precipitation to cease in areas of the sub-grid where they are present, which can stop inaccuracies in precipitation. The trade-off of a mass-flux simulation is the additional complexity of this technique. This requires the model to be accurate in other parameterisations, such as radiative transfer.

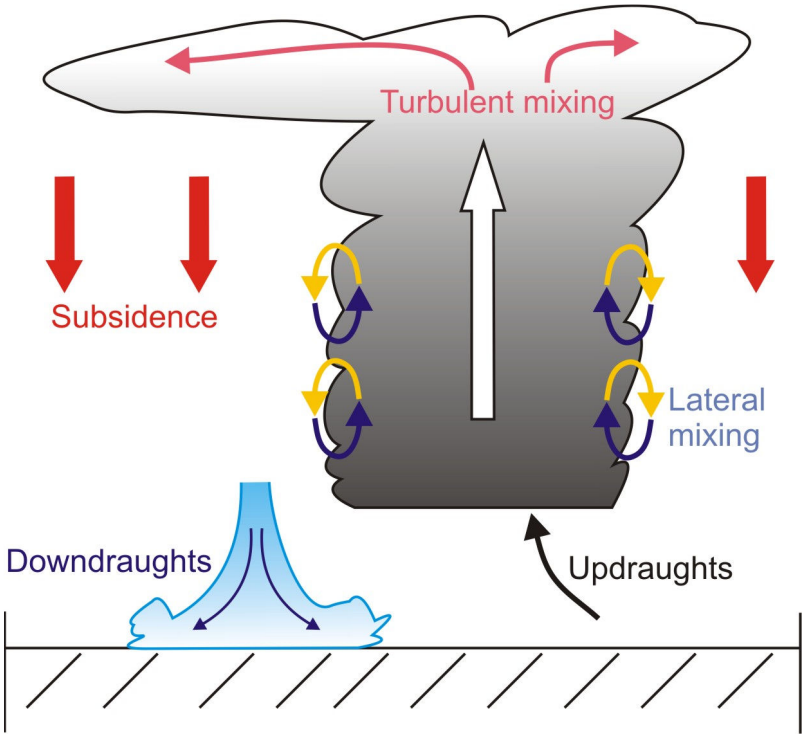

Figure 2.13: Conceptual diagram illustrating the convective mass-flux parameterisation technique. Air is drawn into the cloud (updraughts) as it is vertically lifted and cooled, undergoing turbulent and lateral mixing in the cloud column. This technique includes downdraughts processes which occur in the observed convective environment. Subsidence results from an imbalance between the up/downdraught mass fluxes, so flow is returned to the surface. Once the cloud physical processes have been simulated, precipitation is calculated through a specified closure assumption (adapted from Kain 2006).

2.5.3.3 Explicit convection

In some cases, if the model resolution permits, then simulating cumulus convective processes can be done without the use of a CP scheme. Information regarding explicit

convection is summarised in Table 2.1 at the end of this Chapter. Generally, model grid spacing will need to be small (1–2 km) so that the sub-grid-scale problem is overcome. This is because with fine grid resolution, entire grid cells can be filled with updraught air and condensate while others are filled with downdraughts ('How models produce precipitation and clouds', COMET program 2000). Such a method allows for rapid and tight coupling between the explicit cloud dynamics and the PCP scheme. This results in precise simulation of updraughts and downdraughts in the model without the use of a CP scheme, leading to improved accuracy given that assumptions made by a CP scheme are no longer present. Furthermore, a direct prediction of convective precipitation is possible because a CP scheme can only indirectly predict precipitation as a by-product of the removal of instability.

As with any numerical modelling method, there are still limitations. Firstly, convective initiation in the explicit method is still a largely unresolved issue. This leads to uncertainty in the location and timing of convective initiation. Secondly, high grid resolutions require enormous amounts of computing resources, and computational resources are not yet at the stage where this practice is efficient and cost effective. Finally, even at such high resolutions, convective clouds are still crude. This is a significant limitation because of the dynamic interactions operating within a cloud. This has implications for the hurricane environment, due to the severity and dynamic nature of the cumulonimbus cloud forms that drive a hurricane system.

2.5.4 Convective parameterisation schemes in WRF

This research presents the results of three different CP schemes available in WRF, the Kain-Fritsch (KF) scheme, the BMJ scheme, and the Grell-Devenyi (GD) ensemble. It is important to note that the same CP scheme used in two different models will likely produce contrasting results. This is due to the way the CP scheme interacts with the other components of each individual model ('Convective Parameterisation in Models', Baldwin 1998). It is difficult to make general statements about the quality of one CP scheme over another, so this research will focus on how well each of the schemes resolves precipitation for this event, and in this particular environment. The following section explains the processes involved in each of the CP schemes available in WRF, and a summary is provided in Table 2.1 at the end of this section.

2.5.4.1 Betts-Miller-Janjic convective adjustment scheme

The BMJ scheme (Betts 1986; Betts and Miller 1986; Janjic 1994) is a convective adjustment scheme, which adjusts model simulated soundings toward a pre-determined, post-convective reference profile derived from climatology. For the BMJ scheme to activate, moist soundings and some Convective Available Potential Energy (CAPE) are initially required. The scheme is then designed to check for the possibility of deep (precipitating) convection. The scheme will revert to shallow (non-precipitating) convection if the unstable cloud layer is too dry (termed negative precipitation), and/or the cloud layer is too shallow. Thus, convective depth must exceed a threshold value.

If deep convection is triggered, then the following procedure applies for each grid point where deep convection occurs. This procedure is illustrated conceptually in Figure 2.14a-c. Firstly, the model simulated profiles are used to find the most unstable air in the lowest 200 hPa of the atmosphere. Secondly, a moist adiabat for this unstable air is calculated, which determines the amount of CAPE at that grid point (Figure 2.14a). Thirdly, the initial *first guess* model sounding is compared to the reference profiles to determine what parts of the model sounding are too dry and too moist. Precipitable water for that grid point is also compared (Figure 2.14b). Finally, the adjustment procedure occurs when the model profiles are shifted towards the reference profiles (Figure 2.14c). This process removes excess moisture and latent heat. Precipitation is calculated by the amount of moisture and latent heat removed during this adjustment process. Typically, deep convection will stabilise the cloud layer while heating the middle to upper part of the cloud and drying the lower part. Feedback from this scheme is a reduction in CAPE and precipitable water. This feedback is a method the scheme uses to achieve a balance between the reference profiles and the model profiles. There are no downdraughts accounted for in BMJ because no cloud is modelled, which means cooling of the lower atmosphere must be done through other processes. One such technique is evaporative cooling of model precipitation.

In cases of shallow convection, the scheme still accounts for clouds in the model using adjustment profiles. Unlike the deep convection process, the result of shallow convection in the BMJ scheme is that no net temperature or moisture change occurs. This means enthalpy change is equal to zero, and no precipitation is produced. Differences to the cloud structure include moisture being mixed from cloud base to top while heat is mixed down, which destabilises the cloud layer. There is also no affect on precipitable water. The BMJ

scheme includes a mechanism where shallow convective environments might become deep convective situations if RH increases sufficiently. This is a good component of the BMJ scheme, as it enables a switch between precipitating and non-precipitating environments. This also identifies a controlling factor of the scheme which is cloud layer moisture. In cases of no precipitation being forecast yet some CAPE being present, the cloud layer moisture must be relatively dry.

The BMJ scheme has a number of strengths, which help to account for a variety of complex atmospheric situations. Firstly, this scheme often works well in moist environments with minimal CAPE. So as long as some moisture is present in the simulated profile, large amounts of CAPE are not required as in other cases, for large scale lifting and cloud development to occur. Finally, because of the moisture requirement, the scheme is well suited for tropical and oceanic environment applications.

In contrast, there are some limitations associated with this scheme. Firstly, reference profiles are fixed based on climatological observations. If some flexibility in the reference profiles was available for every forecast situation, then the BMJ scheme might capture a wider range of vertical structures. Secondly, when activated, the scheme often rains out too much water. This is because the reference profile can be too dry for the forecast situation. Finally, because this scheme does not simulate an actual cloud structure, it can only indirectly account for changes below the cloud base. This can impact upon the simulation and intensification of mesoscale highs and lows, and the development and propagation of gust fronts.

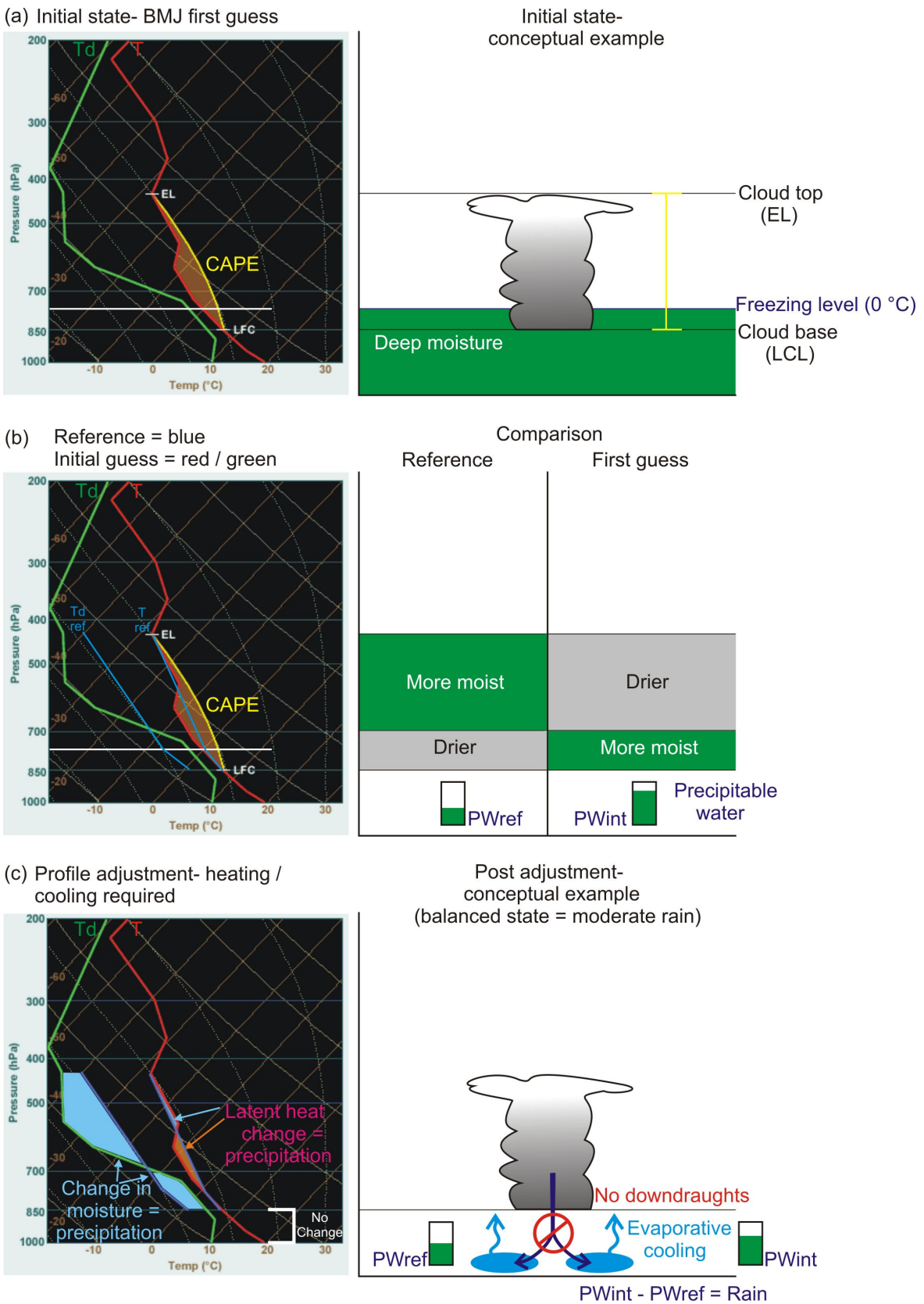

Figure 2.14: The BMJ scheme process for (a) the initial state, (b) the comparison to reference profiles, and (c) the adjustment process. An explanation of this process is given in the text (adapted from 'How models produce precipitation and clouds', COMET program 2000).

2.5.4.2 Kain-Fritsch scheme

The KF scheme is a mass-flux CP scheme, and is regarded as the most comprehensive CP scheme for treatment of in-cloud physical processes (Pielke 2002). The KF scheme operates in a similar way to the BMJ scheme in that both use reference profiles and adjust the model environment towards those reference profiles over a time period. The major difference with the KF scheme, however, is that model profiles are determined by rearrangement of mass in a one-dimensional cloud column, so that CAPE is removed. The cloud column considers moist updraughts and downdraughts, which include the effects of detrainment, entrainment, and microphysics. These are all part of the mass-flux technique previously illustrated in Figure 2.13.

There are a number of steps involved in the KF convective process, as outlined in Figure 2.15a-b. Firstly, KF tests for deep convection by mixing a potential updraught source layer of air near the surface. If the subject parcel reaches the Lifting Condensation Level (LCL), then the second step in the process is initiated. Secondly, the parcel is given a boost from the LCL based on the assumption that low-level convergence creates uplift. If the boosted parcel has sufficient energy to reach the Level of Free Convection (LFC), and cloud depth is greater than 3 km, it is allowed to rise to the Equilibrium Line (EL) (Figure 2.15a). If cloud depth is less than 3 km, then the KF shallow convective scheme is triggered and deep convection ceases. Thirdly, model soundings are then compared to reference profiles. Instead of adjusting the model profiles by convective adjustment, changes to the model sounding occur from actual simulated cloud processes via the mass-flux technique. These cloud processes are shown in Figure 2.15b. Entrainment occurs in many different parts of the cloud, and as the cloud column is cooled from the compensating detrainment process, moisture is released into the atmosphere at many different levels. This allows for more realistic feedback to the PCP scheme. Finally, the adjustment process is completed by the formation of a downdraught from air within 200 hPa of the updraught source layer. Mass is then overturned in the updraught, downdraught and surrounding environment until stabilisation is achieved (Baldwin and Kain 2006). Precipitation is produced as a by-product of moisture removal, and is released in the downdraught. Some precipitation evaporates in the downdraught, and some falls instantly to the surface. The intensity of precipitation is determined by the explicit simulation within the cloud column. Evaporative cooling occurs from falling precipitation which acts to dry and cool the lower-troposphere.

There are a number of strengths associated with this scheme. Firstly, the KF scheme is physically realistic in many ways. For instance, assuming the model boundary layer forecast is accurate, then the trigger mechanism for initiating convection is the most realistic available. The KF scheme also accounts for entrainment and detrainment in the cloud structure better than any other scheme. In addition, the KF scheme can vary its convective response to different forecast scenarios. Finally, this scheme is highly suited to mesoscale models and for coupling with PCP schemes that use clouds (such as the Eta PCP scheme). For example, the KF scheme accounts for microphysical processes in convection, and can be programmed to feed hydrometeors into the PCP scheme.

While the KF scheme has a number of strong qualities, there are also a number of significant limitations. Firstly, the scheme tends to leave unrealistic, deep saturated layers in post-adjustment soundings. This causes the PCP scheme to activate post-convective precipitation, such that the KF scheme is overactive. Finally, CAPE removal is not well suited to tropical or oceanic environments, which can result in over vigorous convection in the PCP scheme and excess precipitation.

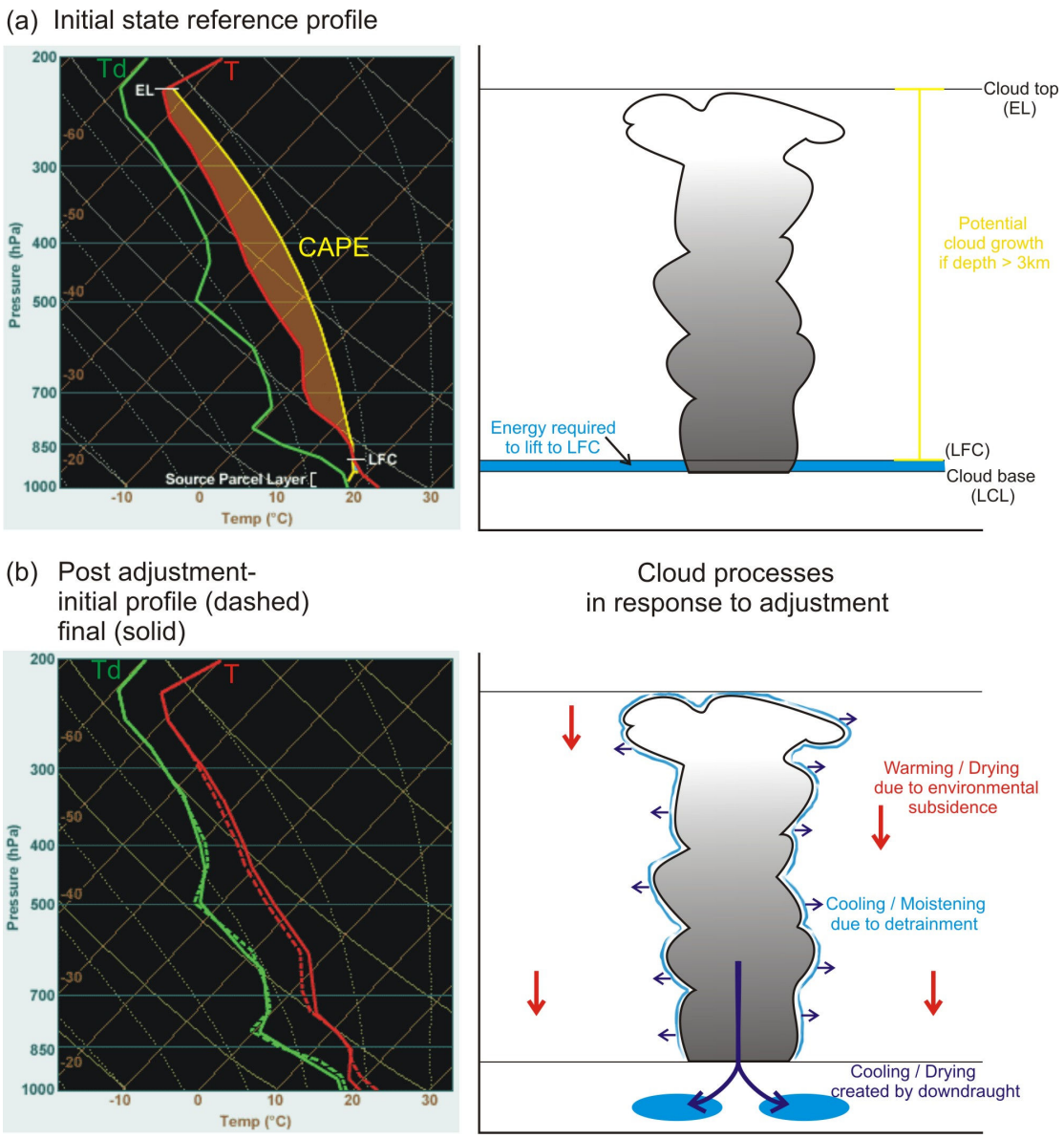

Figure 2.15: A conceptual example of the KF scheme in process for (a) the initial state, and (b) the adjustment phase. An explanation of this process is given in the text (adapted from 'How models produce precipitation and clouds', COMET program 2000).

2.5.4.3 Grell-Devenyi ensemble

The GD ensemble (Grell 1993; Grell and Devenyi 2001, 2002), attempted to overcome what Grell (1993) described as: the many disparate approaches to parameterising the modification of the environment by convection. Fundamentally, the GD ensemble uses multiple mass-flux CP schemes within each grid cell with the convective results averaged to give feedback to the PCP scheme. The ensemble operates by systematically separating the assumptions used in many CP schemes into three mechanisms — the dynamic control; the static control; and feedback. According to Grell (1993), the dynamic control determines the modulation of convection by the environment. This mechanism must know where and how strong the convection will be. The dynamic control uses closures based on

environmental stability or moisture convergence, which assume that the observed change of CAPE is known. Static control determines the updraught or downdraught properties, encompassing cloud physical processes such as entrainment, detrainment and microphysics, as shown in Figure 2.11. The feedback mechanism, which is the modification of the environment by the convection, is strongly dependent on the static control. This is similar to the KF scheme, as the feedback to the PCP scheme is dependent on the mass-flux cloud processes.

In WRF, to calculate the cloud properties, the static control uses 144 different ensemble types. The ensemble types are different combinations of CP schemes and control variations. All 144 ensembles have the same requirements — an unstable layer must exist in the lowest 4 km; and cloud depth must be greater than 500 m. Some ensemble members have additional requirements. For instance, the CAPE of the parcel must exceed 1500 J kg^{-1}, and upward motion must be present at the cloud base, and/or the most unstable layer, and/or any level below the cloud base. These additional conditions vary depending on the arrangement of ensemble parameters selected.

Similarly to the KF CP scheme, post-convective sounding changes are due to the detrainment of moisture at stable layers such as the cloud top, warming and drying due to subsidence, and convective downdraughts cooling the lower-troposphere. Thus, the GD ensemble can be conceptualised as a CP scheme operating similarly to that in Figure 2.15, but making use of many different mass-flux CP schemes in that grid cell with the aim of providing an average condition to eliminate uncertainty.

While a generalised approach can be effective for removing uncertainty between CP schemes, some limitations arise from an ensemble approach. Firstly, the variety of closure assumption choices means that a range of cloud base mass-fluxes can result. This can lead to variation in the treatment of surface radiation, and downdraught parameterisation. Secondly, rounding errors are possible when the dynamic control calculates the cloud work function to analyse the buoyancy force of an air parcel. This can affect the conditions for convective initiation. Finally, according to Jascourt (2004), because not all ensemble members may trigger, the GD ensemble response may appear weak when the large scale forcing is well defined, which is similar to other scheme responses. When the forcing is weak, however, this might be an advantage because intense convection will not initiate at the wrong time or place.

Table 2.1: Summary of the CP schemes and moist-convective techniques used in this study.

Scheme	Type of scheme	Cloud detrainment	Closure	Strengths	Limitations
BMJ	Adjustment	N	Sounding adjustment	1. Well designed for tropical oceans and coarse grids. 2. Can be adapted for the mesoscale. 3. Robust for many applications.	1. No downdraught parameterisation. 2. Mixing-line closure does not generate highs and lows and is not well suited for explosive convection.
KF	Mass-flux	Y	CAPE removal	1. The most complete treatment of in-cloud physical processes. 2. Downdraught parameterisation allows better simulation of mesoscale responses than other schemes.	1. CAPE closure is not well suited to tropical environments, leading to overly vigorous convection.
GD	Mass-flux	Y	Various — CAPE, moisture convergence, vertical velocity	1. Combination of schemes means a generalised parameterisation approach. This can remove uncertainty between schemes.	1. Different choices of closure assumptions may result in a large range of cloud base mass-fluxes. 2. Round-off errors possible when cloud work function is calculated.
No CP scheme	Explicit	Y	None (direct representation)	1. Direct representation of cloud	1. Convective initiation unresolved. 2. Computationally demanding. 3. Convective clouds are still crude.

2.6 Conclusion

In conclusion, this chapter has presented an overview of the controls, mechanisms of formation, and processes involved during the life cycle of a tropical cyclone. A description of numerical modelling, and specific studies of hurricanes using the WRF, helped to set the context for this work. In addition, an explanation of how models produce precipitation and clouds was offered that explains the role of the CP scheme in the model environment.

With an understanding of the background knowledge that this thesis employs, it is now possible to describe the methodological approach and present analytical work that draws upon the concepts outlined in this chapter.

Chapter 3
Methodology

3.1 Introduction

As previously stated, the aim of this study is to use WRF to conduct a series of sensitivity experiments to investigate the dynamics, environmental interactions, convective processes, and life cycle of tropical cyclone Sidr. To gain competency with the numerical model, a period of 4 months was spent experimenting with different model designs. Various model domain sizes and grid cell resolutions were trialled to see how well WRF simulated a hurricane system. Once an appropriate experimental design was reached, advanced simulations were conducted. This chapter explains the general technical principles of WRF including governing equations and physics, and experimental design, detailing how simulations were conducted.

3.2 Data

The United States Naval Research Laboratory (Navy/NRL) tropical cyclone page (Navy/NRL Tropical Cyclone Page 2007) proved to be a valuable resource for observational data of this event. The Joint Typhoon Warning Center (JTWC) *best track* analysis dataset for Sidr was obtained (JTWC Northern Indian Ocean Best Track Data 2007), which provided cyclone track and intensity information. *Best track* data contains tropical cyclone centre location and intensity (maximum 1 minute mean sustained 10 m wind speed) at six-hour intervals. *Best track* is calculated after the cyclone has dissipated, and once enough good quality raw data is available. Intensity estimates are calculated using the Dvorak model (Dvorak 1975, 1984, 1995). This method uses satellite imagery to estimate intensity based on cloud type. This is considered less accurate than in-situ measurements from aircraft and dropsondes, but in regions outside North America is generally the only method available.

The model was initialised with the National Centers for Environmental Prediction/National Center for Atmospheric Research (NCEP/NCAR) reanalysis dataset (Kalnay et al. 1996). This dataset is a 1.5° resolution reanalysis of Global Forecast System (GFS) data. The GFS data is reanalysed once the forecast time has passed, and observational data is available.

This reanalysis process makes the NCEP/NCAR dataset more accurate. This is beneficial for numerical modelling research.

3.3 WRF model technical description

The model used in this study is the NCAR WRF-ARW Version 2.2.1 (Skamarock et al. 2005). WRF is a fully compressible, non-hydrostatic (with hydrostatic option) Euler equations model. It has a terrain-following vertical pressure coordinate, so while the top layer of the model remains constant, the pressure surfaces in between the top layer and the surface change depending on terrain (Figure 3.1). The model uses second and third order Runge-Kutta equations for time integration, and second to sixth order advection schemes for both the vertical and horizontal directions. The advantage of using Runge-Kutta equations is that differential equations that represent atmospheric processes can be solved approximately with a numerical method. Lateral boundary conditions can be periodic, open, symmetric, or specified by the user. For real data cases, initial conditions are three-dimensional based on either forecast data or large scale analysis datasets (such as NCEP/NCAR). Model physics are a combination of microphysics, CP's, surface physics, and atmospheric radiation physics.

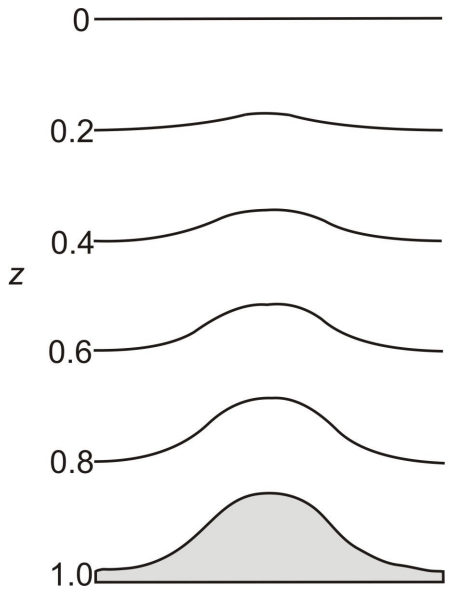

Figure 3.1: Conceptual diagram of the terrain-following vertical coordinate system. The height of each vertical layer (z) denotes the pressure level. Note the top layer of the model (z = 0) remains constant. It is the vertical coordinate that changes in between levels depending on the terrain or surface characteristics. The relationship between z and pressure therefore, is variable. Such that a value of z = 1 will not always equate to 1000 hPa. The height values for z also correspond to model layers (Figure 3.1 adapted from Skamarock et al. 2005).

The WRF model contains a number of improvements to the traditional atmospheric equations (Skamarock et al. 2005). Firstly, the governing equations have been reformed to reduce computational rounding errors that can occur when calculating the vertical pressure gradient and buoyancy. Secondly, the momentum, mass conservation, and geopotential equations are all changed from the thermodynamic formulation of modelling the moist atmosphere devised by Ooyama (1990). The conservation equations for both potential temperature and scalars remain unchanged from Ooyama (1990). Finally, these new equations are defined as perturbations from a balanced reference state. Overall, these changes have created a new conceptualisation of the modelling environment, with the WRF model aiming to overcome some of the complexities that occur from physical interactions and rearrangement of mass inside the model domain.

3.4 The modelling process

The generation of model output was a four step process (Figure 3.2). Firstly, external data files such as meteorological, soil, and topographical data are required for the model to construct a simulation domain. These files are processed in the WRF Pre-processing System (WPS), which forms the second part of the process. In WPS, the external data files are overlain one by one onto a model domain specified by the user. This was done by editing the WPS namelist file for each simulation (Appendix I a-h), and executing three commands: *geogrid* (defining model domains and interpolating geographical data to that domain), *ungrib* (extracting meteorological files and formatting these so WRF can read them), and *metgrid* (horizontally interpolating the meteorological fields extracted by *ungrib* to the model domain defined by *geogrid*). The result of this process was a set of 'met_em' files that were used by the model in step three of the process. In this third step, input data can either be initialised for a real case, or an ideal case. As this was a case study of a real event, the real data method applied, which simply executes the *real.exe* program in the WRF-ARW model. To prepare *real.exe*, the WRF namelist files for each simulation (Appendix II a-h) were edited accordingly. The WRF namelist file controls the physics, dynamics and domain options for the model simulation. The specific options used for this study are described in the model setup section. After the *real.exe* program is executed, the model is ready to run the actual simulation using the file generated by *real.exe*. This file is called *wrf.ll*, and was submitted to the International Business Machines Power Series 5 Model 575 (IBM-P575) supercomputer running at the University of Canterbury. It should be noted here that all simulations need a high speed processor to run on, which is separate

from the actual WRF model. Once computation is complete, the last step in the modelling process, preparing model output for visualisation, can be completed. There are a number of graphics packages available for this task, and version 4 of the Read/Interpolate/Plot (RIP4) program was used. The RIP4 namelist file (Appendix III) was edited to produce the various plots of each experiment. RIP4 can plot any number of atmospheric variables for analysis. Further information on data preparation and model installation is provided in the WRF users guide by Wang et al. (2008).

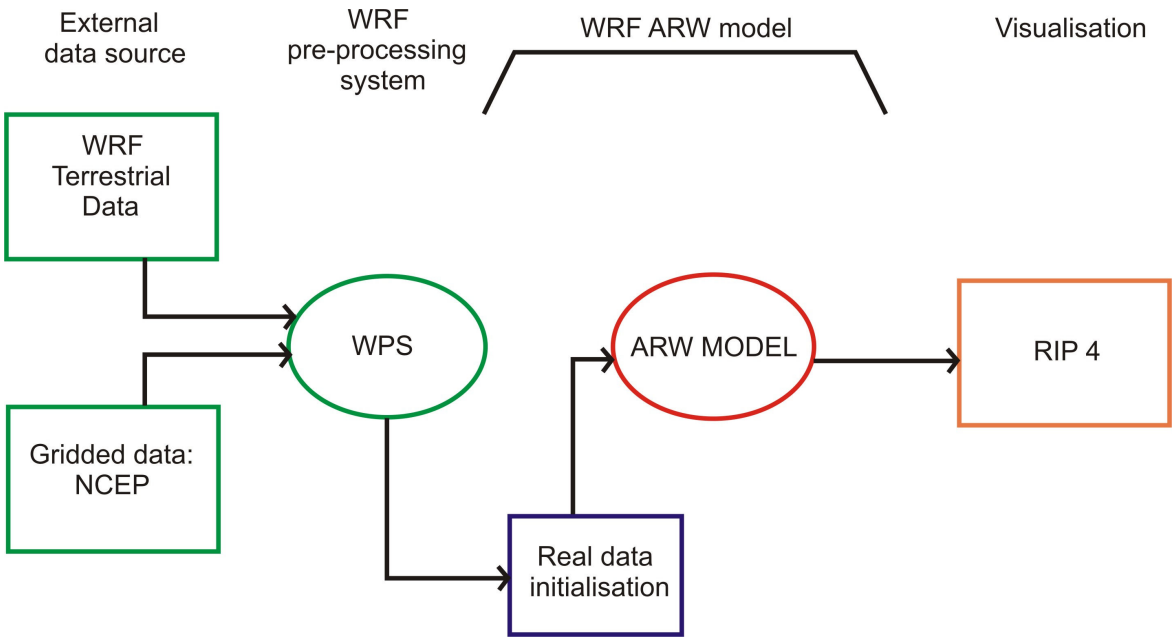

Figure 3.2: Flow diagram showing the components of WRF Version 2.2.1 used in this study. External data is input into the WPS which creates the domain containing meteorological data that is then input into the ARW model solver. There are a number of graphics tools to view output, and in this case RIP 4 was used (adapted from Wang et al. 2008).

3.5 Model setup and experiment configuration

This section outlines the general model setup and then describes specific configurations used for the different experiments. A total of eight simulations were run across three experiment classes — sea surface temperature (1 simulation), initialisation time (3 simulations), and CP scheme (4 simulations). Further information on the configurations used that are not described here can be found in Appendix I a-h and II a-h.

3.5.1 General model setup

A number of conditions remained constant for all simulations. Firstly, lateral boundary conditions were input into the model domain every 12 hours using NCEP/NCAR

reanalysis meteorological data. This process is also referred to as nudging. Secondly, the coarse model domain configuration remained the same (Figure 3.3). The reference coordinates for the centre point of the domain were (15° N, 90° E). The number of grid points was 150 north to south and 150 east to west. Model resolution (Δx and Δy) remained 15 km for each grid cell. Only 1 grid point was in each grid cell. This grid point was located in the centre of the cell. Thirdly, the location of the 33 model pressure levels remained constant for all simulations. The terrain-following vertical coordinate was placed at values of z = 1.000, 0.999, 0.998, 0.997, 0.995, 0.993, 0.991, 0.989, 0.987, 0.985, 0.982, 0.979, 0.976, 0.973, 0.970, 0.950, 0.900, 0.850, 0.800, 0.750, 0.700, 0.650, 0.600, 0.550, 0.500, 0.450, 0.400, 0.350, 0.300, 0.250, 0.200, 0.100, and 0. Finally, the time step for model integration was 60 seconds. Thus, model calculations were performed every 60 seconds throughout the duration of the simulation.

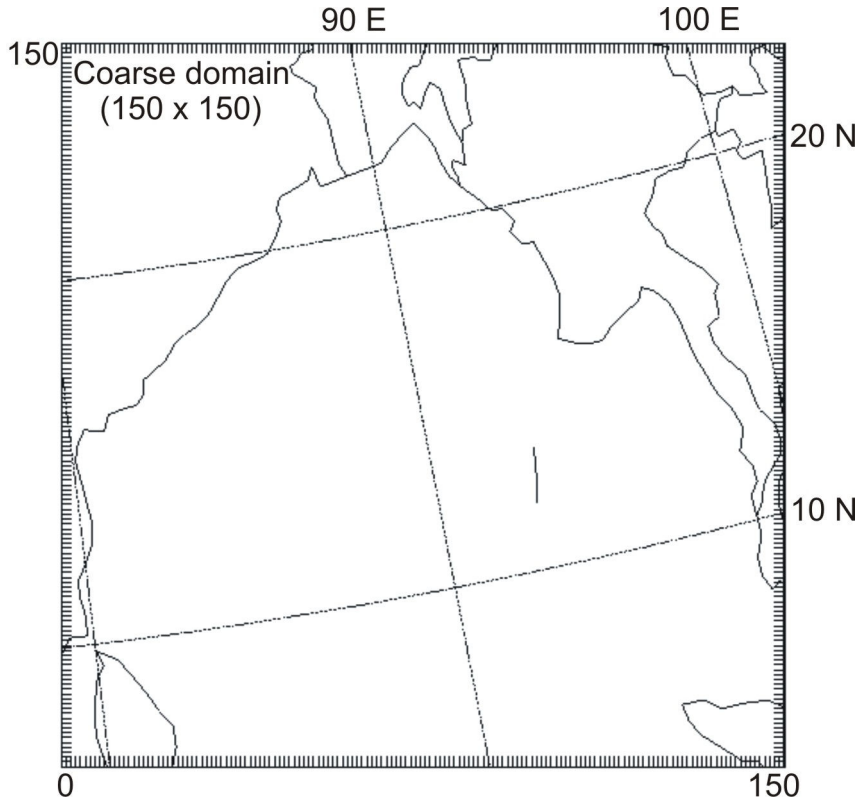

Figure 3.3: Coarse domain configuration for the SST, initialisation, and CP experiments shown in two-dimensional form. The grid points are shown as tick marks along each side ranging from 0 to 150. There were 150 grid points east to west and north to south. The grid spacing of each grid cell was 15 km. One grid point was located at the centre of each grid cell.

3.5.1.1 Physics and dynamics options

The range of physics options in WRF is vast, adding to the complication of model setup. Any number of options can be selected and combined in different ways. Some are more computationally costly than others, but offer more sophistication. Finding a balance

between sophistication, appropriateness of physics option to tropical cyclone simulation, and computation time efficiency, was a challenge. Limitations are inevitable in this work because of balancing those factors. These are discussed in the context of this study in the discussion chapter.

The physics and dynamics options used in this study can be divided into four categories. Firstly, the Eta microphysics PCP scheme represented the cloud and precipitation processes. Secondly, radiation processes use longwave and shortwave schemes. The longwave scheme is the rapid radiative transfer model (Mlawer et al. 1997), which uses a spectral band scheme of 16 wavelengths. Pre-set tables accurately represent longwave processes, including a parameter for cloud depth. Shortwave radiation is accounted for using the Dudhia scheme (Dudhia 1989). It accounts for clear-air scattering, water vapour absorption, and cloud albedo while calculating downward solar flux. Similarly to longwave, pre-set tables (Stephens 1978) are used to determine the influence of clouds. Radiation physics were run (*radt* setting in the WRF namelist) every 8 minutes. Thirdly, surface layer physics are accounted for using the Eta similarity theory, which is based on the Monin-Obukhov scheme. Surface layer schemes calculate two quantities — velocities associated with friction; and energy exchanges in the Planetary Boundary Layer (PBL), enabling heat and moisture calculation. The Eta surface layer scheme (Janjic 1996, 2002) uses a viscous sub-layer of water surfaces. The advantage of using an Eta surface layer scheme is to compensate for the effects of impendence to turbulent mixing in the lowest 1% of the PBL. Finally, the PBL scheme used is the Mellor-Yamada-Janjic (MYJ) (Mellor and Yamada 1982; Janjic 1990, 1996, 2002), which must be used in conjunction with the Eta surface scheme. The PBL scheme accounts for vertical sub-grid scale fluxes, similar to how a CP scheme works. A PBL provides atmospheric tendencies of temperature, moisture and horizontal momentum in the atmospheric column. The MYJ scheme does this using threshold values for a stable and unstable atmosphere, which determines mixing in the boundary layer. PBL physics were run continuously (*bldt* setting in the WRF namelist was set to 0 minutes) throughout the simulation. Furthermore, selecting a PBL scheme meant a dynamic vertical diffusion scheme was not used, as the PBL scheme incorporates this dynamic requirement. The model was run non-hydrostatically, which means the hydrostatic approximation was not made, so that the vertical momentum equation was solved. This option was selected so that small scale mesoscale circulations and cumulus convection could be resolved during simulation.

3.5.2 Specific configurations for the numerical experiments

3.5.2.1 Sea surface temperature experiment

Table 3.1 summarises the conditions of the sea surface temperature (SST) sensitivity simulation. The SST experiment was a 36 hour simulation initialised at 0600 LST on 11/11/07, at the end of Sidr's tropical storm phase. The KF CP scheme was used. The sea surface temperature values (known as *skintemp* in the WRF NCEP file) of the NCEP/NCAR reanalysis dataset were edited to a constant value of 10 °C (283.15 K) across the entire sea surface.

3.5.2.2 Initialisation experiment

The conditions of the three initialisation experiments, namely, KF_108; KF_72; and KF_48, are outlined in Table 3.1. The only condition varied was model start time, which was calculated based on the time of observed landfall, at 1800 LST on 15/11/07. So in this case the KF_108 simulation corresponds to a start time of 108 hours prior to landfall, and so on.

Table 3.1: List of simulations with fundamental conditions for the SST and initialisation experiments.

Simulation name	Grid points	Grid resolution (Δx, Δy)	Model start time(LST)	CP scheme	*Skintemp*
SST	150 x 150	15 km	0600 11/11/07	Kain-Fritsch	10 °C
KF_108	150 x 150	15 km	0600 11/11/07	Kain-Fritsch	Unchanged from NCEP dataset
KF_72	150 x 150	15 km	1800 12/11/07	Kain-Fritsch	Unchanged from NCEP dataset
KF_48	150 x 150	15 km	1800 13/11/07	Kain-Fritsch	Unchanged from NCEP dataset

3.5.2.3 Convective parameterisation experiment

For the CP simulations a high resolution nested domain, of 5 km grid resolution, and 139 grid points was nested within the coarse model domain to resolve dynamical processes. The nested domain was held stationary because of the computational demands and advanced modelling skills that a moving nest requires. A moving nest setup is beyond the scope of this study. This meant an initial coarse grid simulation was required for each of the CP experiments to evaluate where on the coarse domain the cyclone reached maturity. Once this was established the coordinate locations of where each cyclone matured on the coarse domain were specified for the nested domain. The nested grid locations for each of the CP simulations are shown in Figure 3.4, and the coordinate locations are defined in Table 3.2. The run time of each nested domain remained the same to save computational time. This meant that the start time of the nested domain varied for each simulation because of the different maturation times observed for each CP simulation in the initial runs. This does not have any affect on the variability of results for the inner nest, because the inner nest receives its initial conditions from the coarse domain at that time. In most cases, the inner nest was turned on 24 hours before maturity and ran through to the end of the simulation period.

The most important initial condition that was changed between simulations was the CP scheme. Simulations are named according to the scheme used (Table 3.2). As previously stated, three implicit CP schemes were used, the KF scheme, the BMJ scheme and the GD ensemble. CP was run on both domains in each of the experiments. In addition, a simulation that resolved cumulus convection explicitly, named No Cu was also conducted.

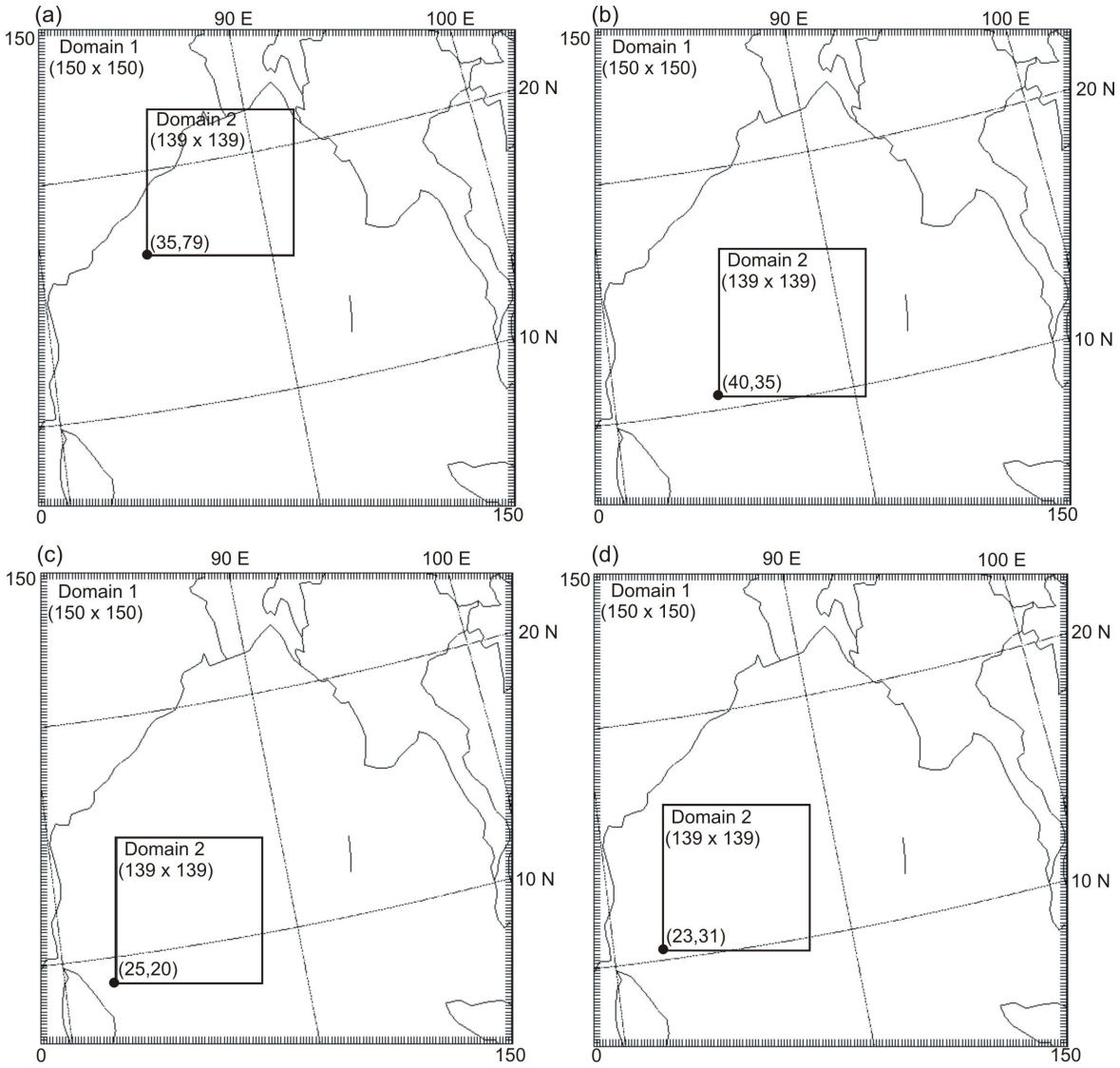

Figure 3.4: Domain configuration used in the CP experiments for (a) KF, (b) BMJ, (c) GD, and (d) No Cu. For each simulation the nested domain was held stationary at a set location in the coarse domain (indicated by the grid point coordinates at the bottom of domain 2) to capture the cyclone during its maturity. The number of grid points is indicated below the domain name. The nested domain had a grid cell resolution of 5 km, while the resolution of domain 1 remained at 15 km.

Table 3.2: Description of simulations and important model conditions used in the CP experiment.

Simulation name	Coarse domain grid points (N–S, E–W)	Coarse domain grid resolution (Δx, Δy)	Coarse domain start time and date (LST)	Nest domain location (on coarse domain)	Nest domain grid points (N–S, E–W)	Nest domain grid resolution (Δx, Δy)	Nest domain start time and date(LST)	CP scheme
KF	150 x 150	15 km	0600 on 11/11/07	35,79	139 x 139	5 km	1800 on 14/11/07	Kain-Fritsch
BMJ	150 x 150	15 km	0600 on 11/11/07	40,35	139 x 139	5 km	0600 on 13/11/07	Betts-Miller-Janjic
GD	150 x 150	15 km	0600 on 11/11/07	23,31	139 x 139	5 km	0600 on 13/11/07	Grell-Devenyi
No Cu	150 x 150	15 km	0600 on 11/11/07	25,20	139 x 139	5 km	1800 on 13/11/07	Explicit convection (no CP)

3.6 Methods of analysis

This section describes the analytical techniques specific to each experiment, and also includes methods of observational analysis that form the basis of Chapter 4.

3.6.1 Observational analysis

Tropical cyclones are difficult to measure by direct methods, and the range of observational data is often limited to indirect techniques ('The Joint Typhoon Warning Center Tropical Cyclone Best Tracks, 1945-2000', Chu et al. 2002). Indeed, remotely sensed data is often the most widely used data unless cyclone detection radar or aircraft reconnaissance are available. Direct measurements from aircraft very rarely occur outside of the United States. Bangladesh has no cyclone detection network, in fact, the nearest facility that is able to provide such detection is in India. Despite these issues, it was still possible to analyse the development and intensification of tropical cyclone Sidr.

The synoptic description of Sidr was analysed from a combination of *best track* analysis and Navy/NRL manipulated imagery. These included: Moderate Resolution Imaging Spectrometer (MODIS) satellite images; Aqua Earth Observing System (EOS) 89 GHz polarisations; Advanced Microwave Scanning Radiometer for Earth Observing System (AMSR-E) integrated water vapour images; Special Sensor Microwave Imager (SSMI) colour composites; and Tropical Rainfall Measuring Mission (TRMM) precipitation surveys.

3.6.2 Sea surface temperature experiment

Numerical simulations of the cyclone circulation development, precipitation intensity, CAPE, wind speed, and equivalent potential temperature were compared with observed recordings to investigate the impact of changing sea surface temperature in a cyclone environment. This experiment tested the model to check correct diagnostic performance, and served as a good exercise in applying theory of environmental control on tropical cyclones. Furthermore, the experiment served as a good assessment of how well WRF is suited to simulating combined ocean-atmosphere processes. A final research objective was to examine the influence of sea surface temperature on tropical cyclone intensity, energy exchange, life cycle and structure.

3.6.3 Initialisation experiment

The research objective of this experiment was to examine the role of model initial conditions on the intensity and track of cyclone Sidr. This was achieved using a variety of analytical techniques. Firstly, an analysis of track error was undertaken. This is a comparison between observed *best track* and simulated tracks. It incorporates a latitude and longitude displacement technique similar to that used by Goerss (2007). In addition, the behaviour of simulated tracks was also studied, once initial errors had been accounted for. This was accomplished by comparing the change in simulated cyclone centre latitude and longitude between selected times. These changes were then compared to the observed centre deviation between the same times. Finally, the influence of initial conditions on predicted cyclone intensity was analysed. In addition, cyclone track was analysed using upper-level analyses. Similar to the SST experiment, pressure, wind speed, and reflectivity were used as a means of analysing cyclone intensity. Upper-level PV and wind fields assisted with the analysis of cyclone track. Using PV fields followed a similar analytical technique as used by Davis and Bosart (2002).

3.6.4 Convective parameterisation experiment

The objective of this experiment was to examine the role of a number of CP schemes and investigate parameterisation implications for the model forecast. For the purpose of analysis, cyclone life cycle was divided into the three stages outlined in Chapter 2 — development, maturity, and decay. Because the hurricane developed and decayed outside of the high resolution domain, analysis of these stages comes from the coarse grid. Development was defined as the tropical storm phase, before category 1 hurricane status was achieved. Maturity was at the time of maximum wind speed and central pressure in the nested domain, and decay was the point after maturity when these parameters decreased.

A number of analytical techniques were used in this experiment. Firstly, after defining the stages of life cycle for each simulation, the intensities were compared. This was a simple wind speed and central pressure analysis. Secondly, the tracks of each were compared and upper-level features identified, noting similarities and differences that could be attributed to the CP scheme used. Thirdly, the CP experiments were compared for their ability to resolve CAPE and convective precipitation processes. Resolved precipitation was compared to observational data where available, which satisfied the objective of finding

the most realistic CP for this event. Furthermore, model simulated vertical soundings were extracted from the nested domain at cyclone maturity to examine the effectiveness of each CP scheme at removing instability. Finally, analysis was extended to study the cyclone intensity structures that each of the CP simulations produced. This was conducted using an analysis technique similar to that of Liu et al. (1997), where vertical plots of different cloud microphysical quantities were used to examine the generation of cyclone reflectivity structures.

3.7 Conclusion

In conclusion, this chapter has outlined the general technical principles of WRF, detailed the experimental design, and explained how the simulations were conducted. The generation of model output is a four step process run through the WPS, WRF-ARW solver and RIP4 model components respectively. A total of eight simulations were run across three experiment classes — sea surface temperature (1 simulation), initialisation time (3 simulations), and CP scheme (4 simulations). A number of conditions remained constant for all simulations, namely lateral boundary conditions, coarse domain configuration, position of model pressure levels, and model time step. The physics and dynamics options used in this study come from four categories comprising microphysics, longwave and shortwave radiation schemes, surface layer physics, and the PBL scheme. The schemes selected were the Eta microphysics, rapid radiative transfer model, Dudhia scheme, Eta similarity theory, and the MYJ scheme, respectively.

The specific changes for each simulation were discussed. Firstly, the SST experiment was a 36 hour simulation initialised at 0600 LST on 11/11/07, at the end of Sidr's tropical storm phase. The KF CP scheme was used. Secondly, in the initialisation study, the only condition changed was model start time. Three experiments were created — KF_108, KF_72, and KF_48, all based on hour from observed landfall. Finally, for the CP simulations, a high resolution nested domain of 5 km grid resolution was nested within the coarse model domain. Three implicit CP schemes were used, the KF scheme, the BMJ scheme, and the GD ensemble. A simulation that resolved cumulus convection explicitly, named No Cu was also conducted.

Methods of analysis were also discussed. Firstly, the synoptic description of Sidr was analysed from a combination of *best track* analysis and Navy/NRL manipulated imagery.

Secondly, the SST simulation was analysed using a variety of atmospheric measures such as CAPE, reflectivity, and wind speed. Thirdly, for the initialisation experiments an analysis of track error was undertaken which compared observed *best track* and simulated tracks. Upper-level analyses were also used. Finally, for the CP experiments, cyclone life cycle was divided into three stages — development, maturity, and decay, and CP performance was analysed and compared at each of those stages. Analysis was undertaken using a combination of simulated CAPE, precipitation, wind speed, central pressure, and structural features.

Limitations that arose during this study are presented in Chapter 8 to provide context for the results. The results of this study are now presented in the forthcoming chapters.

Chapter 4
Tropical cyclone Sidr

4.1 Introduction

Tropical cyclone Sidr officially claimed the lives of 4234 people in Bangladesh (CRED 2008). According to the Bangladesh Ministry of Disaster Management (2007), an estimated 8.9 million people were affected, 563 877 houses damaged, and total damages in the order of $450 million estimated. Sidr's death toll was much less than that of the 1991 *Bangladesh Cyclone* (143 000 people), and Cyclone Bhola (approximately 500 000 people), the two deadliest Bangladesh cyclones on record. The impact of Sidr in this instance fell on many of the survivors, who struggled for assistance. Indeed, while warning times and procedures have improved in this region, the aftermath of these events remains highly significant. The objective of this chapter, therefore, is to describe the pertinent atmospheric processes that led to the formation of this destructive event. To accomplish this, Sidr is studied during each phase of cyclone life cycle. An analysis of observed precipitation is also provided.

4.2 Development and life cycle

4.2.1 Genesis

Sidr's precursor was a tropical disturbance originating as an area of deep convection 235 nautical miles southeast of the Andaman Islands. This disturbance was rapidly developing in the vicinity of a developing low-level circulation centre near the Nicobar Islands at 0830 LST on 10/11/07. Convection was enhanced by a region of diffluent upper-level flow, and an expansive warm sea surface of 29 °C, but further development of this circulation centre was impeded by moderate vertical wind shear at this time. Surface winds were also weak at 12 m s^{-1}. Over the following 24 hours to 0600 LST on 11/11/07, the shear reduced sufficiently for the JTWC to upgrade their advisory and issue a tropical cyclone formation alert. Development of this circulation centre continued, as warm, moist boundary layer air converged to the west of the Nicobar Islands. Deep convection associated with the tropical disturbance north of the circulation became more organised, and enhanced vertical motion led to a small central pressure drop of 5 hPa from 1005 hPa to 1000 hPa (Figure 4.1).

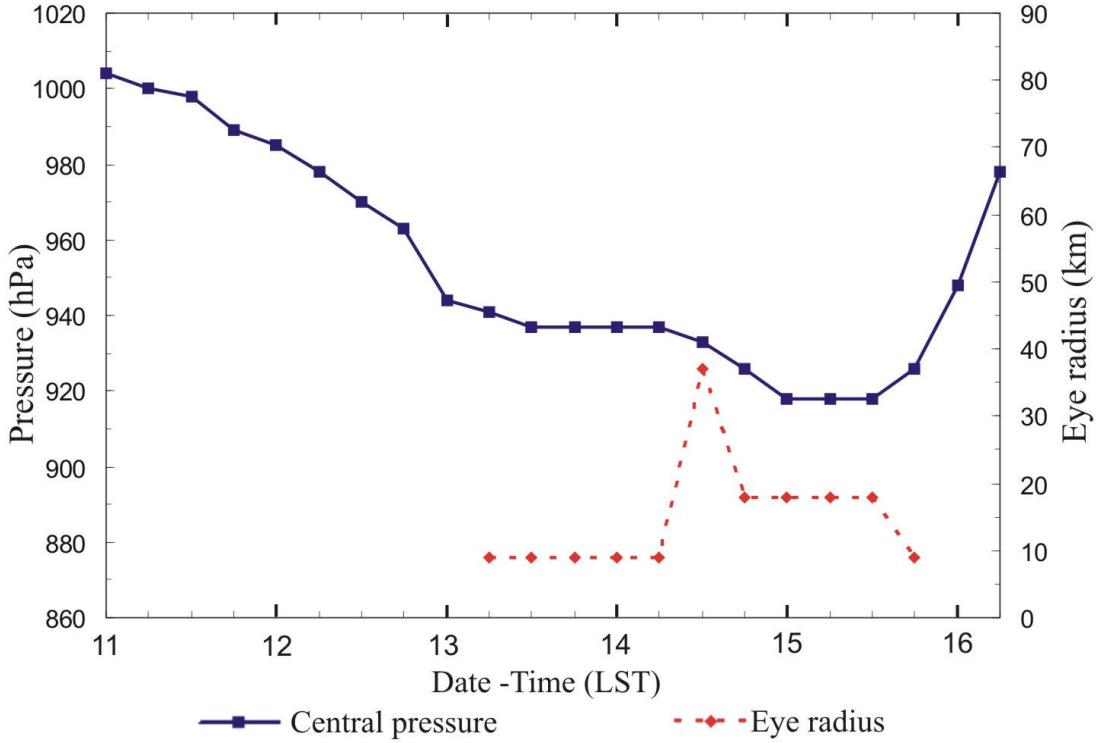

Figure 4.1: Sidr's central pressure in hPa (solid curve), and radius of eye in km (dashed curve) from 0000 LST on 11/11/07. Bold tick marks indicate midnight Bangladesh local time, while small ticks are 6 hourly intervals.

Less than 6 hours later at 1200 LST on 11/11/07, the JTWC issued their first tropical cyclone warning for tropical depression 06B (No name), minimum central pressure at the circulation centre was 998 hPa. Surface winds increased to tropical storm intensity at 18 m s^{-1} (Figure 4.2). A MODIS 250 m resolution satellite image for 1200 LST on 11/11/07 (Figure 4.3 a) showed initial development of significant tropical cyclone structural features. The storm was absent of an eye at this stage, but an area of significant organised convection about a rotating centre was evident, as was the development of two spiral rain bands comprising smaller convective cells to the southwest of the Andaman Islands. To the north, the deep convection associated with the initial boundary layer disturbance spiralled in (due to the influence of rotation at the centre) towards the developing eye wall, and was a source of inflow for the northern extent of the cyclone. As this convective mass flowed across the rough, warm ocean surface, further amounts of water vapour were entrained providing thermal energy that was increasingly converted into mechanical energy through latent heat release. This process assisted convection and further cyclone development. Areas of cirrus around the centre and to the northwest marked the outflow regions in the stratosphere. This divergence aloft allowed for some air recycling back into the boundary layer, and continued convergence at the surface. This period of cyclone intensification is identifiable in Figure 4.1 where an observed pressure fall of 22 hPa occurred over 24 hours

from 0600 LST on 11/11/07 to 0600 LST on 12/11/07, supported also by an increase in surface wind speed (Figure 4.2). The storm was on a west northwest heading of 290° and increased its translation speed from 1 m s^{-1} to 2.6 m s^{-1} during this time.

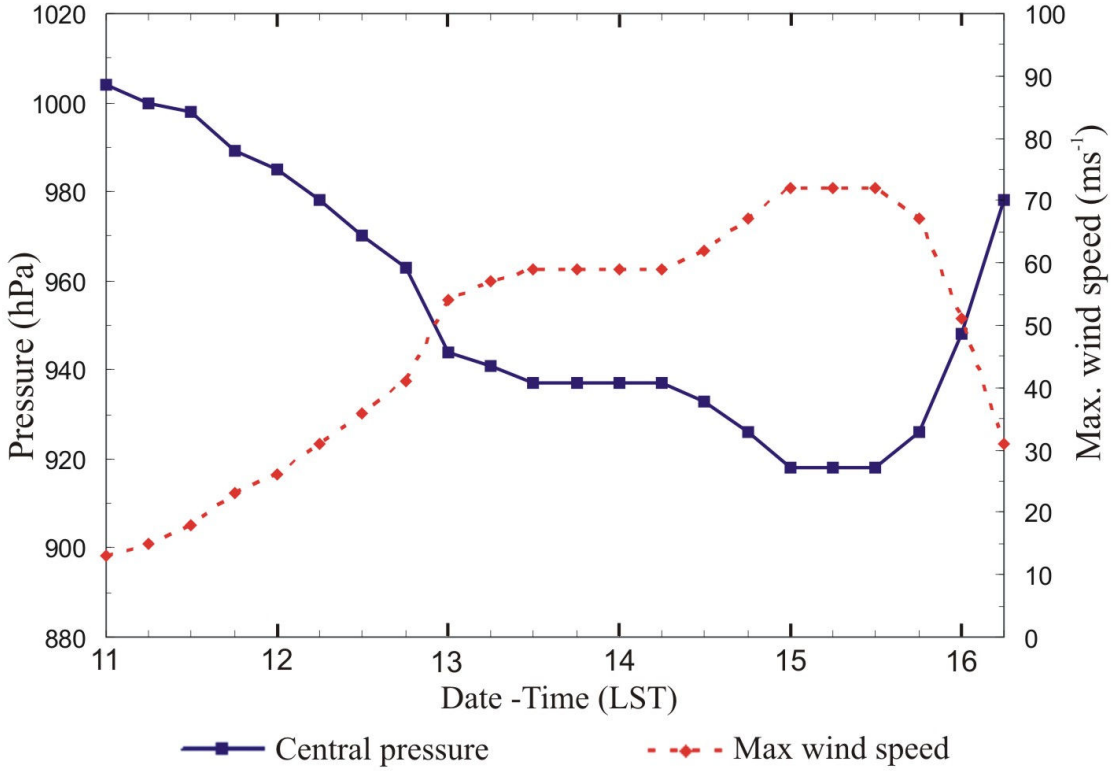

Figure 4.2: Sidr's central pressure in hPa (solid curve), and maximum sustained wind speed in m s^{-1} (dashed curve) from 0000 LST on 11/11/07. Bold tick marks indicate midnight Bangladesh local time, while small ticks are 6 hourly intervals.

This development can also be analysed using Aqua EOS 89 GHz microwave (Figure 4.3a and 4.3b) and AMSR-E integrated water vapour (Figure 4.4a and 4.4b) images, which show a number of features. The first such feature was a developing rotational structure as evident in the MODIS image, and defined by the brightness temperatures and moisture characteristics of the sensor images. Examining the Aqua EOS 89 GHz sensor analysis (Figure 4.3b) reveals deep convection (red brightness temperatures) developing in the northern inflow region (A), and ice particles above freezing level (indicated by green and yellow brightness temperatures) near this convection and present in the spiral bands. There is also low level cloud water present in the southern inflow region (B), indicating shallow clouds, but no convection. Likewise, the integrated water vapour image (Figure 4.4a) which identifies low-level precipitable water, confirms the incidence of convection and low-level cloud water. The majority of this circulation had high precipitable water values (greater than 60 mm), which is indicative of sustained cyclone development. The northern extent had values over 70 mm which supports deep convection in this region. To the south,

shallow clouds were represented by 50–60 mm of precipitable water. Significantly, this image indicates the amount of moisture available to the developing circulation, and where it has come from. The SSMI colour composite (Figure 4.4b) suggested a greater amount of deep convection than that shown in Figure 4.3b. This is due to the collating of three separate polarisation angles into one image, which will be explained and shown to be highly effective at later stages of analysis in this chapter.

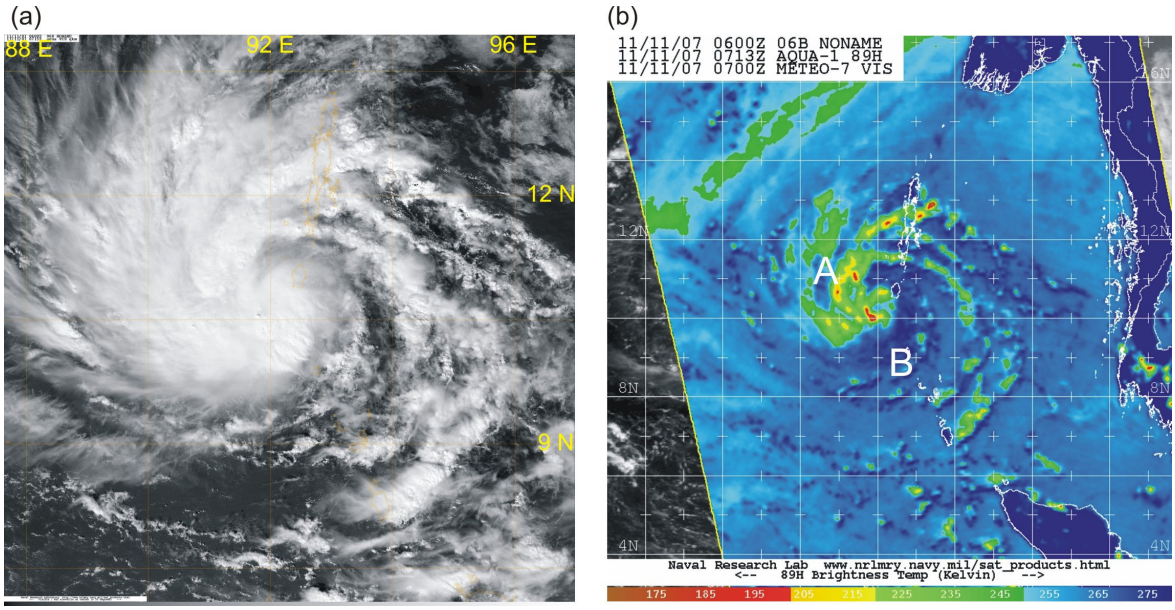

Figure 4.3: (a) MODIS 250 m resolution image for 1200 LST on 11/11/07 indicating the developing circulation, and (b) 89 GHz horizontally polarised Aqua EOS image for 1313 LST on 11/11/07. There is evidence of deep convection initiation in red areas of region A, and low level liquid precipitation throughout region B (Navy/NRL Tropical Cyclone Page 2007).

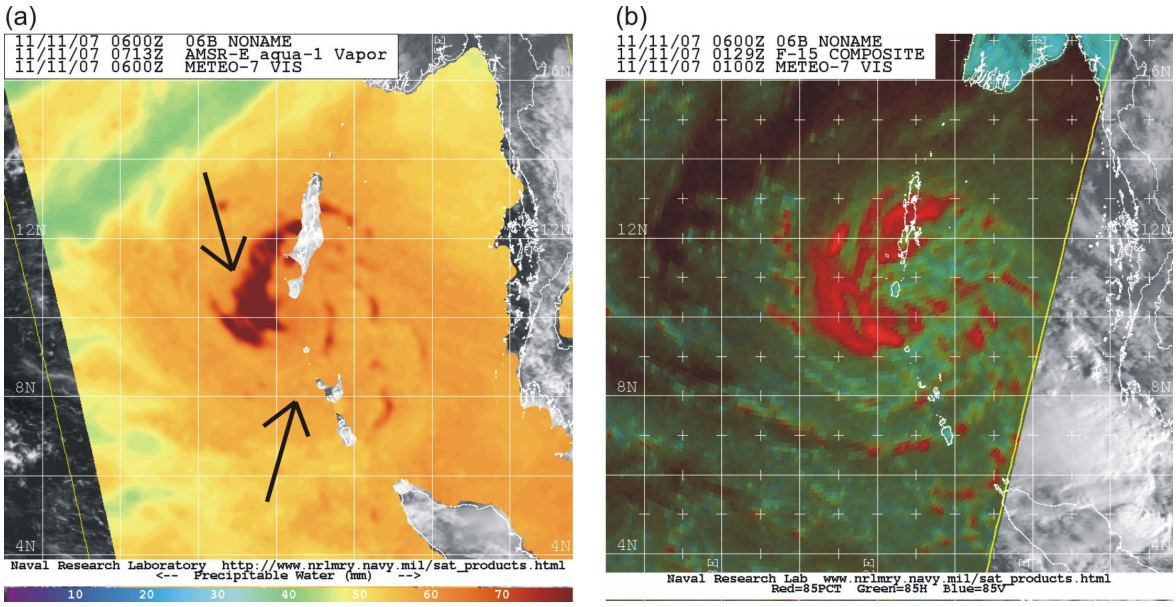

Figure 4.4: (a) AMSR-E integrated water vapour image for 1313 LST on 11/11/07 showing low-level precipitation. The black arrows indicate regions of sustained convective development and intensification (top), and moisture inflow from the south (bottom). (b) 85GHz SSMI colour composite for 0729 LST on 11/11/07, which confirms areas of convection (red), and areas of low level cloud circulation (light blue and green), (Navy/NRL Tropical Cyclone Page 2007).

Tropical storm 06B (Sidr) was classified as a category 1 hurricane at 1200 LST on 12/11/07, when surface winds exceeded 33 m s^{-1}, and central pressure fell to 970 hPa. The centre was southwest of the Andaman Islands at (10° N, 92° E), and tracking northwest with a translation speed of 3.1 m s^{-1}. Tropical cyclone Sidr was upgraded to a category 3 hurricane 12 hours later at 0000 LST on 13/11/07, as a further period of intensification lowered surface pressure to 944 hPa and increased wind speed to 54 m s^{-1}. Central pressure was lowered by adiabatic warming having a positive feedback on the rest of the circulation, since lower surface pressure enabled the low- level air to increase its equivalent potential temperature. This allowed for lower pressures in the eye wall which accelerated the inflow of moist air and increased the release of latent heat. The MODIS image for 1200 LST on 12/11/07 (Figure 4.5a) showed Sidr was becoming a developed hurricane, with a newly developed eye at (11° N, 90° E). A distinct spiral nature became clear due to increased centrifugal force at the centre, as surface winds became stronger. The intensification of Sidr is supported by the development of an eye, a well structured eye wall containing developed convective thunderstorms, the development of more organised and intense spiral rain bands to the northwest, and the marked increase of cirrus around the outflow regions in the stratosphere. The relatively clear sky around Sidr's periphery indicates the effect subsiding air in the outflow regions had on drying the atmosphere.

These features are identifiable in the SSMI 85 GHz analysis image for 2248 LST on 12/11/07 (Figure 4.5b) which shows considerable hurricane intensification compared to its predecessor (Figure 4.3b). The formed eye of Sidr is visible as an area of sparse low-level cloud, or clear sky with a brightness temperature of 255 K, the same as for ocean waters (low-level cloud is often common in the eye). The eye wall is distinguishable as a concentric ring of deep convection, which is better defined than in the MODIS image (Figure 4.5a). The extent of deep convection in the northern inflow region had grown since 1200 LST on 11/11/07, and was a significant driver in the deepening of Sidr's central pressure. An area of low-level precipitable cloud continued to flow towards the centre from the south, and this region did not yet host intense spiral rain bands like those of the northern part of the cyclone. Indeed, it appeared only the upper northeast quadrant showed signs of developing deep convection. The southern quadrant remained either free of convection (shown as light blue in Figure 4.5b) or contained liquid precipitation, with few incidences of convective clouds. Although, as is shown by the TRMM Microwave Imager (TMI) 85 GHz colour composite image (Figure 4.6) this was not entirely the case.

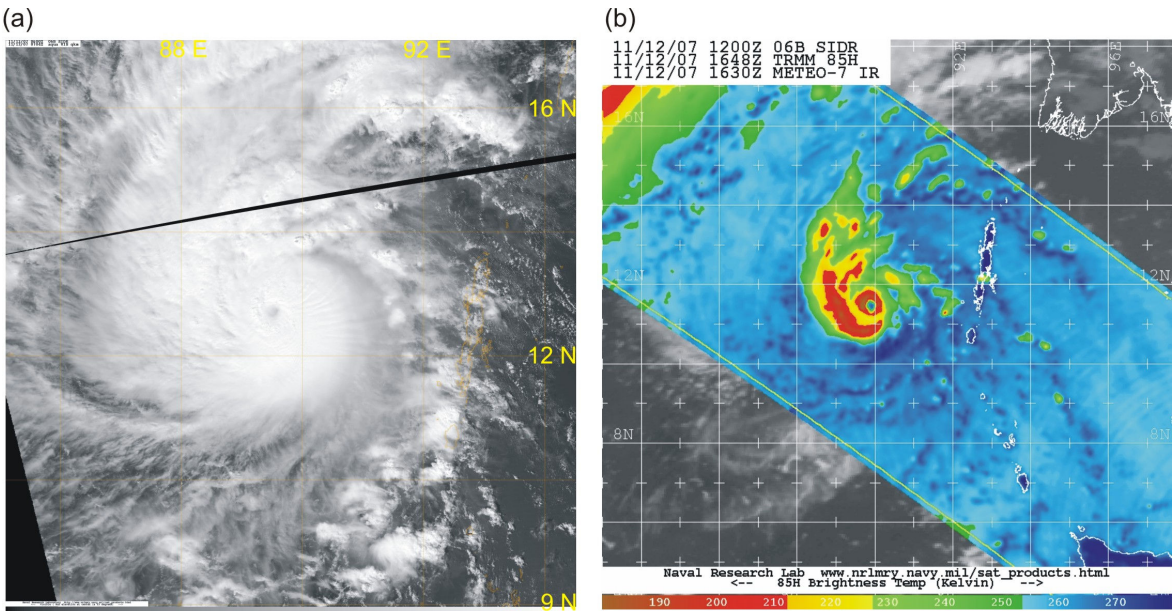

Figure 4.5: (a) MODIS 250 m resolution image for 1200 LST on 12/11/07, and (b) 85 GHz horizontal polarisation SSMI image for 2248 LST on 12/11/07, showing a developing eye, eye wall, and enhanced convective region indicating the intensification of Sidr (Navy/NRL Tropical Cyclone Page 2007).

One advantage of the TMI colour composite image is that it combines the selected horizontal, vertical, and Polarization Corrected Temperature (PCT) images into one. This is particularly useful for identifying features that may be missed in one plane but shown in another, and collating them into one image. There is also the added benefit of identifying intensification and decay of cyclones by examining the extent of 'red' area coverage change (representing deep convection) over time. Such a case was identified at this time in Sidr's development. While it appeared in the SSMI image that there was no deep convection in the northeast and southeast quadrants, but rather ice particles (Figure 4.5b), the colour composite actually showed two regions of deep convection from the southern inflow of the cyclone. Some smaller convective cells were also present in the southern inflow region associated with the intensifying organised spiral bands. Furthermore, the composite shows the northern extent of convection was much more expansive than the SSMI image recorded.

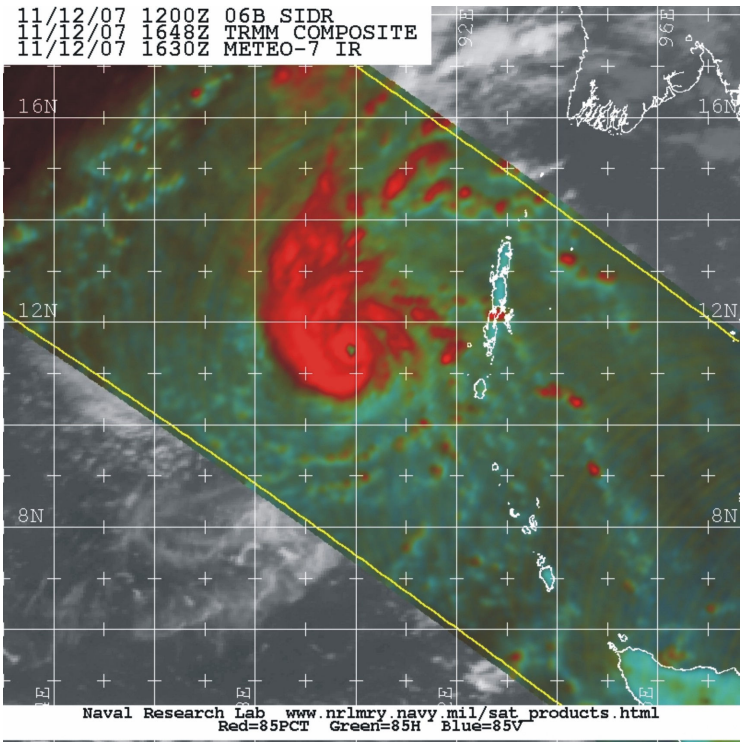

Figure 4.6: TMI 85 GHz colour composite for the same time as in Figure 4.5b. Note the differences between this and Figure 4.5b, here the extent of deep convection (red) is greater than the SSMI horizontal plane image. Sidr appears as a well developed hurricane, with a well organised eye wall, and developing spiral bands (Navy/NRL Tropical Cyclone Page 2007).

4.2.2 Maturity

Over the course of the evening of 12/11/07 to the morning of 13/11/07, Sidr went through a phase of rapid deepening, with central pressure falling 19 hPa in 6 hours. There were a number of factors influencing this deepening. Firstly, a surface pressure analysis for 1200 LST on 13/11/07 (Figure 4.7) showed significant synoptic scale features affecting Sidr. These features were a ridge of high pressure extending over India, and a northeasterly flow over Bangladesh and the northern Bay of Bengal. These features influenced the low-level circulation and directed boundary layer air from the coast of India and Bangladesh towards Sidr's convergence zone. The presence of an anticyclone forced air to the south along the western extent of Sidr's feeder bands, and this eventually steered Sidr northeastwards over the course of the next two days. Another influence was a more favourable upper-level flow that enhanced mid-tropospheric lifting and convective development. A 200 hPa analysis image for 1200 LST on 13/11/07 (Figure 4.8) showed an upper-level westerly trough of divergent air that acted to drive a pressure decrease in the lower-troposphere, and remove the moist rising air from the system. The development of this trough was an important factor in driving further large scale lifting. By 1200 LST on 13/11/07, Sidr was in its

mature phase and had reached category 4 status, with a central pressure of 937 hPa, eye radius of 9 km, and sustained wind speed of 59 m s^{-1}.

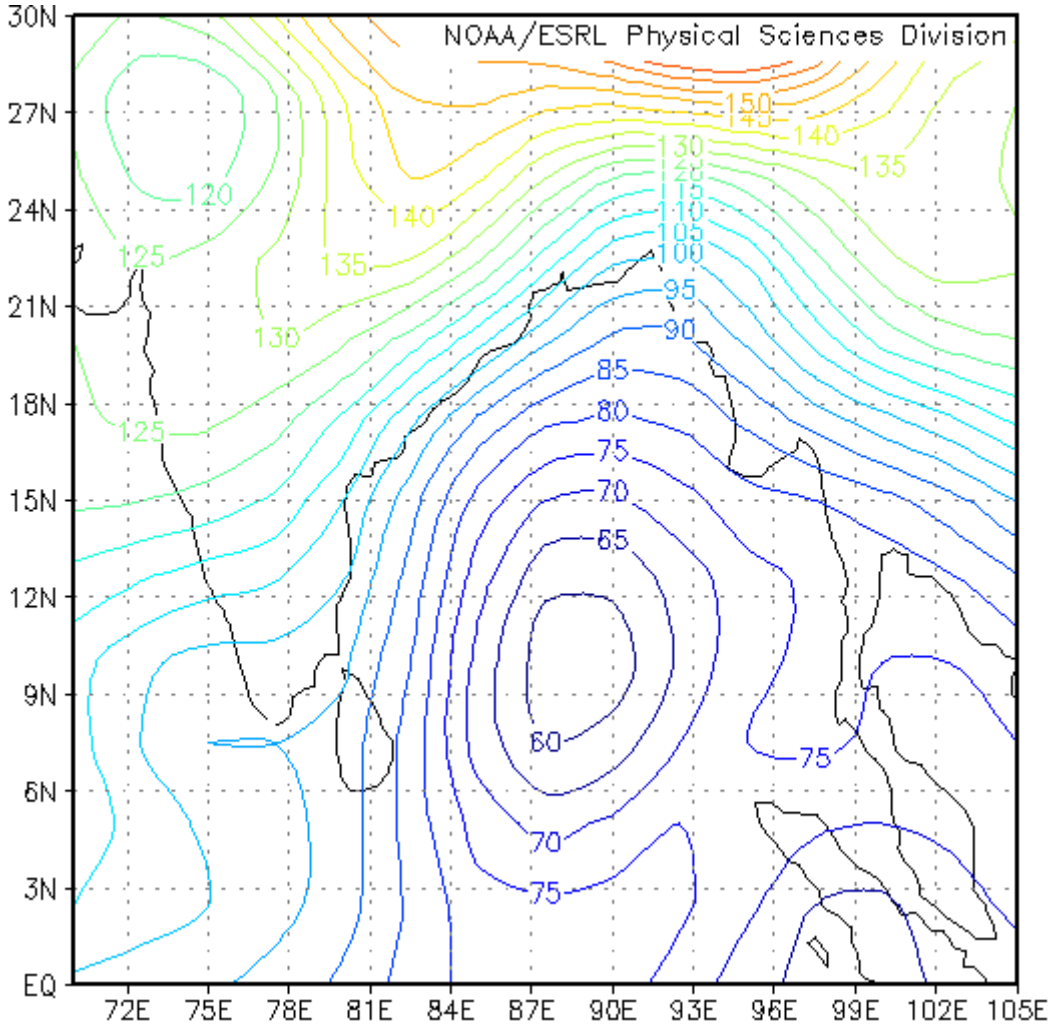

Figure 4.7: NCEP/NCAR surface synoptic analysis for 1200 LST on 13/11/07. Minimum central pressure was observed to be 957 hPa, but JTWC *best track* data recorded observed pressure to be 937 hPa. To obtain a pressure value in these images, 900 hPa is added to the indicated contour value (NCEP/NCAR Reanalysis dataset).

Over the next 18 hours to 0600 LST on 14/11/07, Sidr remained in a steady-state as a category 4 cyclone and held a bearing of 350°, with a translation speed of 3.6 m s^{-1}. The centre was located at (14° N, 89° E) and the JTWC's *tropical cyclone warning number 5* predicted landfall in the vicinity of Calcutta. The observational data for those 18 hours revealed that Sidr maintained a constant surface wind speed and central pressure of 59 m s^{-1} and 937 hPa respectively, yet there was an expansion of Sidr's eye radius from 9 km to 37 km (Figure 4.1).

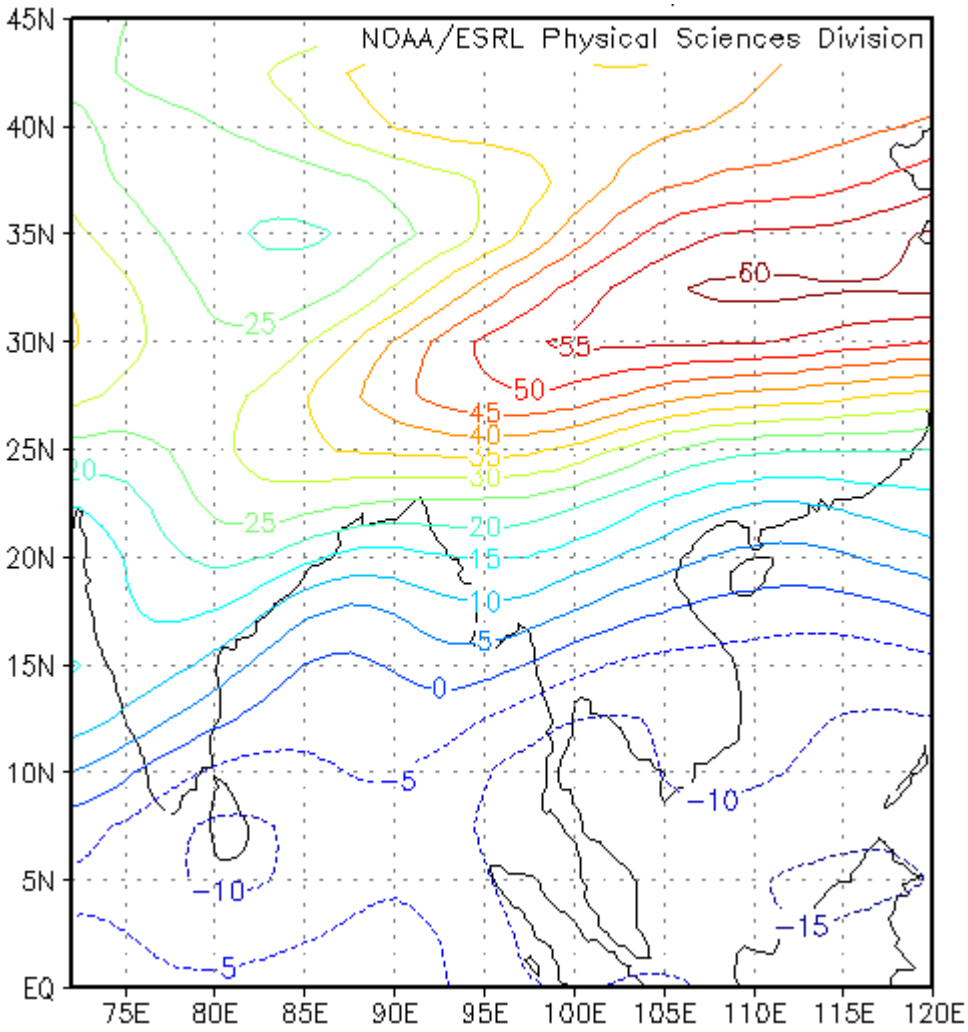

Figure 4.8: NCEP/NCAR 200 hPa horizontal *u* wind (west to east wind component in m s^{-1}) analysis chart for 1200 LST on 13/11/07. The development of an upper-level westerly trough over the Bay of Bengal aided the intensification of Sidr through divergence aloft driving a pressure decrease through the lower-troposphere. Note that negative numbers represent an easterly wind, and positive numbers a westerly wind (NCEP/NCAR Reanalysis dataset).

The changes that occurred to Sidr's structure between 13/11/07 and 14/11/07 are shown in Figures 4.9a and 4.9b. Figure 4.9b indicated that the northeast quadrant had a well organised convective spiral rain band, with a weaker band in the opposite quadrant. For the first time, Sidr showed a large axisymmetric component supporting storm maturity. Axisymmetric is defined as being symmetric about an axis of rotation (Anthes 1982). In this case, a horizontal line through the centre of Sidr would reveal perfect symmetry of the eye and eye wall regions. The eye wall in Figure 4.9b had developed significantly from that in Figure 4.9a, which supported intensification driven by thunderstorm activity in this region.

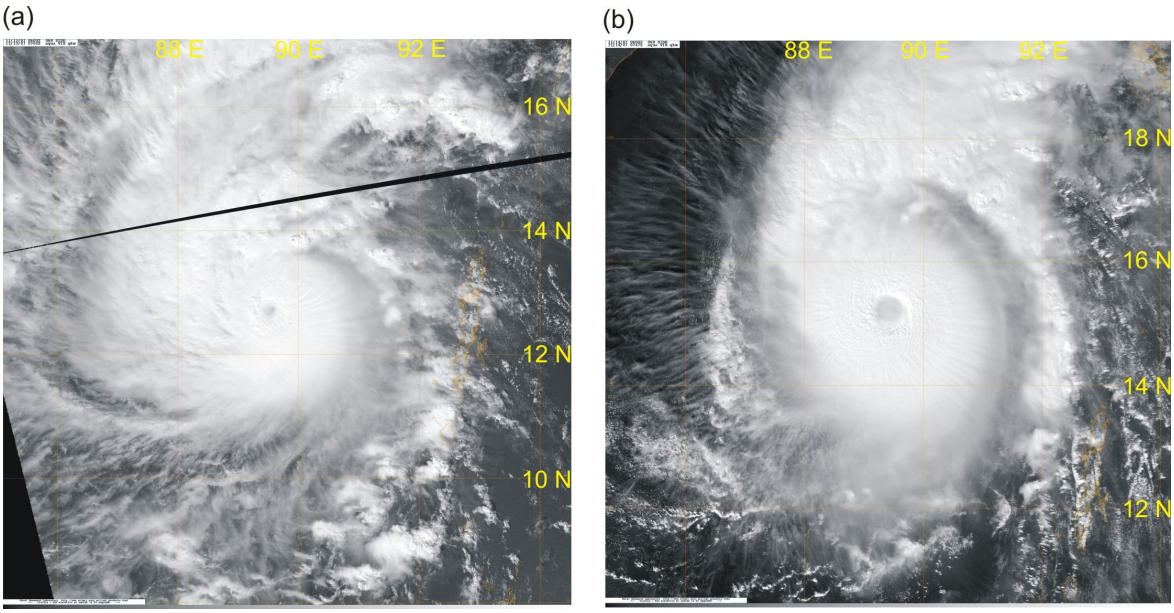

Figure 4.9: MODIS 250 m resolution satellite imagery showing the structural change of Sidr over 24 hours from (a) 1304 LST on 13/11/07, to (b) 1347 LST on 14/11/07. The system had translated approximately 2° north-northeast during this time period. There had been extensive growth of the eye wall and a major spiral rain band in the northeast quadrant. Most of this structural change had occurred from 0600 LST on 14/11/07, as Sidr maintained steady pressure and winds from 13/11/07 until that time (Navy/NRL Tropical Cyclone Page 2007).

Sidr went through another phase of intensification sometime between 0600 LST on 14/11/07 and 0000 LST on 15/11/07, which was sufficient for it to become the second and final category 5 cyclone of the 2007 northern Indian Ocean cyclone season. At 0000 LST on 15/11/07 minimum central pressure had fallen to 918 hPa the lowest Sidr would record, eye radius had contracted from 37 km to 18 km, and the maximum sustained wind was 140 knots (72 m s^{-1}). This intensification was supported by the sensor data over this time period (Figure 4.10a and 4.10b), which showed the contraction of the eye, and a growth of the eye wall. According to the JTWC's *tropical cyclone warning number ten*, the eye was located at (16° N, 89° E), the storm itself moving due north at 4.6 m s^{-1}. Landfall was now forecast 100 nautical miles (185 km) west of Calcutta. During the next 12 hours, Sidr made a 10° shift to the northeast, and increased its translation speed to 7.7 m s^{-1}. Such a shift is not uncommon for cyclones in this region and is often the result of steering from an upper-level trough, which was the case for Sidr (not shown). This shift resulted in landfall predictions being slightly inaccurate.

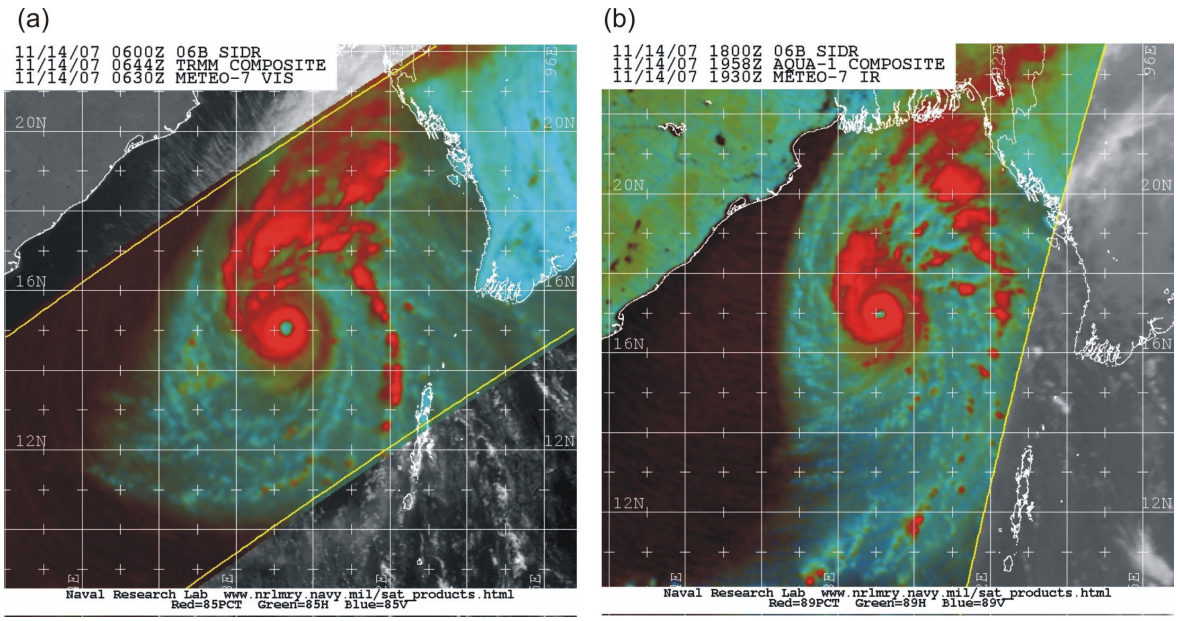

Figure 4.10: (a) the TMI 85 GHz colour composite for 1244 LST on 14/11/07, and (b) the Aqua EOS 89 GHz colour composite for 0158 LST on 15/11/07. The eye contraction is shown by the latter image, which indicates intensification and a pressure decrease (Navy/NRL Tropical Cyclone Page 2007).

The actual landfall occurred somewhat further east of the forecast, in the low-lying Bangladesh delta district of Khulna, near the settlement of Barguna, at about 1800 LST on 15/11/07. Sidr made landfall as a category 4 cyclone with maximum sustained surface winds of 67 m s^{-1}, and a central pressure of 926 hPa. The associated storm surge in most parts of this low-lying delta was in the order of 16 feet (5 m). It was fortunate that the storm lost intensity before landfall, and that people were evacuated promptly or the death toll could have been much higher.

4.2.3 Decay

There were a number of processes that led to the rapid decay of Sidr soon after it made landfall. Firstly, Sidr lost its source of heat as it moved over a cooler land surface, leading to a weakening of thunderstorms within the eye wall. This resulted in a decoupling between the lower- and upper-troposphere and a central pressure rise, which assisted disintegration of the eye wall. Secondly, the source of water vapour from the ocean was removed, and the consequent lack of latent heat release could not maintain strong thunderstorms in the eye wall. Finally, the increased surface roughness retarded the surface wind speed which led to a significant intensity decrease. These effects are evident in Figures 4.1 and 4.2, which show a marked fall in maximum sustained wind speed, a rise in central pressure, and decay of Sidr's eye at the approximate time of landfall.

4.3 Precipitation

High rainfall is one of the major hazards associated with a tropical cyclone. Studying precipitation rates for a cyclone gives insight into its structure and intensity. A selection of TRMM and Flight 16 (F-16) sensor images showed a number of interesting features and significant changes during Sidr's life cycle. Firstly, during the development phase at 2152 LST on 13/11/07, a number of isolated intense convective cells were converging towards the developing centre (Figure 4.11a). The precipitation intensities of these cells were 15–20 mm/hr, matching that of the main convective band at the centre. This is quite normal for an intensifying cyclone. Secondly, during maturity at 0751 LST on 14/11/07 (Figure 4.11b) significant precipitation and cyclone intensification had occurred. This was indicated by a number of structural developments. For example, a well developed eye of light precipitation (5 mm/hr), and an eye wall of heavy precipitation (30 mm/hr) indicated structural development. In addition, a significantly sized convective zone to the north of precipitation intensity 15–20 mm/hr represented a squall line. Finally, an indication of the dynamical change that these systems can undergo is shown in Figure 4.11c. Indeed, a TRMM image at 1244 LST on 14/11/07, 6 hours later, showed a considerable decrease in precipitation rate at the eye wall. Further changes were also evident to the north, as the extent of the squall had decreased, but the spiral rain band to the east had actually intensified.

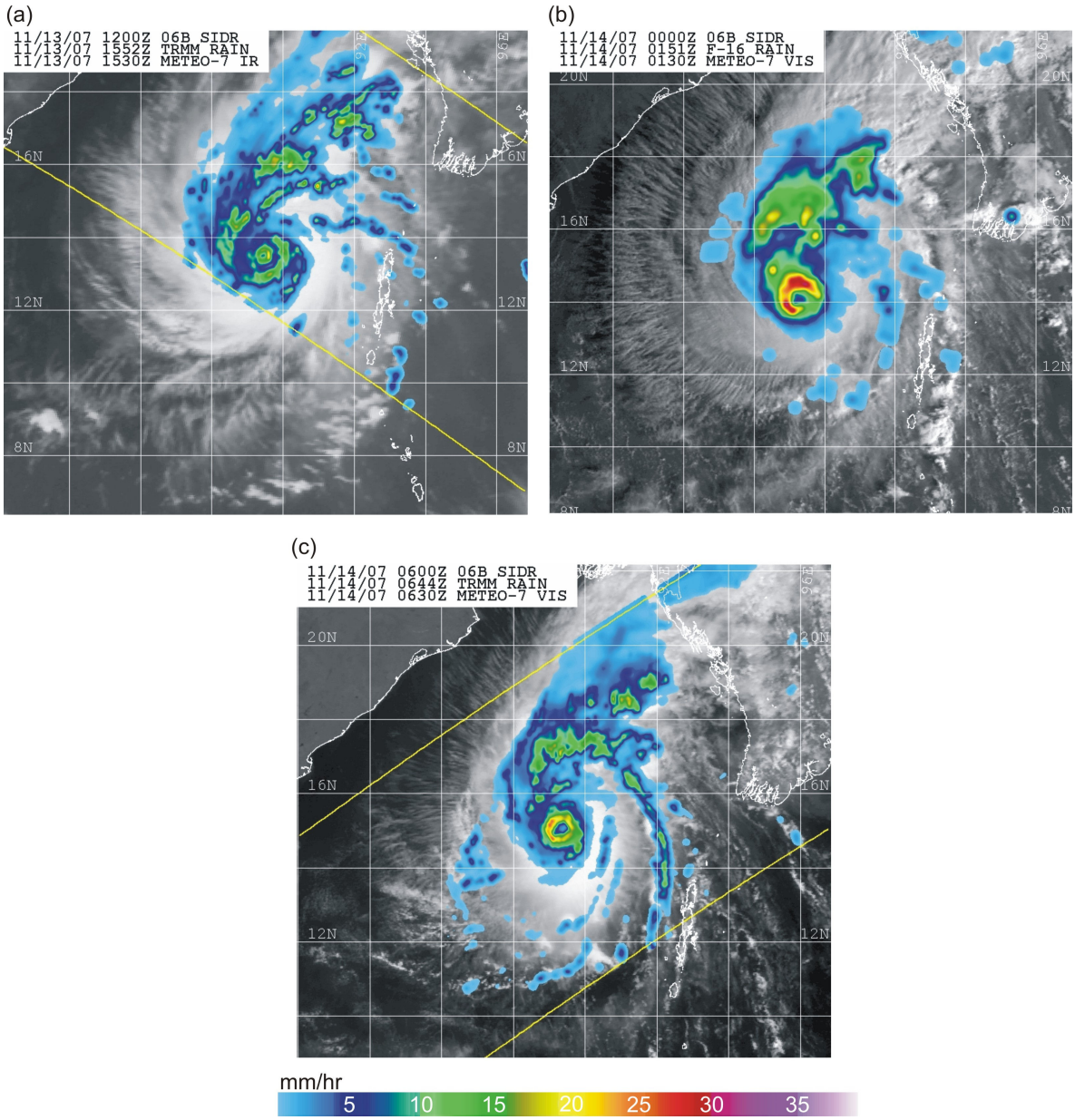

Figure 4.11: Satellite precipitation measurements at (a) 2152 LST on 13/11/07 during the development, (b) during maturity at 0751 LST on 14/11/07, and finally (c) 6 hours later at 1244 LST on 14/11/07, indicating the dynamic change in rainfall intensity that can occur in a short time frame (Navy/NRL Tropical Cyclone Page 2007).

4.4 Cyclone Sidr's track

Figure 4.12 shows the life cycle of Sidr represented by JTWC *best track*, from its classification as a tropical storm, to its dissipation at 0000 LST on 16/11/07. It is interesting to note that Sidr skipped a category in the Saffir-Simpson intensity scale, increasing from a category 1 to a category 3 cyclone at 0000 LST on 13/11/07. This supports the first period of rapid deepening shown in Figure 4.1. The second and final phase of deepening shown in Figure 4.1 was the peak of maturity when Sidr reached

category 5 status shortly before landfall. As previously stated, Sidr's bearing was consistently between 350° and 360° throughout the duration of its mature stage.

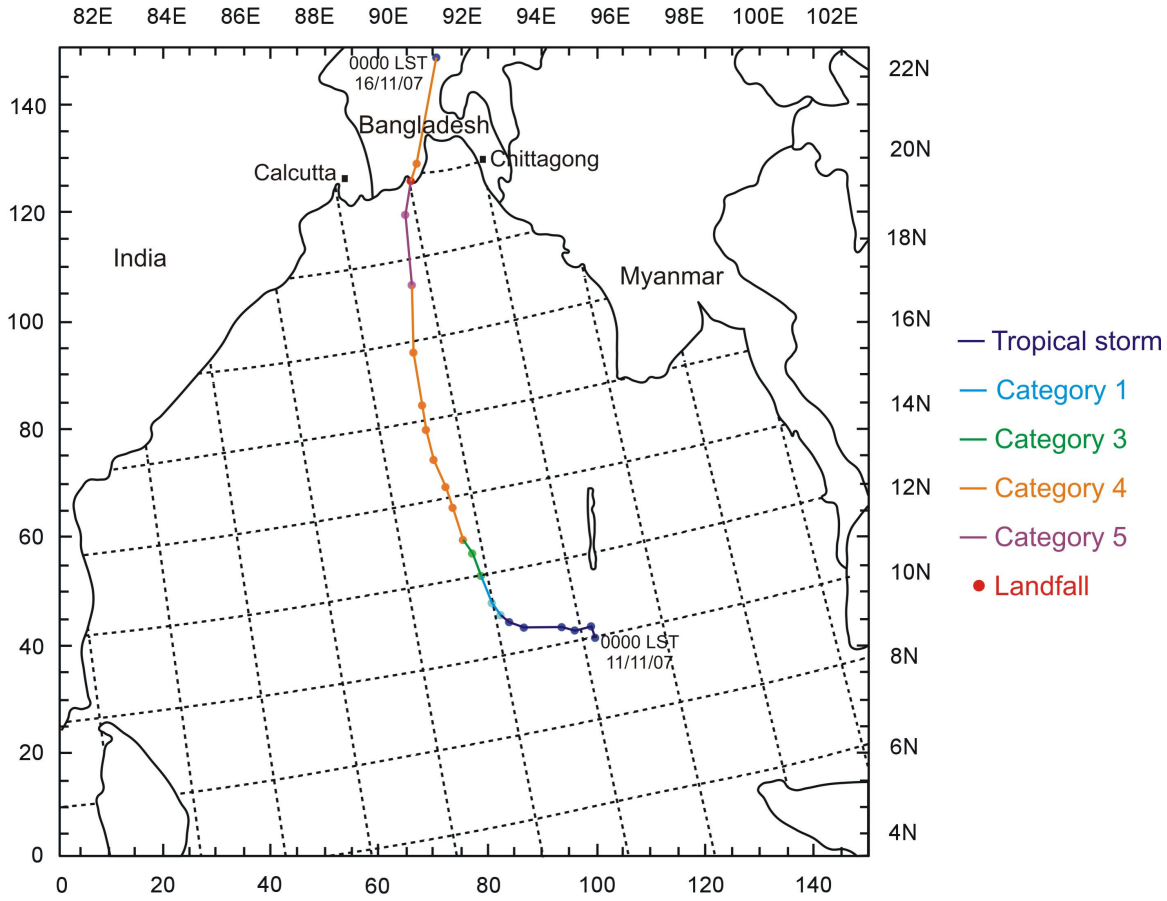

Figure 4.12: JTWC observed *best track* of cyclone Sidr. Each stage of the Saffir-Simpson hurricane intensity scale is indicated by the colour of the circle and line. Cyclone track is plotted every 6 hours beginning at 0000 LST on 11/11/07, and ending at 0000 LST on 16/11/07. Landfall of Sidr is marked by the red circle.

4.5 Conclusion

In conclusion, cyclone Sidr was the second category 5 cyclone of the northern Indian Ocean 2007 hurricane season, which made landfall over Bangladesh at 1800 LST on 15/11/07, claiming the lives of 4,234 people.

Sidr developed from the organisation of deep convective clouds present in a perturbation of a low-level circulation southeast of the Andaman Islands. Sidr gradually intensified towards maturity from latent heat release throughout the troposphere, and assistance from an upper-level westerly trough. Decay was inevitable as Sidr eventually made landfall because the supply of moisture from the ocean was removed, and dry air was input into the lower- and middle- troposphere.

Sidr displayed structural characteristics common to that seen in other hurricanes, and as described by texts such as Anthes (1982). In the development stage, the intense rotation and organisation of deep convection led to the development of an eye, and eye wall respectively as forces within the hurricane environment intensified. During the mature stage, other significant features were the presence of a large squall line to the north of the eye, and an impressive spiral rain band to the east. Sidr also displayed a pronounced axisymmetrical component. Finally, as Sidr tracked over land a typical disintegration of cyclone structure took place. The cyclone became increasingly asymmetrical before the eye and eye wall disintegrated completely. Sporadic cells of convection marked the remnant cyclone.

Naturally, any study of a tropical cyclone event can be limited by a lack of observational data, especially in the northern Indian Ocean region. There is a lack of advanced observational equipment in this region, which must be addressed if further studies are to be undertaken. Indeed, this study relies heavily upon remotely sensed data which can be unavailable at times due to the nature of such methods. Fortunately some good data were available at the most important times of this event. Every effort was made to ensure an accurate, representative coverage of the dynamic evolution of this event.

Chapter 5

Sea surface temperature experiment

5.1 Introduction

Pielke (1990) stated that, as one of five controls on tropical cyclone development, a warm ocean surface is necessary. As stated in Chapter 2, sea surface temperatures greater than 26 °C penetrating to a depth of at least 60 m are required for genesis. It is well known that intensification of tropical cyclones occurs as a result of latent heat release from a warm ocean, which drives condensation (Gray 1982). When temperature falls over the sea surface, the amount of energy released as latent heat declines, so that the deep convection required for a cyclone to intensify cannot be sustained. This is why cyclones often decay over cool waters or land surfaces, when the warm moisture source of energy is removed. To test this theory, an experiment named SST (see Table 3.1 in Chapter 3) was formulated. This involved a constant sea surface temperature value of 10 °C being initialised within the NCEP/NCAR reanalysis dataset. The objective of this experiment was to examine the influence of sea surface temperature on tropical cyclone intensity, energy exchanges, life cycle, and structure. This experiment also tested the ability of WRF for coupling ocean-atmosphere processes.

5.2 Initialisation and development

The experiment SST, was initialised at the end of Sidr's tropical storm phase, and slightly before it was upgraded to a tropical cyclone. A comparison between JTWC *best track* and WRF simulated cyclone central pressure (Figure 5.1) indicates that the initial (0-hour) forecast of central pressure was quite accurate — only 4 hPa higher than observed central pressure. The effect of cool sea surface temperature on the cyclone environment became evident into the forecast as, while Sidr was observed to deepen significantly, simulated pressure slightly increased and the storm did not intensify. This is reflected in Figure 5.1 at forecast hour 36, as the model recorded a minimum pressure of 1008 hPa, compared to the observed value of 937 hPa. Having set sea surface temperature to 10 °C in the simulation, the required heat and moisture source from the ocean that drives tropical cyclone development was removed. Without latent- and sensible heat, and moisture from the underlying ocean, the boundary layer air converging towards the centre of low pressure has

less potential to be converted into kinetic energy (Ahrens 2007). Thus in this case, cyclone intensification was inhibited.

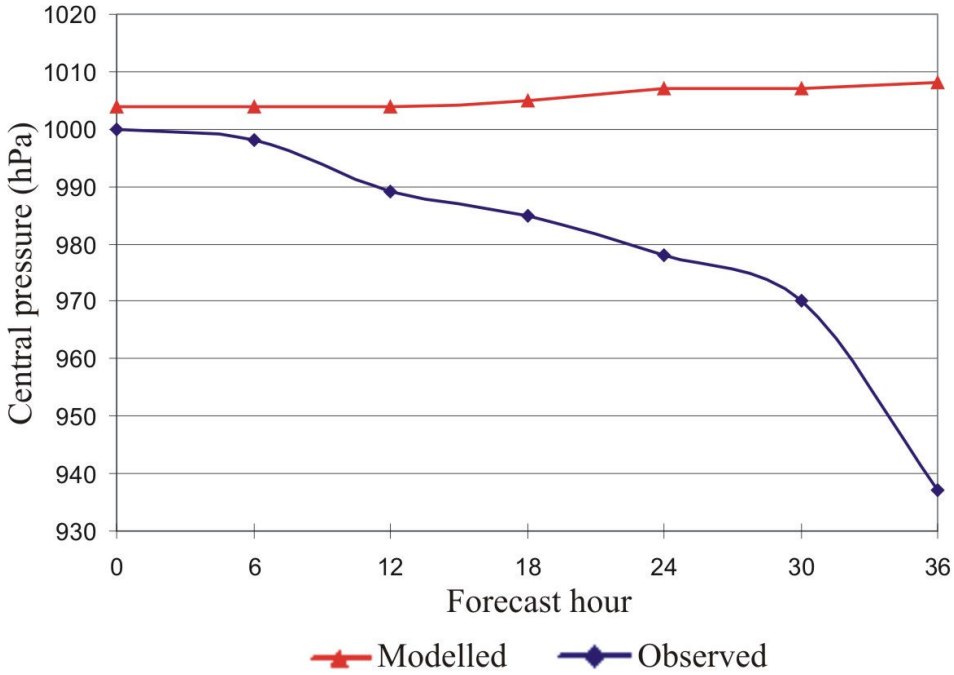

Figure 5.1: Comparison of the trend in modelled and observed central pressure for the selected forecast period (0600 LST on 11/11/07 to 1800 LST on 13/11/07). The effect of cooler than required sea surface temperature for tropical cyclone formation is evident, with the simulated central pressure increasing slightly over the forecast while the observed pressure is falling rapidly during intensification.

5.3 Synoptic life cycle

Simulated synoptic charts for this forecast period reflect the changes to Sidr under an altered sea surface temperature environment (Figure 5.2a-d). The initial forecast (not shown) had a warm pool of 28 °C north of the disturbance; and the remaining ocean was between 26–28 °C. After 6 hours into the simulation, the surface air temperature at the centre had decreased significantly to 14 °C (Figure 5.2a). As radius increased from the centre of the weak circulation, temperature rose to about 18 °C. Air temperatures over the remaining ocean were in the order of 20–24 °C, only a small warm pool of 26 °C remained to the north. At forecast hour 12 (valid at 1800 LST on 11/11/07) a significant area of the circulation of air temperature between 10–12 °C was evident (Figure 5.2b). A warm core was simulated, but it was not overly warm (12–14 °C). It would be reasonable to conclude that tropical cyclone structure was still simulated, although due to cooler sea surface temperature the intensity and temperature of the cyclone was not normal. After 24 hours of simulation (Figure 5.2d): the forecast being valid at 0600 LST on 12/11/07, air temperature

had fallen to 10 °C at the centre. The remaining ocean ranged from 12–16 °C. Winds were mainly light, around 5 m s^{-1}; and the circulation had almost entirely dissipated.

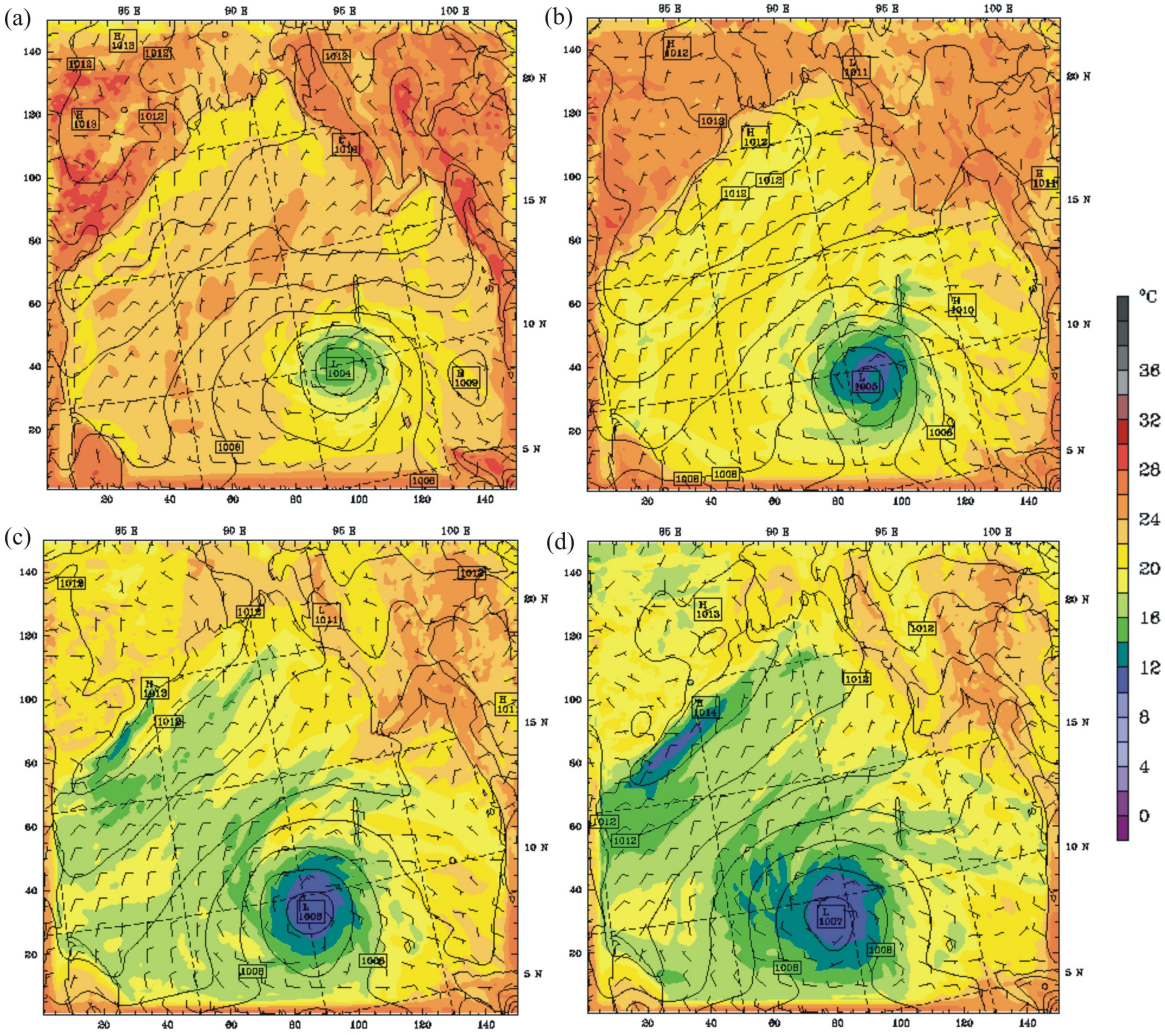

Figure 5.2: Time evolution of simulated synoptic situation including surface air temperature for experiment SST, at (a) 1200 LST on 11/11/07, (b) 1800 LST on 11/11/07, (c) 0000 LST on 12/11/07, and (d) 0600 LST on 12/11/07. A gradual cooling around the cyclone centre was evident, in association with the weakening pressure gradient. The simulations are for model forecast hours 6–24. The contour interval for sea level pressure is 1 hPa, and 2 °C for temperature. Latitude and longitude are shown on the right and top axes respectively and grid points for the model grid are marked in intervals of 5 along the bottom and left axes.

5.4 Potential vorticity and upper-level airflow

As previously stated, the impact of sea surface temperature on decoupling the air-sea environment is well known. Such affects are evident in this experiment, as seen in the upper-level PV and airflow plots (Figure 5.3a-d). Firstly, over the first 12 hours of simulation, an upper- level anticyclone was forming, and after 24 hours this had weakened and was replaced by cyclonic flow aloft. This indicates a lack of adequate anticyclonic outflow for the cyclone had developed. Finally, the wind flow at 300 hPa showed two distinct changes. The first of these was the strengthening of a westerly jet stream across the

northern region of the Bay of Bengal. This would enhance cyclone outflow, however, rather than oppose it. So for the cyclone to have dissipated a negative change was required. Crucially, the second change, diminishing rotational flow after 24 hours, was what contributed to the dissipation. The impact of latent heat decrease from cooler sea surface temperature meant that the transport of heat and energy to the upper- level ceased. Without this heat transport, the coupling between the surface and upper-level was effectively cut off. As a result, the strong rotational circulation normally seen in mature hurricanes at upper-levels was not apparent. The lack of upper-level rotation effectively meant that the cyclone had no influence on the perturbation of the westerly wind field.

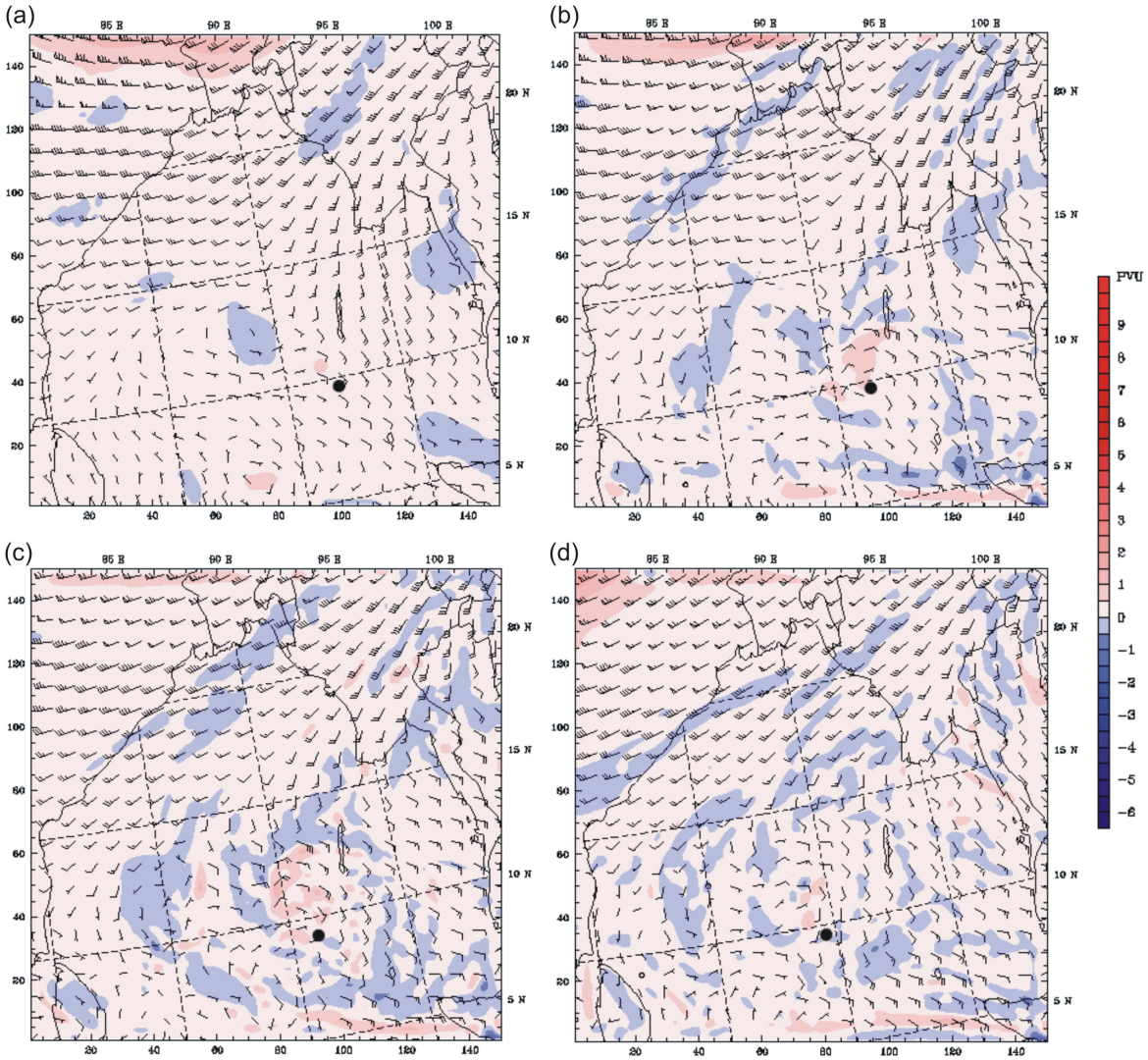

Figure 5.3: Time evolution of 300 hPa simulated potential vorticity measured in potential vorticity units (PVU) for experiment SST at (a) 0600 LST on 11/11/07, (b) 1200 LST on 11/11/07, (c) 1800 LST 11/11/07, and (d) 0600 LST 12/11/07. Two features are evident over time. The first was the development of cyclonic PV indicated by blue PVU; and the second was a decoupling with the lower-levels indicated by diminishing rotational flow over the cyclone region after 24 hours. The simulations are for model forecast hours 0–24 (the 18-hour forecast has been omitted). The position of the surface cyclone is indicated by the black circle. Note that 1 PVU is equal to 1.0×10^{-6} m^2 s^{-1} K kg^{-1}.

5.5 Reflectivity (precipitation intensity)

Radar reflectivity is a measure of the efficiency of a radar target intercepting and returning radio energy. It depends upon the size, shape, aspect, and dialectic properties of a target (American Meteorological Society, Glossary of Meteorology n.d.). In the study of the atmospheric sciences, radar measures precipitation intensity and location. The unit of measurement is the decibel (dBz). Reflectivity is especially effective for locating convective cells in the tropical cyclone environment, and identifying different structural features.

The surface reflectivities (Figure 5.4a-d), show the degeneration of Sidr's structure in less than 24 hours, which can be attributed to cool sea surface temperature. The forecast at 6 hours into the simulation (Figure 5.4a), valid at 1200 LST 11/11/07, was similar to the observed 89 GHz Aqua EOS image for the same time (see Figure 4.3b in Chapter 4). There was an area of moderate convection (15–40 dBz) to the north, similar to what was seen in the observed case, although the simulated convection was slightly weaker. The model predicts the developing rotational structure well at this time, but failed to simulate the lighter liquid precipitation observed (see Figure 4.3b in Chapter 4). An unexpected result occurred 12 hours into the forecast (Figure 5.4b). A greater area of moderate convection developed (15–35 dBz), and while some weakening took place further from the centre, a 5 km area of deep convection (45 dBz) not previously seen appeared in the northern inflow region. No significant structural change reflecting increased intensity had occurred, for instance, the development of an eye. This reflects the cool sea surface temperature starting to impact upon development.

The effect of an unfavourable environment for intensification became clear after 18 hours into the forecast (Figure 5.4c). The forecast, valid at 0000 LST on 12/11/07, showed signs of cyclone decay: convective cells were gradually becoming less organised, and precipitation intensities were declining. This is different from the organised tropical cyclone structure of a developing eye, eye wall, and numerous spiral rain bands observed at this time (see Figure 4.3a and 4.5a in Chapter 4). In addition, the southern extent of simulated reflectivity does not reflect the observed precipitation intensity at this time. The forecast showed a wider region of light precipitation intensity (0–10 dBz) to the south. The affect of strong vertical shear, enhanced by cool sea surface temperature was likely to be the cause of these weak and sporadic intensities. The final forecast shown for 0600 LST on

12/11/07 (Figure 5.4d), 24 hours after model initialisation, indicates little change during the past 6 hours, except for the continued decay of precipitation intensity to the north.

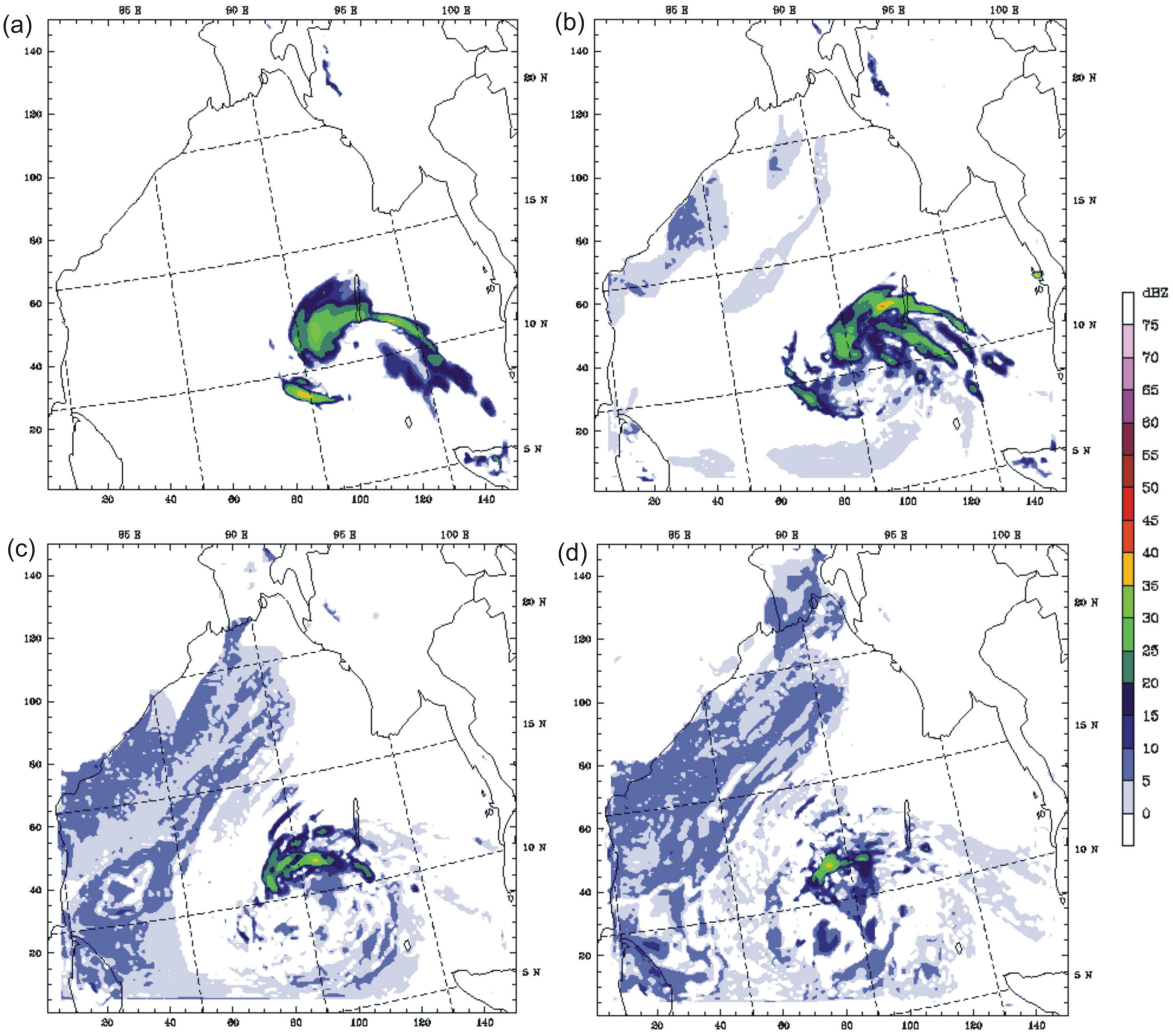

Figure 5.4: Time evolution of simulated radar reflectivity (in dBz) at the surface for experiment SST at (a) 1200 LST on 11/11/07, (b) 1800 LST on 11/11/07, (c) 0000 LST on 12/11/07, and (d) 0600 LST on 12/11/07. Deep convection is indicated by red and moderate convection dark blue to green. Lighter precipitation intensities are shown by light blue to blue. A destabilisation of cyclone structure is evident, a result of sea surface temperature cooling and shear. The simulations are for model forecast hours 6–24.

5.6 Convective available potential energy

Another atmospheric measure that accounts for the failing of the SST experiment to generate a developed cyclone is that of CAPE. CAPE is the amount of potential energy available to accelerate a parcel vertically, and is an indicator of atmospheric instability (American Meteorological Society, Glossary of Meteorology, n.d.). It can be used as a surrogate for atmospheric stability, and indicates the potential for deep convection. As stated, tropical cyclones undergo intensification through deep convective processes when the energy available for that convection is abundant. In this case, by effectively removing

the latent heat source by cooling the ocean, the energy transfer from ocean to atmosphere was diminished. During the simulation, evidence of this energy loss appears in the CAPE forecast (Figure 5.5a-d).

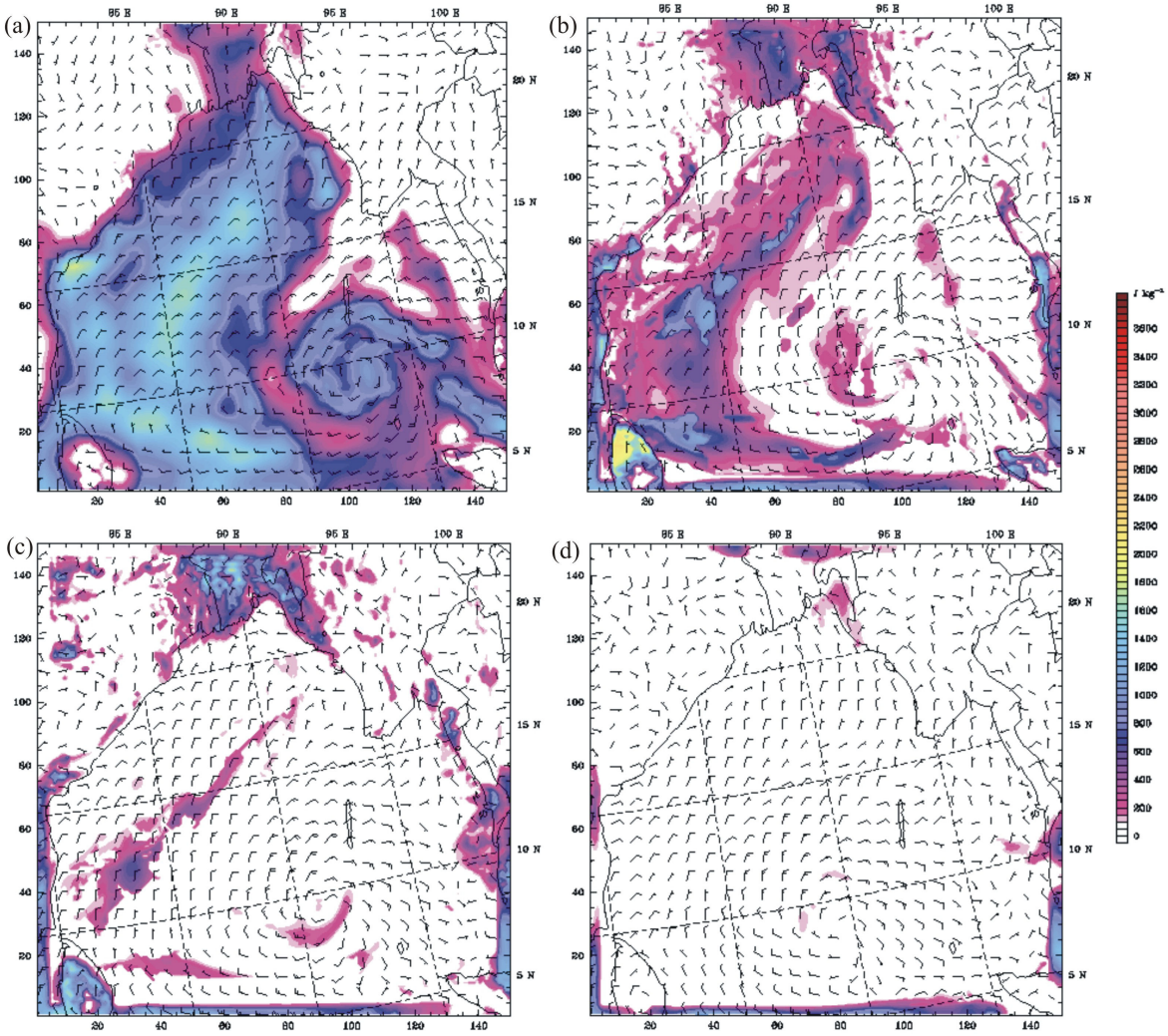

Figure 5.5: Time evolution of simulated CAPE (in J kg^{-1}) for experiment SST at (a) 0600 LST on 11/11/07, (b) 1200 LST on 11/11/07, (c) 1800 LST on 11/11/07, and (d) 0600 LST on 12/11/07. Initially, some energy is available in the cyclone environment to assist convection; and over the next 24 hours that energy dissipates. The simulations are for model forecast hours 0–24 (the 18-hour forecast has been omitted).

The initial forecast valid at 0600 LST on 11/11/07 was indicative of a warm sea environment that was rich in CAPE. The amount of initial energy was minimal, but the forecast reflected the potential for convection. At the circulation centre, CAPE of the order of 600–900 J kg^{-1} was simulated, but it was the regions away from the storm that showed greater amounts (1200–1500 J kg^{-1}) (Figure 5.5a). This is a positive result, as in a warm sea situation an observed disturbance would yield low initial values, with higher amounts of energy for convection away from the centre. As convection is initiated and rotation becomes more intense, convective clouds spiral into the centre and contribute to intensification. After six hours of simulation, however, CAPE had diminished considerably

(Figure 5.5b). Virtually all potential energy had diminished around the circulation itself, and only low values of CAPE (200 J kg^{-1}) were simulated in the northern inflow region.

It is evident that after 12 hours of simulation the impact of cool sea surface temperature had affected CAPE significantly in this environment (Figure 5.5c). The forecast valid at 1800 LST on 11/11/07 indicated low values of CAPE in the order of 200–400 J kg^{-1} northwest of the circulation centre. To the south, CAPE of 200 J kg^{-1} was simulated. Within 24 hours the environment was absent of CAPE, with only trace values simulated near the circulation centre (Figure 5.5d). The reduction of CAPE, and its eventual absence near the circulation core, agrees with the decline in deep convection simulated in the reflectivity forecasts. This illustrates how CAPE is important in the cyclone environment for providing the potential for deep convective development. It also explains why a warm sea surface is required to release latent heat and provide the necessary moisture for convection to be initiated.

5.7 Cyclone structure

Horizontal and vertical fields of wind speed and equivalent potential temperature were used to examine the structure of experiment SST at two forecast times. For the vertical profiles, wind speed and equivalent potential temperature were extracted through the centre of the cyclone at forecast hour 6 (coarse domain location (x, y): 70, 37 to 120, 37), and at forecast hour 18 (coarse location (x, y): 55, 34 to 115, 34). Changes to both variables over forecast time are discussed individually.

5.7.1 Wind speed

Wind speed is an effective way of examining cyclone structure. There were evident changes to the simulated tropical cyclone during the SST experiment, shown by the 6- and 18-hour forecast times (Figure 5.6a-d). At the 6-hour stage, air temperature was still relatively warm across the cyclone environment (Figure 5.2a), and this is reflected in the structure of the radial wind profile (Figure 5.6b). The vertical profile at forecast hour 6 shows signs of a typical theoretical radial wind profile, with a calm eye, and eye wall with greater wind speed. Evidently, the eye wall was not well developed, and only extended to 800 hPa and 660 hPa on the northwest and southeast sides of the storm respectively. Maximum wind speed simulated at this time was 25 m s^{-1}. The circulation vectors on the

vertical profile show two areas of vertical motion around the eye wall. The vertical motion is greater on the northern side of the storm at this stage, which is also consistent with greater precipitation intensity (Figure 5.4a). Also evident was a region of vertical wind shear which appeared at the 820 hPa pressure level and continued aloft to the 400 hPa level.

The forecast at hour 18 was significantly different from the forecast at hour 6. The forecast showed: destabilisation of the eye wall, enhancement of vertical shear, and loss of cyclone structure (Figure 5.6d). At this stage, compared to the observations, an eye wall should have existed, with calm winds at the cyclone centre. Instead, the southeast region of the predicted storm had virtually dissipated, and only the northwest region remained intense in terms of wind speed. The region of calm wind at the centre now extended to only the 680 hPa level. The northern region of maximum wind speed had actually grown in size, although, this is deceiving as enhanced vertical shear was also present at low levels. The enhancement of vertical shear aloft was another feature at this forecast time. The circulation vectors indicated a region of enhanced flow between the 600 hPa and 400 hPa levels. This shear was most likely responsible for inhibiting development of the eye wall to any greater depth in the atmosphere; and certainly was an important factor in the dissipation of the cyclone.

The benefit of using vertical wind profiles in this experiment is evident, as the horizontal wind fields (Figure 5.6a and 5.6c) did not reveal such intimate structural changes. It is clear, from Figure 5.6a and 5.6c however, that the circulation between the two forecast times weakened such that the northerly flow diminished. The extent of no wind to the north and east also increased in size.

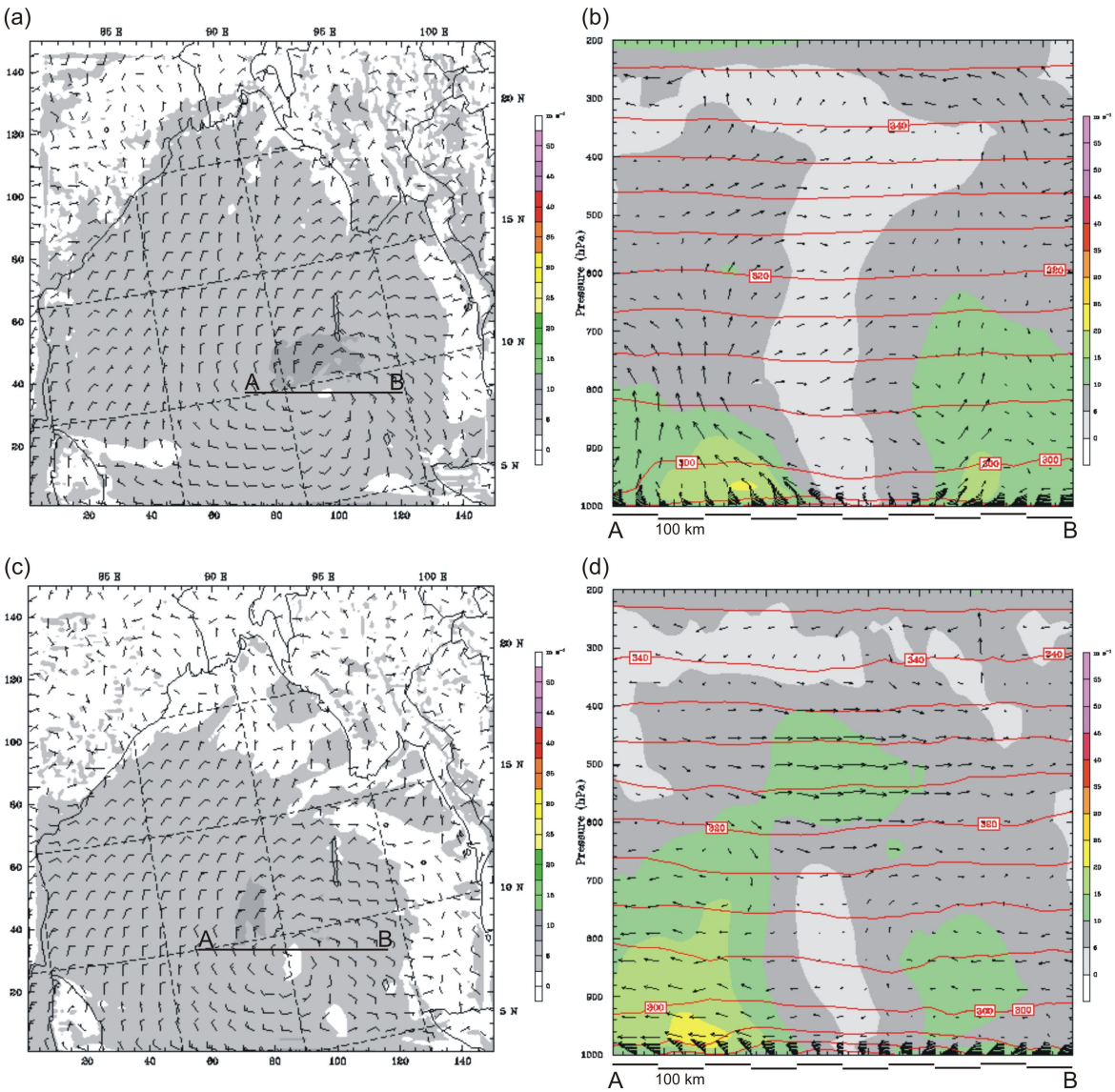

Figure 5.6: Horizontal and vertical wind fields for forecast hour 6 valid at 1200 LST on 11/11/07 (Figure 5.6a and 5.6b), and forecast hour 18 valid at 0000 LST on 12/11/07 (Figure 5.6c and 5.6d). Note the diminished northerly airflow in Figure 5.6c when compared with a slightly more intense rotational field in Figure 5.6a. The cross section at hour 6 showed cyclone structures developing, like a calm eye, and increasing wind speed at the immature eye wall. The situation is quite different at forecast hour 18. The calm region had shrunk, and significant vertical shear was present around 500 hPa. Potential temperature contours are in red, with an interval of 5 K.

5.7.2 Equivalent potential temperature

According to Liu et al. (1997), equivalent potential temperature is a good measure for understanding the thermodynamic structure and origin of different air masses. This is because it represents the static energy of air parcels and is conserved in a non-viscous, pseudoadiabatic flow. Essentially the air mass behaves like an ideal fluid experiencing no resistive force as it flows through the atmosphere.

Equivalent potential temperature in the SST experiment indicated a number of important effects on the cyclone environment. Firstly, a vertical cross section of equivalent potential

temperature for forecast hour 6 showed the movement of the PBL air to higher levels on both sides of the cyclone (Figure 5.7b). The vertical uplift on the northern side of the cyclone assisted the inflow of warm PBL air across this region from the centre to the 800 hPa level. This air-sea interaction resulted in an increase in equivalent potential temperature of the surroundings by 6–10 K at the 800 hPa level. The same effect was evident across the southern extent of the cyclone, although this was not as pronounced as the northern case due to the differing intensity of vertical uplift. The nature of the horizontal wind field at the 6-hour stage confirms this (Figure 5.7a). Secondly, quite a distinct difference was observed at the 18-hour stage of the forecast (Figure 5.7d). A southerly PBL flow across the ocean had eventuated from destabilisation of the cyclone, and the impact of a cooler sea surface. This was evident in the change in equivalent potential temperature of the air mass. A shallow movement of PBL air of temperature 320 K was moving towards the north, and rising to around the 940 hPa level. The temperature change resulting from this movement of air was a decrease of about 10–12 K. These changes are also reflected in the horizontal field at forecast hour 18 (Figure 5.7c), as the majority of the lower-troposphere had cooled to 320 K.

While this was a rather shallow air mass change 18 hours into the simulation, its effect was obvious on the lower part of the system. This reflects the role of air-sea interaction in this experiment. Removing the latent heat source by reducing sea surface temperature caused a loss of available energy for condensation in the cyclone environment. The establishment of a cooler southerly airflow across the surface is the result of that destabilisation of the boundary layer, and is reflected by the air mass change in Figure 5.7d.

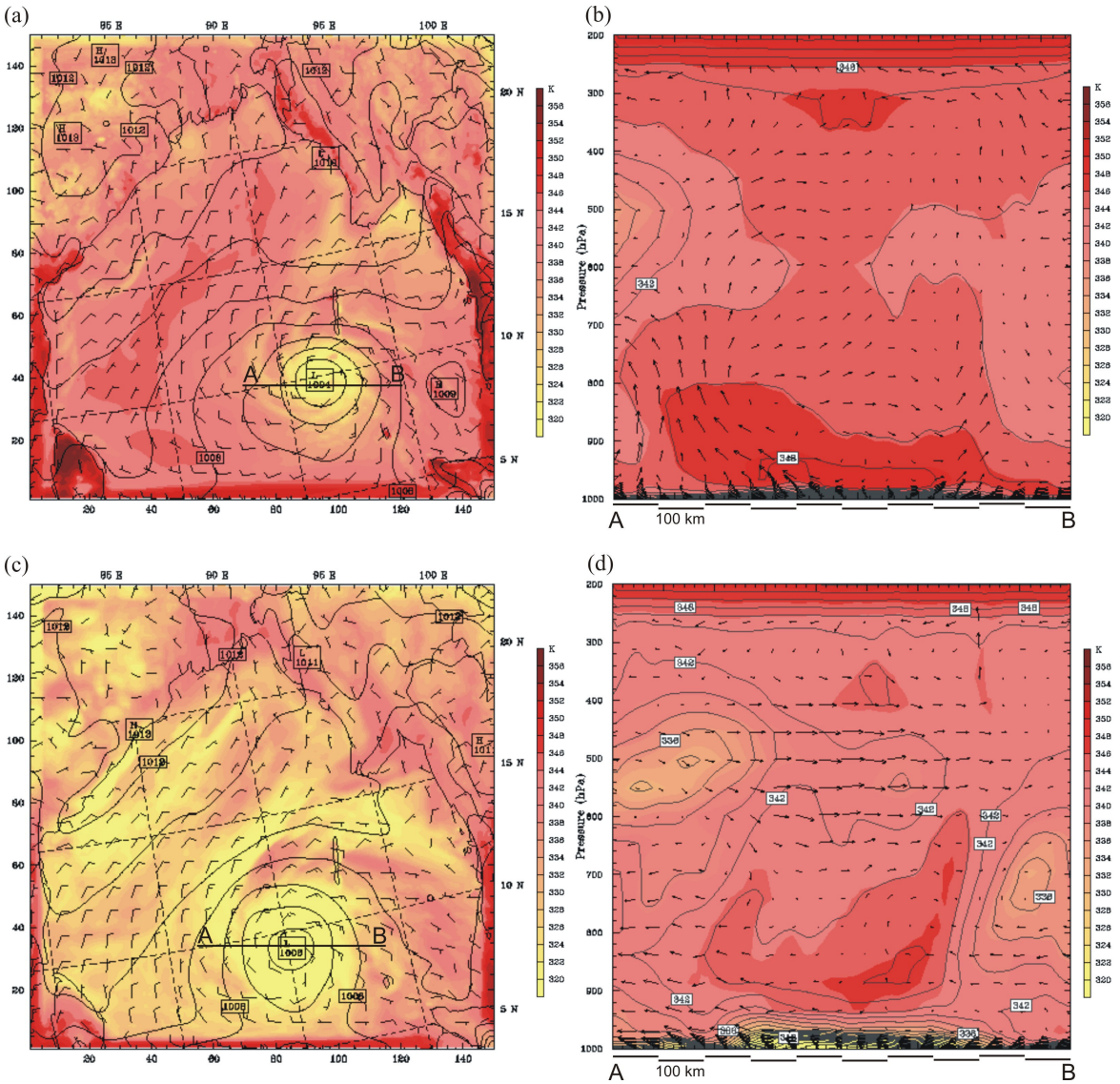

Figure 5.7: Horizontal and vertical equivalent potential temperature fields for forecast hour 6 valid at 1200 LST on 11/11/07 (Figure 5.7a and 5.7b), and forecast hour 18 valid at 0000 LST on 12/11/07 (Figure 5.7c and 5.7d). The change in air mass characteristics over time appears quite evident in the vertical plots: an injection of cooler air at the surface reflects the effect of sea surface temperature. This air mass change was evident on the horizontal plots to: widespread cooling occurs between times. On the vertical plots, equivalent potential temperature contours are in grey. The contour interval is 2 K.

5.8 Conclusion

In conclusion, this chapter has presented the results of an experiment that altered sea surface temperature across the entire model domain. The value of sea surface temperature in the NCEP/NCAR reanalysis dataset was altered to 10 °C, and held constant at that value for the entire simulation period.

Simulations for central pressure, synoptic development, PV, upper-level wind flow, precipitation intensity, CAPE, and horizontal and vertical wind fields, were analysed to

illustrate the impact of changing sea surface temperature in a cyclone environment. All results were in agreement with the preconceived theories surrounding sea surface temperature and cyclone development: if sea temperature is not warm enough, a cyclone will not develop. Simulated central pressure showed that as the forecast progressed, Sidr never really intensified, or matched the observations at the time. Synoptic development showed a destabilisation of the cyclone within 24 hours, and the cooling of surface air temperature. The PV analyses showed that initially an upper-level anticyclone was forming assisting divergence, but after 24 hours this had weakened and was replaced by cyclonic flow aloft. This cyclonic convergence aloft filled the cyclone assisting decay. Precipitation intensities confirmed this decay as deep convection gradually became less intense, and any apparent tropical cyclone structure dissipated within 24 hours. Such dissipation was proven by the reduction of CAPE in the environment. It was shown that as sea surface temperature cooled, the amount of latent heat release diminished, resulting in less energy available for convection. These findings indicate the intimate link between the atmosphere and ocean and how changes at that interface impact upon tropical cyclones. Furthermore, this exercise showed that the model was performing its calculations correctly, and is capable at coupling ocean-atmosphere processes. This is a positive result because how a model treats sea surface temperature and ocean processes is important to the operation of other components in the model, such as boundary layer schemes and CP.

Chapter 6
Initialisation experiment

6.1 Introduction

Forecasting of tropical cyclones remains one of the most challenging problems facing numerical weather forecasters. This is because the complexity of numerical models, and the inability to account for all conditions occurring in nature, means that it is impossible to represent atmospheric events exactly. This constantly creates difficulties when attempting to predict the track and intensity of tropical cyclones. Accurate prediction of tropical cyclone track and intensity from a short initialisation time, around 48–72 hours, is another goal of forecasters. According to Davis and Holland (2007), the forecast of cyclone tracks has improved steadily over the past 30 years due to improvements in the quality of global data available for input. Forecasting intensity, however, remains a long standing problem requiring continued research.

This chapter presents the results of one data assimilation technique that was tested. The objective was to examine the effects of model initial conditions on tropical cyclone track and intensity. Allowing for complexity and the range of inputs that go into a numerical model, the initialisation time was selected as the parameter to change. A number of studies have been conducted in recent times (Davis et al. 2005; Davis et al. 2006; Davis and Holland 2007) that investigated the role of WRF model initialisation time on both track and intensity. The majority of these studies have focused on the North American environment, and few have been conducted using WRF. Those that have used WRF test different data assimilation techniques, so it could be argued that these experiments alter more than one condition. As stated in the methodology, three times from the observed landfall were chosen to initialise the model simulations — 48 hours from landfall (simulation KF_48); 72 hours from landfall (simulation KF_72); and 108 hours from landfall (simulation KF_108) (see Table 3.1 in Chapter 3).

6.2 Cyclone track

There are a number of elements to consider when analysing simulated track forecasts. The first of these is what differences exist between the observed and the simulated track. Goerss (2007) presented an analysis of forecast track error based on latitude and longitude

displacement, and a similar analysis is used for this study. Simulated track positions for the 108 and 72 hour initialisations are first considered at the start of the 48 hour initialisation, so that a direct comparison is provided. Comparing the observed *best track* and each model initialisation track position (Table 6.1), indicates there was deviation from the observed *best track*. Indeed, both latitude and longitude error for all simulations increased progressively with forecast time. Examination of the results at the observed landfall time showed that the predicted cyclone centre positions for the KF_108 and the KF_48 simulations were to the southwest of the observed position. This is supported by Figure 6.1. At landfall, the KF_108 track was in error of the observed by −2.7° and −2.2° latitude and longitude respectively. For the KF_48 simulation, this error was slightly less: −2.5° and −2.1° latitude and longitude. The KF_72 simulation showed a −4.4° error in latitude, which was the furthest south of all predictions, but its longitude error (−2.5°) was similar to the other simulations. The simulated landfall for each case occurred about 6–12 hours later than was observed.

The second important consideration is to examine the behaviour of the predicted tracks to the observed *best track* behaviour, once initial positional errors have been accounted for. A technique devised in this study was to compare the change in modelled cyclone centre latitude and longitude between times; and for the total period. This was then compared to the observed centre deviation (Table 6.2).

There are a number of points to make regarding the behaviour of the observed cyclone. Firstly, the latitude change of the observed cyclone over 13/11/07 and 14/11/07 was less than a degree every 6 hours; but on 15/11/07, it increased to over 1° every 6 hours (Table 6.2). This was consistent with an increase in translation speed indicated in Chapter 4. Secondly, the observed centre remained steady between a few tenths of a degree of longitude: the centre did not deviate more than 0.5° east or west as it tracked. Indeed, Sidr was observed to hold an almost true north bearing from 1800 LST on 13/11/07 until landfall at 1800 LST on 15/11/07. The observed track of Sidr was more forward moving (northward) than side moving (east or westward). The modelled cyclones, however, show a different result in some aspects of their movement behaviour.

Table 6.1: JTWC observed *best track* latitude (lat) and longitude (long) position for the centre of Sidr, and the error from that observed position for each of the model initialisation experiments. If a latitude error is positive then the model centre is to the north of the observed location, and if it is negative is to the south. If a longitude error is positive then the model centre is to the east of the observed location, and if negative to the west. For instance, if the model centre recorded both negative lat and long errors the predicted centre would be southwest of the observed centre. In the date-time column, LF denotes the observed landfall.

	JTWC observed		**KF_108 error**		**KF_72 error**		**KF_48 error**	
Date – Time (LST)	**Lat (° N)**	**Long (° E)**	**Lat**	**Long**	**Lat**	**Long**	**Lat**	**Long**
13/11/07 1800	13	89.6	−0.8	−0.9	−1.2	−0.3	0.1	−0.2
14/11/07 0000	13.7	89.5	−1.5	−0.8	−1.6	−0.5	−0.1	−0.4
14/11/07 0600	14.3	89.6	−1.6	−1.1	−1.8	−1	−1.4	−1.6
14/11/07 1200	15	89.3	−1.5	−1.3	−2.2	−0.9	−1.7	−0.9
14/11/07 1800	15.7	89.3	−1.7	−1.7	−2.2	−1.3	−0.5	−0.7
15/11/07 0000	16.6	89.3	−1.7	−1.8	−2.5	−1.6	−0.9	−0.8
15/11/07 0600	17.8	89.2	−2	−1.8	−2.9	−2	−1.8	−1.3
15/11/07 1200	19.3	89.3	−2.3	−2	−3.7	−2.4	−1.9	−1.8
15/11/07 1800 (LF)	20.9	89.5	−2.7	−2.2	−4.4	−2.5	−2.5	−2.1

Table 6.2: Comparison of observed and simulated change in cyclone centre position every 6 hours for the period 1800 LST on 13/11/07 to 1800 LST on 15/11/07. The total deviation based on the cyclone start and end position is also calculated. Positive and negative values of lat and long are the same as Table 6.1.

	JTWC observed change		**KF_108 change**		**KF_72 change**		**KF_48 change**	
Time period (LST)	**Lat (° N–° S)**	**Long (° E–° W)**	**Lat**	**Long**	**Lat**	**Long**	**Lat**	**Long**
13th 1800–14th 0000	0.7	−0.1	0.5	−0.2	0.3	−0.3	0.5	−0.3
14th 0000–0600	0.6	0.1	0.5	−0.2	0.4	−0.4	−0.7	−1.1
0600–1200	0.7	−0.3	0.8	−0.5	0.3	−0.2	0.4	0.4
1200–1800	0.8	0	0.5	−0.4	0.7	−0.4	1.9	0.2
14th 1800–15th 0000	0.8	0	0.9	−0.1	0.6	−0.3	0.5	−0.1
0000–0600	1.2	−0.1	0.9	−0.1	0.8	−0.1	0.3	−0.6
0600–1200	1.6	0.1	1.2	−0.1	0.7	−0.3	1.4	−0.4
1200–1800	1.6	0.2	1.2	0	0.9	0.1	1	−0.1
Start position 13th 1800	13N	89.6E	11.7	88.9	11.8	89.3	13.1	89.4
End position 15th 1800	21N	89.4E	18	87.3	16.5	87	18.4	87.4
Total change	8	−0.2	6.3	−1.6	4.7	−2.3	5.3	−2.0

The KF_108 simulation showed a similar latitude change to that of the observed, although northward movement began to increase at about 6 hours later than the observed, at 0600 LST on 15/11/07. This probably explains why the KF_108 simulation made landfall after the observed time. The KF_72 simulation did not translate north as fast as the KF_108 simulation. Its movement remained relatively constant, with latitude changes less than 1° every 6 hours of track being recorded (Table 6.2).

The KF_48 simulation was less convincing: the cyclone actually tracked south-westward at one stage. The KF_48 did, however, increase its northward shift at the same time as the KF_108 simulation. Overall, in terms of latitude change, the KF_108 simulation performed the best, with only 1.7° latitude change less than the observed total latitude change. Despite the track problems associated with the KF_48 simulation, it performed slightly better than the KF_72; but still predicted a latitude change 1° less than the total of the KF_108 simulation.

The simulations showed more longitude deviation than the observed cyclone. In fact, the KF_108 and KF_72 simulations progressively tracked west over the simulation time, and never adjusted their tracks back towards the east. This is indicated by the negative longitude error values in Table 7.1. The KF_48 simulation predicted eastward movement twice, but this came directly after a time when the cyclone had readjusted north after incorrectly tracking south. The KF_108 simulation performed the best, with only a −1.6° W deviation, with the KF_72 and KF_48 simulations having deviations of −2.3° W and −2.0° W respectively. Once again, KF_72 performed worst; but in this category the KF_108 simulation had a slight performance edge over the KF_48. This indicates that the 108 hour initialisation time resulted in the most accurate representation of cyclone track behaviour. It is still reasonable to conclude that after allowing for the initial positional errors, the simulated tracks still failed to model observed cyclone behaviour accurately.

Tracks for each simulation are presented in Figure 6.1, to support the data in Tables 6.1 and 6.2. The KF_72 simulation produced a storm that was too far west. Development and translation of the KF_72 simulation occurred slightly later than the KF_108 case, representing a lag of about 12 hours at the end of the simulation. This lag was evident for the KF_48 simulation too, which was placed at the same latitude as the KF_72 cyclone, but further east. Despite the initial error, KF_108 was closest to resembling the behaviour of

the observed track. This supports the conclusion that 108 hours prior to landfall provided the most accurate track of all three initialisation experiments.

As a final consideration of track behaviour, and to help explain differences between the simulated tracks, an analysis of PV can be applied. Research has indicated that one control of cyclone track is upper-level divergence and PV (Chan 1984; Chan 2006). It has been shown in recent years that anticyclonic outflow at 300 hPa, resulting from asymmetry in PV can steer tropical cyclones (Davis and Bosart 2002).

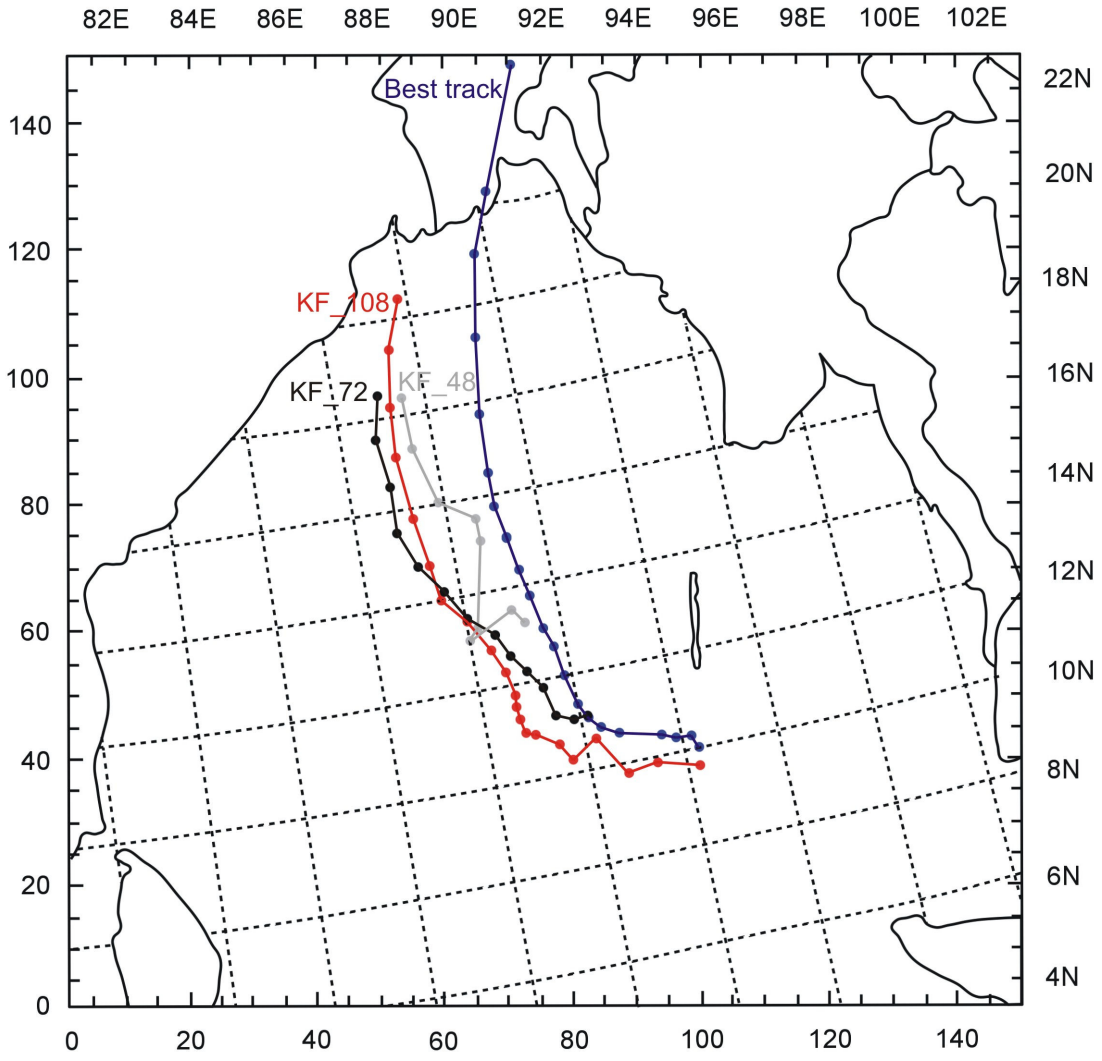

Figure 6.1: Comparison of initialisation track forecasts with the observed *best track*. The simulated tracks show a westward drift compared to the observed track. What is of note is the end position of the KF_48 and KF_72 cases is quite similar, where as the KF_108 case is well advanced of each. The tracks are plotted every 6 hours. The centres of the cyclones are indicated by filled circles.

The upper-level analyses at 0600 LST on 15/11/07 showed a distinct difference in both PV and wind speed for each case (Figure 6.2). Firstly, a highly interesting result was seen in the KF_48 case (Figure 6.2a), was a poleward anticyclone formed from the deformation of the 300 hPa layer from cyclone outflow aloft. The centre at the surface was south of this

upper-level feature, and is consistent with the findings of Davis and Bosart (2002). In the KF_108 and KF_72 simulations, this feature was seen equatorward of the surface cyclone, and perhaps explains why the KF_48 track was steered further east than the other cases. Furthermore, there is also a slight flow difference in the KF_48 case. The westerly flow was oriented more northwest than seen in the other cases, which would help move the cyclone further east than in the other cases. The lack of anticyclonic PV intensity was responsible for the reduced northward transition of the cyclone because the lack of shear suppressed the rotation of the easterly wind to the north between 5–10° N. This latter observation raises another interesting point.

Finally, because the anticyclonic PV in the KF_108 and KF_72 simulations was more intense than in the KF_48 case, meant the tracks were further north. It appears the greater intensity of the anticyclonic outflow aloft created a more intense perturbation of the easterly flow. The result was a stronger southerly flow and less westerly flow which steered both cyclones further north. Because the KF_108 anticyclonic PV was the most intense, it was the furthest north, which is consistent with Figure 6.1. In addition, a greater cyclonic PV was present at 300 hPa in the KF_72 experiment, which explains why the track was further west than the other simulations. This is because of the competition between the 300 hPa anticyclonic flow attempting to steer the surface cyclone north, and the cyclonic flow working to resist that movement.

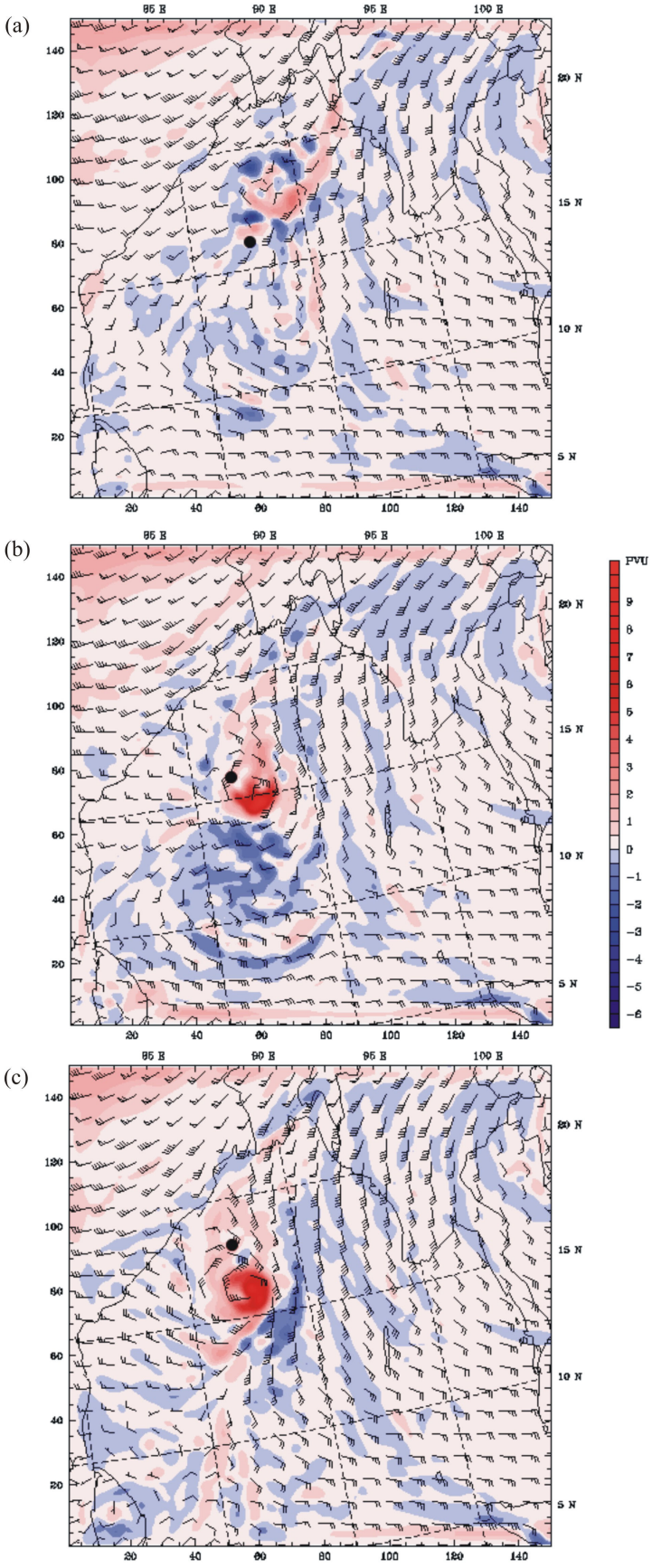

Figure 6.2: 300 hPa PV and wind comparisons for (a) the KF_48 simulation at 0600 LST on 15/11/07, (b) the KF_72 simulation at 0600 LST on 15/11/07, and (c) the KF_108 simulation at 0600 LST on 15/11/07. The analyses show that anticyclonic PV represented in red and positive PVU increases with simulation time. The position of the surface cyclone is marked by the black circle. Note that 1 PVU is equal to 1.0×10^{-6} m^2 s^{-1} K kg^{-1}.

6.3 Cyclone intensity

Intensity is a defining indicator of simulation performance, and must be studied in conjunction with track. There are a range of measures available to analyse cyclone intensity for the three simulations including, central pressure, maximum wind speed, precipitation intensity, and wind intensity.

6.3.1 Cyclone central pressure

Cyclone central pressure recordings were extracted at intervals of 6 hours beginning at 1800 LST on 13/11/07, which was the start time of the KF_48 simulation (Figure 6.3). Distinct pressure differences were found between the three simulations indicating that initialisation time impacts upon intensity. None of the model runs were able to match observed central pressure. The KF_108 simulation performed best, consistently predicting the lowest central pressure of the three runs, with a lowest recorded central pressure of 949 hPa (a category 3 cyclone). The KF_108 case was still some 35 hPa in error of the observed on average.

Despite the error, the KF_108 case displayed similar characteristics to that of the observed, deepening and remaining steady at similar times. Indeed, the central pressure change between 0600 LST on 14/11/07 and 0000 LST on 15/11/07 (the second phase of Sidr's intensification, see Figure 4.2 in Chapter 4) was an 11 hPa decrease, only 8 hPa less than the observed decrease.

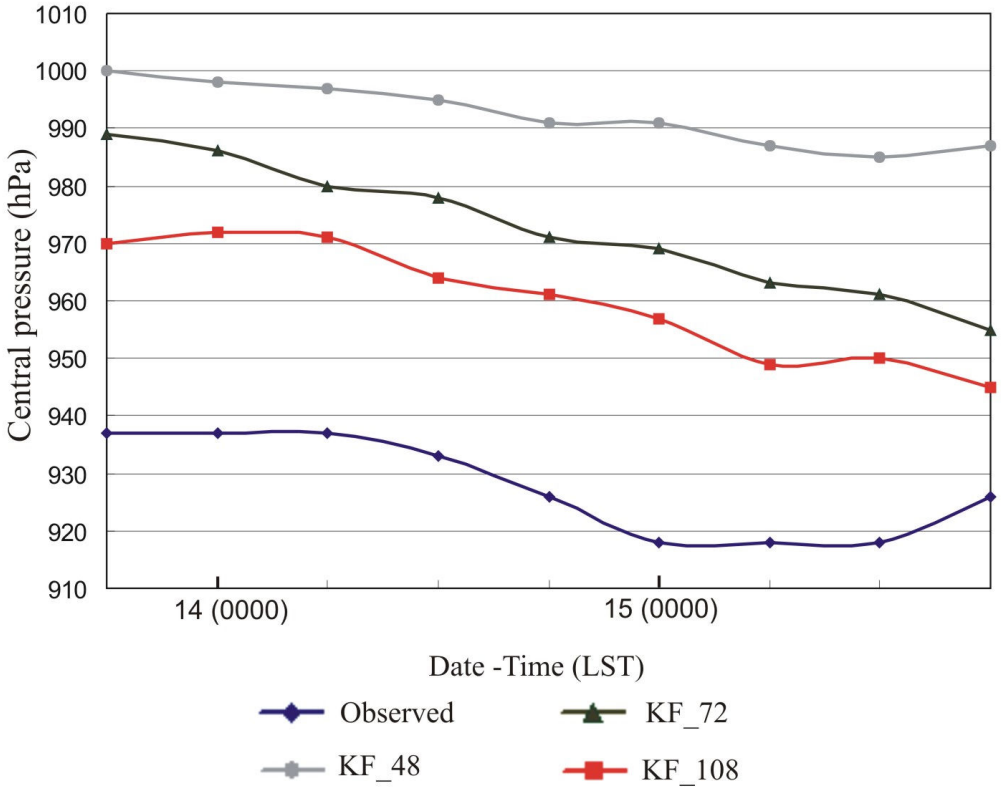

Figure 6.3: Comparison of the trend in simulated central pressure for the initialisation forecasts with the observed central pressure. The simulations were not able to match the observed pressure at any stage, and were consistently greater. The time interval is 6 hours for each reading, starting from the time of the KF_48 initialisation at 1800 LST on 13/11/07.

There was minimal difference between the KF_108 and KF_72 simulations, as the KF_72 simulation continued to deepen throughout the forecast. The error in pressure for the KF_72 case was on average 47 hPa. The KF_72 simulation did not display similar pressure characteristics to the observed, like the KF_108 case. The KF_72 recorded its lowest pressure of 960 hPa (a category 2 cyclone) at the time of observed landfall, which is consistent with the KF_108 experiment. The 18 hour change during the second period of intensification was 9 hpa — 2 hPa less than the KF_108 simulation, and is also a function of initialisation time. The KF_108 and KF_72 simulations did not show an increase in pressure at the observed landfall time, but as shown in Section 6.2, this was to be expected as landfall occurred later in these simulations. Finally, the KF_48 experiment, being the poorest performing of the three runs showed minimal intensification over the forecast period. Indeed, the 18 hour central pressure change during the second intensification period was only 5 hPa, considerably lower than the observed. The lowest central pressure simulated was 986 hPa which meant the KF_48 simulation was only classified as a tropical storm. In addition, the average central pressure error between the KF_48 case and the observed central pressure was 65 hPa. This can be attributed to the short spin up time of

the cyclone. Clearly, there is a relationship between initialisation time and cyclone intensity.

6.3.2 Maximum wind speed

As previously stated, maximum wind speed is factored into the Saffir-Simpson scale of hurricane intensity, and is an important measure of cyclone strength. From the observational analysis in Chapter 4, it is known that Sidr reached category 4 status at 1200 LST on 13/11/07, and category 5 sometime near 2200 LST on 14/11/07. The simulated cyclones were much weaker than this. In terms of wind on the Saffir-Simpson scale, the KF_108 simulation achieved a maximum of category 2 status for 18 hours (0600 LST–1800 LST on 15/11/07). The KF_72 simulation achieved category 2 for only 6 hours (1200 LST–1800 LST on 15/11/07); and was simulated as a tropical storm for the period 1800 LST on 13/11/07 to 1200 LST on 14/11/07. The KF_48 simulation failed to reach tropical cyclone classification, and remained a weak tropical storm throughout its life cycle. When comparing these classifications to the simulated pressure analysis, it is clear that some inconsistency arises when classifying by either central pressure or wind speed.

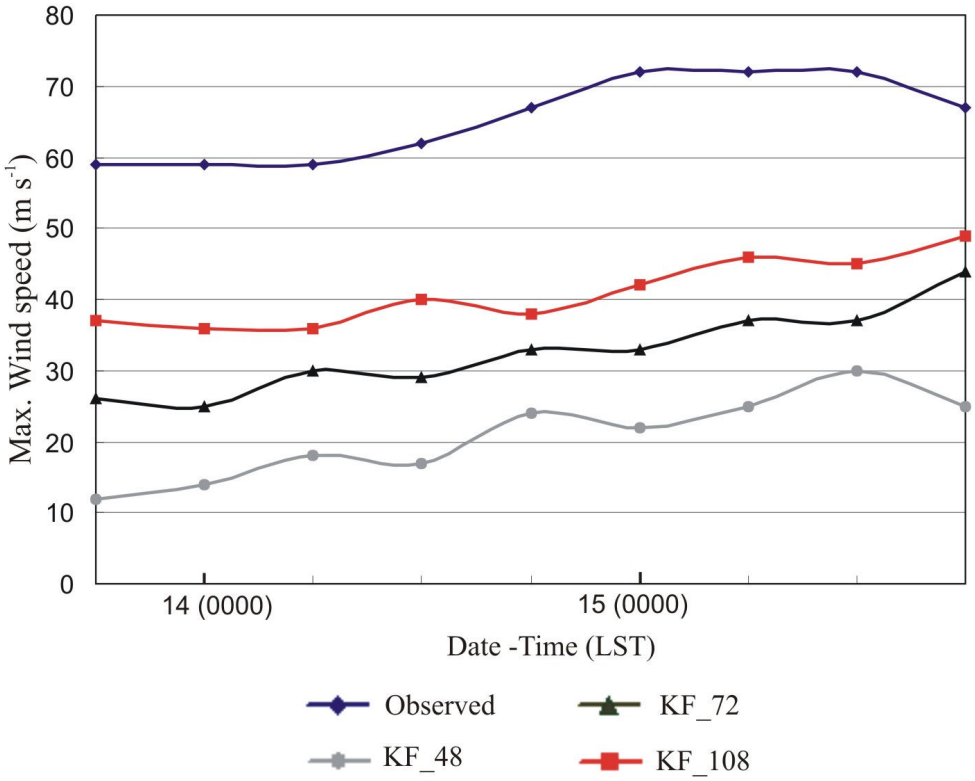

Figure 6.4: Comparison of the trend in maximum wind speeds for the initialisation forecasts with the observed wind. There is a clear relationship between initialisation time and maximum wind speed. All initialisations were unable to meet the observed readings. The time interval is 6 hours for each reading, starting from the time of the KF_48 initialisation at 1800 LST on 13/11/07.

The simulated wind speed results (Figure 6.4) showed a similar pattern to the central pressure results. Indeed, maximum winds fell well short of observed cyclone wind speeds. Furthermore, the wind strengths were ordered in terms of initialisation time, with the KF_108 case producing the best result, and the KF_48 the worst. In addition, wind speed tended to increase with time, reflecting the time taken for the cyclone to spin-up in the simulations. The behaviour of the predicted maximum wind was quite different to the observed wind speed. There were frequent fluctuations in each of the simulations during the forecast. The observed cyclone, however, displayed a period of steady wind speed, a period of steady increase, and another period of steady wind speed at maturity.

6.3.3 Reflectivity (precipitation intensity)

Predicted reflectivity fields for the three simulations were analysed at 1800 LST on 15/11/07 (Figure 6.5a-c), to coincide with the observed landfall time. From the analysis images it was clear where each of the cyclones was in relation to land. The cyclone structures were also well represented. The reflectivity images are consistent with the other measurements of intensity, showing that initialisation time affects the predicted development of this cyclone event.

The short spin-up time of the KF_48 simulation resulted in poorly developed cyclone structure (Figure 6.5a). The northern inflow region of the cyclone was reproduced reasonably well, a well defined deep convection zone of 40–55 dBz was evident, and some rotational aspect of this zone of the cyclone can be identified. There was no reproduction of the southern inflow region, resulting in a poorly simulated cyclone. A number of squalls of medium intensity (30 dBz) were apparent and one distinct squall line was shown to be crossing Bangladesh. Prior reflectivity analyses for this simulation (not shown) did not show any better structural features to contrast this result. The system remained immature for its entire life cycle, which was the only simulation of the three to do so.

The KF_72 experiment provided an improved result. Given the additional spin-up time, the cyclone was able to intensify sufficiently to model a number of features (Figure 6.5b). Firstly, an eye of little to no precipitation of max radius 45 km (east-west) and 37 km (north- south) existed. This contrasted the observed eye radius of 9 km at this time (see Figure 4.1 in Chapter 4), indicating the difference that existed in intensity. Secondly, a moderately developed eye wall extended from the centre to the north and west. The most

intense reflectivities were recorded as a band of deep convection (45–50 dBz) along the outer region of this eye wall. The inner regions of the wall were yet to fully develop, with only moderate convection of liquid precipitation (30–35 dBz) simulated. The eye wall was asymmetric because the rotation at the southern part of the storm had not developed sufficiently to enhance convection in the eastern region. Thirdly, there was evidence of a spiral band of cellular deep convection west of the centre. Between the eye wall and the outer band was an area of light precipitation intensity, consistent with the theory outlined in Stull (1999). Unlike the observed case, however, no other distinct spiral bands were simulated. Finally, comparing the simulated analysis to the observed Aqua EOS 89 GHz colour composite (see Figure 4.10b in Chapter 4), shows several features lacking or poorly developed — lighter liquid precipitation surrounding the cyclone, deep convection to the northeast, axisymmetrical structure, and a spiral rain band to the east.

It is without surprise that the KF_108 simulation produced the best result (simply because more time was allowed for spin-up). Firstly, the simulated cyclone was almost fully axisymmetrical, indicating maturity was nigh. Indeed, a concentric eye wall of radius 150 km on the western side, and 75 km on the eastern side, had developed with severe convective falls in the order of 45–55 dBz. Secondly, the eye that had formed was well developed, being of maximum radius 37 km (east to west) and 37 km (north to south), which was still greater than the observed eye radius at this time (see Figure 4.1 in Chapter 4). The eye was better defined than the KF_72 case, indicating greater intensity. Thirdly, a spiral rain band to the southeast of the cyclone was simulated, and a number of squalls to the northwest were apparent. While the positional accuracy and number of these features was not correct when compared to the observed event, their simulation was indicating that the model was accomplishing the task of accounting for certain structural features. Finally, while the northern extent of the storm simulated the observed conditions quite well, the southern and northeastern regions of the cyclone were still limited. For instance, a number of heavy thunderstorms were observed to the northeast of Sidr, but these were not accounted for by the model for this initialisation time. Furthermore, the model continued to ineffectively resolve light precipitation intensities as the Aqua EOS image showed (see Figure 4.10b in Chapter 4). This indicates a potential problem with the type of CP scheme chosen, and the resolving of cloud parameters in the model. This will be discussed in depth in Chapter 7.

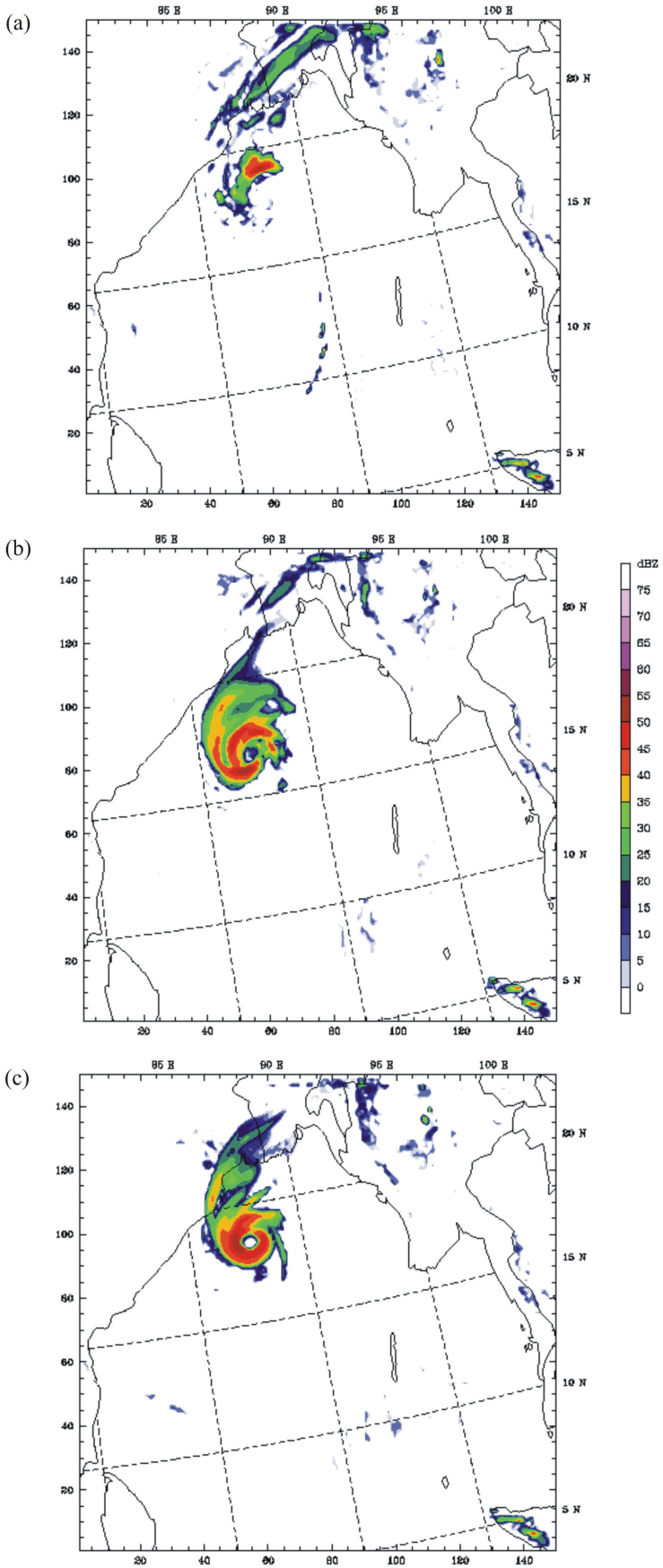

Figure 6.5: Comparison of simulated radar reflectivity for (a) the KF_48 simulation, (b) the KF_72 simulation, and (c) the KF_108 simulation. The simulations are all valid at observed landfall, at 1800 LST on 15/11/07. It is indicative that as initialisation time increases from landfall, the model is more effective in representing structure and precipitation intensity. Note that the simulated cyclones do not make landfall at the same time as the observed, it was some hours later.

6.3.4 Cyclone wind field intensities

In addition to the wind data shown in Figure 6.4, it is possible to examine the 10 m horizontal and 1000 hPa–100 hPa vertical wind fields for the three initialisation cases. This section completes the analysis of structure, showing that initialisation time affected the horizontal extent and vertical depth of maximum wind and cyclone structure.

The predicted wind plots for the KF_48 simulation agreed with the other results, that this cyclone was the most poorly developed of all initialisation times. Firstly, the horizontal field for 1200 LST on 15/11/07 showed a rotational circulation, but winds about the cyclone centre were only 20–25 m s^{-1} (Figure 6.6a). An eye of relatively calm winds was simulated, and the maximum wind of 30 m s^{-1} was slightly to the northwest of this. The cyclone structure was not well defined, as no intense concentric development of wind was modelled. The lack of wind speed, and poor structural features indicated that intensity was poor. The maximum east-west extent of winds greater than 15 m s^{-1} was approximately 1500 km. Secondly, the vertical profile (Figure 6.6b) across the line A–B on Figure 6.6a concurred with the lack of development suggested by the horizontal plot. The first important feature to note is the lack of development through the troposphere, as the eye region represented by calm winds, only extended to about 600 hPa (Figure 6.6b). There was evidence of vertical shear above this height, although it was not intense enough to warrant it being the main factor in the lack of development. Indeed, it appears that the eye could have extended to as high as 300 hPa before the shear developed, as a region of light wind did still exist at 300 hPa. The second notable feature is the lack of symmetry between the east and west sides of the cyclone. On the western side, a region of 40 m s^{-1} wind speed extending from the surface to 850 hPa represented the most intense part of the eye wall, and it was interesting that this did not appear on the horizontal plot. Within the western eye wall a core of 45 m s^{-1} was simulated. The eastern side of the cyclone did not show an eye wall quite as intense, but did show a wider extent of wind speed greater than 25 m s^{-1}, and this is consistent with the rotation shown in Figure 6.6a. The depth of this maximum wind was to about the 550 hPa layer on the eastern side, and 700 hPa on the western side. The centre and eye wall was roughly 200 km in diameter, and the entire system roughly 300 km in diameter.

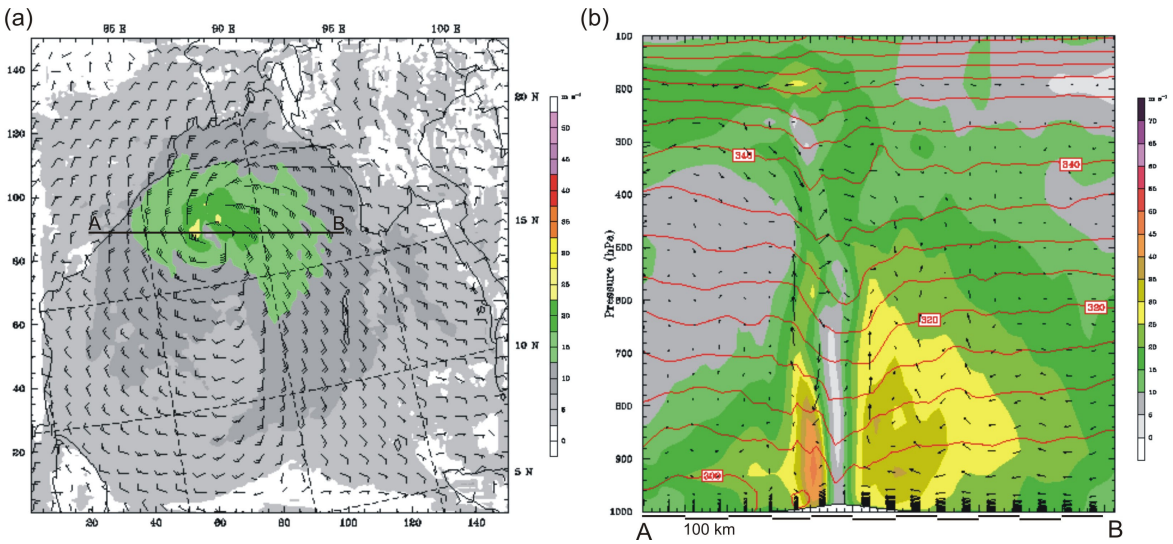

Figure 6.6: KF_48 simulated wind intensity for (a) horizontal wind field at 10 m height at 1200 LST on 15/11/07, and (b) vertical profile through line A–B on the horizontal plot at the same time. Note that the wind speed scale is different for both plots.

The KF_72 predicted wind field was an improvement on the KF_48 simulation, confirming that it performed better as other results have shown. Firstly, the horizontal plot for 1200 LST on 15/11/07 showed a more intense rotational circulation than the KF_48 case. For example, winds about the centre were in the order of 30 m s^{-1} (Figure 6.7a). Wind speed decreased away from the eye, with a 1050 km east-west extent of 15 m s^{-1} or greater wind speed, which was less than that of the KF_48 case. This was offset by the greater intensity around the centre. Indeed, a well defined concentric circulation was simulated, and the cyclone region of most intense wind speed (25 m s^{-1} or greater) was roughly 300 km. Furthermore, the vertical structure through the line A-B in Figure 6.7a indicated that the simulated intensity was an improvement on the KF_48 simulation, and also showed quite similar structural characteristics. The eye appeared to extend to a greater depth in the atmosphere. In fact, it is reasonable to suggest that it extended to about 100 hPa (Figure 6.7b). The eye wall indicated greater cyclone intensity for two reasons. The first was the extension of both the east and west sides of maximum wind speed to a greater depth in the troposphere, particularly on the eastern side yet again. The western eye wall extended to about 600 hPa, and on the eastern side, up to 200 hPa, which was of significant depth. The second reason for greater intensity than the KF_48 case was the more intense simulated wind speed about the eye wall. Indeed, the western side of the storm had simulated winds in the order of 50 m s^{-1} near the eye, while on the eastern side winds about the eye were around 45 m s^{-1}. The size of the eye and eye wall was 250 km in diameter which was greater than the KF_48 case. The entire cyclone was roughly 400 km in diameter. This represented a more intense rotational circulation than that in the KF_48 simulation.

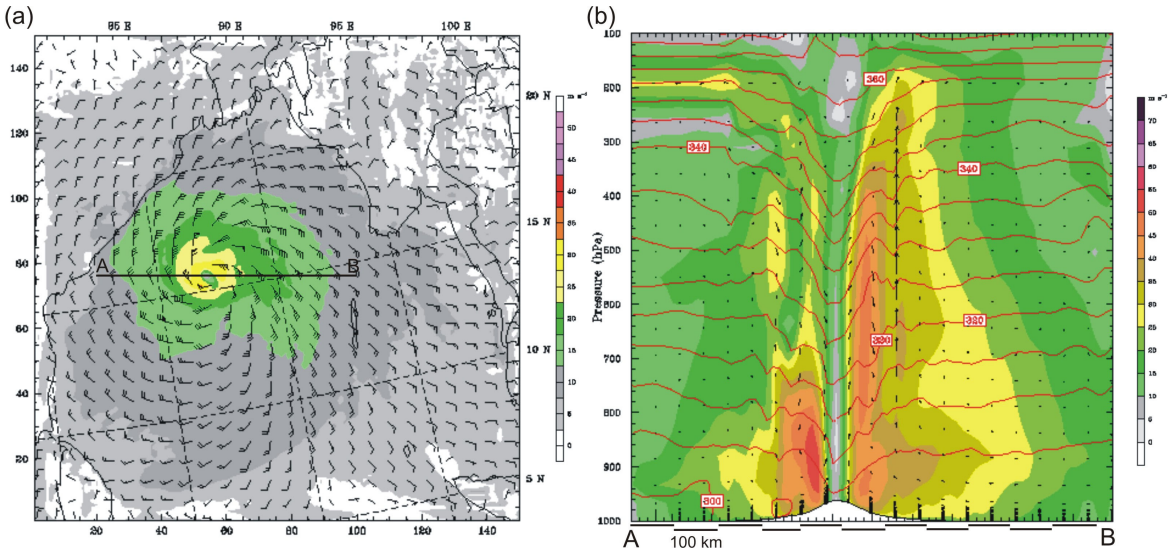

Figure 6.7: KF_72 simulated wind intensity for (a) horizontal wind field at 10 m height at 1200 LST on 15/11/07, and (b) vertical profile through line A–B on the horizontal plot at the same time. Note that the wind speed scale is different for both plots.

The KF_108 predicted wind field results proved that given ample spin up time, well defined structures and intensities are effectively resolved. The KF_108 simulation showed the most intense winds and best developed structural features of all the runs, and this is consistent with the other results. The horizontal plot of wind speed for 1200 LST on 15/11/07 (Figure 6.8a) showed a well developed concentric structure of a calm eye, and a radial wind band of 35 m s^{-1} that represented the eye wall. The wind field extending outwards from the eye wall was similar to that of the KF_72 simulation. The vertical structure of the KF_108 case (Figure 6.8b) across the line A–B on Figure 6.8a showed a number of similarities to the KF_72 and KF_48 cases except in this simulation it was more developed, and a slight radial tilting of the eye wall was simulated. This is common for intense, mature cyclones as shown by Liu et al. (1997). While the structure showed similarities to the other simulations, the wind speed was quite different. Wind speeds at the most intense part of the eye wall were 65 m s^{-1} (west side) and 60 m s^{-1} (east side), some 10 m s^{-1} faster than in the KF_72 simulation. The depth of the region of winds greater than 50 m s^{-1} extended to the 700 hPa layer on the west side, and 380 hPa layer on the east side. The cyclone was axisymmetrical up to the 700 hPa layer. The diameter of the eye and eye wall was 160 km at its longest east-west extent, which was 40 km less than in the KF_72 simulation, indicating that the cyclonic circulation was even more intense than that predicted in KF_72. The longest extent of the cyclone was 450 km east-west, which was 50 km greater than the KF_72 prediction, and showed that the region of wind greater than 25 m s^{-1} covered a greater area than that of the other simulations.

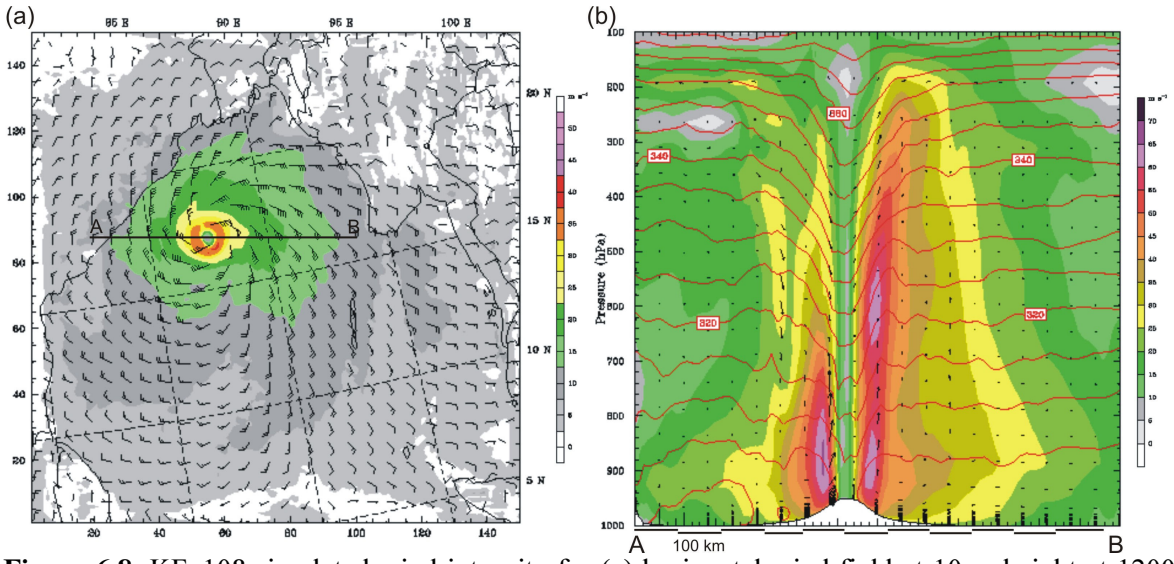

Figure 6.8: KF_108 simulated wind intensity for (a) horizontal wind field at 10 m height at 1200 LST on 15/11/07, and (b) vertical profile through line A–B on the horizontal plot at the same time. Note that the wind speed scale is different for both plots.

Across all the simulations, the vertical profiles indicate that the west side of the circulation was the most intense with faster wind speeds, while the extent of intense wind speeds on the east side of the cyclone was greater, but with weaker winds. This is quite common for cyclonic systems of the northern hemisphere, as shown by Emanuel (2005).

6.5 Conclusion

In conclusion, this chapter has presented the results of track and intensity simulations for three initialisation experiments — KF_48, KF_72, and KF_108. An analysis of track error using an effective technique based on that of Goerss (2007) showed that all simulated cyclone tracks were in error, but that neither the KF_108 simulation nor the KF_48 simulation (the KF_72 was clearly the worst performing) could be identified as being the most accurate. Indeed, there was minimal difference in the error between the KF_108 and KF_48 simulations, which was 0.2° and 0.1° latitude and longitude error respectively. None of the initialisation experiments simulated landfall at the observed time, it occurred about 6–12 hours later in all simulations. When considering the behaviour of simulated track, however, it is evident that the KF_108 performed best. In addition, PV and wind speed fields at 300 hPa were used to support the track behaviour of the surface cyclone. It was found that the KF_108 simulation had the most intense anticyclonic PV and westerly wind field aloft, assisting the northward translation at the surface. Overall, it is reasonable to conclude based on this result, that the KF_108 simulation, using a longer initialisation time, provided the best simulated track.

While determining the best simulated track based on initialisation time proved difficult, it was clear that cyclone intensity was directly related to simulation start time. It was shown that by allowing WRF more time to simulate, a more intense cyclone was produced, in terms of central pressure, wind speed, and structural features. In this regard, the KF_108 simulation was the most intense cyclone. Differences in categorisation of cyclone intensity using the Saffir-Simpson scale for pressure and wind were also found. Indeed, central pressures for the KF_108 and KF_72 simulations indicated slightly stronger category cyclones using this scale, but the wind speed analysis classified slightly weaker category cyclones using the same scale. The KF_48 simulation remained a tropical storm regardless of pressure and wind speed results. It is unclear why these differences occur, and therefore how to best classify an event.

While track and intensity can be studied separately, it is important to recognise that both have an important role in the forecast. Predicting cyclone tracks accurately seems pointless without accurate predictions of cyclone intensity at landfall, so a holistic approach to cyclone analysis is certainly the most preferred option. When taking this into consideration, it becomes clear that the KF_108 simulation was consistently the best performing simulation. Such a lengthy initialisation time, however, is not ideal when considering weather forecasting. In this sense, it is more ideal to achieve a similar result to the KF_108 simulation anywhere between 48–72 hours.

This might be considered a fundamental experiment for an event-specific study, but it is important to conduct such analysis to determine what model conditions produce the most accurate representation of nature, and learn about data assimilation in the numerical modelling environment. Indeed, with such work one is able to improve forecast accuracy, and this is crucial for successful weather forecasting and research.

Chapter 7

Convective parameterisation experiment

7.1 Introduction

Convective parameterisation is a highly complex, yet essential component of numerical modelling. As previously stated, convective processes need to be accounted for by parameterisation schemes in models, because they cannot resolve these processes accurately on such large scales. This poses another challenge for forecasters and researchers, because there are inaccuracies with any CP scheme devised to estimate convective effects. The choice of CP scheme is important for the environment for which it is being modelled, and for producing a reliable forecast. In the case of a tropical cyclone, the way convection is accounted for is crucial to the dynamics of the system. For instance, deep convection drives energy transfers that lead to intensification, and if this is under (or over) predicted, errors in the type and amount of convection can occur. This also creates uncertainty in the intensity and location of precipitation that these cloud systems produce, and can become troublesome for response planning. The objective of this chapter, therefore, is to examine the sensitivity of tropical cyclone Sidr to various CP schemes.

The results from Chapter 6 have shown the variability in cyclone track and intensity that can occur from varying initialisation time in WRF. This too can be studied for CP schemes available in WRF. As discussed in Chapter 3, three CP schemes, the KF, BMJ, and GD ensemble, were used to examine precipitation resolving processes and test model sensitivity. A simulation of explicit convection (No Cu) was also undertaken to test model performance without the use of CP. Available observational data are referred to in the analysis, as a means of providing some validity to the schemes. Furthermore, it was decided that an initialisation time of 108 hours from landfall would be used to simulate the cyclones, as this proved to be a successful model start time in Chapter 6. In addition, a high resolution nested domain of 5 km grid resolution was used in this experiment to study the dynamics and structure at the most mature stage.

The CP scheme analysis section is divided into three categories: development, maturity and dissipation. In this study, development is defined as being the tropical storm phase before the cyclone reaches category one status. Maturity is defined as being the point in the cyclone life cycle where intensity is at a maximum (this was determined from the nested

domain). The dissipative stage was when the cyclone showed signs of an increase in pressure and wind speed after maturity. For each stage of Sidr's life cycle, simulations of CAPE and precipitation are analysed. Simulated vertical soundings are used for the maturity phase also. Finally, analysis is extended to study the cyclone intensity structures that each of the schemes simulated. This involves an analysis technique similar to that of Liu et al. (1997), in which vertical plots of different cloud microphysical quantities were used to examine the generation of cyclone reflectivity structures.

7.2 Cyclone life cycle

The choice of CP had an effect on life cycle. Table 7.1 shows the times of development, maturity and decay for each experiment. Firstly, the development phase indicated that the KF, GD, and No Cu experiments all reached category 1 hurricane status at the same time. The BMJ experiment did not reach category 1 status at any stage of the simulation. To account for this, an arbitrary time was selected that marked the end of cyclone development. This time was based on central pressure and wind speed observations. Secondly, in regard to maturity, the KF scheme did not mature until 0000 LST on 16/11/07; and the GD and No Cu experiments were 24 and 18 hours prior to the KF maturity respectively. The BMJ experiment matured at 0000 LST on 15/11/07. Finally, the dissipation times were variable. The GD cyclone was the first to decay at 0600 LST on 15/11/07; the BMJ and No Cu cyclones decayed 6 hours after this; and the KF cyclone was the last to decay because of its later maturity.

The small separation in maturation time for the experiments, and the fact that all but one simulation reached category 3 status (Table 7.1), does not indicate that the schemes performed similarly. In fact, later sections will show that track, intensity, and precipitation patterns varied for each of these experiments. This is a positive result, as it was expected that the experiments would show such variation.

Table 7.1: Cyclone life cycle stages for each of the CP experiments. Development was before the storm reached category one status; maturity was the time at which deepest pressure and maximum wind speed was recorded on the nested domain; and decay refers to the time the cyclone began to increase in pressure rapidly. The Saffir-Simpson scale classifications for each are given in brackets at the mature stage.

Experiment	End of development	Maturity (from 5 km grid)	Dissipation
KF	1800 LST on 12/11/07	0000 LST on 16/11/07 (category 3)	0600 LST on 16/11/07
BMJ	0600 LST on 13/11/07	0600 LST on 15/11/07 (tropical storm)	1200 LST on 15/11/07
GD	1800 LST on 12/11/07	0000 LST on 15/11/07 (category 4)	0600 LST on 15/11/07
No Cu	1800 LST on 12/11/07	0600 LST on 15/11/07 (category 4)	1200 LST on 15/11/07

7.3 Cyclone intensities

Cyclone intensity measured in terms of cyclone central pressure and wind speed is a good indicator of how each CP scheme performed. Results for pressure and wind speed in this section are from the coarse, 15 km domain. It is important to note that differences in pressure and wind speed between a coarse domain and a higher resolution nest are quite common, and normal. This was explained in Chapter 2 to be related to the number of grid points in a grid cell, and the resolution of that grid cell. It is necessary, therefore, to remember the model grid resolution when examining these results. For instance, while the nested domain simulated a more intense cyclone for some of the CP schemes when measured on the Saffir-Simpson scale, the coarse domain simulated a slightly weaker cyclone, as will be shown in the following sub-sections.

7.3.1 Cyclone central pressure

There are a number of important findings to discuss from the simulation of central pressure by the CP schemes. The variation between each of the schemes is a good indication of how different CP affected the spin-up of the cyclone at various stages. Firstly, in the development stage, the simulated pressures are reasonably even. For example, at the 12 hour time in the forecast there was only a 1–2 hPa central pressure difference between each

of the CP schemes (Figure 7.1). After 30 hours of the simulation, however, a spread in central pressure was quite evident. For instance, 28 hPa separated the KF and BMJ schemes, while the GD and No Cu schemes were in between KF and BMJ. The KF scheme was able to simulate the development of the cyclone better than the other cases, as over the first 48 hours of development the predicted central pressure was deepest. Secondly, the period of intensification which led to maturity is quite different for each simulation. While the KF scheme performed best at initial cyclone development, it was the GD ensemble that performed best at intensifying the cyclone towards maturity from the period starting 1800 LST on 12/11/07 to 0600 LST on 15/11/07. The KF scheme resulted in cyclone deepening by 28 hPa, the GD by 47 hPa, and the No Cu by 30 hPa over this period. The BMJ scheme did not show any significant deepening similar to the other simulations and remained a weak tropical storm. As a result of this second period of intensification, the GD ensemble produced the deepest simulated central pressure overall (942 hPa) for the coarse domain.

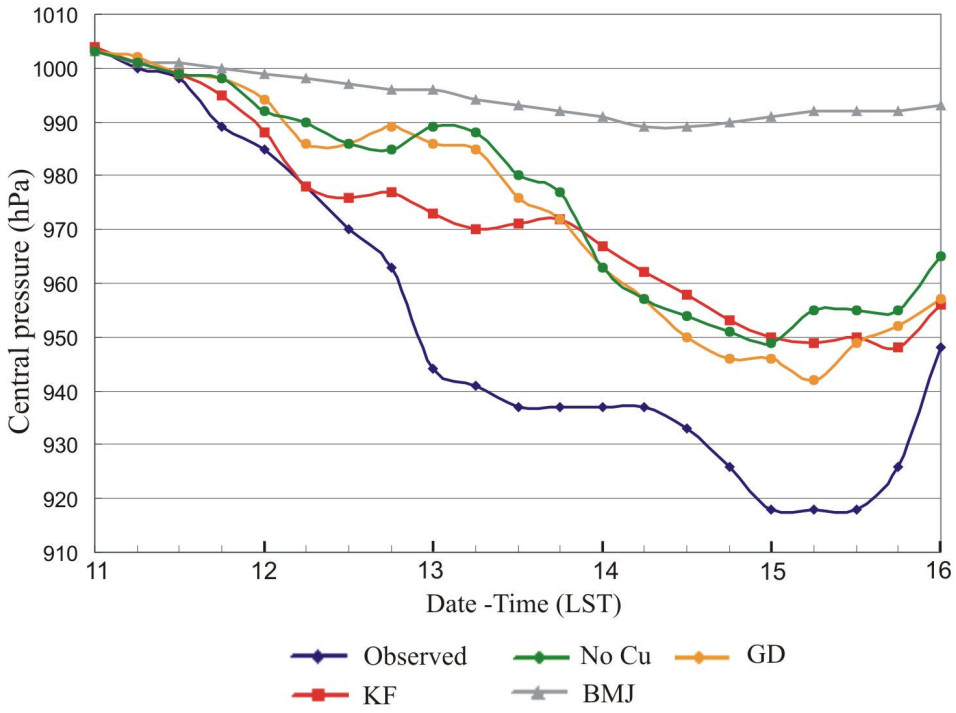

Figure 7.1: Comparison of the trend in observed central pressure to those for the different CP schemes. There is minimal separation between KF, GD, and No Cu, but BMJ was significantly different from the others. Pressures are from the coarse domain. Bold tick marks on the x-axis indicate midnight local time, and the interval is 6 hourly.

Finally, all simulations showed an increase in central pressure near the end of the forecast, which indicated dissipation after maturity. The rate of this dissipation in terms of central pressure was more rapid for the KF and No Cu schemes than for BMJ and GD. For instance, the GD ensemble increased the cyclone central pressure by 16 hPa over 18 hours, but KF and No Cu schemes both showed a more rapid pressure increase in the 6 hours

leading up to 0000 LST on 16/11/07, with 8 hPa and 10 hPa increases respectively. These results indicate the variation that occurred between the CP schemes, although there is also the need to compare the simulations to Sidr's observed central pressure.

The performance of each scheme when compared to the observed central pressure is now discussed. As described in Chapter 4 and reiterated in Figure 7.1, Sidr went through two distinct phases of rapid intensification separated by a period of steady-state maintenance. Firstly, while the KF scheme pressure prediction was in error, the scheme performed with reasonable skill at matching the development stages of the observed event. For example, the initial development nearly matched the observed up to 0600 LST on 12/11/07, but the scheme failed to simulate the rapid part of the observed initial deepening up to 0000 LST on 13/11/07. Furthermore, the KF scheme started simulating the steady state period at 0600 LST on 13/11/07, 6 hours before the observed; and entered its final phase of intensification at 1800 LST on 13/11/07, 12 hours before the observed. The central pressure increase at landfall did not match the observed pressure increase at landfall because of the error in track (Figure 7.1 and 7.3). Secondly, because of the failure of the BMJ simulation to develop, predictions were much higher than observed central pressure. At no stage (apart from the first 6 hours) did the BMJ scheme show any indication of matching the observed pressure variations. The BMJ predictions deepened quite slowly for the majority of its life cycle, and then increased its pressure in a similar pattern from 0600 LST on 14/11/07. This was considerably different to the observed pressure. Finally, because of the similarity between the results of the GD and No Cu schemes, they are comparable when measured against observed pressure. This was despite some minor differences, such as times and rates of deepening, and the increase of pressure at landfall. For instance, both intensified similarly in the initial stages, although the No Cu simulation extended its deepening for 12 hours after the GD simulation. Both simulations increased their central pressure after this deepening, but because the No Cu simulation had deepened for longer, there was a lag in this increase. This lag appeared to influence the remainder of the simulation. These factors meant that neither simulation realistically matched the observed situation. In summary, the most important difference was the inability of the simulations to deepen sufficiently during the development phase, which meant the simulations were effectively in considerable error for the remainder of the forecast.

7.3.2 Maximum wind speed

The results of simulated wind speed (Figure 7.2) showed a similar pattern to that of simulated pressure. Firstly, during the development stage, the KF, No Cu, and GD simulations were in close agreement. These schemes were inseparable for the first 18 hours and after 24 hours only 1 m s^{-1} separated the KF and No Cu schemes, although the GD scheme had fallen slightly. The BMJ scheme was unable to predict intensification at the same rate, which was similar to its pressure result. Secondly, between the simulation period 0600 LST on 12/11/07 to 1200 LST on 13/11/07, the schemes showed different characteristics. From development to 1200 LST on 13/11/07, the KF predicted an increase in its wind speed of 1–2 m s^{-1} every 6 hours, and as such was the most intense cyclone. The No Cu scheme maintained a steady-state wind speed for this period, not increasing or decreasing by more than 2 m s^{-1} every 6 hours. This initially lead to the GD prediction becoming more intense than for No Cu, which had continued a gradual increase since the start time. During the evening of 12/11/07, however, GD began to decrease its wind speed, decreasing by 5 m s^{-1} in 12 hours. The BMJ scheme produced less intense development than the other CP schemes, but did show a slight increase of 4 m s^{-1} in its wind speed during this period. Thirdly, two important developments occurred at or around 1800 LST on 13/11/07, as the simulated cyclones began their final intensification towards maturity. In the previous 12 hours leading up to this point, the GD cyclone increased its predicted wind speed by 5 m s^{-1}, which now meant it was only 3 m s^{-1} less than the KF cyclone. This was matched by a similar decrease in wind speed of the No Cu cyclone 6 hours later at 1200 LST on 13/11/07, so that it was now 10 m s^{-1} less than for the KF cyclone. Finally, it was evident that these latter developments were important to how the wind speeds compared at the maturation stage. For instance, the period from 0000 LST on 14/11/07 to 0600 LST on 15/11/07 showed that the GD cyclone continued to increase its predicted wind speed to become the most intense of the matured simulated cyclones. While the KF simulation was the most intense cyclone for the time leading up to this point, it did not show the same rapid intensification as for the GD simulation. Furthermore, the No Cu cyclone, which had just undergone a pressure fall, also went through a rapid intensification of 16 m s^{-1} over 24 hours to 1800 LST on 14/11/07. The 6 hour decrease of No Cu predictions just before this point appeared to be the reason why it was 3–4 m s^{-1} less intense than the KF and GD predictions during 14/11/07 and 15/11/07. Indeed, it is clear from Figure 7.2 that the wind speed prediction of the No Cu simulation intensified at a

faster rate than for the KF and GD simulations, but not significantly, as GD went through a 13 m s^{-1} intensification during that same period.

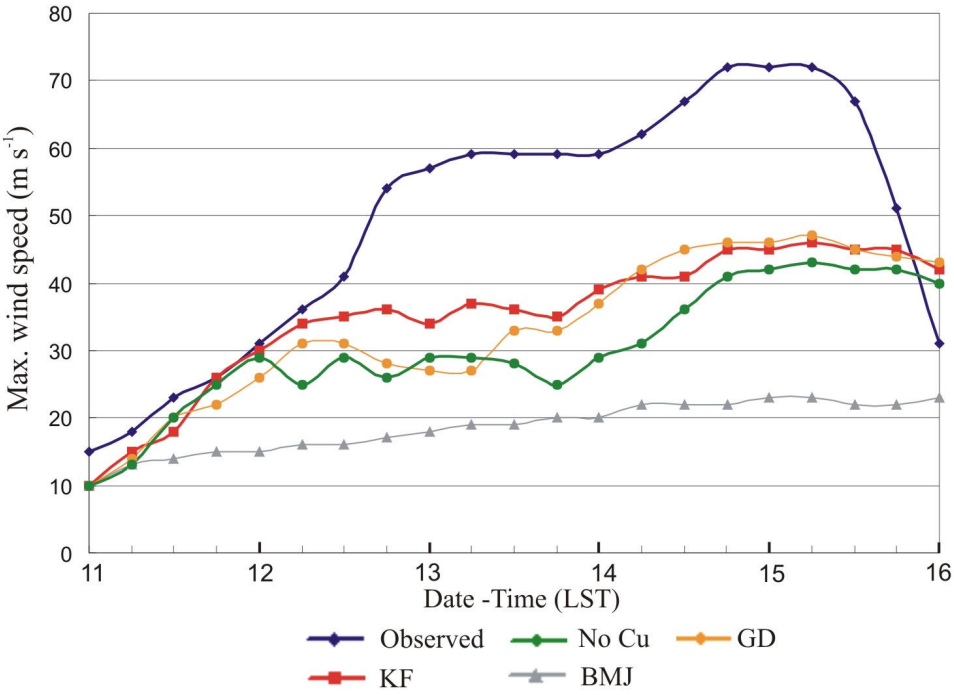

Figure 7.2: Comparison of the trend in observed maximum wind speed to those for the different CP schemes. The simulated wind speeds show three distinct stages, an initial increase from development, a steady-state period, and then another increase towards maturity. Wind speeds are from the coarse domain. Bold tick marks on the x-axis indicate midnight local time, and the interval is 6 hourly.

The developments on 13/11/07 appear to have influenced the CP schemes over the last part of the simulation, which ultimately indicates why there was little difference between KF and GD predicted wind speed. It is reasonable to conclude, therefore, that while the CP schemes showed differences throughout the simulation period, all CP schemes except for BMJ displayed little variation in the final stages of simulation.

The comparison of trends in the simulated wind to those of the observed wind revealed that the model was unable to match observed wind after 24–30 hours of simulation. After the first 24 hours to 0000 LST on 12/11/07, the model began to show that it was unable to simulate the further intensification of the cyclone represented by the steady nature of simulated wind speed. Indeed, the observed Sidr continued to intensify rapidly for another 12–18 hours before maintaining a steady-state. The simulated cases reached a steady-state much earlier than the observed Sidr. Furthermore, it is clear that the simulated cases remained in error for the remainder of the simulation. For example, at the time of maximum recorded observed wind at 1800 LST on 14/11/07, the KF predicted wind speed

was simulated to be 27 m s^{-1} in error, with the GD 26 m s^{-1}, No Cu 31 m s^{-1}, and BMJ 50 m s^{-1} in error of the observed.

7.4 Cyclone tracks

It was shown in Chapter 6 that initial conditions had some consequence for prediction of the cyclone track, and this was explained through PV and upper-level wind flow. The initial conditions in this experiment remained the same, so the objective in this chapter was to assess whether the CP scheme directly affects the track for this event. A recent study by Davis and Bosart (2002) showed that CP schemes can indeed have an effect on PV, which affects the storm track. No studies have used WRF to examine this.

The simulated tracks for each scheme show that variation did arise in cyclone path (Figure 7.3). In fact, more variation was seen in these tracks than the tracks with different initialisation time. The KF scheme produced the most accurate track, with a westward displacement and a lag from the observed of about 18 hours the only notable errors. The BMJ track initially performed well, and was the closest to the observed after 42 hours, but produced a more westward track during the remainder of the simulation. Both the GD and No Cu predicted tracks were quite similar to each other, but resolved a much more westward movement, making each rather inaccurate.

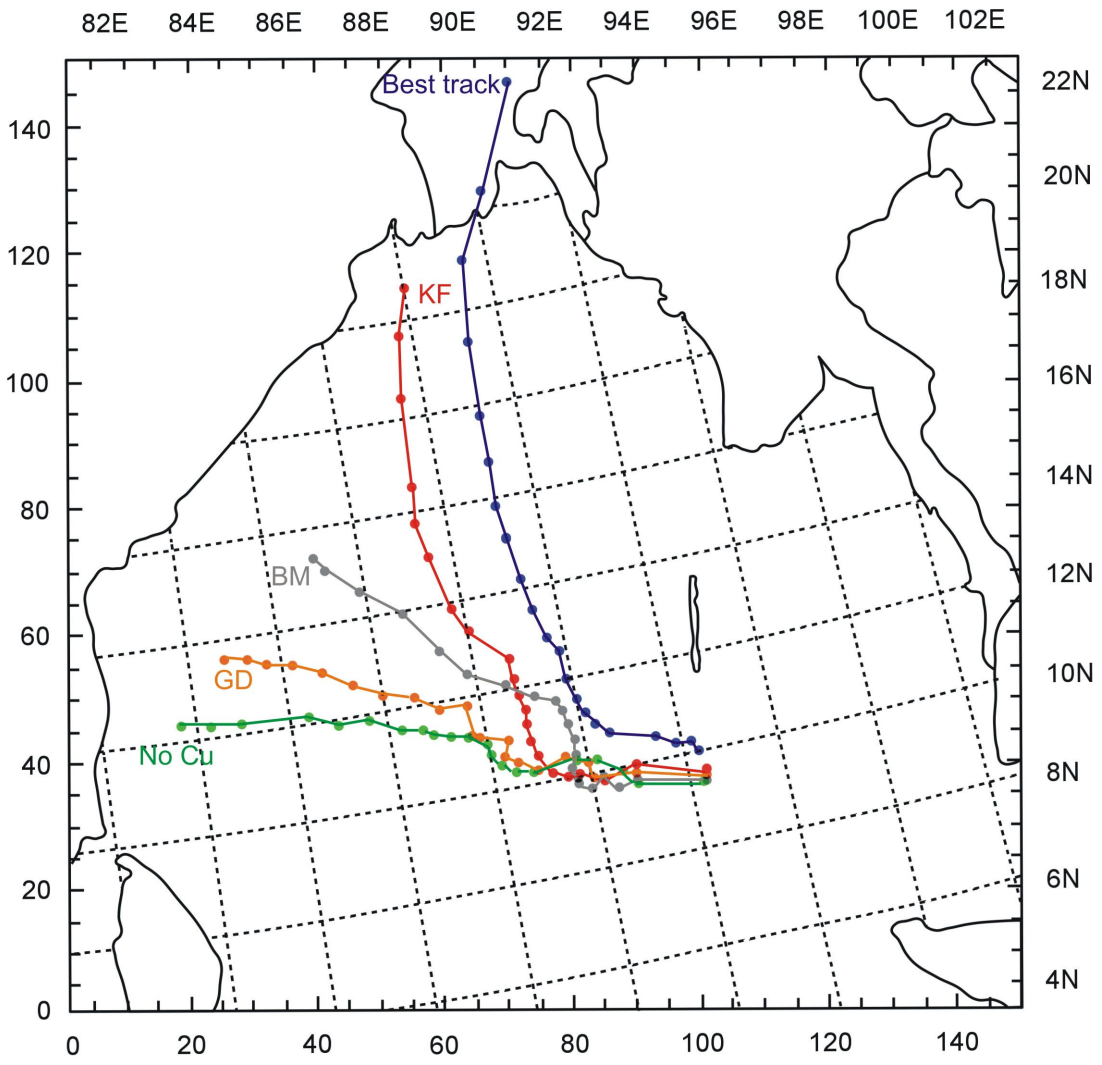

Figure 7.3: Comparison of tracks for simulations with different CP schemes to that of the observed *best track*. The KF track was most accurate but displaced westward, and the remaining schemes drifted west without significant northward adjustment.

Again, upper-level analyses of PV and wind are quite informative as to the processes aloft that influence the cyclone track. In the case of the CP scheme, it is evident that differences in the supply of latent heat from the CP scheme lead to variation in the upper-level PV and wind field. These differences in upper-tropospheric flow are highlighted in the 300 hPa analysis images for 1800 LST on 14/11/07 (Figure 7.4). Notably, the KF predicted surface cyclone was most advanced at this time, but the anticyclonic PV was equatorward and southeastward, not poleward. The BMJ and GD simulations showed the anticyclonic PV directly east of the surface cyclone; and in the case of No Cu the anticyclone was slightly poleward of the surface feature. It appears the intensity of the anticyclonic PV in the KF case was sufficient to steer the cyclone accurately by virtue of the resulting rotation of the 300 hPa wind field to create westerly flow.

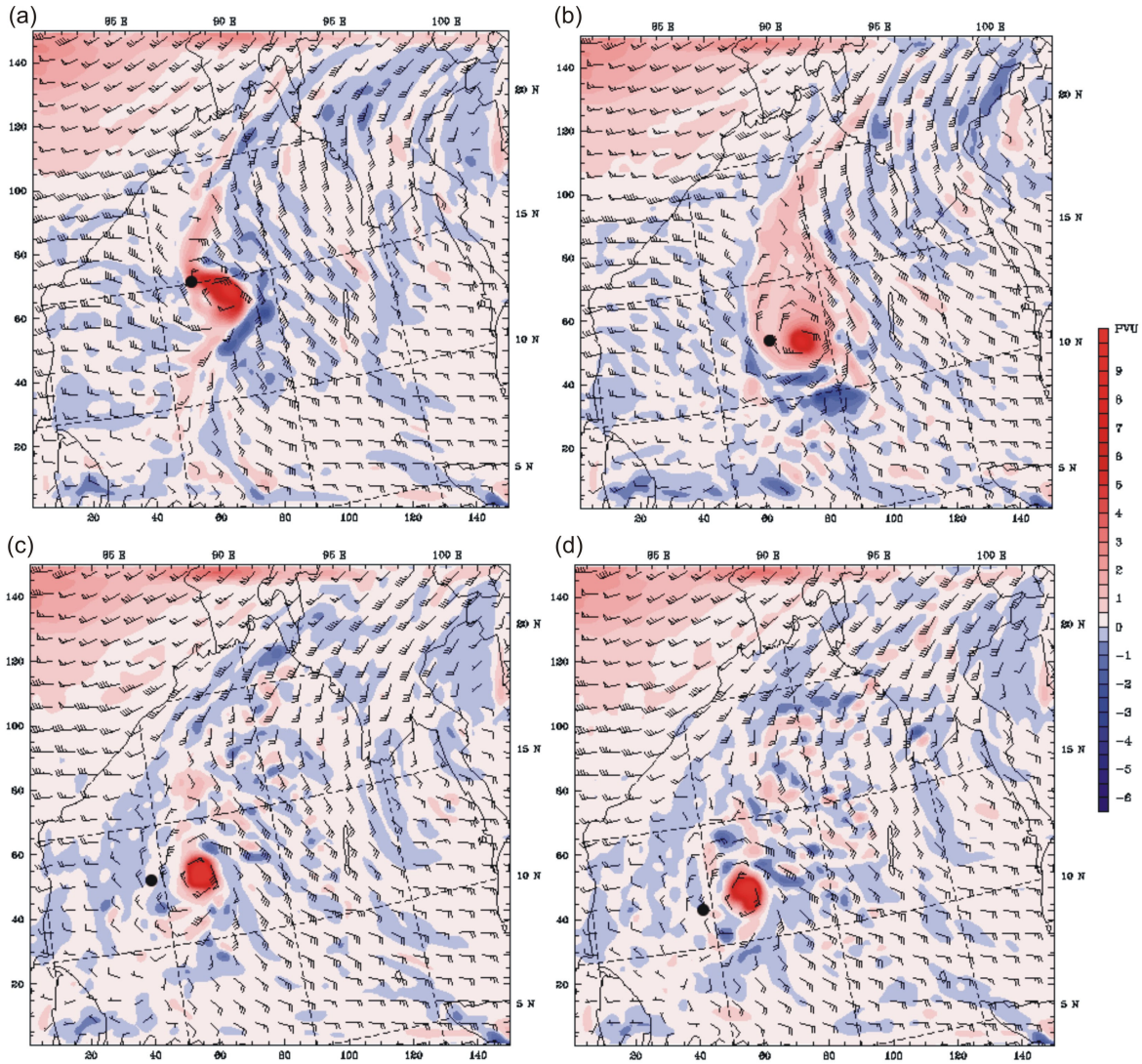

Figure 7.4: 300 hPa PV and wind analyses for (a) KF at 1800 LST on 14/11/07, (b) BMJ at 1800 LST on 14/11/07, (c) GD at 1800 LST on 14/11/07, and (d) No Cu at 1800 LST on 14/11/07. Black circles mark the location of each surface cyclone. The KF and BMJ schemes showed stronger westerly flow than the GD and No Cu, which steered those cyclones north. The analyses are from the coarse domain. Note that 1 PVU is equal to 1.0×10^{-6} m^2 s^{-1} K kg^{-1}.

As stated, the tracks of the other schemes were not as good as for KF, despite the other schemes simulating the position of anticyclonic PV more accurately. This is partly due to the upper-level wind field that resulted from the weaker intensity of anticyclonic outflow aloft. For instance, the KF simulation produced a stronger southerly and westerly flow from the greater PV anomaly at 300 hPa, but the GD and No Cu cases both produced much weaker flows. The flows in these cases tended southwest rather than south, which suppressed the westerly flow. The southwest airflow effectively steered the GD and No Cu cyclones east. It is reasonable to conclude that differences in parameterisation of convection in each scheme resulted in track variation. Indeed, Dengler and Reeder (1997) found that relatively minor changes to the CP have a relatively large effect on the motion of the tropical cyclone. This can also be said for changing the CP scheme within a model,

which will change the way the parameterised clouds transport momentum. These momentum changes have been shown to impact upon the upper-level structure of simulated cyclones (Davis and Bosart 2002). It is reasonable to conclude that this was the case here.

7.5 Convective parameterisation analysis

Having described the effects of the schemes on central pressure, wind speed, and cyclone track, it is time to examine how each of the CP schemes performed in relation to CAPE and precipitation. As previously stated, the CP schemes resolve CAPE using reference profiles which are adjusted after initial simulation. At this stage, it is important to restate what CAPE is, and how it affects tropical cyclones. CAPE is the amount of potential energy available to accelerate a parcel vertically, and is an indicator of atmospheric instability. This is important for tropical cyclogenesis, as an unstable environment will assist convective development. In relation to CP in numerical models, if a scheme manages to lift a parcel of air to the LFC, then the amount of CAPE from the LFC to the EL (see Figure 2.15 in Chapter 2) will represent the instability of the atmosphere within a grid cell. CAPE is, therefore, an excellent measure to use for this analysis, as it reflects the intensity of any convection that eventuates.

It is important to note that because CAPE represents potential energy, the energy will only be used if the CP scheme is able to lift the subject air parcel to the LFC and trigger convection. The precipitation fields will therefore indicate where on the grid domain each CP scheme triggered precipitation, and the intensity of that precipitation is determined by the amount of CAPE at that grid point. Recall that it is the PCP scheme that parameterises the cloud structures. It is the role of the CP to account for the PCP convective effects through the redistribution of temperature and moisture in a grid column. CP acts to prevent the PCP from creating un-realistic large scale convection. Thus, by analysing precipitation fields, it is possible to comment on the accuracy of the CP scheme.

The following section examines CAPE and precipitation simulation across three stages of Sidr's life cycle: development, maturity, and decay. An overall summary of the accuracy of the CP schemes in relation to this work concludes this section.

7.5.1 Development

The reference times for the end of the development period were indicated in Table 7.1. CAPE and precipitation results are from the coarse domain.

7.5.1.1 Convective available potential energy

The results of simulated CAPE during the development phase confirm what the pressure and wind speed intensity has shown about cyclone development. During the first 36–48 hours of simulation it is evident that intensity differences between the schemes were the result of instability differences throughout the cyclone environment. The KF scheme simulated CAPE that occurred near the peak of cyclone development at 1800 LST on 12/11/07 (Figure 7.5a) resolved a stable convergence zone of no CAPE at the cyclone centre, consistent with theories on eye development. The rotational aspect of the developing cyclone is evident. The immediate surroundings were convectively unstable, and adjacent to the centre moderately unstable conditions were simulated. Further from the centre, particularly to the south, embedded in a moderately unstable zone was a very unstable convective environment of CAPE in excess of 2500 J kg^{-1}. The airflow indicates that this unstable air was slowly being entrained in the rotational circulation.

The BMJ scheme simulated CAPE showed quite a different environment at the peak of the development phase (Figure 7.5b). The circulation was weaker, as indicated by the wind barbs and previous data in Figure 7.2. This was likely due to the weaker convective instability compared to the KF case. Indeed, about the storm centre, the environment was only marginally unstable, with CAPE in the order of 200–400 J kg^{-1}. There was no stable convergence centre like that seen in the KF case, and the moderately to very unstable convective region was smaller and further west of the cyclone environment.

An interesting result was found with the GD and No Cu cases, in that CAPE was quite similar during their respective development phases. Firstly, the GD scheme simulated CAPE for 1800 LST on 12/11/07 (Figure 7.5c) resolved a stable convergence zone. This was similar to that of the KF, but of a smaller extent. The environment was not as highly unstable as the KF, but directly east of the centre was a region of very unstable air not simulated in the KF case. Another interesting result was the development of subsidence regions to the north of the cyclone centre, indicated by areas of stable air and no CAPE

embedded in the flow. The No Cu case (Figure 7.5d) simulated the same stable convergence zone, a similar convectively unstable atmosphere, and subsidence to the north, but all were not quite as prevalent as in the GD case. The very unstable region about the centre was slightly more extensive than for the GD simulation. Overall, it is clear that the KF predicted environment contained the greatest amount of convectively unstable air, which might explain why it was more intense during the development phase.

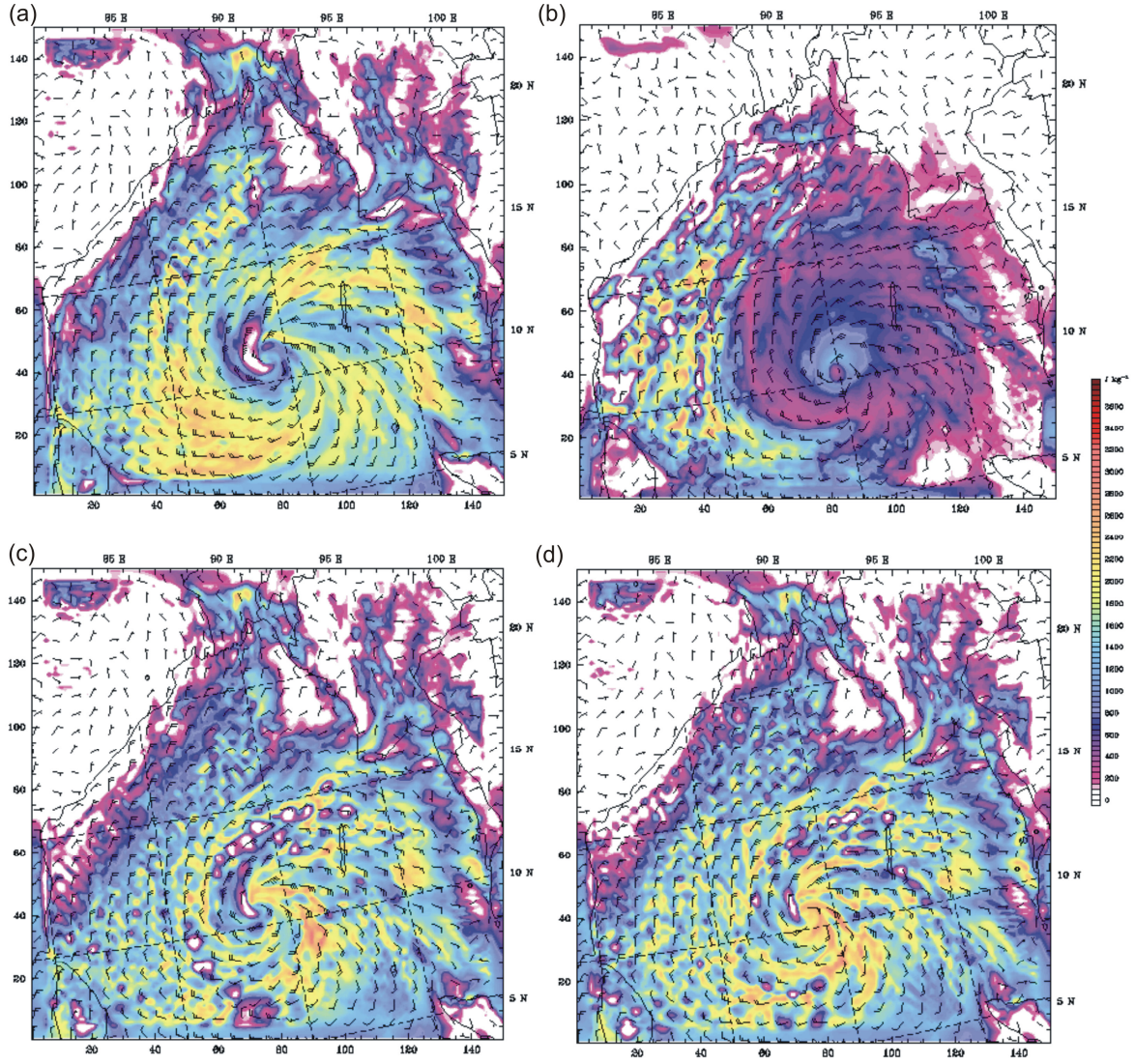

Figure 7.5: Simulated CAPE in J kg^{-1} during the development phase for (a) KF at 1800 LST on 12/11/07, (b) BMJ at 0600 LST 13/11/07, (c) GD at 1800 LST on 12/11/07, and (d) No Cu at 1800 LST on 12/11/07. The CAPE fields are from the coarse grid domain.

7.5.1.2 Precipitation

Rainfall totals for one hour during the development phase are shown in Figure 7.6a-d. The choice of CP scheme was found to affect the developing disturbance in quite different ways. Firstly, with the BMJ scheme (Figure 7.6b) the intensity of the storm is reduced relative to the other schemes. The area coverage of light precipitation (2–8 mm/hr),

however, is consistent with observations at this time (see Figure 4.11 in Chapter 4). In comparison, the KF scheme (Figure 7.6a) triggered light, yet sporadic, convection across the same region, and a rotational component to the precipitation field was evident. Furthermore, the intensity of precipitation about the southern inflow was best resolved by the KF scheme. The GD (Figure 7.6c) and No Cu schemes (Figure 7.6d) did not resolve lighter precipitation throughout this part of the grid, but instead resolved individual deep convective cells with a rotational aspect. Such a finding is consistent with observations of developing tropical disturbances, as shown by Mayfield et al. (1994).

An interesting finding was that the KF, GD, and No Cu schemes appear to have resolved the storm centre quite similarly at this time. Indeed, the intensity and position of rainfall at the centre were similar, but spurious by about 15–20 mm/hr when compared with the observed analysis (see Figure 4.11 in Chapter 4). This would indicate that these CP schemes failed to adequately control the PCP scheme, so that excess precipitation was produced. Furthermore, the developing concentric eye and intense precipitation rates at the centre of the KF scheme cyclone confirm that it was the fastest to develop into a category 1 cyclone. In addition, the No Cu scheme performed remarkably similarly to the GD simulation. This indicates that the use of explicit convection renders a similar result to that of a combination of implicit schemes that the GD ensemble uses for this event. This is an interesting result, as modelling convection explicitly is physically questionable on grids over 9 km (Molinari and Dudek 1992).

Another interesting result was found when comparing the CAPE simulations in Section 7.5.1.1 to the amount of precipitation actually resolved across the domain. Firstly, it is apparent that despite an abundance of CAPE in the KF, GD, and No Cu schemes, only precipitation around the cyclone region was resolved. One explanation for this is that because the KF scheme requires 90% of CAPE to be removed for CP closure, it was simply not reached in these regions, and precipitation could not result. Another explanation is that the CP scheme is effectively controlling the PCP scheme, providing feedback to the PCP that no deep convective cloud can form in these regions. In all likelihood the KF shallow convection scheme (no precipitation) would trigger. These explanations are valid for the GD ensemble also, which uses CAPE as one of its many closure assumptions. Difficulty arises when attempting to account for the explicit No Cu case. The fact the No Cu simulated precipitation field is similar to that for the GD ensemble would indicate that the PCP performs well regardless of the use of a CP scheme. This is a fascinating finding,

but should be treated with caution. Finally, the BMJ scheme triggered precipitation surrounding the cyclone from only moderately unstable air, but not from very unstable air to the west. This can be explained by the triggers required for the BMJ CP scheme to activate. It is likely that in these regions convective cloud depth did not exceed the threshold value and the reference soundings were not moist.

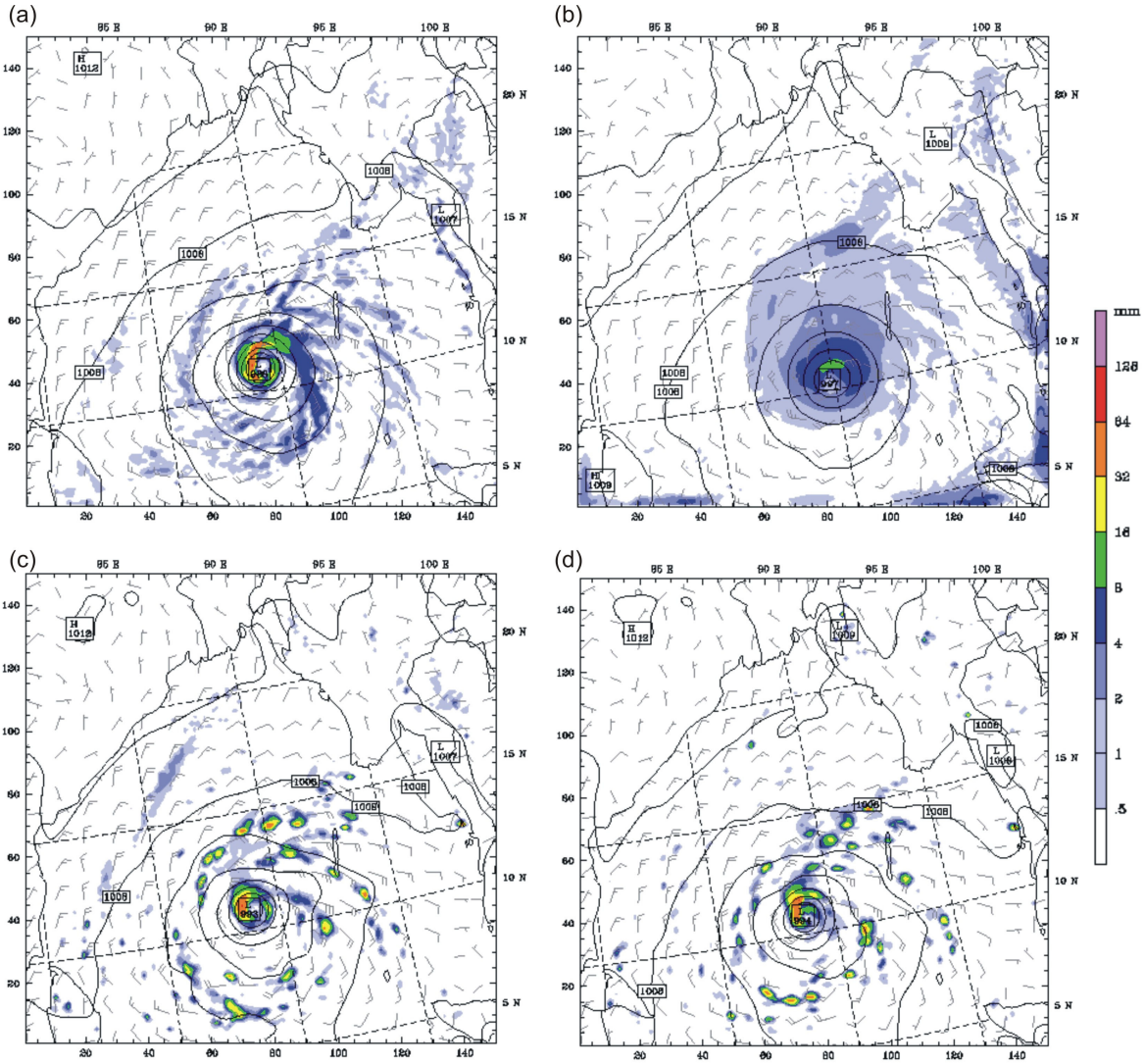

Figure 7.6: Rainfall totals for one hour during simulation development for (a) KF at 1800 LST on 12/11/07, (b) BMJ at 0600 LST on 13/11/07, (c) GD at 1800 LST on 12/11/07, and (d) No Cu at 1800 LST on 12/11/07. The contour interval for sea level pressure is 2 hPa. The precipitation fields are from the coarse domain.

7.5.2 Maturity

The high resolution domain revealed some interesting features at the maturation stage of each of the simulated cyclones. Despite the differences in track, it is still possible to compare the simulations, but it is important to note that because the KF simulation was nearing landfall, some effects of land were evident. This was particularly the case for CAPE. The reference times for the maturity phase were previously listed in Table 7.1.

7.5.2.1 Convective available potential energy

The higher resolution domain enabled more explicit definition of CAPE in the immediate area surrounding the cyclone. It was possible to assess the stability of the eye, and of the air mass circulating about the centre.

The KF scheme resolved a strong rotational vortex indicated by the wind barbs (Figure 7.7a). At the KF simulation's most mature stage at 0000 LST on 16/11/07 (note this was the time of peak wind and pressure), the centre of the eye was marginally unstable. A marginally unstable eye can be common for a cyclone, as shown by Anthes (1982); and will often mean low-level cloud is present. In addition, the affect of land is evident as diminished CAPE to the north and west of the cyclone resulted from dry stable air flowing south from the Bangladesh coastline. This air was seen to be rotating into the centre, which would eventually assist dissipation, and further filling of the eye. To the southeast, there was a region of very unstable air of 2600 J kg^{-1}, this reflected the energy still available from the ocean. The simulation resolved this air to be flowing north, and into the right front region of the cyclone.

The BMJ scheme prediction at maturity was in sharp contrast to the KF scheme. At the peak of the BMJ simulation life cycle at 0600 LST on 15/11/07, no significant change in CAPE from the development phase was found (Figure 7.7b). The eye was close to neutral stability, with the air mass resolved to be marginally unstable, with CAPE of 200 J kg^{-1}. Directly adjacent to the eye was a region of marginal to moderate instability, but as will be shown in a later section, this moderate instability (1500 J kg^{-1}) had minimal effect on the amount and intensity of convection resolved. The outer edges of the domain to the east were resolved to have very unstable air, but this was limited and appeared to be having minimal influence on the cyclone. The circulation was weak and gently rotating.

The CAPE environment in the GD case was significantly more unstable than the other experiments. The GD CAPE simulation at 0000 LST on 15/11/07 (Figure 7.7c) resolved a north to south oriented eye of stable air which was marginally unstable around the periphery. In contrast to the KF and BMJ schemes, the simulation produced very unstable air surrounding the cyclone core. The GD ensemble represented a CAPE rich environment that provided considerable potential energy for convective development, as was shown via precipitation that was triggered by the scheme (see Section 7.5.2.2).

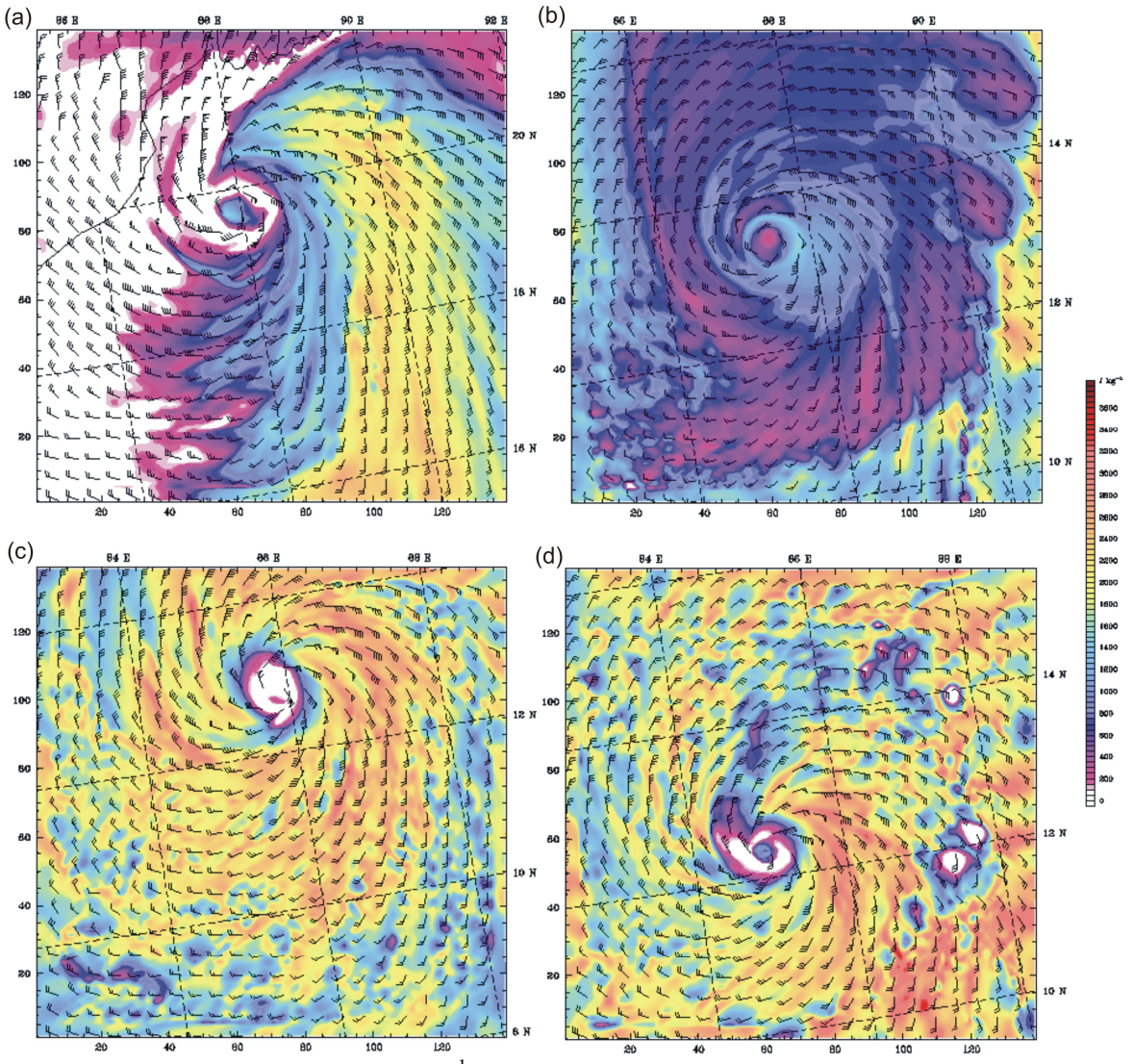

Figure 7.7: Simulated CAPE in J kg^{-1} during the maturity phase for (a) KF at 0000 LST on 16/11/07, (b) BMJ at 0600 LST on 15/11/07, (c) GD at 0000 LST on 15/11/07, and (d) No Cu at 0600 LST on 15/11/07. The CAPE fields are from the nested domain.

The same can be said for the No Cu simulation which was similar to the GD simulation at its maturation on 15/11/07 at 0600 LST (Figure 7.7d). Directly in the centre of the eye was marginally unstable air, but the remainder of the eye was stable. There was less very unstable air to the north when compared to the south. In addition, two notable features that were not seen in the other cases appeared in the No Cu simulation. The first feature was the existence of a number of subsidence regions to the east of the actual cyclone, represented by areas of stable air of no CAPE. The second feature was a minimal amount of extremely unstable air (CAPE in excess of 3500 J kg^{-1}) embedded in the southern air flow. It is likely that having no CP scheme allowed for more variation between stable and unstable conditions throughout the cyclone environment, which might explain the subsidence regions at this time of the analysis.

Overall, the results of CAPE for the maturation phase show quite distinct differences in the amount and distribution of potential energy in the cyclone environment for each CP scheme. This did have an effect on the intensity of each cyclone, as will be shown in relation to the precipitation rates and cyclone structure, in the following sections.

7.5.2.2 Precipitation

The high resolution domain resolved cyclone precipitation structure at maturity rather well. All schemes show reasonable representation of common precipitation characteristics expected of a mature cyclone. An eye of little to no precipitation was simulated, with a region of heavy precipitation directly adjacent to the eye representing the eye wall. Precipitation also decreased with increasing radius from the eye wall. No significant spiral rain bands were simulated, which was an incorrect result in comparison with observations.

Considering the performance of each CP scheme in turn reveals some similarities and differences in the way each resolved precipitation across the domain. Firstly, the KF scheme showed a distinct asymmetry at its maturity, which none of the other schemes showed. Indeed, the eye wall was not concentric like the GD and No Cu predictions, but split, with an intense region to the northwest, and one further to the southeast (Figure 7.8a). Secondly, precipitation rates at the eye wall appear to be reasonably similar for the KF, GD, and No Cu schemes, but not BMJ. It is evident that a maximum hourly total between 84–128 mm was resolved by the KF, GD, and No Cu schemes, with only the extent of maximum precipitation coverage varying. The GD scheme appears to have resolved the most extensive amount of intense precipitation about the eye wall (Figure 7.8c). When compared to TRMM observations (see Figure 4.11c in Chapter 4) around this time, it is clear that the KF, GD, and No Cu schemes have predicted excessive precipitation in the eye wall. This would indicate that these CP schemes were under-active in this environment, and have failed to control the amount of cloud development by the PCP scheme. Finally, while the BMJ scheme may not have resolved cyclone structure well, it would appear to be the most accurate CP scheme for the high resolution domain. The BMJ simulated precipitation rate is quite similar to observations for the mature stage, indicating that perhaps the convective adjustment technique is the best performing type of scheme for this event. Indeed, rainfall totals for one hour (Figure 7.8b) are quite accurate. For example, the deep convection in the northeast region was between 32–64 mm/hr. Furthermore, in relation to the amount of precipitation triggered for each grid point across

this domain, it is interesting to note that the BMJ scheme appears to have triggered convective precipitation over a greater extent. This is certainly the case for light precipitation. When examining the area coverage of the cyclone itself, however, the KF prediction is significantly greater than all others. Indeed, a more significant eye wall and eye were resolved.

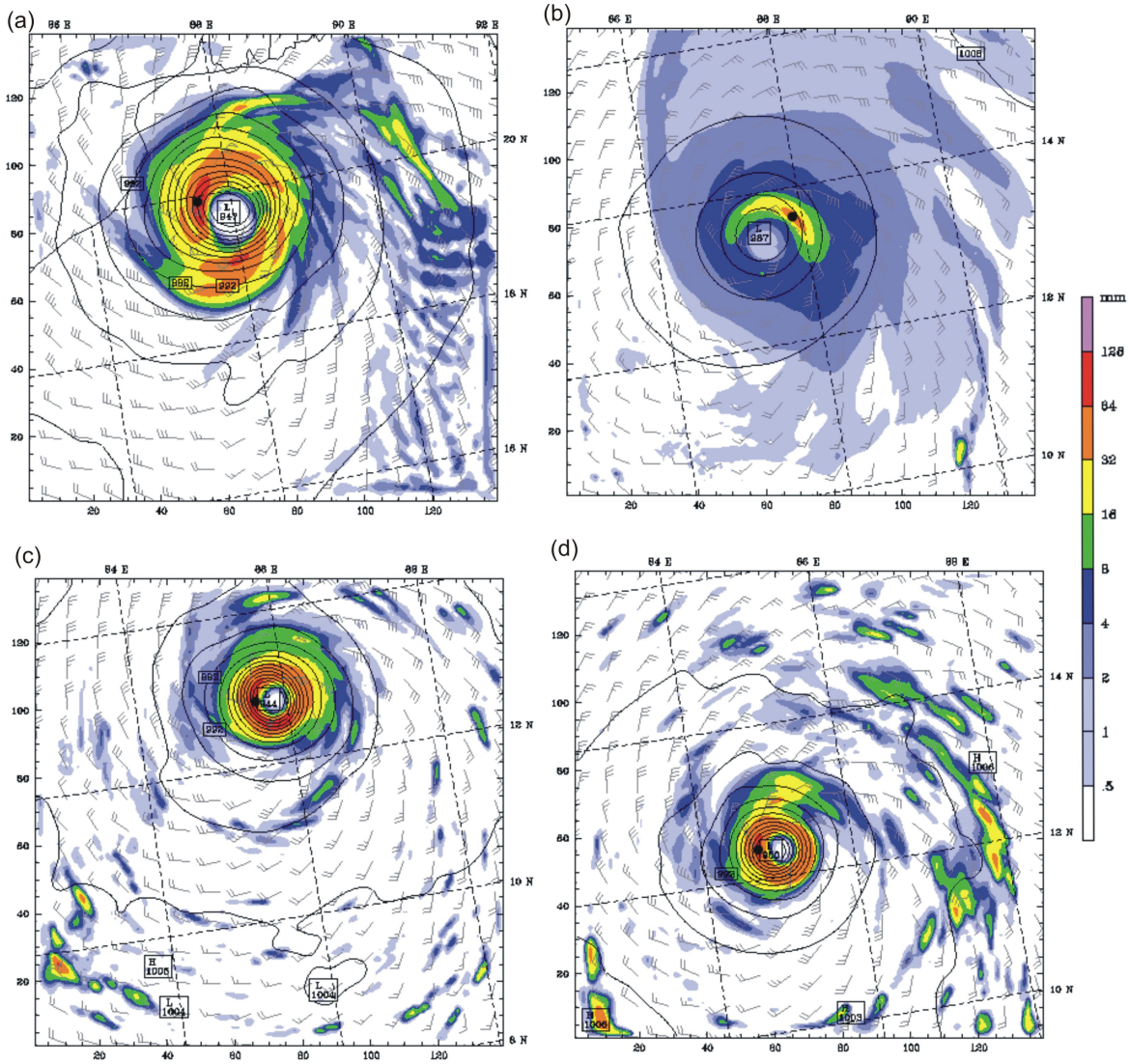

Figure 7.8: Rainfall totals for one hour during simulation maturity for (a) KF at 0000 LST on 15/11/07, (b) BMJ at 0600 LST on 15/11/07, (c) GD at 0000 LST on 15/11/07, and (d) No Cu at 0600 LST on 15/11/07. The contour interval for sea level pressure is 4 hPa. Note the grid resolution is 5 km, and the black circle marks the location of the eye wall sounding for each cyclone.

As in the development phase, the comparison of CAPE to the final amount of precipitation resolved and type of cyclone structure simulated can be studied. Firstly, the asymmetrical nature of the KF simulation is likely to have resulted from an imbalance of CAPE at this time because the cyclone was near land. As discussed, the dry air flowing into the cyclone centre from the north has likely perturbed the convergent cyclonic flow, creating an imbalance in stability. Furthermore, with the only moisture and latent heat supply coming from the south, it is reasonable to conclude that asymmetry in flow would occur. Secondly,

the axisymmetrical nature of the GD and No Cu simulations is perhaps a consequence of being over open water, and having convective energy available to both the north and south inflow regions. Finally, as discussed the BMJ scheme resolved the lowest levels of CAPE, but triggered the most precipitation over the domain. It appears, therefore, that only a moderately unstable environment is required for the BMJ scheme to trigger deep convection in this instance. This conforms to the theoretical explanation of the BMJ scheme outlined in Chapter 2.

7.5.2.3 Vertical soundings

At this point, it is of interest to examine how the model-simulated soundings in the eye and eye wall compare for each of the CP schemes at maturity. Soundings were extracted from locations on the nested domain. Eye soundings were taken from the centre of the cyclone, and the location of the eye wall soundings are marked in Figure 7.8.

There are a number of comments to make regarding the eye soundings. Firstly, the eye soundings show that the KF (Figure 7.9a), GD (Figure 7.9c), and No Cu schemes (Figure 7.9d) reflect similar air mass characteristics, while BMJ differs. It is evident that the BMJ simulation (Figure 7.9b) was moister than all other schemes above the 700 hPa layer, and especially above the 350 hPa layer, but was not saturated at the surface. Indeed, the KF, GD, and No Cu schemes were all saturated at the surface to approximately 800 hPa, 900 hPa, and 900 hPa respectively, after which they were dry. An interesting feature that was observed in the GD simulation at 300 hPa was a shallow moist layer of high potential temperature, and a temperature inversion above. This marked a distinct separation between moist boundary layer air and descending warm, dry air. The exact same feature was also observed in the BMJ simulation, but at 500 hPa, not 300 hPa. This would indicate that in the BMJ simulation, the descending warm air was able to penetrate further into the middle-troposphere.

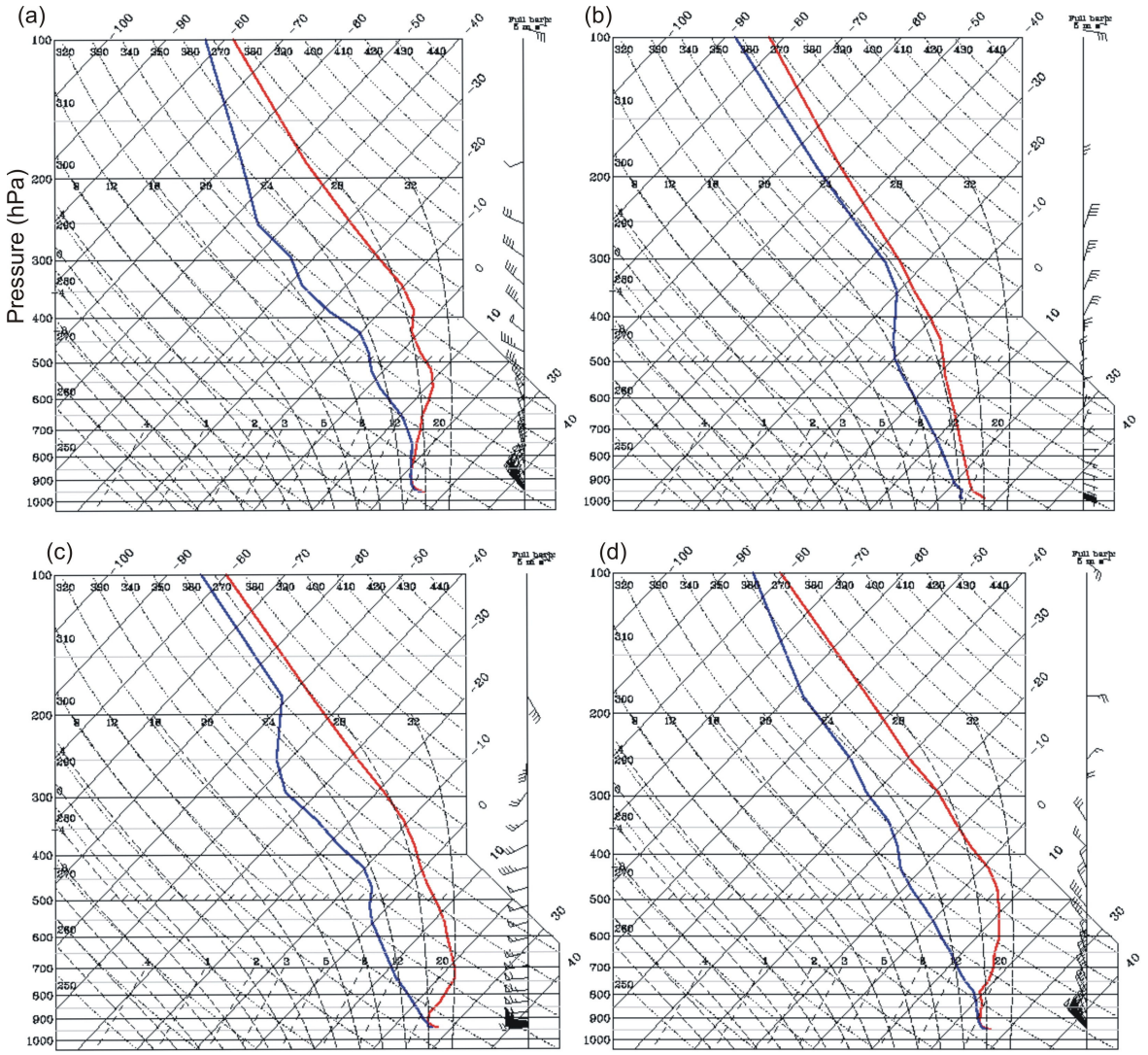

Figure 7.9: Skew T soundings located within the eye at maturity for (a) KF at 0000 LST on 16/11/07 (x, y location on the nest domain: 53,84), (b) BMJ at 0600 LST on 15/11/07 (58,78), (c) GD at 0000 LST on 15/11/07 (72,100), and (d) No Cu at 0600 LST on 15/11/07 (57,54). The blue curve is dew-point temperature, and the red curve is the air temperature. The bracketed values are the grid locations from Figure 7.8a-d. The sounding locations were directly in the centre of each cyclone eye in Figure 7.8a-d.

The simulated soundings from within the eye wall revealed some interesting features. Firstly, a commonality between all schemes was the near-saturated thermal structure extending to various levels in the troposphere. It was interesting that the BMJ simulation was saturated to 500 hPa, higher than any other scheme, as the KF (680 hPa), GD (700 hPa), and No Cu schemes (700 hPa) were saturated at much lower-levels. Secondly, the temperatures are much cooler than those in the eye. This was to be expected because the eye contained dry, subsiding air and the eye wall moist, rising air. Finally, a very interesting finding was that all eye wall soundings except for the BMJ simulation were dry above their respective levels of saturation. The BMJ simulation, however, remained closer to saturation throughout the troposphere. This reveals some interesting findings regarding the activity of the CP schemes.

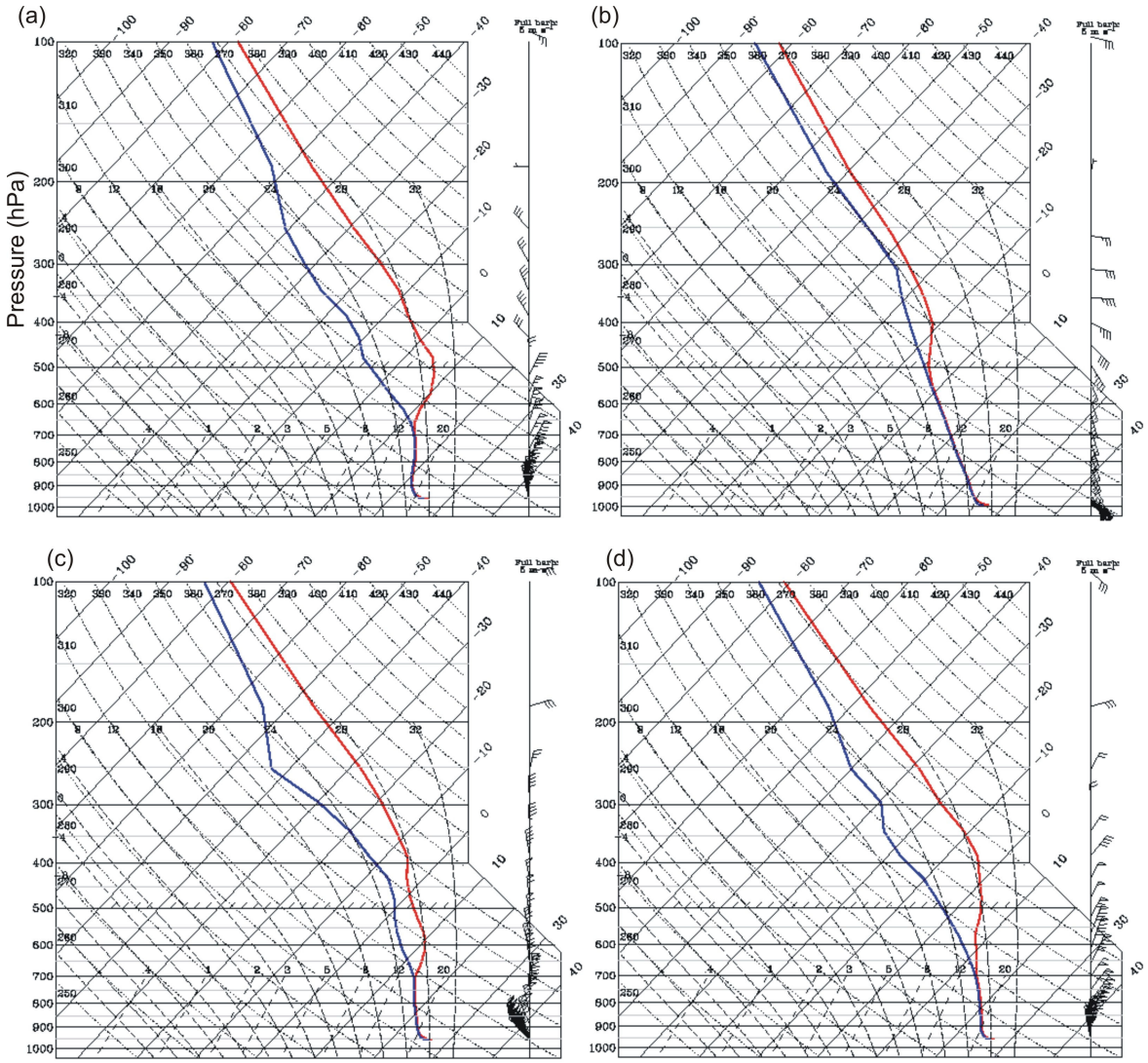

Figure 7.10: Skew T soundings located within the eye wall at maturity for (a) KF at 0000 LST on 16/11/07 (51,88), (b) BMJ at 0600 LST on 15/11/07 (66,83), (c) GD at 0000 LST on 15/11/07 (65,102), and (d) No Cu at 0600 LST on 15/11/07 (55,57). The blue curve is dew-point temperature, and the red curve is the air temperature. The bracketed values are the grid locations from Figure 7.8a-d, and for the sounding locations refer also to Figure 7.8a-d.

The eye and eye wall soundings give some indication as to the activity of the CP schemes in the model simulations. Recalling that the primary purpose of a CP scheme is two fold — to reduce instability and remove moisture and to give feedback to the PCP scheme. Precipitation is only a by-product of instability removal. It is possible to infer from both a sounding and a precipitation field whether a scheme has been too active (removed too much instability and moisture) or under- active (removed too little). Firstly, it is evident from the simulated eye soundings that the KF, GD, and No Cu CP schemes are all under-active because their profiles are too moist at low levels. This is likely the result of missing convective downdraughts that would normally cool the low levels and remove excess moisture. In fact, it seems that the BMJ scheme has accounted for convective downdraughts well in the adjustment process, although not actually having modelled a

cloud like the other schemes. Indeed, the BMJ profile was sub-saturated at low levels, indicating that moisture was removed in the adjustment process. Furthermore, studying the precipitation fields (Figure 7.8a-d) confirms this theory. The BMJ scheme (Figure 7.8b) has resolved a light amount of precipitation in the eye associated with low-level clouds, which is a by-product of moisture removal. The other schemes (Figure 7.8a, 7.8c, and 7.8d) resolved no precipitation in the eye, indicating that the model was unable to produce sub-grid-scale convection with the PCP scheme for this region. The finding using the BMJ scheme is consistent with the observed situation (see Figure 4.11, Chapter 4); further proving that it resolved the eye the best at this stage. Finally, using the eye wall soundings and precipitation fields in Figure 7.8, it is possible to indicate whether the CP schemes were performing correctly for this region of the cyclone. As previously stated, from the examination of the precipitation fields (Figure 7.8a-d) the KF, GD, and No Cu CP schemes all predicted excessive precipitation in the eye wall region. Indeed, the eye wall soundings confirm this as the mid-level regions in KF, GD, and No Cu are all too dry and stable. This means that these schemes have removed too much instability and created too much precipitation. The BMJ simulated sounding is representative of how the other eye wall soundings should be, as the profile remains near saturation to an appropriate level, and is not too dry above that point. This allows for an appropriate amount of precipitation to be released from the environment, rather than too much instability and moisture removal producing excessive amounts of precipitation as a result. To rectify predictions of excessive precipitation, changes can be made to temperature and moisture of the environment downstream of the surface cyclone.

7.5.3 Decay

Computational demands meant that the simulations could not run for as long as desired, so the results for cyclone decay were not as had been anticipated. Despite this issue, the simulations were either showing good evidence of decay, or were just entering the decay phase. The reference times for the decay phase were previously listed in Table 7.1.

7.5.3.1 Convective available potential energy

There was minimal change found in the KF simulation from the time of maturity to what was observed during decay at landfall. Indeed, CAPE across the Bay of Bengal remained relatively the same as the maturity analysis, despite the different domain resolutions. There

were some notable changes however, and these were evident at 0600 LST on 16/11/07 (Figure 7.11a). Firstly, CAPE was completely absent from the left front and left rear of the cyclone. The KF simulated cyclone was positioned off the coast of Bangladesh and as previously stated CAPE was reduced due to the effect of land. This was a contrast to the maturity phase, as in this analysis no unstable air was observed to be filling into the centre from the west. At the decay phase, the coarse domain resolved less very unstable air to the south compared with the maturity analysis. There was still an abundant amount of unstable air further south of the storm, and the wind flow across the bay was assisting the transportation of this northward.

The BMJ simulated CAPE during decay at 0600 LST on 16/11/07 (Figure 7.11b) was rather difficult to assess for storm decay, as the system never actually made tropical cyclone status. Indeed, there appeared to be minimal change in CAPE between maturity and decay. The centre of the storm actually showed an increase in instability, with CAPE in the order of 1000 J kg^{-1} resolved. Further south a region of moderate to very unstable air was resolved embedded in a marginally unstable flow. This appeared to have no influence on the storm at this time, as it was well south of the centre. The storm was tracking northwest towards land, and the initial signs of CAPE reduction in this region were evident. As this was the start of the decay phase, the effect of land would probably not be seen for another 12–18 hours of simulation.

At the same time, the GD simulation (Figure 7.11c) was further advanced toward India than the BMJ scheme and showed similar decay characteristics to that of KF. The effect of the Indian coast was quite evident on the reduction of potential energy to the southwest of the cyclone. In particular, dry stable air was filling into the centre by means of strong rotation from the south. The northern sector was still abundant with very unstable air, and the northern inflow was still feeding this air into the centre. The cyclone was clearly in the process of dissipation as the removal of potential energy from the left and right rear of the cyclone would ultimately fuel the destabilisation of the structure.

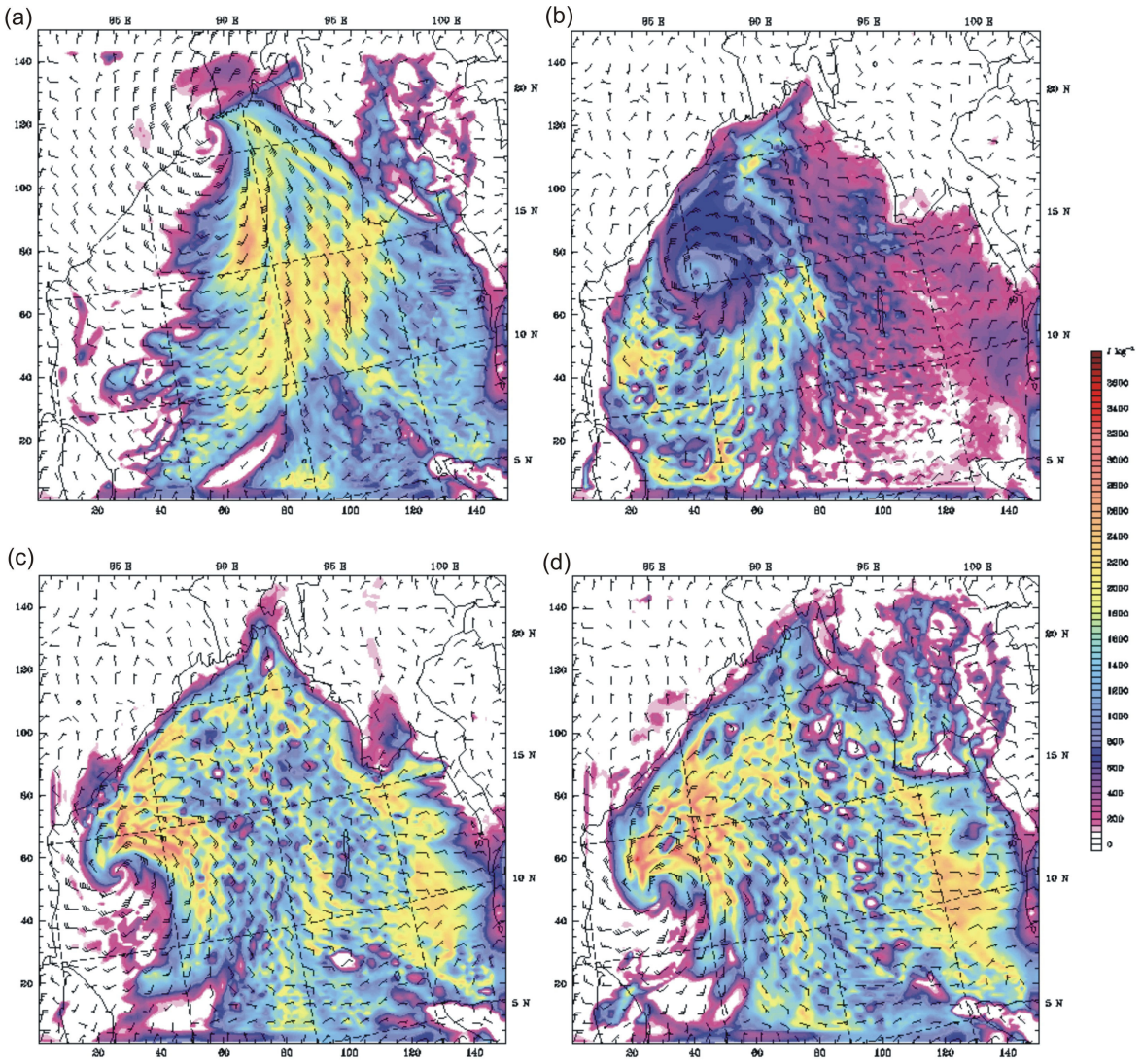

Figure 7.11: Simulated CAPE in J kg^{-1} during the decay phase for (a) KF at 0600 LST on 16/11/07, (b) BMJ at 0600 LST on 16/11/07, (c) GD at 0600 LST on 16/11/07, and (d) No Cu at 0600 LST on 16/11/07. The CAPE fields are from the coarse domain.

The No Cu simulation at 0600 LST on 16/11/07 (Figure 7.11d) continued the trend of similarity with the GD case into the decay phase. The rotation in the No Cu simulation was weaker than that seen in the GD simulation, explaining why the immediate centre of the storm was yet to fill with stable air. Arguably, this cyclone was further advanced in its dissipation compared to GD, primarily due to the lack of intense rotation. The No Cu simulation also had a greater amount of very unstable air north of the centre.

In summary, the effect of land on decay was quite evident in the KF, GD, and No Cu cases. Depending on the storm position relative to land, the southern section of each cyclone showed the infilling of stable air as potential energy was removed from the environment. This is part of the decay process commonly illustrated in cyclone theory.

7.5.3.2 Precipitation

Precipitation for the coarse domain during the decay phase showed characteristics common for this period of cyclone life cycle. Firstly, the KF simulation predicted landfall near Calcutta, southwest of the observed landfall site. It showed distinct characteristics of dissipation, namely a perturbation of the pressure field as frictional forces of land impacted upon the airflow at the surface, and an increasing asymmetrical component. For example, it is evident in Figure 7.12a that the eye wall was disintegrating, and the eye had started the process of filling. KF simulated precipitation rates remained high in the northwest and southwest parts of the eye wall (32–64 mm/hr). In addition, a trail of light precipitation stretching from the tail of the cyclone to the south of the Bay of Bengal was an interesting feature. This corresponded to a similar trail feature in the CAPE simulation (Figure 7.11a), except CAPE indicated more unstable air than the CP scheme appears to have resolved in terms of precipitation. Secondly, the BMJ simulation showed a decrease in precipitation rate from the mature stage, but when compared to the coarse domain at development, there was no decrease. Indeed, both BMJ simulated precipitation fields at development and decay are remarkably similar, further proving that this cyclone did not undergo dynamic changes like the other simulated cases. Finally, the trend of similarity between the GD and No Cu cases continued at decay. In both cases, the simulated cyclones were approaching the east coast of India, and their structures were similar. For example, both cyclones resolved a number of deep convective cells to the north, and the southern extent of the eye wall was similar. In contrast, the extent of the No Cu simulated cyclone was greater than for GD, and had also resolved more intense precipitation to the north of the eye. From the time of analysis it appears that the GD predicted cyclone was further decayed than that of the No Cu scheme.

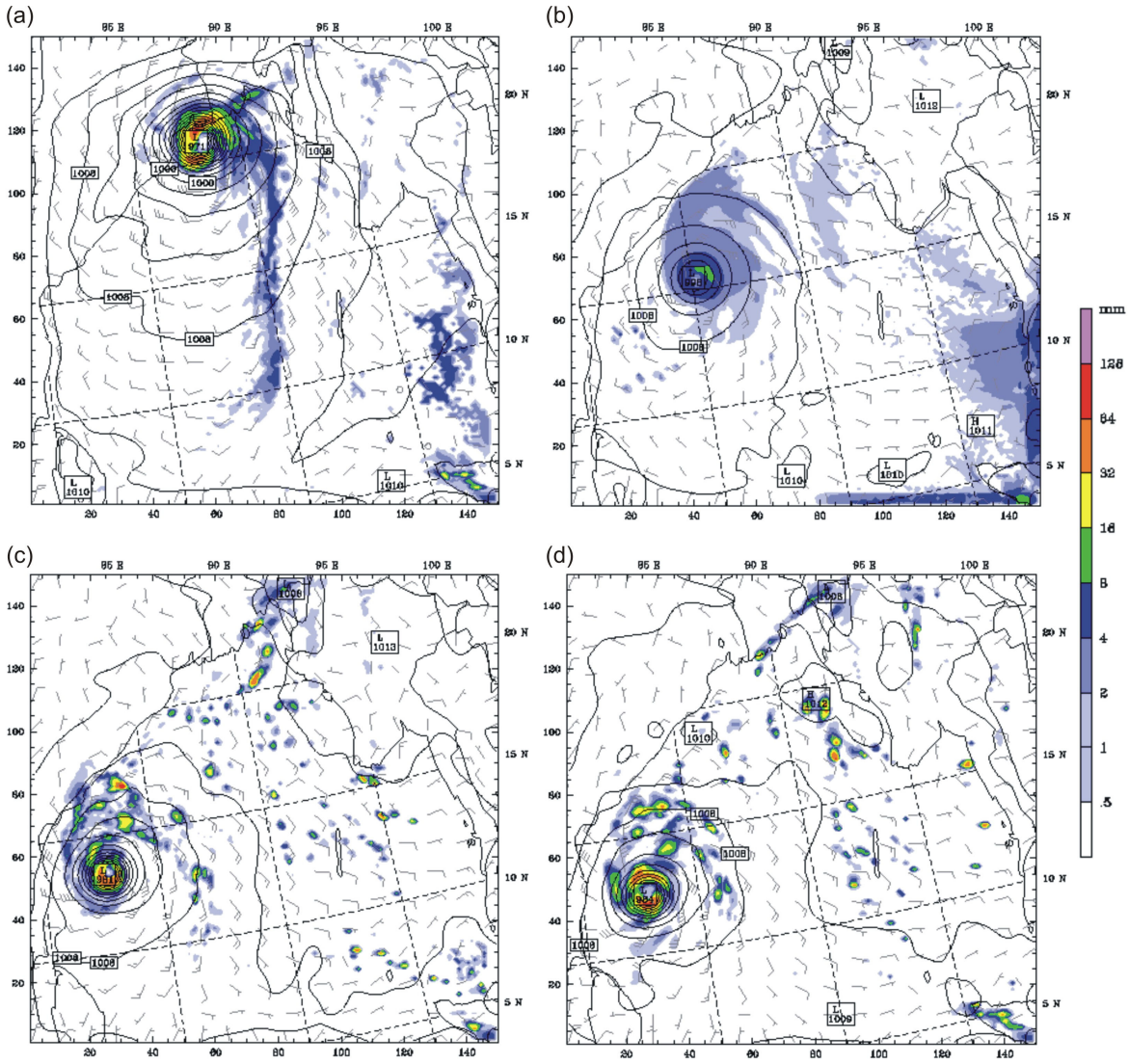

Figure 7.12: Rainfall totals for one hour during simulation decay for (a) KF at 0600 LST on 16/11/07, (b) BMJ at 0600 LST on 16/11/07, (c) GD at 0600 LST on 16/11/07, and (d) No Cu at 0600 LST on 16/11/07. The contour interval for sea level pressure is 2 hPa. The precipitation fields are from the coarse domain.

7.5.4 Summary of the CP experiments

A summary of the CP experiments is given in Table 7.2. In summary, the KF, GD, and No Cu simulations recorded excessive rates of precipitation; and the BMJ simulation was the most realistic. In addition, the excessive amount of instability removed from the environment by the KF and GD schemes, indicates that these CP schemes were over-active. The feedback to the PCP, therefore, was such that over-vigorous convection was initiated. Modelling of convection explicitly in the No Cu simulation also resulted in excessive instability removal and over-vigorous convection. The BMJ scheme removed a realistic amount of instability in some regions, and was under-active in others.

Table 7.2: Summary table showing the performance of the CP schemes.

Experiment	Precipitation rate* (mm/hr)			Instability removal*	Overall CP scheme performance; and feedback to PCP scheme
	Development	Maturity	Decay		
KF	32–64	64–128	32–64	Excessive — sounding too dry and stable (see Figure 7.10a)	Over-active — KF scheme removed too much instability which resulted in excess precipitation. Feedback to PCP — PCP scheme produced too much deep convective cloud.
BMJ	8–16	32–64	8–16	Realistic — sounding saturated to appropriate height (see Figure 7.10b)	Mixed — CP realistic in some regions; under-active in others (see Figure 7.11b). The BMJ scheme was never over-active. Feedback to PCP — also mixed. In under-active regions the PCP was unable to produce deep convection.
GD	32–64	64–128	32–64	Excessive — sounding too dry and stable (see Figure 7.10c)	Over-active — GD scheme removed too much instability which resulted in excess precipitation. Feedback to PCP — PCP scheme produced too much deep convective cloud.
No Cu (no implicit CP scheme)	32–64	64–128	32–64	Excessive — sounding too dry and stable (see Figure 7.10d)	Explicit convection removed too much instability which resulted in excess precipitation. Feedback to PCP — PCP scheme produced too much deep convective cloud on the sub-grid.

Note * indicates maximum recorded precipitation rate from the eye wall, and instability removal derived from the simulated eye wall soundings in Figure 7.10.

7.6 Cyclone structure and microphysical quantities

The following section presents high resolution horizontal and vertical reflectivity fields for each simulation during the mature phase. These are used to illustrate the nature and type of precipitation, and cyclone structure. For the vertical fields, reflectivity is combined with mixing ratio contours of graupel to indicate where frozen precipitation was located in the cloud structure.

7.6.1 KF simulated cyclone

The horizontal reflectivity field of the KF simulation (Figure 7.13a) is in reasonable agreement with the KF predicted precipitation (Figure 7.8a). Firstly, a deep convective band of 55 dBz was located in the correct location northwest of the eye, matching the most intense precipitation rates in Figure 7.8a. Secondly, reflectivity decreased with increasing radius from the eye wall, consistent with resolved precipitation. Finally, in contrast to the simulated precipitation, lighter precipitation intensities of 5–20 dBz were not resolved in the surrounding environment, and the isolated convective cells to the northeast appear to be too intense. Indeed, grid cells to the east in Figure 7.8a were found to be lightly precipitating (2–4 mm/hr), and the squall line to the northeast was somewhat less intense than the reflectivity suggests (16–32 mm/hr).

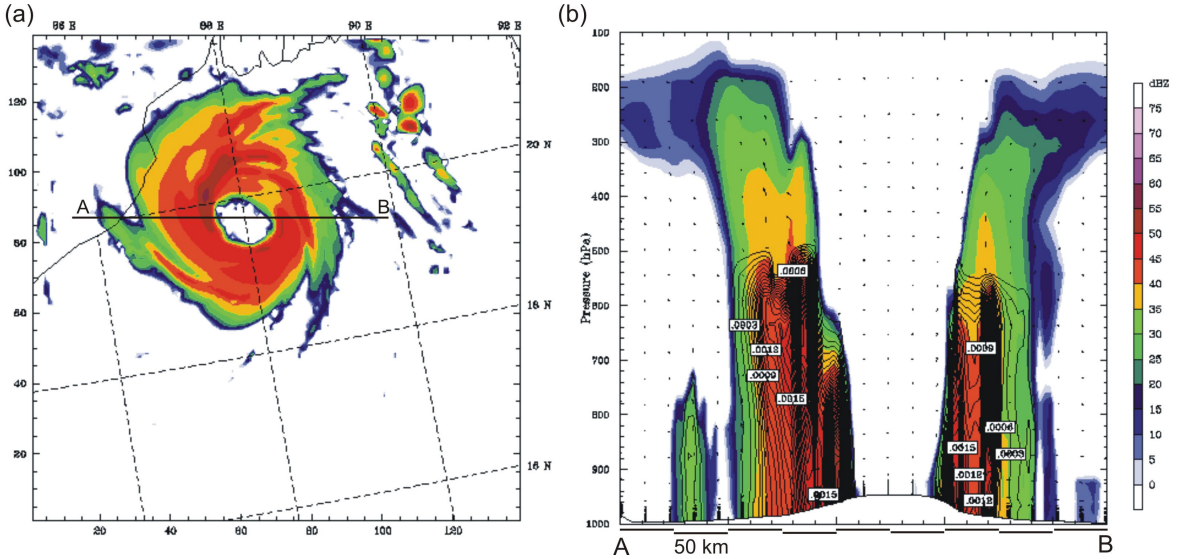

Figure 7.13: KF simulated reflectivity showing (a) horizontal extent of the predicted cyclone at 0000 LST on 16/11/07, and (b) vertical profile with mixing ratio contours for graupel, through the line A–B on Figure 7.13a, for the same time. Note the contour interval for the graupel mixing ratio is 0.1 x 10^{-9} g kg^{-1}.

The vertical structure indicates a number of interesting features (Figure 7.13b).The first was the radial tilting of the eye wall with increasing height. This is a common feature of

mature cyclones, and was also shown by Liu et al. (1997). The second feature was outflow at 200 hPa indicated by the suppression of rising motion capped by the upper-troposphere. The third was a dramatic decrease in reflectivity as air entered this outflow region. The decrease in reflectivity represents cooling aloft and a change from deep convecting precipitation associated with cumulonimbus to ice crystals associated with cirrus. Finally, the size of the eye was roughly 75 km, and eye wall 125 km (on the western side), and 75 km (on the eastern side) indicating that this was a particularly large, intense hurricane at maturity.

The contours in Figure 7.13b indicate the location of graupel in the eye wall. It is interesting to note that the mixing ratios are rather small, and that in the KF simulation, no graupel was resolved above 500 hPa. The most intense regions of graupel were not surprisingly located around the innermost part of the eye wall, and another region of intense precipitation was located at the mid-level (500–700 hPa) on both sides of the cyclone. This can be attributed to intense vertical motion through these regions.

7.6.2 BMJ simulated cyclone

The horizontal and vertical reflectivity fields of the BMJ simulation (Figure 7.14a and 7.14b) confirm the less intense nature of this cyclone compared to both the observed and simulated results. The vertical profile, however, does suggest a weak hurricane developed, which contradicts the Saffir-Simpson classification. Similar to the KF simulated cyclone, reflectivity appears to only register falls greater than 15 dBz intensity, and only the immediate cyclone environment was simulated. There was reasonable agreement between the most intense precipitation simulated and reflectivity. The location of intense precipitation matches in both instances.

The vertical profile (Figure 7.14b) indicates some interesting differences in structure compared to the KF simulation. Firstly, the western side of the cyclone was much less developed. The eye wall only extended to 700 hPa, and did not show intensities similar to those in the KF simulation. A 25 km region of deep convection extending to 970 hPa formed the most intense part of the eye wall on the western side, compared to 70 km and 500 hPa respectively in the KF simulation. Finally, the distinct lack of symmetry between the east and west sides of the BMJ simulated cyclone is illustrated well from the vertical profile. The eastern side of the BMJ simulation showed a more intense eye wall, and

greater amounts of graupel than the western side of the cyclone. For example, the most intense region of the eye wall (reflectivity greater than 40 dBz) covered 35 km and extended to 600 hPa. The eastern eye wall was roughly 75 km in diameter, and extended to 450 hPa. In addition, there was no apparent radial tilting of the eye wall like that seen in the KF simulation, probably due to the expansion of the eye at low levels.

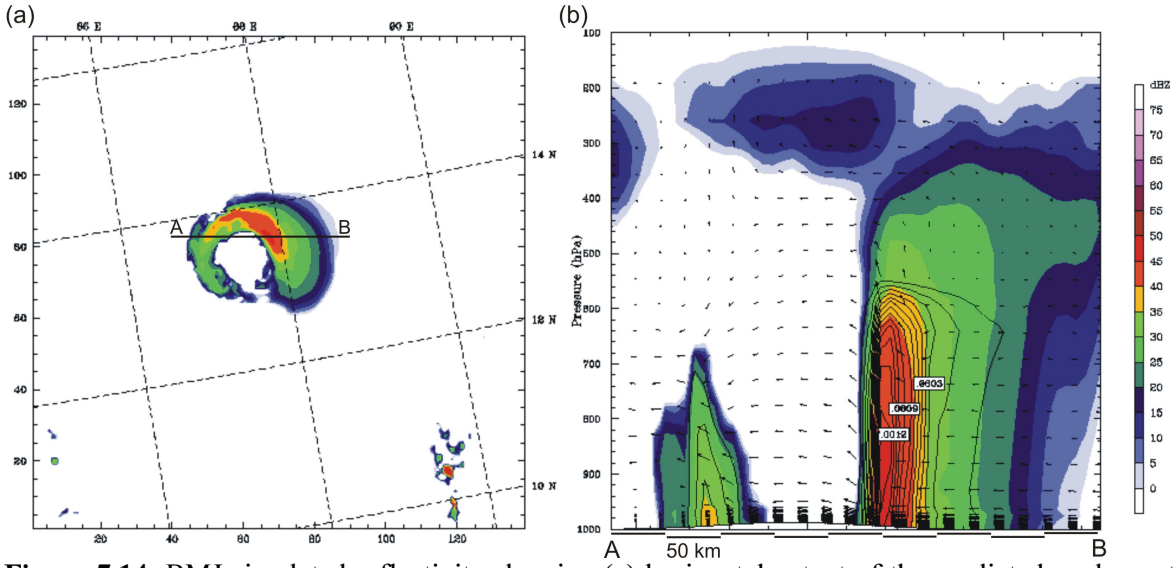

Figure 7.14: BMJ simulated reflectivity showing (a) horizontal extent of the predicted cyclone at 0600 LST on 15/11/07, and (b) vertical profile with mixing ratio contours for graupel, through the line A–B on Figure 7.14a, for the same time. Note the contour interval for the graupel mixing ratio is 0.1 x 10^{-9} g kg^{-1}.

7.6.3 GD simulated cyclone

The reflectivity field of the GD simulation in Figure 7.15a is in close agreement with its respective precipitation field shown in Figure 7.8c, despite a few contrasts. Firstly, reflectivities within the spiral rain band appear too intense. For example, the reflectivity field shows the spiral rain band to have deep convective cells (greater than 40 dBz), but the precipitation rates in Figure 7.8c only resolved 8–16 mm/hr, which is considered light precipitation in a hurricane environment. Furthermore, to illustrate the inconsistency, the reflectivities recorded in the spiral band match those in the eye wall, where precipitation rates of 64–128 mm/hr were simulated. Finally, the eye wall exhibited some inconsistency also. For example, the reflectivity of the eye wall was not exactly consistent with the rates of precipitation. The GD simulated cyclone resolved a concentric eye wall indicated by the precipitation rates in Figure 7.8c, but the reflectivity analysis showed an elongate, slanted cyclone in the north to south direction. In addition, the zone of maximum reflectivity (55–60 dBz) did not agree with the position of the maximum precipitation rate in Figure 7.8c.

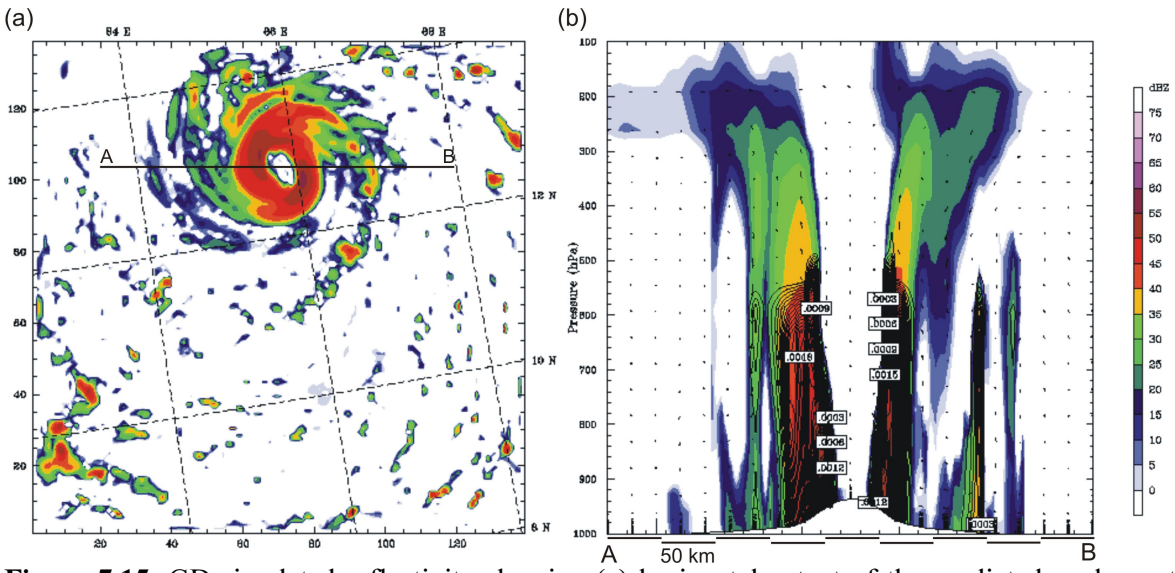

Figure 7.15: GD simulated reflectivity showing (a) horizontal extent of the predicted cyclone at 0000 LST on 15/11/07, and (b) vertical profile with mixing ratio contours for graupel, through the line A–B on Figure 7.15a, for the same time. Note the contour interval for the graupel mixing ratio is 0.1 x 10^{-9} g kg^{-1}.

In comparison to the KF simulation, there are a number of points to note. Firstly, it is evident that the KF scheme predicted a larger cyclone, but not necessarily as intense as the GD scheme at maturity. For instance, comparing the eye walls for each cyclone shows that the GD scheme resolved two regions of intense reflectivity (greater than 55 dBz) both to the northwest and to the southwest. This corresponded to the radius of maximum winds (not shown) at both the north and south feeder regions. In the KF simulated cyclone, however, only one region of intense convection to the northwest was resolved. Furthermore, the vertical structure of the GD cyclone (Figure 7.13b) proved to be quite different from that of the KF scheme. Noticeably, the distribution of graupel was more symmetrical between the east and west sides of the cyclone than was resolved in the KF simulation. The GD predicted eye wall was also smaller than for the KF scheme on both the east and west sides. In addition, the radial tilting between the two cases was similar, although the size of the eye was considerably larger in the KF simulation. This would indicate that the KF cyclone was less intense than that predicted by the GD scheme, which supports the previous observation that the GD cyclone was the most intense simulated cyclone. It is apparent, however, that the overall diameter of the KF cyclone proves that it was more accurate structurally than the GD simulation.

7.6.4 No Cu simulated cyclone

The No Cu simulated cyclone resolved reflectivity similarly to the GD simulation but with a number of differences. Firstly, examining the reflectivity structure in Figure 7.16a shows

that the eye wall of the No Cu cyclone was more concentric than that of the GD simulation. There was no southeast to northwest slant of the cyclone as in the GD simulation. Secondly, the region of maximum reflectivity around the eye wall showed differences to the GD simulation. It is likely that the cyclonic rotation associated with the radius of maximum winds was more intense than that in the GD case. This is because eye wall reflectivity associated with deep convection (greater than 50 dBz) could be seen to circulate from the northwest of the eye wall to the southeast of the eye wall. There was another band of this same convection to the northeast. This ring of maximum reflectivity was not seen in the GD simulation. Finally, there was no significant spiral rain band like that seen in the GD case, but a number of squall lines were simulated northeast of the system. These squalls had deep convective centres of the order of 50 dBz.

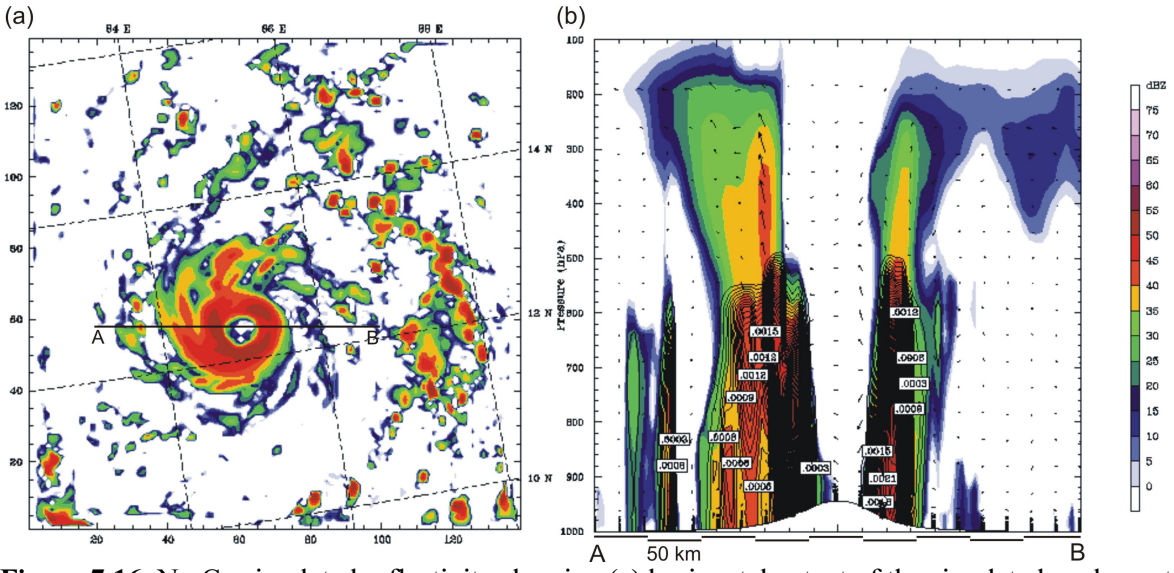

Figure 7.16: No Cu simulated reflectivity showing (a) horizontal extent of the simulated cyclone at 0600 LST on 15/11/07, and (b) vertical profile with mixing ratio contours for graupel, through the line A–B on Figure 7.16a, for the same time. Note the contour interval for the graupel mixing ratio is 0.1 x 10^{-9} g kg^{-1}.

A comparison between the No Cu simulated reflectivity and the No Cu precipitation rate (Figure 7.8d) did show some agreement. Firstly, the maximum hourly rainfall total recorded for the eye wall in Figure 7.8d was 64–128 mm/hr. This agrees with the simulated reflectivity for the eye wall, but an inconsistency in the extent of this rainfall is apparent. The maximum rate was simulated in the northwest corner of the eye wall, but as stated the reflectivity field showed deep convection occurring over a greater area than this. Finally, the squall lines appear to be in good agreement. There appears to be a general smoothing of precipitation rate in Figure 7.8d when compared to the organisation and distribution of deep convective squall centres, but the model did resolve some of these intense centres. Indeed, there are 3 such centres of deep convection represented by a rainfall rate of 32–64 mm/hr to the east of the main system.

It is also important to examine how the vertical structure of the cyclone was resolved by the use of no implicit CP scheme. The result appears remarkably similar to that of the GD scheme, with the exception of the western side of the eye wall. In the No Cu case, the western side of the cyclone appears more intense than for the GD case, and this can be explained by the concentric nature illustrated in Figure 7.16a. This is reflected in the size and extent of the eye wall. The diameter is approximately 125 km, while the most intense section of the eye wall extends to the 600 hPa layer.

7.6.5 Comparison to eye wall soundings

It is important to compare the simulated eye wall soundings (Figure 7.10) to the vertical reflectivity profiles. The soundings extracted from the eye wall appear to agree with the reflectivity structures. Indeed, all CP schemes were saturated to the correct levels according to the vertical reflectivity profiles. It is important to stress that this is highly dependent on the location of the sounding within the eye wall. Indeed, considerable variability in the depth of saturation in the troposphere might have been found had the position of the simulated soundings changed. For this reason, it is important to note that while the BMJ scheme showed saturation to a higher layer than the other schemes, it did not necessarily have the most intense eye wall, as indicated by the reflectivity structures. This shows it is essential to examine each method of analysis in relation to the whole.

7.7 Conclusion

In conclusion this chapter has presented a thorough investigation of three CP schemes: KF, BMJ, and GD. A simulation of no CP scheme (No Cu) was also undertaken to test model performance of simulating convection explicitly.

Returning to the research questions that examined the impact of CP scheme on cyclone intensity, this experiment has found the following. Firstly, the results of central pressure and wind speed indicate that the BMJ scheme resolved the weakest of all simulated cyclones. The KF scheme was consistently the best performing during the development phase, but as the cyclones matured the GD cyclone became the most intense. There was minimal separation between the KF, GD, and No Cu schemes when analysing the central pressures and wind speeds of the simulated cyclones. Finally, despite similarities found in

the intensities, cyclone tracks were quite different. The KF scheme produced the most accurate cyclone track when compared against the observed *best track*. The BMJ track initially performed well, and was the closest to the observed after 42 hours, but produced a more westward track during the remainder of its life. Both the GD and No Cu predicted tracks were quite similar to each other, but resolved a greater westward movement than the other schemes and the observed, making each rather inaccurate. Furthermore, when analysing the upper-level PV, it appears the intensity of the anticyclonic PV in the KF case was sufficient to steer the cyclone accurately by virtue of the resulting rotation of the 300 hPa wind field to create westerly flow. This upper-level steering effect seemed to be more intense than in the other cases, which is why the KF track was steered further northeast than the other cyclones.

The analysis of precipitation and cyclone structure also resulted in a number of interesting findings. Firstly, comparison of simulated rainfall rates at each stage of life cycle to the observed data consistently showed that the BMJ scheme was the most reliable for precipitation prediction. The KF, GD, and No Cu simulations all produced spurious precipitation on the model grid, especially in the eye wall. Thus it is clear that the BMJ scheme was the most effective at removing instability during the convective process. Secondly, despite the BMJ scheme producing the most accurate precipitation rates throughout the simulation, it failed to accurately predict cyclone structure. The KF, GD, and No Cu simulations all produced well developed cyclones at the maturity stage. Indeed, an eye, eye wall, and feeder bands appeared to be present. It is reasonable to conclude, therefore, that for a 5 km grid resolution for this event that the KF and GD schemes predicted significant cyclone structure, but as a trade off precipitation rates were too intense. This was also found for the explicit convection simulation. Finally, conclusions can be made regarding the operation of the CP schemes, and their feedback to the PCP scheme. The BMJ scheme was the most effective scheme for inhibiting the PCP from producing over-vigorous deep convection. In contrast, the KF and GD schemes have shown that they are ineffective at controlling the PCP scheme because too much deep convection was simulated by the PCP on the sub-grid scale. This was indicated by the amount of CAPE predicted by each CP scheme. The use of no CP scheme returned a similar result to the GD scheme which indicates that the use of no implicit CP scheme was as effective as the GD on these model resolutions. This is a very interesting finding, and will be discussed in Chapter 8.

Chapter 8
Discussion

8.1 Introduction

The aim of this research was to use WRF to conduct a series of sensitivity experiments investigating the dynamics, environmental interactions, and life cycle of tropical cyclone Sidr. This aim was divided into four research objectives:

- Examine the synoptic and mesoscale atmospheric processes that led to the development of tropical cyclone Sidr.

- Examine the influence of sea surface temperature on tropical cyclone Sidr's intensity, energy exchanges, life cycle, and structure; and test the suitability of WRF for coupling ocean-atmosphere processes.

- Examine the role of model initial conditions on the intensity and track of cyclone Sidr.

- Examine the sensitivity of tropical cyclone Sidr to choice of CP scheme.

The following research questions were developed to answer these objectives:

1. What were the observed atmospheric developments that lead to the genesis of Sidr, and its continued intensification? What significant hurricane structural characteristics existed?

2. What effect does a cool sea surface temperature have on hurricane intensification and energy exchange?

3. How important is model initialisation time for prediction of cyclone track and intensity?

4. What differences in cyclone track, intensity, and structure exist between the CP experiments?

5. Which CP experiment resolved the most realistic precipitation rates?

6. What do the precipitation rates indicate about the operation of each CP scheme, and what implications does this have for the operation of the PCP scheme?

8.2 Key results

The following points summarise the findings of this research:

1. Sidr developed from the organisation of deep convective clouds in a perturbed easterly flow, warm sea surface temperatures, and minimal vertical wind shear. Intensification occurred through latent heat release from the ocean into the troposphere, supported by divergence at upper-levels. Significant structural features included an eye, eye wall, and spiral rain bands.

2. Cool sea surface temperature caused Sidr to dissipate within 24 hours of model start time. The amount of latent heat released into the atmosphere also diminished significantly.

3. Model initialisation time affected both track and intensity. In this study, allowing WRF more time to simulate cyclone development produced a more intense cyclone. There was, however, some difficulty determining the most accurate track, but after a more investigatory approach, KF_108 was determined to be the most accurate.

4. Considerable differences in cyclone track, intensity, and structure were found when using different CP schemes. The KF simulation produced the most accurate track, while the BMJ, GD, and No Cu simulations produced tracks with too much westward displacement. It appears that upper-level PV, influenced by the CP scheme, affects the cyclone track. Cyclone central pressures and wind speeds show that the BMJ experiment produced the weakest cyclone. The KF, GD, and No Cu experiments showed similar pressure and wind intensities, with all predicting

intense cyclones. The cyclone precipitation and reflectivity structures confirm these trends of intensity.

5. The BMJ simulation resolved the most realistic precipitation rates throughout Sidr's life cycle. The KF, GD, and No Cu simulations produced too much precipitation on the sub-grid-scale. The explicit convection simulation rendered highly similar precipitation results to the GD experiment, which was an interesting finding.

6. The KF and GD schemes removed too much instability from the model. This caused the PCP to produce too much deep convective cloud and thus excess precipitation. The same result was found for the No Cu case, indicating that explicit simulation of convection did not provide realistic feedback to the PCP. No Cu, however, was no worse than the KF and GD schemes. The performance of the BMJ scheme was better here than KF, GD, and No Cu, but still mixed. The scheme removed realistic amounts of instability in some regions, but not enough in others. This was reflected in the cyclone structure.

8.3 Discussion of results

This section elaborates on the findings outlined in Section 8.2. To set the results of this study in context, comparison to similar studies is made where possible.

8.3.1 Tropical cyclone Sidr

8.3.1.1 Sidr in context

To set cyclone Sidr in context, the 10 most intense hurricanes in United States history are shown in Table 8.1. On this list, Sidr is ranked the fourth most intense cyclone, determined solely by the Saffir-Simpson category rating at landfall. Other factors such as death toll show that Sidr is ranked second only to the Galveston hurricane of the year 1900. This illustrates the significance of Sidr providing justification for this research, as outlined in the rationale. Indeed, it is advantageous to continue studying Indian Ocean cyclones because awareness must be raised of the significance of these storms in a social context.

A number of other points of discussion are evident from the data in Table 8.1. These go beyond the scope of this research, but are important to recognise. The implications of poor forecasting and disaster preparedness reflect in the death toll figures for both the Galveston hurricane and hurricane Katrina. As stated by Emanuel (2005), the Galveston hurricane was a great tragedy that could have been avoided. This was essentially due to United States forecasters failing to acknowledge their Cuban counterparts who predicted that the storm would track across the Gulf of Mexico. Their prediction and forecast that the storm would track towards New England remained, and as a result many lives were lost when the hurricane made landfall at Galveston, Texas. Since that time forecasting techniques have improved so that the death toll of Galveston has not been repeated in the US, but this is not the case in countries like Bangladesh. There is a lack of quality forecasts and warnings for people in countries like Bangladesh when a hurricane occurs, and this is a reflection of a social and economic problem. Indeed, this region has an insufficient meteorological network, and lack of decent warning measures and relief programmes to help save lives. In effect, when a hurricane strikes, it is often the people in the low delta regions, some of whom have no warning at all, that are worst affected or even killed.

Table 8.1: Comparison of cyclone Sidr to the ten most intense US hurricanes (at landfall) from 1900 to 2005. Sidr ranks fourth on the list; and only second to the Galveston hurricane in terms of deaths (adapted from Ahrens 2007).

Rank	Hurricane	Year	Central pressure (hPa)	Category	Death toll
1	Florida (Keys)	1935	892	5	408
2	Camille	1969	909	5	256
3	Andrew	1992	922	5	53
4	Sidr	2007	918	4	4234
5	Katrina	2005	920	4	1300
6	Florida (Keys) / South Texas	1919	927	4	600
7	Florida (Lake Okeechobee)	1928	929	4	1836
8	Donna	1960	930	4	50
9	Texas (Galveston)	1900	931	4	6000
10	Louisiana (Grand Isle)	1909	931	4	350
11	Louisiana (New Orleans)	1915	931	4	275

Gaps still remain in the United States disaster preparation programme, however, and this was illustrated during hurricane Katrina of the year 2005. This leads to the final point: even if good forecasting techniques are available, the social policy and disaster planning must also be in place. Indeed, hurricane Katrina was well forecast, and the location of landfall was well predicted, but a tardy evacuation decision left the people of New Orleans with insufficient time to leave. The impact of this event was amplified when the associated

storm surge damaged the levee system protecting the city. Up to 20 feet of water inundated the city before some people had evacuated (Ahrens 2007). The failings of both the state government and the levee system resulted in approximately 1300 deaths, the second largest hurricane death toll in United States history (Table 8.1). This illustrates the point made at the start of this thesis that lessons learnt from successes and failures in reducing vulnerability to hurricanes have the potential to contribute to efforts to reduce societal vulnerability to extreme weather events more generally (Pielke and Pielke 1997). In this study, the testing of model sensitivity to certain parameters is a fundamental part of that aim.

8.3.1.2 Observations

As expected, tropical cyclone Sidr conformed with common theories and observational studies of tropical cyclone genesis and intensification. These theories and studies were described in Chapter 2. Firstly, Sidr developed from the organisation of deep convective clouds about a centre of low pressure, originating from a perturbation in the easterly flow. This atmospheric situation is well described by Anthes (1982). In addition, the controls of formation as outlined in Pielke (1990) were satisfied during the initial stages of development. For example, a sea surface temperature analysis for the Bay of Bengal (Appendix IV) indicated warm ocean waters in excess of the required 26 °C. As stated, there was a low-level region of horizontal convergence, while a satellite image of precipitable water indicated abundant moisture in the lower troposphere (see Figure 4.4a Chapter 4). Vertical wind shear was too difficult to analyse due to lack of data. Sidr's location was also greater than 5° N of the equator, so that the Coriolis force required to support initial rotation was present. Secondly, Sidr underwent further intensification as the latent heat release increased, the cyclonic rotation intensified, and as significant feeder bands developed north and south of the storm. The latent heating associated with deep convection and the intense cyclonic rotation were inferred from observations from the 85 GHz horizontal polarisation SSMI image (see Figure 4.5b in Chapter 4), which showed rotating spiral rain bands and an eye wall. These are all significant factors required for intensification indicated in the example decision tree shown in Chapter 2 (see Figure 2.3 in Chapter 2). Finally, these findings also agree with other observational hurricane studies by Mayfield et al. (1994) and Willoughby and Black (1996). Willoughby and Black (1996) showed that the formation of hurricane Andrew occurred from the same type of perturbation in an easterly flow. While Mayfield et al. (1994) described the focussing of convection in a region of cyclonic cloud rotation during hurricane Andrew's development.

The structure of Sidr at maturity was also as expected. This was evident from the range of observational data analysed in Chapter 4. Firstly, a well developed eye was present. Secondly, an eye wall of intense precipitation and wind speed was identified. These two features contributed to the distinct axisymmetrical nature of Sidr at maturity. Thirdly, significant spiral rain bands were observed to the southeast, west and northeast of the storm centre. A severe line of deep convective squalls to the northeast was also apparent (Figure 8.1d). Such features indirectly illustrate the severe rotational force and deep convective processes operating in this environment. Indeed, it was not possible to obtain directly measured data which meant a composite view of the hurricane structure could not be constructed for this event. Because of the evidence of these features, however, it is reasonable to suggest that Sidr displayed the idealised characteristics described and illustrated by the mature hurricane profile in Stull (1999) (see Figure 2.5 in Chapter 2). For example, the formation of an eye suggests pressure differences caused by subsidence in the eye and rising motion in the eye wall resulted in a similar pressure profile to that shown in Figure 2.5b in Chapter 2. The development of an eye wall suggests that both the tangential velocity and vertical velocity profiles in the conceptual model by Stull (1999) apply to Sidr. These assumptions are confirmed in part by the minimum central pressure and maximum wind speed data obtained from the *best track* dataset (see Figure 4.4 in Chapter 4). Finally, these cyclone features were concealed by an extensive band of cirrus aloft, which is commonly observed with mature hurricanes.

As a final point of discussion, it is worthwhile to directly compare Sidr to another event. Figure 8.1a-f is a collection of remotely sensed images of hurricane's Katrina and Sidr at their respective times of maturity. There are a number of points to make regarding features and intensity. Firstly, both hurricanes show similar features. For example, the precipitation rates (Figure 8.1a and 8.1b) indicate intense falls associated with the eye wall, minimal precipitation in the eye, and a number of deep convective squalls and rain bands emanating from the centre. Colour composite images show the extent of the eye wall and deep convective bands in both storms (Figure 8.1c and 8.1d).The MODIS satellite images show similar patterns of divergence aloft reflected by the cirrus cover (Figures 8.1e and 8.1f). Finally, the images help to confirm the data in Table 8.1 that Sidr was of greater intensity. Indeed, it is reasonable to suggest that at maturity, Sidr was more intense because of greater intensity rainfall in the eye wall (Figure 8.1b), and a contracting eye (Figure 8.1d). Hurricane Katrina did not show as intense rainfall rates in the eye wall, but did however, have a number of squalls associated with deep convective rain bands that were of greater

intensity than Sidr (not shown). A simple comparative analysis such as this one helps to identify possible factors creating differences in hurricane intensity between regions. For instance, regional anomalies in sea surface temperature, or positions of oscillatory cycles such as El Niño might have an influence. This creates a number of avenues of research that could explore the regional differences in hurricane genesis and intensity using a numerical modelling based approach.

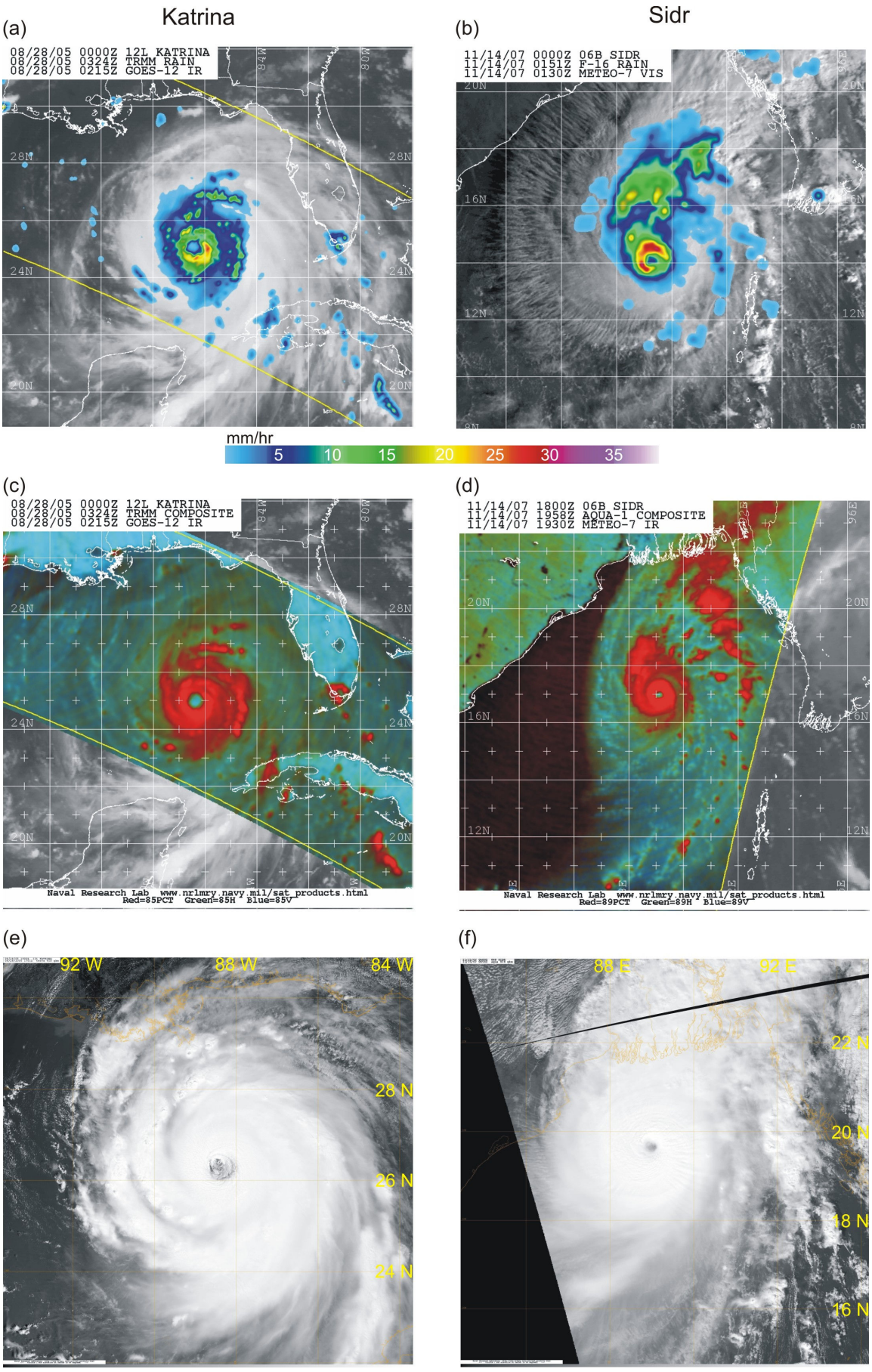

Figure 8.1: Remotely sensed images of hurricanes Katrina (a, c and e) and Sidr (b, d and f) (Navy/NRL Tropical Cyclone Page 2005, 2007).

8.3.2 Sea surface temperature experiment

Realistically, a hurricane will never develop in ocean waters as cold as those simulated here. The significance of this study, therefore, was to show how the theoretical principles of physical processes in a hurricane operate. In addition, this study served as a means of testing the suitability of WRF for investigating ocean-atmosphere interactions.

The findings of this experiment can best be explained by their effect on the physical processes of hurricane formation outlined in Chapter 2. Firstly, considering the CISK hypothesis, it was clearly demonstrated in this study that a reduction in sea surface temperature resulted in a negative feedback to the cyclone environment. This is because the rate of heating in the boundary layer was diminished such that cumulus development was inhibited. This was shown in the amount of CAPE simulated during the forecast, which decreased dramatically within 24 hours (see Figure 5.5a-d in Chapter 5). Radar reflectivities of cyclone structure also indicated that Sidr dissipated in a cooling environment, and supports the decline of cumulus convection (see Figure 5.4a-d in Chapter 5). Furthermore, CISK states that as heating decreases, so does horizontal convergence. This was also shown to be the case here, as the simulated horizontal wind fields reflected a decrease in rotation and convergence towards the storm centre, associated with cooling (see Figure 5.6a and 5.6c in Chapter 5). Finally, the impact of cooling on the interactions between the ocean and atmosphere was clearly evident. As shown by Emanuel (1986), the hurricane can be regarded as a Carnot heat cycle. This theory accounts for the limitations of CISK and incorporates the role of the ocean in hurricane dynamics. It was shown in this study that cooling of sea surface temperature had a negative impact on the operation of the Carnot heat cycle. Normally, boundary layer air converging from point A to point B in the Carnot Cycle would warm as it acquires moist entropy from a warm sea surface (see Figure 2.6 in Chapter 2).

In this experiment, warming was effectively shut down due to cool ocean temperatures. Indeed, the horizontal and vertical profiles of equivalent potential temperature showed cooling of boundary layer air during the course of the simulation (see Figure 5.7a-d in Chapter 5). This had subsequent effects for the remaining parts of the cycle. The exchange of latent heat from the lower- to upper-troposphere (flow B to C in Figure 2.6 in Chapter 2) diminished as the amount of cumulus convection decreased. This in turn caused the return

flow from the upper- to lower-levels (flow C to D in Figure 2.6 in Chapter 2) to be reduced, and thus the overall breakdown of the cycle.

The findings of this experiment agree with the general theoretical studies of Emanuel (1986, 1998). This experiment appears to be a first for the WRF model, but this is of little consequence as the effect of sea surface temperature on tropical cyclones is a well known theory. If, however, this experiment was viewed as more of a test of the ability of WRF to couple ocean-atmosphere processes, then this experiment can be regarded as a success. The results have shown the clear potential of this model for accurately accounting for interaction between the ocean and atmosphere.

8.3.3 Initialisation experiment

As stated, model initialisation time affects both track and intensity. In this study, allowing WRF more time to simulate tropical cyclone development appeared to produce a more accurate track, and a greater intensity cyclone. The results indicated that 108 hours prior to landfall was an appropriate time for WRF to spin-up a realistically intense cyclone. It was apparent that the model required at least 24–48 hours to adjust its environment to the intensity of the hurricane.

All simulated cyclone tracks were in error compared to the observations. Initially, it was unclear whether a model start time of 48 hours (experiment KF_48) or 108 hours (experiment KF_108) from landfall, produced a more accurate track. An interesting result was the performance of the 72 hour case (experiment KF_72), which was the most erroneous of the three simulated tracks (see Figure 6.1 in Chapter 6). When analysing the behaviour of the tracks after initial errors were removed, however, it became clear that the KF_108 simulation performed best at simulating the observed track (see Table 6.2 in Chapter 6). Indeed, KF_108 was the most northward cyclone of all three simulations, and its latitude and longitude changes were similar to those of the observed cyclone in the final stages of simulation.

It is evident that the predicted cyclone tracks were able to trend northeastwards during the later stages of simulation. Indeed, from Figure 6.1 it appears the greatest errors occur at the start of each simulation. The initial vortex position of all simulations was inaccurate, and all tracks for the remainder of the simulation were in error as a result. This indicates that

the initial position and intensity of the hurricane vortex is essential for accurate track prediction, and explains attempts to produce more effective initialisation techniques. A similar finding has been shown in other studies such as Davis et al. (2006), and Wang et al. (2006), albeit using more advanced methods than those in this study. The Davis et al. (2006) study tested a number of different initialisation techniques. Findings indicated that WRF 3DVAR, and the EnKF, produced a more accurate track than simply changing model start time (Figure 8.2). Evidently, Davis et al. (2006) showed that a longer initialisation time (track AVN2512 in Figure 8.2) produced a more accurate track than when using a start time closer to landfall (track AVN2600 in Figure 8.2); and this concurred with the study undertaken here.

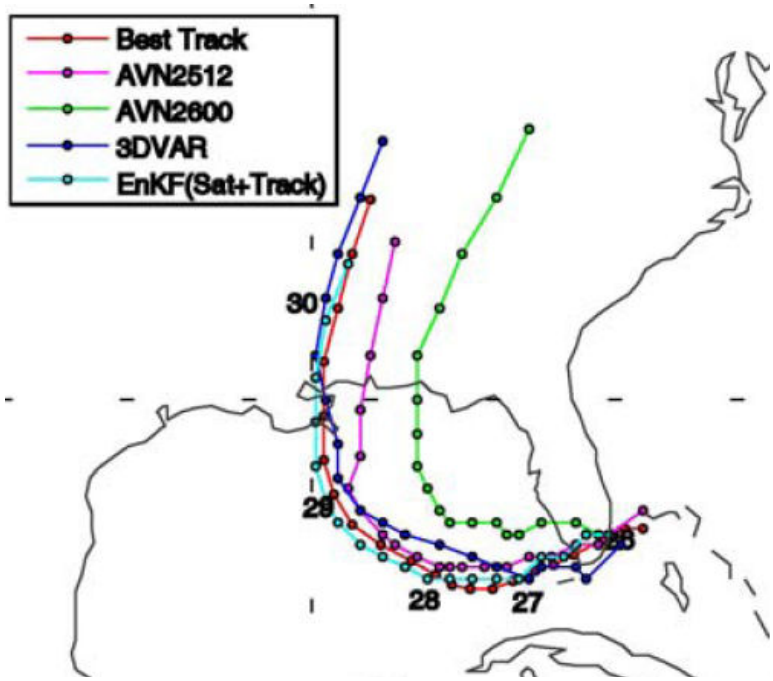

Figure 8.2: WRF tracks of hurricane Katrina using different initialisation techniques. The green and pink tracks were experiments that changed model time only. The dark blue and light blue tracks tested new initialisation methods, and resulted in a greater accuracy of simulated track (Davis et al. 2006).

There is certainly a lack of other comparable studies that have used model initialisation time similar to this research. A recent study by Pattanayak and Mohanty (2008), however, provided an excellent comparison: they conducted initialisation simulations of tropical cyclone Sidr. The Pattanayak and Mohanty (2008) study used the GD ensemble with the Eta PCP scheme, but a different PBL scheme, namely, the Yonsei University (YSU) scheme. The grid resolution was also different: 27 km. The tracks of cyclone Sidr from the Pattanayak and Mohanty (2008) study are shown in Figure 8.3. When compared to the initialised tracks of Figure 6.1 in Chapter 6, it appears that Pattanayak and Mohanty (2008) have achieved a more accurate representation of track using a different physical set up.

Furthermore, Pattanayak and Mohanty (2008) have produced reasonably accurate tracks ranging from 72 hours prior to landfall, to 18 hours prior to landfall. This indicates the choice of CP scheme and PBL scheme affects the track.

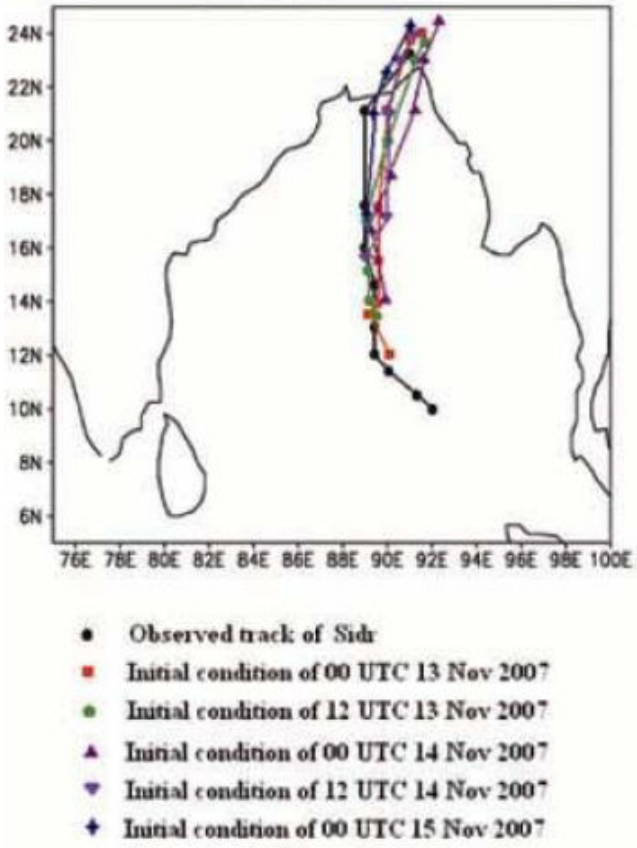

Figure 8.3: WRF tracks of tropical cyclone Sidr at various initialisation times using the GD ensemble, and YSU PBL scheme (Pattanayak and Mohanty 2008).

There is one point to consider regarding cyclone intensity. It has been shown that the number of grid points and grid resolution affects intensity (Davis and Holland 2007). This is relevant in this study because only one grid point was used per 15 km grid cell. As explained in Chapter 2, a greater number of grid points will result in less interpolation by the model between points, which reduces errors. Clearly, in this study, the lack of grid points was a factor in the simulated cyclone intensity. This is because the grid point was placed in the centre of the grid cell. According to Stull (1999), it is worthwhile to have multiple grid points per cell and have each calculating a different parameter, programmed according to the specifics of the study. Because all the data were computed at one point indicates the overall dynamical processes may not have been best represented within each grid cell. In addition, the coarse grid resolution that was used meant that a single grid point interpreted data for a greater area. Thus, if the grid resolution can be reduced in conjunction with increasing the number of grid points, then improved accuracy might result. This has been shown in related studies such as Gentry and Lackmann (2006), where

high resolution grids in the order of 1.5 km and 4 km were used. The results in Chapter 6 indicate that the predicted central pressures and maximum wind speeds for each cyclone never matched the observed. This illustrates the errors that arose from the model interpolating over too large an area.

8.3.3.1 Concluding remarks

There are some possible changes that can be made to this study, which might improve the result. The first such change would be to sample a greater range of tracks using a variety of initialisation times. It is hypothesised, however, that this would result in minimal difference of track and intensity for this event. This is because a large spread of times was used in this study. Further investigation surrounding the 72 hour case, however, would be advantageous because this track was the most inaccurate. Another possibility is to change the model initial conditions. The changes that could be made to model initial conditions are limitless, some of which might improve the results of the experiments provided here. For example, a selection of changes includes, initialising the model with higher resolution forecast data; initialising the model with a synthetic vortex with correct position and intensity at the start of the simulation; initialising the model with the YSU PBL scheme; and initialising the model with a different PCP scheme.

8.3.4 Convective parameterisation experiment

There are a number of significant points to make in relation to this experiment and other studies used to discuss the CP findings of Chapter 7. Firstly, it should be recalled from Chapter 2 that the same CP scheme used in two different models will likely produce contrasting results (‘Convective Parameterisation in Models’, Baldwin 1998). This is because every numerical model has unique physical characteristics, and different ways of calculating the solution. The same applies to using the same model, but with a different PCP scheme. This is because of the unique coupling that occurs between the PCP scheme and other parameters. Every PCP scheme treats microphysical processes differently, and this creates variability between simulations. Secondly, the limited number of WRF studies examining the role of CP schemes, means that it was difficult to find appropriate comparisons. Indeed, no 1 WRF CP study is the same because of the different PCP schemes or PBL schemes used, so caution is required. Finally, these points mean, therefore, that only vague conclusions can be drawn regarding the best CP scheme to use

for hurricane simulation. In fact, it would be irresponsible to make bold assumptions about the best CP scheme because of the event-specific nature of this study. Indeed, it is fairer, and more appropriate to suggest possible avenues of further research and possible improvements to the CP schemes. The following sections compare the CP experiment results of this study to those of others, keeping in mind these points.

8.3.4.1 Track and intensity

Considerable differences in cyclone track and intensity were found when using different CP schemes, or no implicit CP scheme. Tracks of the simulated cyclones were shown in Figure 7.3 in Chapter 7. The KF simulation was the most accurate, while the BMJ track was accurate early into the forecast, but drifted west during the later stages of simulation. The GD ensemble produced a similar track to the use of no implicit CP scheme. To help explain the differences in track, a study of PV and wind flow was used.

As stated previously, it has been shown by Emanuel (2005) that: the upper-level anticyclone forming from divergence aloft can effectively steer the surface cyclone. From the results of this thesis, it appears that the intensity of the upper-level anticyclonic PV and wind flow was influenced by the choice of CP scheme. The KF, GD, and No Cu simulations all predicted similarly intense upper-level anticyclones, while the BMJ simulation predicted a weaker anticyclone (see Figure 7.4a-d in Chapter 7). There were, however, noticeable differences in the tracks despite the similarities between the KF, GD, and No Cu simulations. For there to be such differences, other factors must be influential. This can be partly explained by the upper-level wind flow. As found in Chapter 7, it appears the strength of the upper-level westerly and southerly flows influenced the upper-level anticyclone and thus the cyclone track (see Figure 7.3 and Figure 7.4a-d in Chapter 7). A further explanation, which relates to this study, was provided in Davis and Bosart (2002).

Davis and Bosart (2002) stated that CP schemes that allow for more grid-scale overturning, resulting from mass-flux, enhanced the anticyclonic flow aloft. This is because convection transports heat and moisture through the troposphere (see Section 2.4 in Chapter 2). If the convection is intense enough to penetrate to great depths of the atmosphere, then the intensity of the divergent airflow will be affected, which will in turn affect cyclone track. This study has found that to be the case when comparing the mass-flux simulations of the

KF, GD, and No Cu schemes, to the BMJ simulation. There is still no explanation, however, for the similarity in anticyclonic PV between the KF, GD, and No Cu simulations in spite of the quite different tracks. This suggests there is another process at work that needs to be examined. Indeed, a possible cause might be that another control on tropical cyclone movement has influenced these tracks. It is possible that the background flow of the cyclone environment has displaced the GD and No Cu tracks further west relative to the KF track. This requires further investigation and is recommended for future studies.

Linked intimately to track and PV, are cyclone intensity and precipitation. The remainder of this section discusses the intensities of the simulated cyclones. In particular, consideration is given to the role of the Eta PCP scheme in cyclone intensity when coupled to the various CP experiments used here.

The experiments in this study showed that when using the Eta PCP scheme coupled to the KF and GD schemes, intense cyclones developed. The same observation was found when convection was simulated explicitly. The BMJ scheme, however, failed to intensify. These findings are reflected in the central pressure results over the simulation period (see Figure 7.1 in Chapter 7). In a similar study, Bassill and Morgan (2008) found that the Eta PCP scheme seemed to have difficulty intensifying tropical cyclones when coupled to CP schemes, with all but one exception: the KF scheme. This finding contrasts the results presented here. Indeed, in Bassill and Morgan (2008), 14 simulations of each CP scheme at 30 km grid resolution, returned minimum cyclone central pressure averages of: 960.5 hPa for the KF scheme; 991.1 hPa for the BMJ scheme; and 993.0 hPa for the GD scheme respectively. In comparison, the findings of this research found minimum central pressure was 948 hPa for the KF scheme, 989 hPa for the BMJ scheme, and 942 hPa for the GD scheme. In addition, explicit convection predicted a minimum pressure of 949 hPa. These results suggest, therefore, that for a 15 km grid resolution, the KF and GD CP schemes have worked efficiently with the Eta PCP scheme at resolving an intense cyclone. Furthermore, the use of explicit convection was also shown to be effective for intensity prediction. The performance of the BMJ scheme agrees with Bassill and Morgan (2008). This suggests that the BMJ scheme does have difficulty intensifying a hurricane when coupled to the Eta PCP scheme.

A similar finding was noted by Rosier (2005) in a WRF study of hurricane Charley. In that study, Rosier (2005) showed that noticeable variability existed in cyclone intensity when

the CP scheme was changed. For instance, at the time of Charley's maturity the central pressure when using the KF scheme was 8 hPa deeper than when using the BMJ scheme. The findings of this thesis, however, showed that a much greater central pressure difference existed between the KF and the BMJ CP schemes (see Figure 7.1 in Chapter 7). This is perhaps explained by the different PCP scheme used in this study to the one used in Rosier (2005).

A study by Gentry and Lackmann (2006) showed quite contrasting results to this research. Their study used a coarse domain of 27 km, and nested domains of 9 km and 3 km grid resolution respectively. In their study, the BMJ scheme was found to simulate the lowest central pressure, which is in contrast to this research. The difference between the results here and those of Gentry and Lackmann (2006) can perhaps be explained by the use of a different PCP scheme. Gentry and Lackmann (2006) was a CP study using the WRF Single Moment 6 Class (WSM6) PCP scheme. Indeed, this further proves the point raised by Bassill and Morgan (2008) that the use of a different combination of PCP with CP produces different hurricane intensities. One similar finding, however, was that the central pressures between all schemes used in Gentry and Lackmann (2006) were found to vary by as much as 28 hPa later into the forecast (Figure 8.4). A similar variation between CP simulations was evident in this study, but was greater earlier in the forecast (see Figure 7.1 in Chapter 7). The notable exception in this case was of course BMJ, which did not intensify, and thus varied considerably from all CP experiments.

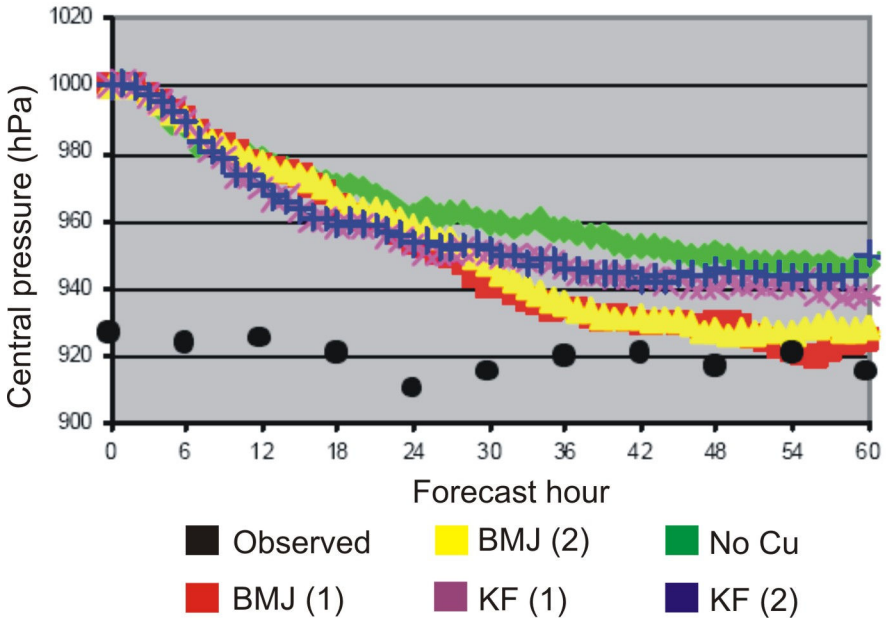

Figure 8.4: Comparison of the trend in minimum central pressures from the Gentry and Lackmann (2006) CP experiment. Note that BMJ/KF (1) refers to experiments run with CP on the 27 km and 9 km grid, but no CP run on the 3 km grid. BMJ/KF (2) refers to experiments run with CP scheme on all three domains (adapted from Gentry and Lackmann 2006).

None of these aforementioned CP studies focussed on the influence on the track. This is a factor that requires further investigation using WRF. This is because of the findings noted by Davis and Bosart (2002), and the findings of this study, which have raised questions surrounding the influence of CP scheme on the cyclone track that was not fully explained by PV. In addition, the CP results in this study are complicated by the fact that the BMJ scheme actually resolved the most realistic hourly precipitation rates, despite poorly predicting hurricane intensity. Such a finding was not seen in the Bassill and Morgan (2008) and Rosier (2005) studies. The precipitation rate and cyclone structure are discussed in the following section.

8.3.4.2 Precipitation rate and cyclone structure

The relative success of the BMJ scheme at simulating realistic peak hourly rainfall conforms to other studies using this CP scheme for tropical environments. Throughout the BMJ simulation, however, the southwest side of the hurricane was under-developed. This was especially prevalent during the mature stage, indicated by the relatively light precipitation rate (Figure 7.8b in Chapter 7), and the poor cyclone structure in that region. Indeed, the BMJ simulated reflectivity shown in Figure 7.14a in Chapter 7 indicated an imbalance of intense hydrometeors between the right front and left rear of the hurricane.

The failing of the BMJ scheme to sufficiently represent the eye wall and banding structure in a hurricane has been found in prior studies, such as Rosier (2005). One explanation for this is that the BMJ scheme has successfully removed a realistic amount of instability in the accurate precipitation areas, but too little instability in the lighter areas. This can perhaps be attributed to the amount of low-level moisture in those regions, and that the BMJ scheme does not explicitly simulate downdraughts. It is reasonable to suggest that the BMJ scheme has accounted for surface processes more accurately in the northern region of the cyclone. This is a function of radiative transfer in the model, and available moisture for convection.

The BMJ scheme also tended to produce a smoothed precipitation field throughout the cyclone life cycle (see Figure 7.8b in Chapter 7). This effect was also found in the Rosier (2005) study, and is shown in Figure 8.5a. The distribution of precipitation of the BMJ scheme in Rosier (2005) is similar to the BMJ precipitation distribution predicted for Sidr. This is interesting given the BMJ cyclone in Rosier (2005) had a deeper central pressure

and greater maximum wind speed than the other CP schemes, where in this study it was less intense. The BMJ precipitation rate in Rosier (2005), however, was not as accurate as the KF scheme (Figure 8.5b) when both were compared to the observed radar image (Figure 8.5c). The BMJ precipitation rate was also more intense than the KF scheme.

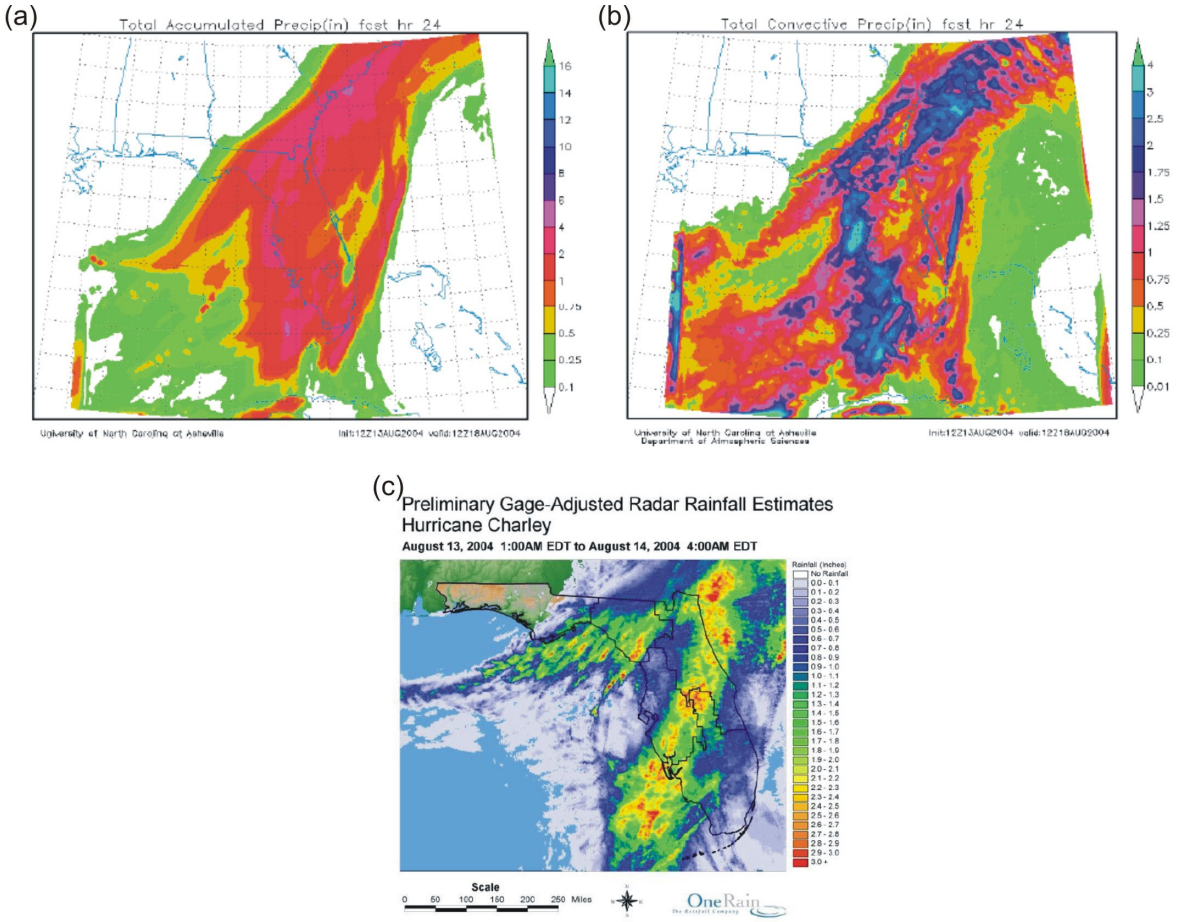

Figure 8.5: 24 hour total accumulated precipitation from the Rosier (2005) WRF study of hurricane Charley for (a) the BMJ scheme, (b) the KF scheme, and (c) the observed radar image (adapted from Rosier 2005).

Gentry and Lackmann (2006) also showed that the BMJ scheme produced more precipitation than the KF scheme. Figure 8.6a shows the predicted precipitation rates from their study. Precipitation rate is shaded every 10 mm/hr and every 1 mm/hr. Clearly, the BMJ scheme produced greater intensity rainfall when precipitation was shaded every 1 mm/hr. When shaded every 10 mm/hr, the BMJ scheme produced a less extensive area of intense precipitation, but resolved a concentric eye wall, which the KF scheme did not predict. The simulated reflectivities (Figure 8.6b) also support the precipitation rates predicted in the Gentry and Lackmann (2006) study. One explanation for the contrast between the Gentry and Lackmann (2006) study and this study, is that a different PCP scheme was used. This is a fair point as it has been established that differences exist between PCP schemes. Clearly, it needs to be established which PCP scheme more accurately represents the microphysical processes occurring in hurricane environments,

when simulated with WRF. This is beyond the scope of this research, but is a suggestion for further work in this field.

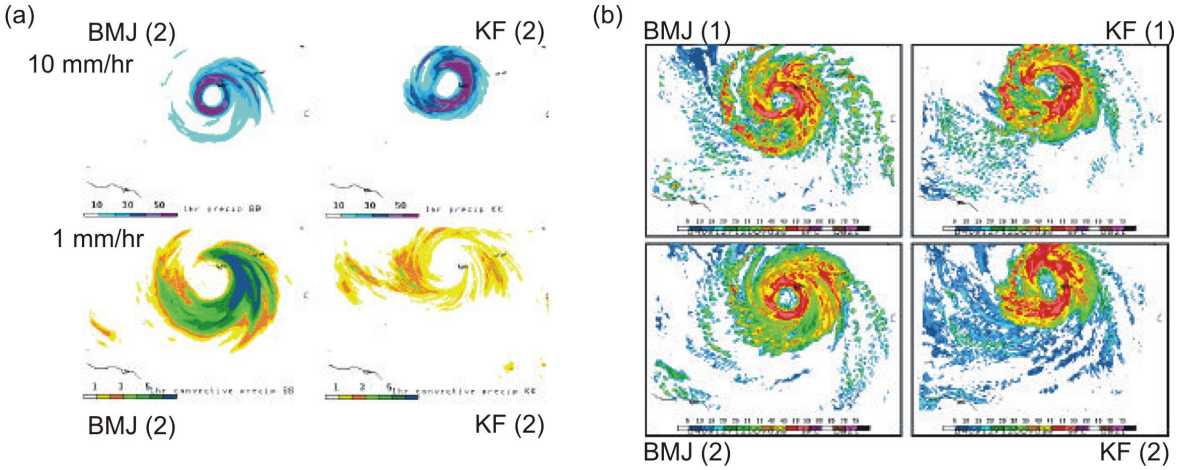

Figure 8.6: Results from the Gentry and Lackmann (2006) CP study for (a) total hourly precipitation shaded every 10 mm/hr, and every 1 mm/hr, at forecast hour 36, and (b) simulated reflectivity at forecast hour 36. The explanations for KF and BMJ are the same as in Figure 8.4 (Gentry and Lackmann 2006).

The other CP schemes did not show the ability to suppress the PCP scheme from producing deep convection on both model domains. This was indicated by the spurious, peak hourly rainfall rates. Indeed, it was established from the high resolution precipitation fields and the vertical soundings in Chapter 7 (see Figures 7.8a-d and 7.10a-d), that the KF and GD CP schemes were over-active. Simulating convection explicitly also produced too much grid-scale convection. Furthermore, the inaccuracy in precipitation rates for the KF scheme appears to contrast other studies. Indeed, Rosier (2005) established that the KF scheme was the most accurate CP scheme for simulating hurricane Charley, albeit with a different PCP scheme. In addition, Gentry and Lackmann (2006) using the WSM6 PCP scheme, showed that the KF scheme was also more accurate than the BMJ scheme, but had difficultly resolving cyclone structure. Clearly, there are issues surrounding the choice of PCP scheme for simulating cloud and precipitation processes.

As stated, the GD ensemble has been shown by Pattanayak and Mohanty (2008) to work well with the YSU PBL scheme in WRF. This research, however, has found the GD ensemble to be over-active. Some points regarding the GD ensemble can, therefore, be raised. Firstly, it should be recalled from Chapter 2, that the GD ensemble operates using a dynamic and static control mechanism. The dynamic control must know the location and intensity of the convection, and the observed change of CAPE to obtain closure. Thus, it is possible that inaccuracies in this process have occurred when simulating cyclone Sidr. For example, errors may have resulted from the interaction between the GD ensemble with the

PCP and the PBL scheme. In fact, it is likely the MYJ PBL scheme used here influenced the GD ensemble rather significantly. For instance, inaccuracies in moisture and momentum transport from the PBL scheme will affect the location and quantity of moisture available for convection. In addition, any error in the dynamic control will be compounded when the static control attempts to simulate the cloud physical processes. The impact of the PBL scheme on the performance of the GD ensemble requires further investigation.

It should also be recalled from Chapter 2, that because of its generalised approach, the GD ensemble can remove uncertainty between schemes. The results indicate, however, that this did not occur. For example, it was shown that there was minimal difference between the GD and KF precipitation fields. Indeed, the precipitation rates given in Table 7.2 in Chapter 7 show the KF and GD maximum hourly rates were identical. In addition, both CP schemes were over-active. The simulated soundings indicated that too much instability was removed from the selected eye wall region. Furthermore, even greater similarity was identified between the GD and No Cu simulation. This further illustrates that an ensemble approach has proven ineffective in this case with the selected physics schemes.

Based on the CP results of this study, and having identified that other PCP and PBL schemes might be better for hurricane simulation than the Eta PCP, leads to the following conclusions. Firstly, the Eta PCP scheme is quite possibly too simple to model the complex cloud processes occurring in a hurricane. Indeed, the Eta scheme is an example of a PCP that predicts clouds based on the cloud water in a grid cell. This is not as accurate as a complex scheme, which predicts precipitation from internal cloud processes, and multiple cloud types. Secondly, it should be recalled from Chapter 2 that grid-scale convective interactions in the Eta PCP scheme are limited. Indeed, the high RH threshold of 98% for coarse domains means that little grid-scale precipitation occurs in advance of convection. This would explain why the CP schemes were over-active in this study because they had to work harder to simulate convection that the PCP scheme failed to resolve. Finally, the MYJ PBL scheme is perhaps insufficient for representing the PBL interactions in a hurricane environment. This was not a significant focus of this study, but it would be worthwhile examining the effectiveness of a different PBL scheme for this event.

Cyclone structure is the final point for discussion. It was established from the reflectivity fields that some structural differences arose between the CP experiments. These

differences included: the shape and size of the eye; the extent of the eye wall; the nature of symmetry; and the vertical structure of the eye wall. The first explanation for this relates to the treatment of hydrometeors by the PCP scheme, as a result of feedback from the CP scheme. The intensity structures simulated (see Section 7.6 in Chapter 7) indicated that there were differences associated with precipitation intensity. This was particularly evident in the eye wall of each simulated cyclone. Another possible explanation relates to the amount of CAPE resolved, and instability removed by each CP scheme. Indeed, notable differences were found in the prediction of CAPE. The vertical soundings also reflect that the CP schemes which removed the greatest amount of grid-scale instability also resulted in more convective cloud. Because of the similarity between the KF, GD, and No Cu simulations, however, it would appear that the amount of predicted CAPE is more important for structural development, than the amount of instability removed. This should be treated with caution, however, because the BMJ scheme does not need much CAPE to trigger convection. Thus, it would be worthwhile to examine this issue, and perhaps adjust the thresholds for deep convective development.

8.3.4.3 Concluding remarks

It is difficult to assess the quality of the CP schemes used here, and there are two reasons for this. Firstly, the KF and GD schemes resolved intense hurricanes represented by accurate cyclone structures, but with excessive hourly precipitation rates. The BMJ scheme, however, resolved a weak cyclone, but with more realistic precipitation rates. Finally, further compounding the situation, was that the use of no implicit CP scheme rendered a similar result to the use of the GD ensemble, which is a CP scheme. It is reasonable to conclude that no one approach for incorporating cumulus convection into WRF for this event, using these model conditions, has been successful.

To examine cyclone track, intensity, precipitation, and structure more intently, a number of other studies are possible. It would be worthwhile re-testing these CP simulations with a different PCP and PBL scheme. Another study might follow a similar methodology to that of Gentry and Lackmann (2006). Furthermore, a number of simulations could be conducted that run CP for all domains, as well as some that do not run CP on the highest resolution domain. Finally, the issue surrounding the influence of PV on cyclone track needs further investigation. It would be reasonable to extract mid-level data such as vertical velocity to examine vorticity through the troposphere. This has been shown by

Emanuel (2005) to have an affect on environmental flow of hurricanes and as a result cyclone track.

8.4 Limitations of methodology and results

A number of methodological limitations are evident in this research. Firstly, the sparse amount of observational data meant that observational analysis was limited to indirect measurement. This is because Bangladesh and the surrounding areas do not have an established cyclone tracking network. Cyclone detection radar is located in Calcutta, but cannot provide the area coverage needed to observe cyclones over the whole northern Indian Ocean area. There are no known reconnaissance aircraft to make direct cyclone measurements. Without direct measurements it becomes difficult to evaluate simulated results. For example, direct measurements from the eye wall of Sidr would have improved the analysis of model simulated soundings. Secondly, computational demands and time constraints surrounding this research meant the quality of model simulation was limited. For example, had more time been available a high resolution moving nest would have been used to track the cyclone from the time of development. This would have allowed for high resolution simulations for all stages of cyclone life cycle, not just maturity. In addition, another nested grid could have been employed to resolve the inner core structure at even higher resolution than the 5 km nest. Finally, issues surround model initialisation. The quality of forecast data, and the choice of physics options, ultimately affects the simulation process. Furthermore, user inexperience also meant model initial conditions were limited. For example, had a synthetic vortex been implemented then the initial cyclone position and intensity might have been improved. This might lessen the effect of errors that compound during computation.

8.5 Suggestions for improvements to this work

From the discussion of the results, and the identification of several issues raised by the literature, the following improvements can be made:

- Increase the number of grid points per grid cell, to allow for more accurate model interpolation between points.

- Initialise the model with a synthetic vortex. This might improve the initial accuracy of intensity and track.

- Run a high resolution nested domain for the entire simulation period, in the CP experiment. In addition, implement a moving nest to track the hurricane centre as its life cycle progresses.

- Isolate the background flow for each of the CP simulated cyclones, and examine whether this influenced the track.

- Compare CP scheme precipitation rates for the 15 km and 5 km grid resolutions at maturity.

- Choose a different PBL scheme and a more complex PCP scheme, to represent microphysics more accurately in the hurricane environment.

- Select different ensemble parameters for the GD scheme to improve the static control function.

- Analyse the convection triggers for each CP scheme, with a closer examination of the CAPE closure mechanism.

8.6 Conclusion

In conclusion, this chapter has brought together the entire thesis, linking the results to the theoretical background provided in Chapter 2. In addition, this study was placed in context using similar hurricane studies. This contextual analysis has identified a number of issues arising from hurricane simulation using WRF, namely:

- What factors other than PV, CP, and upper-level wind flow influence a cyclone's track?

- What are the impacts of the PBL and PCP schemes for hurricane intensity prediction?

- Why did explicit convection predict a similar hurricane to the GD ensemble, for this event?

These questions unlock avenues for further research. These are reviewed in the concluding chapter of this thesis.

Chapter 9
Conclusion

9.1 Suggestions for future research

As stated in Chapter 8, a number of questions requiring further investigation were identified. The following points are, therefore, future research avenues:

- Examine the causal factors for regional differences in hurricane intensity.
- Examine which WRF PCP scheme most accurately represents microphysical processes of a hurricane.
- Examine more intently the PCP/GD coupling.
- Conduct more event-specific studies focussing on the impact of CP on cyclone track prediction.

9.2 Summary of thesis

In this study, the dynamics of tropical cyclone Sidr were simulated using WRF — a non-hydrostatic, two-way interactive, triply-nested-grid mesoscale model. Three experiments were developed examining model sensitivity to ocean-atmosphere interaction; initialisation time; and choice of CP scheme. All experiments were verified against analysed synoptic data. The ocean-atmosphere experiment involved one simulation of a cold sea surface temperature, fixed at 10 °C; and simulated using a 15 km grid resolution. The initialisation experiment involved three simulations of different model start time: 108-, 72-, and 48-hours before landfall respectively. These were simulated using a 15 km grid resolution. The convective experiment consisted of four simulations, with three of these using a different implicit convective scheme. The three schemes used were, the KF scheme, the BMJ scheme, and the GD ensemble. The fourth case simulated convection explicitly. A nested domain of 5km grid spacing was used in the convective experiment, for high resolution modelling. In all experiments, the Eta-Ferrier microphysics scheme, and the MYJ planetary boundary layer scheme were used.

As verified against available observations, the model showed considerable sensitivity in each of the experiments. The model was found to be well suited for combining ocean-atmosphere interactions: a cool sea surface caused cyclone Sidr to dissipate within 24 hours. The initialisation simulations indicated moderate model sensitivity to initialisation time: variations were found for both cyclone track and intensity. Of the three simulations, an initialisation time 108 hours prior to landfall, was found to most accurately represent cyclone Sidr's track and intensity. Finally, the convective simulations showed that considerable differences were found in cyclone track, intensity, and structure, when using different convective schemes. The KF scheme produced the most accurate cyclone track and structure, but the rainfall rate was spurious on the sub-grid-scale. The BMJ scheme resolved realistic rainfall on both domains, but cyclone intensity was poor. Of particular significance, was that explicit convection produced a similar result to the GD ensemble for both model domain resolutions.

Overall, the results suggest that the modelled cyclone is highly sensitive to changes in initial conditions. In particular, in the context of other studies, it appears that the combination of CP, PBL, and PCP scheme are most significant for accurate track and intensity prediction. This requires further investigation.

References

Ahrens, CD 2007 '*Meteorology Today: An introduction to weather, climate, and the environment. Eighth edition*', Thomson Brooks/Cole, California.

American Meteorological Society, Glossary of Meteorology n.d., *Radar reflectivity*. Retrieved August 28, 2008, from http://amsglossary.allenpress.com/glossary /search?id=radar-reflectivity1/.

American Meteorological Society, Glossary of Meteorology n.d., *Convective Available Potential Energy*. Retrieved August 28, 2008, from http://amsglossary. allenpress.com/glossary/search?id=radar-reflectivity1/.

Anthes, RA, Rosenthal, SL, and Trout, JW 1971a 'Preliminary results from an asymmetric model of the tropical cyclone', *Monthly Weather Review*, vol. 99, pp. 744–758.

Anthes, RA, Trout, JW, and Rosenthal, SL 1971b 'Preliminary results from an asymmetric model of the tropical cyclone', *Monthly Weather Review*, vol. 99, pp. 759–766.

Anthes, RA 1972 'The development of asymmetries in a three-dimensional numerical model of the tropical cyclone', *Monthly Weather Review*, vol. 100, pp. 461–476.

Anthes, RA, and Chang, SW 1978 'Numerical simulation of the ocean's nonlinear, baroclinic response to translating hurricanes', *Journal of Physical Oceanography*, vol. 8, pp. 468–480.

Anthes, RA 1982 *'Tropical Cyclones. Their evolution, structure, and effect*s', American Meteorological Society, Science Press, Pennsylvania.

Baldwin, M 1998 'Convective Parameterization in Models: Background Information'. Retrieved July 27, 2007, from http://www.comet.ucar.edu/nwplessons /precipproclesson3/.

Baldwin, M, and Kain, J 2006 'The Betts-Miller-Janjic Convective Scheme.' Retrieved September 15, 2008, from www.unidata.ucar.edu/community/2006workshop /PresenterPowerPoint/Wednesday%20Afternoon/BMJ_Unidata.pps.

Bassill, NP, and Morgan, MC 2008 'Tropical cyclone forecast track and intensity sensitivities to various parameterisations using the WRF-ARW model. Part II: Intensity sensitivities'. Retrieved November 10, 2007, from http://aurora.aos .wisc.edu/~bassill/2008-WRF%20User%27s%20Meeting-noGIF.ppt

Bender, MA, Ginis, I, and Kurihara, Y 1993 'Numerical simulations of tropical cyclone-ocean interaction with a high-resolution coupled model', *Journal of Geophysical Research*, vol. 98, pp. 23245–23263.

Bender, M, Liu, Q, Surgi, N, Pan, HL, Marchok, T, Tuleya, R, and Lord, S 2004 'Hurricane initialisation in high resolution models', *proceedings of the Twenty-Sixth Conference on Hurricanes and Tropical Meteorology*, American Meteorological Society, Miami, Florida.

Betts, AK, and Miller, MJ 1986 'A new convective adjustment scheme. Part II: Single column tests using GATE wave, BOMEX, ATEX, and Arctic air-mass data sets', *Quarterly Journal of the Royal Meteorological Society*, vol. 112, pp. 693–709.

Black, ML, Corbosiero, KL, Molinari, J, and Rogers, R 2006 'Aircraft observations of concentric eye wall formation and evolution in Hurricane Rita on 22 September 2005', *proceedings of the Twenty-Seventh Conference on Hurricanes and Tropical Meteorology*, American Meteorological Society, Monterey, California, pp. 13A.4.

Black, PG, D'asaro, EA, Drennan, WM, French, JR, Niiler, PP, Sanford, TB, Terrill, EJ, Walsh, EJ, and Zhang, JA 2007 'Air-sea exchange in hurricanes. Synthesis of observations from the coupled boundary layer air-sea transfer experiment', *Bulletin of the American Meteorological Society*, vol. 88, pp. 357–374.

Center for Research on the Epidemiology of Disasters (CRED), International Disaster Database, Retrieved 4 March, 2008, http://www.emdat.be/Database/CountryProfile/countryprofile2.php?disgroup=technological&country=Bangladesh&period=2007$2007.

Charney, JG, and Eliassen, A 1964 'On the growth of the hurricane depression', *Journal of the Atmospheric Sciences*, vol. 21, pp. 68–75.

Chan, JCL 1984 'An observational study of the physical processes responsible for tropical cyclone motion', *Journal of the Atmospheric Sciences*, vol. 41, pp. 1036–1048.

Chan, JCL, Ko FMF, and Lei, YM 2002 'Relationship between potential vorticity tendency and tropical cyclone motion', *Journal of the Atmospheric Sciences*, vol. 59, pp. 1317–1336.

Chang, SW, and Anthes, RA 1979 'The mutual response of the tropical cyclone and the ocean', *Journal of Physical Oceanography*, vol. 9, pp. 128–135.

Chu, JH, Sampson, CR, Levine, AS, Fukada, E 2002 'The Joint Typhoon Warning Center Tropical Cyclone Best Tracks, 1945-2000'. Retrieved August 18, 2008, from http://metocph.nmci.navy.mil/jtwc/best_tracks/.

Cione, JJ, Black, PG, and Houston, SH 2000 'Surface observations in the hurricane environment', *Monthly Weather Review*, vol. 128, pp. 1550–1561.

COMET program 2000 'How models produce precipitation and clouds.' Retrieved September 15, 2008, from http://www.meted.ucar.edu/nwp/pcu1/ic3/.

Davis, C, and Bosart LF 2002 'Numerical simulations of the Genesis of Hurricane Diana (1984). Part II: Sensitivity of Track and Intensity Prediction', *Monthly Weather Review*, vol. 130, pp. 1100–1124.

Davis, CA, Wang, W, and Holland, G 2005 'Real-time forecasts of Frances, Ivan, and Jeanne (2004)', *proceedings of the Sixth WRF Users' Workshop*, National Center for Atmospheric Research, Boulder, Colorado.

Davis, CA, Wang, W, Chen, Y, Corbosiero, K, Dudhia, J, Holland, G, Klemp, J, Michalakes, J, Rotunno, R, Snyder, C, and Xiao, Q 2006 'Advanced research WRF developments for Hurricane prediction', *proceedings of the seventh WRF Users' Workshop*, National Center for Atmospheric Research, Boulder, Colorado.

Davis, CA, and Holland, G 2007 'Realistic simulations of intense Hurricanes with the NCEP/NCAR WRF modelling system', *proceedings of the Tenth International Workshop on Wave Hindcasting and Forecasting and Coastal Hazard Symposium*, Oahu, Hawaii.

Dengler, K, and Reeder, MJ 1997 'The effects of convection and baroclinicity on the motion of tropical-cyclone-like vortices', *Quarterly Journal of the Royal Meteorological Society*, vol. 123, pp. 699–725.

Devaney, RL 2003 '*An introduction to chaotic dynamical systems. Second edition*', Westview Press, New York.

Dudhia, J 1989 'Numerical study of convection observed during the winter monsoon experiment using a mesoscale two-dimensional model', *Journal of the Atmospheric Sciences*, vol. 46, pp. 3077–3107.

Dvorak, VF 1975 'Tropical cyclone intensity analysis and forecasting from satellite imagery', *Monthly Weather Review*, vol. 103, pp. 420–430.

Dvorak, VF 1984 'Tropical cyclone intensity analysis using satellite data', NOAA Technical Report NESDIS 11, 47 pp.

Dvorak, VF 1995 'Tropical clouds and cloud systems observed in satellite imagery: Tropical cyclones. Workbook Volume 2. Available from NOAA/NESDIS, Washington DC, 20233.

Emanuel, KA 1986 'An air–sea interaction theory for tropical cyclones. Part I: Steady–state maintenance', *Journal of the Atmospheric Sciences*, vol. 43, pp. 585–604.

Emanuel, KA 1988 ‘The maximum intensity of Hurricanes’, *Journal of the Atmospheric Sciences*, vol. 45, pp. 1143–1155.

Emanuel, KA, DesAutels, C, Holloway, C, and Korty, R, 2004 ‘Environmental control of tropical cyclone intensity’, *Journal of the Atmospheric Sciences*, vol. 61, pp. 843–858.

Emanuel, KA 2005 ‘*Divine Wind. The history and science of Hurricanes’,* Oxford University Press, New York.

Estoque, ME 1962 ‘Vertical and radial motions in a tropical cyclone’, Scientific report number 1, Meteorology Division, University of Hawaii.

Ferrier, BS, Jin, Y, Lin, Y, Black, T, Rogers, E, and DiMego, G 2002 ‘Implementation of a new grid-scale cloud and precipitation scheme in the NCEP Eta Model’, *proceedings of The Nineteenth Conference on Weather Analysis and Forecasting, and the Fifteenth Conference on Numerical Weather Prediction*, San Antonio, Texas, American Meteorological Society, pp. 280–283.

Fritsch, JM, and Chappell, CF 1980a ‘Numerical prediction of convectively driven mesoscale pressure systems. Part I: Convective parameterisation’, *Journal of the Atmospheric Sciences*, vol. 37, pp. 1722–1733.

Fritsch, JM, and Chappell, CF 1980b ‘Numerical prediction of convectively driven mesoscale pressure systems. Part II: Mesoscale model’, *Journal of the Atmospheric Sciences*, vol. 37, pp. 1734–1762.

Gallacher, PC, Rotunno, R, and Emanuel, KA 1989 ‘Tropical cyclogenesis in a coupled ocean–atmosphere model’, proceedings *of 18th Conference on Hurricanes and Tropical Meteorology*, American Meteorological Society, San Diego, California.

Gentry, MS, and Lackmann, GM 2006 ‘The sensitivity of WRF simulations of Hurricane Ivan to choice of Cumulus parameterisation’, *proceedings of the Twenty-Seventh Conference on Hurricanes and Tropical Meteorology*, American Meteorological Society, Monterey, California.

Goerss, JS 2007 ‘Prediction of consensus Tropical Cyclone track forecast error’, *Monthly Weather Rview,* vol. 135, pp. 1985–1993.

Gray, WM, and Shea, DJ 1973 ‘The hurricane’s inner core region. Part II: Thermal stability and dynamic characteristics’, *Journal of the Atmospheric Sciences*, vol. 30, pp. 1565–1576.

Gray, WM 1982 ‘Tropical cyclone genesis and intensification’, *Intense Atmospheric Vortices*, Bengtsson, L, and Lighthill, J, (Editors), Springer–Verlag, Berlin.

Grell, GA, Kuo, YH, and Pasch, R 1991 ‘Semi-prognostic test of cumulus parameterisation schemes in the middle latitudes’, *Monthly Weather Review*, vol. 119, pp. 5–31.

Grell, GA 1993 ‘Prognostic evaluation of assumptions used by cumulus parameterisation’, *Monthly Weather Review*, vol. 121, pp. 764–787.

Grell, GA and Devenyi, D 2002 ‘A generalised approach to parameterising convection combining ensemble and data assimilation techniques’, *Geophysical Research Letters*, vol. 29, no. 14, pp. 38–1 – 38–4.

Guo, YR, Lin, HC, Ma, XX, Huang, XY, Terng, CT, and Kuo, YH 2006 ‘Impact of WRF-Var (3DVar) background error statistics on typhoon analysis and forecast’, *proceedings of the Seventh WRF Users’ Workshop*, National Center for Atmospheric Research, Boulder, Colorado.

Henderson, JM, Lackmann GM, and Gyakum, JR 1999 ‘An analysis of Hurricane Opal’s forecast track errors using quasi–geostropihic potential vorticity inversion’, *Monthly Weather Review*, vol. 127, pp. 292–307.

Jacobsen, MZ 1999 ‘*Fundamentals of atmospheric modelling*’, Cambridge University Press, Cambridge.

Janjic, ZI 1990 ‘The step-mountain coordinate: physical package’, *Monthly Weather Review*, vol. 118, pp. 1429–1443.

Janjic, ZI 1994 'The step-mountain coordinate model: Further developments of the convection, viscous sub-layer, and turbulence closure schemes', *Monthly Weather Review*, vol. 122, pp. 927–945.

Janjic, ZI 1996 'The surface layer in the NCEP Eta Model, *proceedings of the Eleventh Conference on Numerical Weather Prediction*, American Meteorological Society, Norfolk, Virginia.

Janjic, ZI 2000 'Comments on: Development and Evaluation of a Convection Scheme for use in Climate Models', *Journal of the Atmospheric Sciences*, vol. 57, pp. 3686–3686.

Janjic, ZI 2002 'Nonsingular Implementation of the Mellor–Yamada Level 2.5 Scheme in the NCEP Mesoscale model', NCEP Office Note, No. 437, 61 pp.

Jascourt, S 2004 'Convective Parameterizations in the NCEP Operational Models and Some Convective Guidance Products'. Retrieved November 12, 2008, from www.meted.ucar.edu/comm_highered/convectpp.ppt

JTWC Northern Indian Ocean Best Track Data 2007. Retrieved June 25, 2008 from http://metocph.nmci.navy.mil/jtwc/best_tracks/2007/2007s-bio/bio062007.txt

Kain, J 2006 'The Kain-Fritsch Convective Scheme.' Retrieved September 15, 2008, from www.unidata.ucar.edu/community/2006workshop/PresenterPowerPoint/Wednesday%20*Afternoon/KF_Unidata.pps*

Kain, JS, and Fritsch, JM 1990 'A one–dimensional entraining/detraining plume model and its application in convective parameterisation', *Journal of the Atmospheric Sciences*, vol. 47, pp. 2784–2802.

Kain, JS, and Fritsch, JM 1993 'Convective parameterisation for mesoscale models: The Kain-Fritsch scheme', *The Representation of Cumulus Convection in Numerical Models*, Meteorological Monographs, Emanuel, KA, and Raymond, DJ, Eds., No. 46, American Meteorological Society, pp. 165–170.

Kalnay, E, Kanamitus, M, Kitsler, R, Collins, W, Deaven, D, Gandin, L, Iredell, M, Saha, S, White, G, Woollen, J, Zhu, Y, Chelliah, M, Ebisuzaki, W, Higgins, W, Janowaik, J, Mo, KC, Ropelewski, C, Wang, J, Leetmaa, A, Reynolds, R, Jenne, R, and Joseph, D 1996 'The NCEP/NCAR 40–year reanalysis project', *Bulletin of the American Meteorological Society*, vol. 77, pp. 437–470.

Kasahara, A 1961 'A numerical experiment on the development of a tropical cyclone', *Journal of Meteorology*, vol. 18, pp. 259–282.

Khain, AP, and Ginis, I 1991 'The mutual response of a moving tropical cyclone and the ocean' *Beitraege zur Physik der Atmosphaere*, vol. 64, pp. 125–141.

Kurihara, Y, and Tuleya, RE 1974 'Structure of a tropical cyclone developed in a three-dimensional numerical simulation model', *Journal of the Atmospheric Sciences*, vol. 31, pp. 893–919.

Kuo, HL 1965 'On formation and intensification of Tropical Cyclones through latent heat release by Cumulus convection', *Journal of the Atmospheric Sciences*, vol. 22, pp. 40–63.

Kurihara, Y, and Bender, MA 1982 'Structure and analysis of the eye of a numerically simulated tropical cyclone', *Journal of the Meteorological Society of Japan*, vol. 60, pp. 381–394.

Kurihara, Y 1975 'Budget analysis of a tropical cyclone simulated in an axisymmetric numerical model', *Journal of the Atmospheric Sciences*, vol. 32, pp. 32–59.

Kurihara, Y, and Tuleya, RE 1981 'A numerical simulation study on the genesis of a tropical storm', *Monthly Weather Review*, vol. 109, pp. 1629–1653.

Lily, DK 1960 'On the theory of disturbances in a conditionally unstable atmosphere', *Monthly Weather Review*, vol. 88, pp. 1–17.

Liu, Y, Zhang, DL, and Yau, MK 1997 'A multiscale numerical study of Hurricane Andrew (1992). Part I: Explicit simulation and verification', *Monthly Weather Review*, vol. 125, pp. 3073–3093.

Malkus, JS, and Riehl, H 1960 'On the dynamics and energy transformations in steady state hurricanes', *Tellus*, vol. 12, pp. 1–20.

Marks, FD Jnr. 1985 'Evolution of the structure of precipitation in hurricane Allen (1980)', *Monthly Weather Review*, vol. 113, pp. 909–930.

Mayfield, M, Avila, L, and Rappaport, EN 1994 'Atlantic hurricane season of 1992', *Monthly Weather Review*, vol. 117, pp. 2248–2259.

Mellor, GL and Yamada, T 1982 'Development of a turbulence closure model for geophysical fluid problems', *Reviews of Geophysics and Space Physics*, vol. 20, pp. 851–875.

Miller, BI 1958 'On the maximum intensity of hurricanes', *Journal of Meteorology*, vol. 15, pp. 184–195.

Mlawer, EJ, Taubman, SJ, Brown, PD, Iacono, MJ, and Clough, SA 1997 'Radiative transfer for inhomogeneous atmosphere: RRTM, a validated correlated-k model for the longwave', *Journal of Geophysical Research*, vol. 102, pp. 16663–16682.

Molinari, J, and Dudek, M 1992 'The parameterisation of convection in numerical models: A critical review', *Monthly Weather Review*, vol. 120, pp. 326–344.

NASA Hurricane Data Analysis portal, Sea surface temperature analysis. Retrieved November 15, 2008, from http://disc.sci.gsfc.nasa.gov/ hurricane/trmm_quikscat _analysis.shtml.

Navy/NRL Tropical Cyclone Page 2007. Images retrieved June 25, 2008 from http://www.nrlmry.navy.mil/tc-bin/tc_home2.cgi

NCEP/NCAR Reanalysis dataset. Images retrieved February 20, 2008 from http://www.cdc.noaa.gov/cdc/data.ncep.reanalysis.html.

NCEP/NCAR surface pressure analysis. Retrieved May 25, 2008, from http://www.cdc.noaa.gov/cgibin/DataAccess.pl?DB_dataset=NCEP+Reanalysis+Surface+Level&DB_variable=Pressure&DB_statistic=Individual+Obs&DB_tid=21896&DB_did=3&DB_vid=28.

Ooyama, K 1964 'A dynamical model for the study of tropical cyclone development', *Geofisica Internacional*, vol. 4, pp. 187–198.

Ooyama, K 1969 'Numerical simulation of the life cycle of tropical cyclones', *Journal of the Atmospheric Sciences*, vol. 26, pp. 3–40.

Ooyama, K 1971 'A theory on parameterisation of cumulus convection', *Journal of the Meteorological Society of Japan*, vol. 39 (special issue), pp. 744–756.

Ooyama, K 1982 'Conceptual evolution of the theory and modelling of tropical cyclones', *Journal of the Meteorological Society of Japan*, vol. 49, pp. 744–756.

Ooyama, K 1990 'A thermodynamic foundation for modelling the moist atmosphere', *Journal of the Atmospheric Sciences*, vol. 47, pp. 2580–2593.

Pattanayak, S and Mohanty, UC 2008 'A comparative study on the performance of MM5 and WRF models in the simulation of tropical cyclones over the Indian seas', *Current Science*, vol. 95, pp. 923–936.

Pielke, RA Snr 1990 *'The Hurricane'*, Routledge, London.

Pielke, RA Snr, and Pielke, RA Jnr, 1997 *'Hurricanes: Their nature and impacts on society'*, John Wiley and Sons Ltd., West Sussex.

Pielke, RA Snr 2002 *'Mesoscale meteorological modelling. Second Edition'*, Academic Press, California.

Price, JF 1981 'Upper ocean response to a hurricane', *Journal of Physical Oceanography*, vol. 11, pp. 153–175.

Puri, K, and Miller MJ 1990 'Sensitivity of the ECMWF analyses forecasts of tropical cyclones to cumulus parameterisation', *Monthly Weather Review*, vol. 118, pp. 1709–1742.

Rosenthal, SL 1964 'Some attempts to simulate the development of tropical cyclones by numerical methods', *Monthly Weather Review*, vol. 92, pp. 1–21.

Rosenthal, SL 1978 'Numerical simulation of tropical cyclone development with latent heat by the resolvable scale. I: Model description and preliminary results', *Journal of the Atmospheric Sciences*, vol. 35, pp. 258–271.

Rosenthal, SL 1979 'The sensitivity of simulated hurricane development to cumulus parameterisation details', *Monthly Weather Review*, vol.107, pp. 193–197.

Rosier, MJ 2005 'Sensitivity of Hurricane Charley simulations to changes in WRF model'. Retrieved October 15, 2008, from http://orgs.unca.edu/nemac/opportunities/studentresearch/presentationresources/RosierPaper.pdf.

Saffir, H, and Simpson, R 1974 'The hurricane disaster potential Scale', *Weatherwise*, vol. 27, pp.169–186.

Schade, LR, and Emanuel, KA 1999 'The ocean's effect on the intensity of tropical cyclones: Results from a simple coupled atmosphere–ocean model', *Journal of the Atmospheric Sciences*, vol. 56, pp. 642–651.

Shapiro, LJ, and Franklin JL 1999 'Potential vorticity asymmetries and tropical cyclone motion', *Monthly Weather Review*, vol.127, pp. 124–131.

Skamarock, WC, Wang, W, Barker, D, Gill, D, Klemp, J, and Powers, JG, 2005 *'A description of the Advanced Research WRF Version 2'*, NCAR Technical Note–468+STR. Retrieved February 12, 2007 from http://www.mmm.ucar.edu /wrf/users/pub-doc.html.

Snyder, C, and Chen, Y 2006 'Initialising a hurricane vortex with an Ensemble Kalman Filter', *proceedings of the Twenty-Seventh Conference on Hurricanes and Tropical Meteorology*, American Meteorological Society, Monterey, California, pp. 8A.5.

Stephens, GL 1978 'Radiation profiles in extended water clouds. Part II: Parameterization schemes', *Journal of the Atmospheric Sciences*, vol. 35, pp. 2123–2132.

Stull, RB 1999 '*Meteorology for scientists and engineers. Second edition*', Thomson Brooks/Cole, California.

Sturman AP and Tapper NJ 2006 *'The weather and Climate of Australia and New Zealand. Second edition'*, Oxford University Press, Melbourne.

Summary of cyclone situation. Bangladesh Ministry of Disaster Management. Retrieved July 15, 2007, from http://www.mofdm.gov.bd/sidr%20damage.htm.

Syono, S 1953 'On the formation of tropical cyclones', *Tellus*, vol. 5, pp. 179–185.

Wang, Y, and Holland GJ 1996a 'The beta drift of baroclinic vortices. Part I: Adiabatic vortices', *Journal of the Atmospheric Sciences*, vol. 53, pp. 411–427.

Wang, W, Barker, D, Bray, J, Bruyère, C, Duda, M, Gill, D, and Michalakes, J 2008 'ARW Version 2 Modelling System Users Guide', NCAR Mesoscale and Microscale Meteorology Division. Retrieved July 12, 2008 from http://www.mmm.ucar.edu/wrf/users/pub-doc.html.

Wang, Y, and Holland GJ 1996b 'The beta drift of baroclinic vortices. Part II: Diabatic vortices', *Journal of the Atmospheric Sciences*, vol. 53, pp. 3737–3756.

Weatherford, C, and Gray, WM 1988 'Typhoon structure as revealed by aircraft reconnaissance. Part II: Structural variability', *Monthly Weather Review*, vol. 116, pp.1044–1056.

Willoughby, HE, Clos, JA, and Shoreibah, MG 1982 ‘Concentric eye wall, secondary wind maxima, and the evolution of the hurricane vortex’, *Journal of the Atmospheric Sciences*, vol. 39, pp. 395–411.

Willoughby, HE, and Black, PG 1996 ‘Hurricane Andrew in Florida: Dynamics of a disaster’, *Bulletin of the American Meteorological Society*, vol. 77, pp. 543–549.

Wu, CC, and Emanuel, KA 1993 ‘Interaction of a baroclinic vortex with background shear: Application to hurricane movement’, *Journal of the Atmospheric Sciences*, vol. 50, pp. 62–76.

Wu, CC, and Emanuel, KA 1995a ‘Potential vorticity diagnosis of hurricane movement. Part I: A case study of Hurricane Bob (1991)’, *Monthly Weather Review*, vol. 123, pp.69–92.

Wu, CC, and Emanuel, KA 1995b ‘Potential vorticity diagnosis of hurricane movement. Part II: Tropical Storm Ana (1991)’, *Monthly Weather Review*, vol. 123, pp.93–109.

Yamasaki, M 1977 ‘A preliminary experiment of the tropical cyclone without parameterising the effects of cumulus convection’, *Journal of the Meteorological Society of Japan*, vol. 55, pp. 11–31.

Yanai, M 1961 ‘A detailed analysis of typhoon formation’, *Journal of the Meteorological Society of Japan*, series 2, vol. 39, pp. 187–213.